Development of Different Natural Polymeric Biocompatible Materials for Wound Healing

Thesis submitted to Jadavpur University

for the degree of

Doctor of Philosophy in Science

by

ISHITA SAHA

Under the supervision of

Prof. Parimal Karmakar

Department of Life Science and Biotechnology

Jadavpur University

Kolkata, West Bengal, India

2024

CERTIFICATE FROM THE SUPERVISOR

This is to certify that the thesis entitled "*Development of Different Natural Polymeric Biocompatible Materials for Wound Healing*" Submitted by **Smt. Ishita Saha** who got her name registered on **04/10/2018** for the award of Ph. D. (Science) degree of Jadavpur University, is absolutely based upon his own work under the supervision of **Prof. Parimal Karmakar** and that neither this thesis nor any part of it has been submitted for either any degree / diploma or any other academic award anywhere before.

Parimal Karmakar 01/04/24

(Signature of the Supervisor(s) date with official seal)

Parimal Karmakar, Ph.D.
PROFESSOR
Department of Life Science & Biotechnilogy
JADAVPUR UNIVERSITY, KOL-32
Email:pkarmakar_28@yahoo
(M) 943

DECLARATION

I do hereby declare that the work embodied in the thesis entitled "***Development of Different Natural Polymeric Biocompatible Materials for Wound Healing***", submitted for the award of Doctorate of Philosophy (PhD) in science, is the completion of the work carried out under the supervision of Prof. Parimal Karmakar at the Department of Life science and Biotechnology, Jadavpur University. Neither this thesis nor any part of it has been submitted for any degree/diploma or any other academic award.

Date: Signature of the candidate

                                             Department of Life Science and Biotechnology

                                             Jadavpur University, Kolkata

                                             West Bengal, India

DEDICATION

I dedicate this thesis

To

My parents, grandfather, grandmother, all well-wishers,

&

Almighty God.

PREAMBLE

The thesis consists of six chapters. The first chapter includes a general introduction to the wound healing process, different types of skin wound healing and dressing materials, polyherbal extract, hydrogel, mucilage polymer, and microsphere. In the present study, we mostly focused on the development of environment-friendly, natural acute and chronic wound healing materials, their physical characterization, and their therapeutic application on human cell lines and mouse models. In the second chapter, we mentioned some common Methods and techniques used in most chapters. In the third chapter, we emphasized the role and fabrication process of polyherbal extract encapsulated hydrogel matrix for excision wound healing. In the fourth chapter, we focused on the synthesis process of hibiscus mucilage polymer and its application against second-degree burns and excision wounds. In the fifth chapter, we focused on the synthesis process of green silver nanoparticle encapsulated hibiscus mucilage microsphere and its application against pathogen-infected second-degree burn and excision wounds. During this study, we also found that our synthesized materials played a crucial role in preventing acute and chronic wounds. Collectively, in the sixth chapter, we discussed the general conclusion on the basis of the therapeutic effects of our fabricated various polymeric materials.

ACKNOWLEDGEMENT

TABLE OF CONTENTS

Contents	Page No.

Chapter 4: Hibiscus Mucilage Polymer: Natural Fabrication & Innovative Approaches in the Treatment of Second-Degree Burns, Inflammation, and Excision Wounds

Chapter 5: Fabrication process of Green Silver Nanoparticle Embedded Mucilage Microsphere and Applied Against Highly Pathogenic Bacteria Infected Second-Degree Burn And Excision Wound

List of Publications

List of Awards

LIST OF FIGURES

LIST OF TABLES

LIST OF ABBREVIATIONS

AgNO$_3$	Silver nitrate
Akt	Protein kinase B
BET	Brunauer–Emmett–Teller
BSA	Bovine serum albumin
bFGF	Basic fibroblast growth factor
b.w.	Body weight
CFU	Colony forming unit
COL-1	Collagen type-1
DAPI	4',6-Diamidino-2-phenylindole
DCFDA	2,7-dichlorofluorescein di-acetate
DLS	Dynamic light scattering
DMEM	Dulbecco's modified eagle medium
FBS	Fatal bovine serum
FESEM	Field emission scanning electron microscopy
FITC	Fluorescein isothiocyanate
FT-IR	Fourier transform infrared spectroscopy
GSNPs	Green Silver nanoparticles
GAPDH	Glyceraldehyde 3-phosphate dehydrogenase
HM	Hibiscus mucilage polymer
HMMS@GSNP	Green silver nanoprticle encapsulated hibiscus mucilage microsphere
HB-EGF	Heparin-binding EGF-like growth factor
IL-1β	Interleukin-1-beta
IL-6	Interleukin-6

IFN-γ	Interferon-gamma
LB	Luria Bertani
LD50	Lethal dose at 50 % survival
MBC	Minimum bactericidal concentration
MDR	Multi-drug resistant strains
MIC	Minimum inhibitory concentration
MTCC	Microbial type cell culture
MTT	3-(4,5-dimethylthiazol-2-yl)-2,5-diphenyl tetrazolium bromide
NAC	N-acetyl cysteine
NaOH	Sodium hydroxide
NPs	Nanoparticles
OD	Optical density
PBS	Phosphate buffered saline
pAkt	Phosphorylated protein kinase
PEG	Poly ethylene glycol
PVA	polyvinyl alcohol
PLGA	Poly(lactic-co-glycolic acid)
PNVP	Polyvinylpyrrolidone
PDI	Polydispersity Index
PDGF	Platelet-derived growth factor
PI3K	phosphoinositide 3-kinase
ROS	Reactive oxygen species
RT	Room temperature
SD	Standard deviation

SDS	Sodium dodecyl sulphate
SEM	Scanning electron microscope
TGA-DTA	Thermogravimetric Analysis-Differential Thermal Analysis
TNFα	Tumor necrosis factor alpha
TGF-β	Transforming growth factor-β
TGF-α	Transforming growth factor-α
UV	Ultra-violet
WHO	World Health Organization
w/w	Weight/ weight
XRD	X-ray diffraction
X	Xanthan gum hydrogel
X@C	Calendula encapsulated xanthan gum hydrogel
X@H	Hibiscus encapsulated xanthan gum hydrogel
X@C-H	Polyherbal extract encapsulated xanthan gum hydrogel
XG	Xanthan gum powder

LIST OF SYMBOLS

%	Percentage
:	Ratio
+Ve	Positive
<	Less than
=	Equal
>	Greater than
±	Plus-minus
×	Times
°C	Degree centigrade
µg	Microgram
µl	Microliter
µM	Micro molar
µmol	Micromole
cm^{-1}	Centimeter inverse
cm^2	Centimeters squared
gm	Gram
h	Hour
min	Minute
KV	Kilovolt
M	Molar
M^{-1}	Molar inverse
mA	Milliampere
mg	Milligram
min	Minute

ml	Mililiter
mM	Milimolar
mm	Millimeter
mV	Millivolt
mW	Milliwatt
nm	Nanometer
π	Pi
rpm	Rotation per minute
V	Volt
-Ve	Negative
W	Watt
w/v	Weight/volume
α	Alpha
β	Beta
γ	Gamma
λ	Lambda
kg	Kilogram
&	And

Abstract

An injury or wound results in disruption of healthy tissues as well as a breakdown in the skin's protective layer. Replacing damaged skin or other tissues is a dynamic and intricate phenomena known as wound healing. On the basis of the recovery period, the wounds are differentiated into acute and chronic wounds. According to WHO annually maximum mortality rates are induced by burn wounds associated with the growth of various types of pathogenic bacteria and form sepsis. Therefore, various reports suggested that wound dressing or wound care management is the most important for fast wound recovery, reduced wound infection, and subsequently decreased mortality rates. In the last decades, various forms of wound healing materials have developed like hydrogel, nanoparticles, mesosphere, scaffold, ointment, etc., and most of the materials were synthesized from either chemical or natural processes. The naturally synthesized materials are usually high prices and produced very low amounts. In this thesis, we have formulated three types of biocompatible, biodegradable, and cheap-priced skin wound care management products and tested them against acute and chronic wounds.

Firstly, we fabricated polyherbal extract (*Hibiscus rosa-sinensis and Calendula officinalis* flower extract) encapsulated xanthan gum hydrogel matrix (X@C-H) and applied in excision wound. During ancient times, the tribal communities utilized the *Hibiscus rosa-sinensis* and *Calendula officinalis* flowers as herbal remedies for a wide range of health conditions. However, the herbal medicines loading and delivery are significantly tricky process due to the maintenance of their molecular structure against some environmental factors like moisture, temperature, plus other ambient factors. Our synthesized polyherbal extract was phytochemically screened, which revealed the presence of several compounds including alkaloids, flavonoids, terpenoids, saponins, tannins, glycosides, anthraquinones, a few percentages of reducing sugar and amino acids. The polyherbal extract encapsulated xanthan gum hydrogel matrix released the polyherbal extract slowly for extended time. When

tried in in-vitro system, the X@C-H significantly improved the proliferation and migration of human fibroblast and keratinocyte cells compare to undoped excipient treated cells as determined by MTT assay, scratch wound assay, and BrdU assay. Also, the X@C-H treated cells enhanced the expression of the pAkt protein indicating the activation of PI3K signaling pathway. In an in-vivo study, we also noticed that X@C-H treated excision wound-formed male BALB/c murine model resulted reduction in wound area within the 12th day and helped for re-epithelization, granulation process compared to the other groups (untreated, X, X@C, X@H). As a result, we believe that this biocompatible hydrogel could serve as a potential transporter for herbal excipients.

Additionally, we formulated a mucilage polymer (HM) from the leaves of *Hibiscus rosa sinensis* and its potential utilization in the treatment of second-degree burn and excision wounds has been assessed. Mucilage is a sticky material found in diverse plant species and microorganisms, composed of protein and polysaccharides. Due to its stabilizing, emulsifying, moisturizing, and soothing characteristics, it finds widespread application in the food sector and skin care products. The in vitro experiment indicates that the addition of HM polymer promotes the migration and proliferation of human lung fibroblasts (WI-38) and keratinocytes (HaCaT) cells. Furthermore, HM polymer exhibits biocompatibility antioxidant, and anti-inflammatory properties. During an in vivo experiment conducted on BALB/c mice with second-degree burn and excision wounds, it has been observed that the HM-treated mice developed hair follicles, new tissue, and also blood vessels within six days and cured the wound within 11th days.

Finally, we focused on antibiotic-resistant bacteria-infected wound infection. Recently various scientists have developed nanoparticle-mediated antibacterial agents but most of the nanoparticles have some toxic effect. Therefore, we have developed green silver

nanoparticles encapsulated mucilage microsphere (HMMS@GSNP). Both the silver nanoparticle and the mucilage polymer were obtained from *Hibiscus rosa sinensis* leaves. Microspheres are porous and spherical structures made of a variety of materials, including polymers, glass, ceramics, metals, and more. In the current study, we have utilized the HMMS@GSNP microsphere as a therapeutic intervention for the treatment of second-degree burns and excision wounds that have been contaminated by pathogenic bacteria. The HMMS@GSNP microsphere released GSNP nanoparticles from their surface through the control release process. This HMMS@GSNP microsphere showed strong antibacterial, cell proliferation, migration, antioxidant, and anti-inflammation activity compared to untreated, GSNP (green silver Nanoparticle) and HMMS (hibiscus mucilage polymer). In in vivo experiment, we observed that the HMMS@GSNP microsphere treated either MRSA infected second-degree burn or MRSA infected excision wound bearing male BALB/c mice =significantly recovered injured area and decreased bacterial infection within 20th days compared to other groups (untreated, Silverex ionic gel, $AgNO_3$, HMMS, GSNP). Thus, the HMM@GSNP microsphere is an excellent therapeutic material that can be used as a topical agent for the management of chronic wound therapy.

Moreover, our all data suggested that our synthesized X@C-H hydrogel matrix, HM polymer, and HMMS@GSNP microsphere are suitable for acute or chronic wound-healing agents and other biomedical applications for the near future.

Chapter 1

Introduction

&

Review of Literature

1.1. Introduction

Skin is the major appendage in the body and acts as a defence against pathogens, UV radiation, temperature regulation, and environmental injuries. In addition, when exposed to sunlight, the skin participates in the synthesis of vitamin D, which is necessary for maintaining strong bones and a healthy immune system. The skin consists of three layers: the outer, epidermis (up to 600 μm thick), the dermis (a mixture of fibroblast-containing connective tissue; 2–4 mm thick), and the hypodermis (fatty connective tissue; dermal-skeletal attachment). (Bombin *et al* 2020)

A wound is a disruption of normal tissues that can be differentiated into several types depends on various characteristics, including their cause, depth, and whether they are open or closed. Here mentioned are some common types of wounds: incision, excision, burn, Laceration, Abrasions, punctures, and Avulsion. (Herman *et al* 2020) Human skin, are categories as two types of compulsive scarring after damage like hypertrophic scars and keloids. Hypertrophic scars are formed after 6 months of injuries (burns, surgery, trauma, etc.) and typically resolve within six months. However, keloids develop beyond the boundaries of the initial tissue injury and they do not regress spontaneously. In addition, keloids and hypertrophic scars can be distinguished histologically by their distinct collagen fibre arrangement, presence of α-smooth muscle actin (α-SMA)–positive myofibroblasts, and angiogenesis. (Gauglitz *et al* 2011)

In the case of higher organisms, the biological wound-healing process is differentiated into two types: tissue regeneration and wound repair. In humans, after surgical injuries, liver cells have regenerated completely while other organs like skin, heart, lungs, and kidneys, cannot regenerate completely. (Fu *et al* 2009)Modern medicine continues to face difficulties

in the very complicated and dynamic process of wound healing as it depends on various biological and molecular processes like- cellular proliferation, cellular migration, remodeling, and extracellular matrix deposition, etc. (Guo*et al* 2010)In addition to the fact that certain healing processes result in the formation of fibrosis or a scar in the wounded area which is another health concern for the general population. (Wynn *et al* 2012)

Another barrier to the wound recovery process is a polymicrobial infection; the microorganisms impede the injured area and thus delay the repairing process. (Eming *et al* 2014) Here mentioned some wound infection-responsive bacteria like Methicillin-resistant *Staphylococcus aureus* (MRSA), *Pseudomonas aeruginosa*; *Streptococcus pyogenes*; *Escherichia coli*; *Enterococcus* species (*Enterococcus faecalis* and *Enterococcus faecium*). (Puca *et al* 2021) Wound infection refers to the invasion when a wound becomes contaminated with harmful bacteria or other pathogens, it can impede the normal healing process and lead to complications. The appropriate treatment for a wound infection depends on the identification of the particular microorganisms, and identification of their protease levels, such as MMPs or ADAMs, which may help for specific wound treatment processes. (Snyder *et al* 2011). Therefore proper treatment of infected wound is not only tedious but also expensive.

Therefore proper wound care management and wound dressing are very important factors for fast wound healing and reducing scar formation. In ancient time various types of folk medicine like herbal extract has been used for wound healing. The herbal extracts repressed microbial growth along with blood clotting, and upregulated the collagen fibril formation, promoting DNA synthesis. (Rezaei *et al* 2015) However, crude extracts have some side effects like toxicity, allergic reactions, rashes, etc.(Zeng *et al* 2010) However, some scientists coated the crude extract by some natural polymers and used them for various

biomedical application and often reduced the hazardous effect of crude drugs.. Currently, different types of wound dressing equipments are available on the market, like, Foam, Hydrocolloid, Hydrogel, Alginate, Silicone, Collagen dressings, etc. (Nguyen *et al* 2023) Therefore, in this thesis, we synthesized three types of cost-effective, nontoxic wound healing agents for acute and chronic wounds, like polyherbal extract encapsulated xanthan gum hydrogel matrix, hibiscus mucilage biopolymer, and green silver encapsulated mucilage microsphere.

1.2 Review of the wound healing process

Hemostasis, inflammation, proliferation, and remodeling are the 4 distinct stages of the wound recovery process. These stages of wound healing are interrelated and overlap each other, and the timing and advancement of each stage might change based on the size, depth, location, and general health of the patient. Here the four phases of the wound healing process are briefly discussed.

Hemostasis:

In this early stage, blood clots are formed to stop the bleeding and provide a temporary closure over the incision. A fibrin clot forms as a result of substances released by platelets that start the clotting cascade. When blood flow is reduced due to injured blood vessels constricting, inflammatory cells begin to move toward the area of the wound. (LaPelusa *et al* 2019)

Inflammation:

In this phase, immune cells, like macrophages and neutrophils, gather at the damage site to combat infection and remove debris. Inflammation helps to clear away bacteria, damaged

tissues, and foreign particles, creating an environment conducive to healing. (Reinke *et al* 2012) The inflammatory response also triggers the release of growth factors like TGF-β, PDGF, TGF-α, bFGF, and HB-EGF; some pro-inflammatory cytokines-such as TNFα, IL-1β, IL-6, IFN-γ and chemokines CCL2 (monocyte chemo-attractant protein-1), CCL11 (eotaxin) and CXCL1 (chemokine ligand 1)that stimulate cell proliferation and the recruitment of other cells involved in the healing process. However, prolonging the inflammatory phase also leads to a delayed healing process (Eming *et al* 2014) as observed in type II diabetes (T2D).

Proliferation:

During the proliferation phase, the injured tissue is replaced with new tissue like keratinocytes. This phase starts 2–10 days after injury. Fibroblasts play a crucial role by producing collagen, the main protein responsible for wound strength. Mesenchymal stem cells (MSCs) downregulate the expression of pro-inflammatory cytokines and chemokines after the inflammation phase.(Landén *et al* 2016)New blood vessels, called angiogenesis, form to supply oxygen and nutrients to the healing area. The VEGFA (vascular endothelial growth factor A) and FGF-2 (fibroblast growth factor 2; also known as bFGF) are the most significant positive regulators of angiogenesis. Later on, in the healing process, the fibrin matrix is replaced by capillary sprouts connected to fibroblasts and macrophages, and granulation tissue forms a new substrate. This new substrate allows keratinocytes to migrate and the barrier function of the epithelium has been restored. (Gurtner *et al* 2008) TGF-β plays a dual role in re-epithelialization, as it aids in keratinocyte migration while also negatively regulating the overall process. Despite its negative regulation, the combined action of FGF, HGF, and EGF still promotes the migration and proliferation of keratinocytes, ultimately leading to the closure of the wound.

Some transcription factors like Ap-1, STAT3, Fos, Jun, and the Krox zinc finger are also subsequently up-regulated and induced cell proliferation signalling pathway by activation of tyrosine kinases and cytokine-receptor.(Schäfer *et al* 2007) It has also been shown that certain polyunsaturated fatty acids and their derivatives, which activate PPARs (peroxisome proliferator-activated receptors), are significant regulators of re-epithelialization and separately keratinocytes express more PPAR-δ and PPAR-α after skin damage. (Michalik *et al* 2001)Pro-inflammatory cytokines turn on AP1 proteins through the stress-activated protein-kinase signaling cascade. This turns up the production of the gene that codes for PPAR-β (also known as PPAR-δ) and of ligands that haven't been found yet. By increasing the expression of the genes for integrin-linked kinase and 3-phosphoinositide-dependent protein kinase 1, which phosphorylate and activate the anti-apoptotic protein Akt, PPAR-β promotes cell viability. Therefore, a variety of factors can stimulate the intracellular signaling pathways and upregulate the numerous phases of wound re-epithelialization. (Gurtner *et al* 2008)

Remodeling:

The remodeling or maturation phase begins two to three weeks after injury. During this phase, specialized cells called fibroblasts produce collagen, which provides structural support to the healing tissue. Additionally, blood vessels continue to grow and supply oxygen and nutrients to aid in the remodeling process. Collagen fibers are realigned, and remodelled from type III collagen backbone to type I collagen, and excess collagen is broken down and replaced with stronger fibers.(Schultz *et al* 2011) Finally the wound increased tensile strength and decreased scar tissue formation.
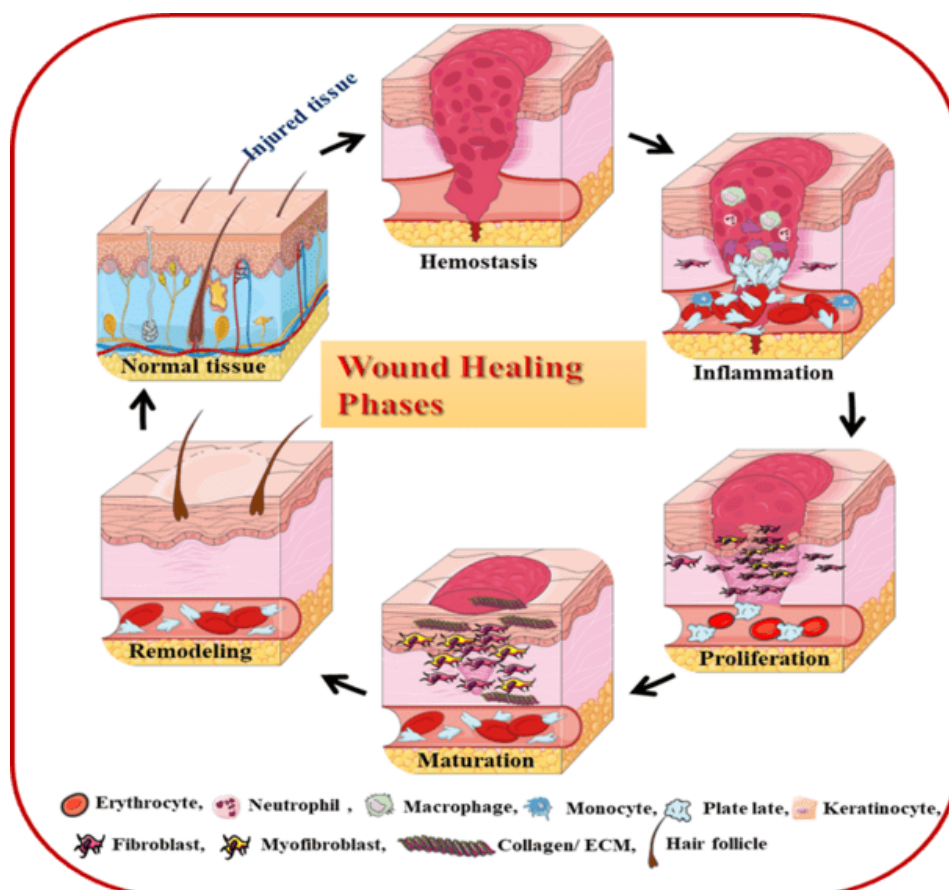
Figure 1.1. *Wound healing phases of injured skin. Some portion of the figure was created using Servier Medical Art, provided by Servier, licensed under a Creative Commons Attribution 3.0 unported license*

1.3. Review of polyherbal extract

Medical science consists of two systems Oriental medicine and Western medicine; herbal treatment is a vital component of Eastern or Oriental medicine (Lai *et al* 2017). Another new concept in medicine is multitarget therapy, which involves the use of various drugs and plant compounds in combination with superior efficacy and lesser side effects than a single plant extract. In this regard use of poly-herbal component is a promising therapeutic process for wound healing. (Budovsky *et al* 2016). In ancient time single herbal extract like *Calendula officinalis, Annona reticulate, Moringa sp., Aloe ver*a, etc. have been used as folk medicine but it was not suitable for complex wound care management. Currently, some scientists have used polyherbal extract because the active phytochemical constituents of single plant extract

are insufficient to achieve the desirable therapeutic effects while combining multiple herbs in a particular ratio, will give a better therapeutic effect and reduce the toxicity. In recent times various types of wound healing gel have been developed from polyherbal compounds like a methanolic fraction of *Plumbago zeylanica* Linn, *Datura stramonium* Linn and *Argemone mexicana* Lin which has been used for anti-bacterial effect. (Dev *et al* 2019). The combination of pomegranate and chamomile has better wound-healing properties than a single herb treatment. It was also found to be quicker to wound induction.(Niknam *et al* 2021) Fahimi *et al.* have synthesized polyherbal cream (PHC), from aqueous leaves extracts of *Solanum nigrum*, *Malva sylvestris*, and petals extract of *Rosa damascene* and it significantly reduced burn wound by upregulation of anti-inflammation, antibacterial and antioxidant effect. (Fahimi *et al* 2015)Therefore this finding suggested that multi-target therapeutic properties of polyherbal extract could be used to treat different phases of wounds at a time. (Dubey *et al* 2023)

Table 1.1. List of polyherbal extract for wound healing activities

Polyherbal extract	Properties	Ref.
Methanolic extract of *Plumbago zeylanica Linn* (stem), *Datura stramonium* Linn (leaf) and *Argemone mexicana* Linn (aerial part)	Antibacterial	Dev *et al* 2019
Aqueous extract of Leaves of *Vitex negundo*, bark of *Emblica officinalis* and whole plant of *Tridax procumbens*	Angiogenasis, antioxidant, wound healing	Talekar *et al* 2017
Hydroalcoholic extract of *Curcuma longa*, *Eclipta alba*, and *Tridax procumbens*	excision, incision, burn and dead space wound healing	Nasir *et al* 2016
Root extract of *Astragalus membranaceus*, &*Rehmannia glutinosa Libosch*	Hindlimb ischemia-induced neovascularization and wound healing	Tam *et al* 2014
Ethanolic extract of *Erythrina indica, Bergenia ciliata*&*Cissampelos pareira*	Wound healing	Patel *et al* 2013
Curcuma longa L. *Zingiberaceae, Orthosiphon aristatus, and Phyllanthus niruri L., Phyllanthaceae*	Antimicrobial, antioxidant	Hamad *et al* 2023

1.4 Review of wound healing materials

Since ancient times, cotton gauze and other materials were used to provide passive protection for wounds. In 1960, George Winter changed the concept of wound care products (Xiang *et al* 2020) and Turner in 1979 gave the outline of "ideal wound dressing" properties. The modern wound dressing concept should maintain various properties such as (a) absorb exudates, absorb wound odor, and harmful substances from the surface of the wounds; (b) keeping the wound/dressing interface humid; (c) permit the flow of fluids and gases; (d) provide thermal protection; (e) maintain the wound against bacterial invasion; (f) non-allergic, non-sensitizing, sterile, non-scarring, excellent biocompatible, and biodegradable (g) be quickly removed without damaging the wound (Choi*et al* 2016; Perchyonok *et al* 2017). A moist wound environment is known to nourish the cells and stimulate the growth of various growth factors. It also provides a situation that is rich in white blood cells cytokines and enzymes (Stashak *et al* 2004). Previously most of the wound healing and dressing materials were synthesized from synthetic polymers like PEG, PVA, PNP, PLGA, and PNVP.etc. The chemically synthesized polymers have some hazardous effects like toxicity, short half-life, low biodegradability, hydrophobic, time-consuming process, etc.(Jin, 2022) Currently, based on George Winter's wet healing theory, a wide variety of natural polymeric dressing materials are available in international markets. Moreover, the natural polymer has also some advantageous characteristics including biocompatibility, biodegradability, well availability, low antigenicity, a soothing effect, a non-irritant nature, antimicrobial and anti-inflammatory properties making it an ideal component of wound healing.(Serpico *et al* 2023)The natural polymer is synthesized from different biological sources like Alginic acid, Pectin Sulfate, Dextran, Chitosan, Collagen Carboxymethyl chitin, Fibrin, Dextran Agarose, Pullulan, guar gum, locust bean gum, gum arabic, alginate, starch, heparin, xanthan, etc.(Fazal *et al* 2023)

Here we have discussed three types of wound protective polymers-hydrogel, mucilage biopolymer, and microsphere.

Table 1.2. Different types of wound healing and wound dressing material (Bhoyar *et al* 2023)

Dressing Type	Synthesis sources	Example
1. Traditional dressing	Natural cotton, wool, cellulose, woven and nonwoven fibres of cotton, rayon polyester	Gauze, natural and synthetic bandage
2. Modern dressing		
Hydrocolloid Dressings (Global utilization rate 24%)	colloidal (gel forming agents) materials combined with elastomers and adhesives	Granuflex^{TM}, Aquacel^{TM} ,Comfeel^{TM} , Tegasorb^{TM}
Alginate Dressings (Global utilization rate 20%)	calcium and sodium salts of alginic acid, a polysaccharide comprising mannuronic and guluronic acid units	Sorbsan^{TM}, Kaltostat^{TM}, Tegagen^{TM}, Comfeel Plus^{TM}
Hydrogel dressing (Global utilization rate 43%)	synthetic polymers and natural polymers	Nu-gel^{TM} and Purilon^{TM}
Semi-Permeable Adhesive film Dressings (Global utilization rate 8%)	polyurethane covered with hypoallergenic acrylic derivatives	Cutifilm^{TM}, Biooclusive^{TM} and Opsite^{TM} .
Foam Dressings (Global utilization rate 5%)	porous polyurethane foam or polyurethane foam film	Tielle^{TM}, Lyofoam and Allevyn
3. Biological Dressings	normal and fresh skin collected from foreigner bodies (human, animals, or cadavers).These material synthesised from collagen, hyaluronic acid ,chitosan, alginates, elastin.	Hyaluronic acid based dressing

1.5 Concept of the hydrogel

In 1954 Wichterle and Lim have been reported a synthetic hydrogels preparation process (Wichterle *et al* 1960), the hydrogel technologies may be applied for various industries like hygienic products, sealing, drug delivery system, artificial snow (Singh*et al* 2010)agriculture (Saxena *et al*2010; Sun *et al*2002), food additives (Chen *et al* 1995), pharmaceuticals (Kashyap *et al* 2005), biomedical applications (Kaihara *et al* 2008), etc. Hydrogel is a three-dimensional cross-linked, insoluble mass composed of a variety of hydrophilic polymeric chains. It can be susceptible to volume alteration against various external factors such as temperature, pH, and light etc (Ganguly *et al* 2020). Based on the configuration of the hydrogel, it can be divided into three groups: amorphous, semicrystalline, and crystalline. The three groups have various physical properties such as cross linking (chemical or physical interaction), physical appearance (matrix, film or microsphere), and network electrical charge (neutral, ionic, amphoteric electrolyte or Zwitterionic). (Mekkawy *et al* 2016) The hydrogel can also be divided into two main groups, other than sources namely, polysaccharide and polypeptides. These hydrogels have various advantages over other sources, such as their high water absorption capability, biocompatibility, cross linking densities, porosity, synthesis process and cost (Ozcelik *et al* 2016). The cross-linking mechanism is initiated by bonding the gel between its neighbouring macromolecules using a cyclic bond. Additionally hydrogen interactions between the side groups, such as hydrogen bonding, ionic associations, dipole interactions, and van der Waals forces also exist. Another type of properties of hydrogel is self-healing capacity or self-repair, establishing safer and longer-lasting products and provide better wound protection and healing.(Okur*et al* 2020) In addition, hydrogels can be used directly to human tissues to prevent the loss of body fluids. They can also stimulate wound

healing by delivering oxygen to the wound and protecting it from bacterial violations. Polysaccharide-based hydrogels have been widely used in the pharmaceutical industry as drug carriers. (Hamidi *et al* 2008)

1.6 Concept of mucilage polymer

Mucilage is a type of biopolymer that refers to a gelatinous or viscous substance produced by plants, bacteria, or fungi. It is often found in the sap, seeds, or roots of these organisms. (Kolhe *et al*, 2014) Mucilage has various functions in nature, including aiding in seed dispersal, water retention, and protection against pathogens. It can also have practical uses for humans, such as in food production, medicine, and industrial applications. It is made up of polysaccharides, proteins, pectin hemicellulose, cellulose and other organic compounds. The Mucilage biopolymer was synthesized by the filtration process. (Tosif *et al* 2021) Currently, various scientists have synthesized mucilage from Okra, Hibiscus, Bryophyllum, Fenugreek, etc. and it is used as a nasal gel, tablet preparation, drug delivery carrier, binging agent, cosmetics preparation, food industry etc. (Kassem *et al* 2021) Overall, mucilage is an important and versatile biopolymer with a wide range of biomedical and commercial significance
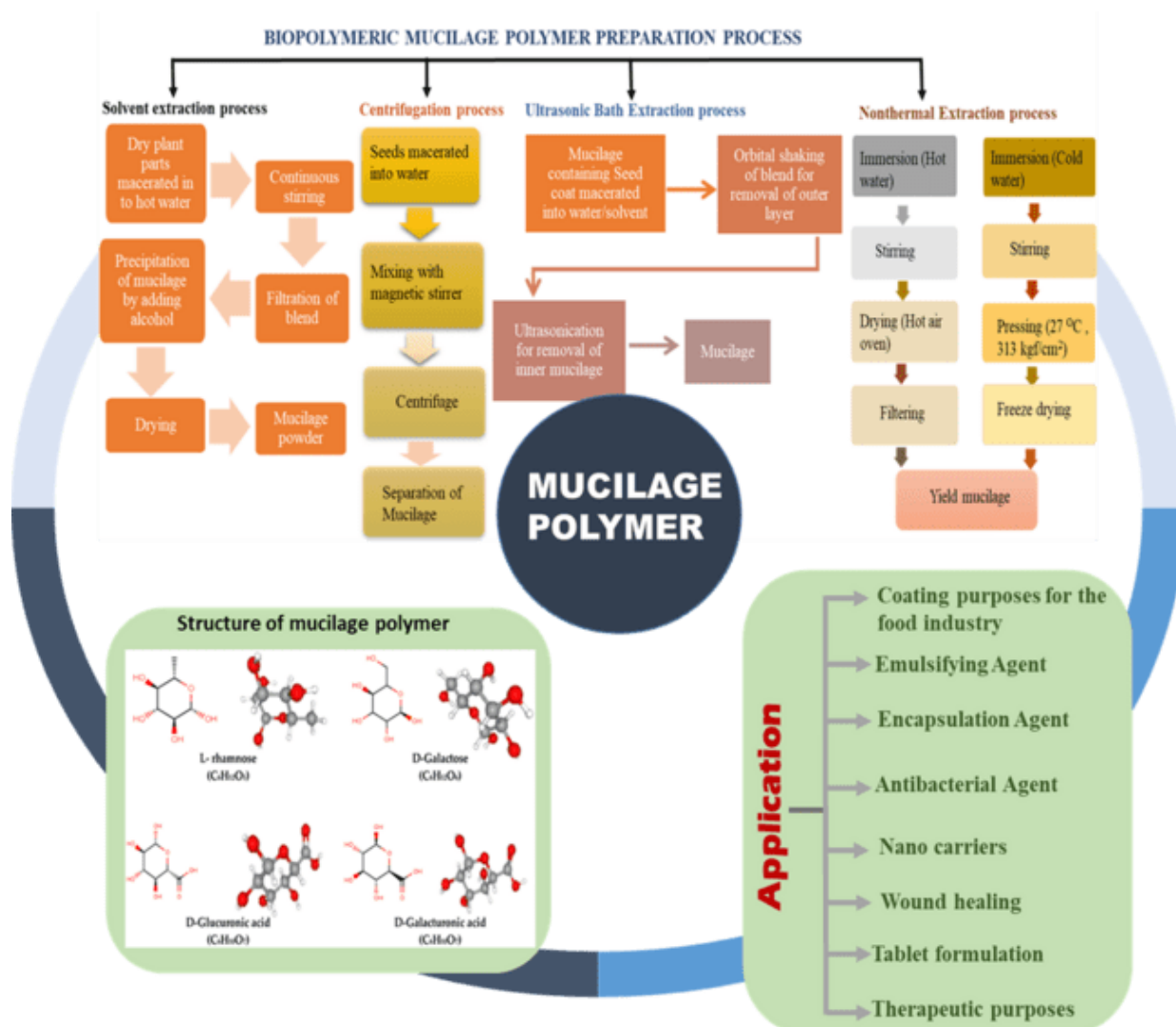
Figure 1.2. *Different properties of mucilage polymer*

1.7 Concept of Microsphere

Microspheres are small spherical and porous particles that deliver different types of small molecules like drugs, proteins, etc. The size range of the microsphere is 1µm to 100 µm. (Lengyel *et al* 2019)The microsphere is made up of different type of natural sources like carbohydrates proteins etc. and synthetic polymer sources like biodegradable polymers (Lactides, Glycolides) and non-biodegradable polymers (Poly methyl methacrylate (PMMA), Glycidylmethacrylate, Acrolein, Epoxy polymers). (Patel *et al* 2011) Different types of microspheres are available in the market like Magnetic microspheres, Floating microspheres,

Bioadhesive microspheres, Radioactive microspheres, and Polymeric microspheres.(Dhadde *et al* 2021) In addition, different microspheres are prepared by different methods such as 1. Solvent Evaporation, 2. Spray Drying, 3. Double emulsion technique, 4. Single emulsion technique, 5. Spray drying and spray congealing, 6. Phase separation coacervation technique, 7. Quassi emulsion solvent diffusion, 8. Solvent extraction. (Mahale *et al* 2019)The microsphere has some advantages like 1. protecting a risky drug before and after it is delivered, 2. reducing drug concentration at that site rather than the tissue or the target organ,3. maintaining the blood concentration and which is decreasing the toxic effect of drugs. 4. Porous surface area is increased water absorption capacity,5. provides a consistent and sustained therapeutic impact. Currently, microspheres are used for different purposes like Tissue regeneration scaffolds; High-speed protein chromatography; transport of biomacromolecules or other compounds to the target organ; tumor therapy, Pulmonary drug delivery; etc. (Cai *et al* 2013) Moreover microsphere was used for wound dressing purposes and they can stimulate tissue remodeling with the ability to deliver drugs, hemostasis, stimulate angiogenesis, anti-inflammation, anti-infection and collagen deposition at the wound site (Yang *et al* 2023). Here we have mentioned some wound-healing responsible microspheres like Xiao wei Wu et al. produced a compact calcium alginate shell coated with porous CS nuclear layer microsphere and applied it for a hemostatic agent, Xiaoling Yu et al. fabricated a porous and pH-responsive polylactic acid-glycolic acid (PLGA)-vancomycin (VAN) microsphere and it showed potent antibacterial activity, Lei et al. developed multifunctional CS microsphere (MCS-Zn^{2+}-VEGF), and it exhibited good angiogenesis ability etc. (Yang *et al* 2023)
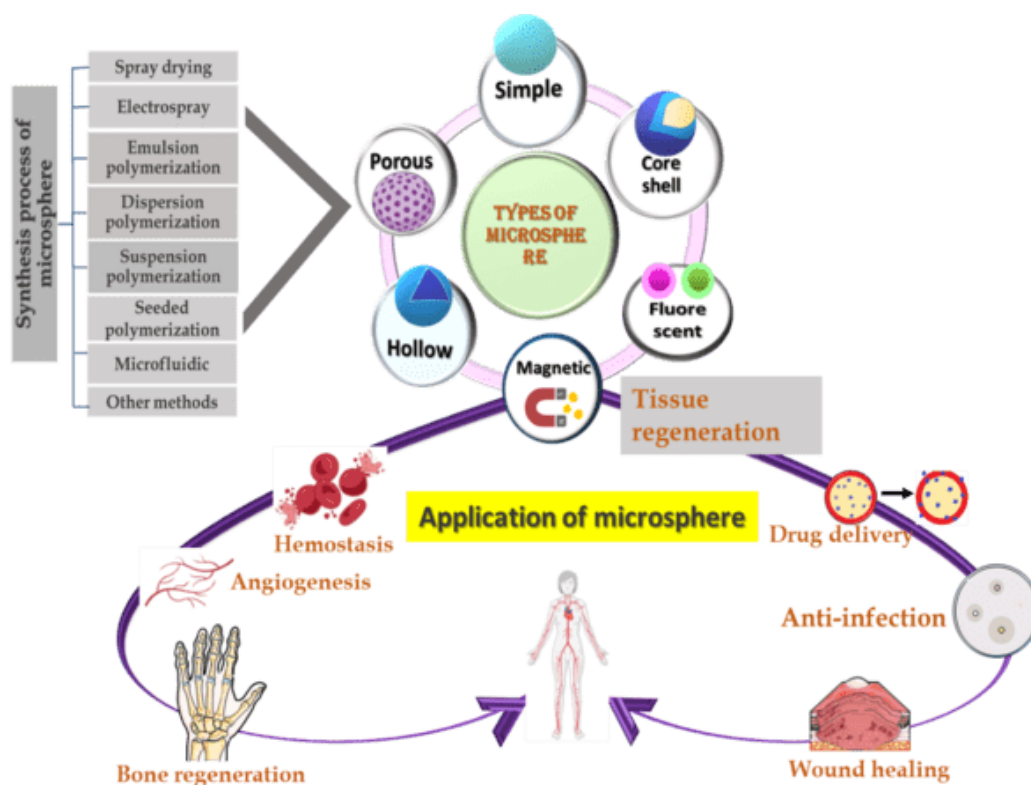
Figure 1.3. *Various properties of microsphere.*

1.8. Scope & Objective of the thesis

Normal wound care management is a very complex, dynamic, and multistep process. Therefore, proper wound protection and subsequent treatment are the most important factor for fast wound healing, According to WHO opinions, most low and middle-income countries peoples are suffering from sepsis disease since the treatment of sepsis is very expensive. The burn wound infection or chronic wound is closely related to sepsis. (Sharma *et al* 2006) After a thorough literature survey, we observed that most of the natural wound dressing materials were cost-effective and most of the researchers used chemically synthesized drugs for the encapsulation process. Therefore, one step further, we developed polyherbal extract (*Calendula officinalis* and *Hibiscus rosa sinensis* flower extract) encapsulated xanthan gum hydrogel and applied it against the excision wound. Xanthan gum is a natural polymer; it is isolated from *Xanthomonas campestris* bacteria. The *Calendula officinalis* flower, which was known to heal burn and ulcer wounds, and the *Hibiscus rosa-sinensis* flower, which was

known to heal wounds and fight microbes, so this polyherbal extract can be used for therapeutic and medicinal substances that help prevent wound infections and speed up the healing of wound tissue. On the other hand, the water absorption capacity of xanthan gum hydrogel was very high therefore it is the perfect delivering agent for wound care management.

Recently, some scientists isolated biopolymeric mucilage from different plant sources like okra, fenugreek, *Aloe vera*, *Bryophyllum sp*, *Asparagus racemosus*, *Cassia angustifolia,* etc. but these mucilage polymers have not been evaluated for wound-healing activity. Therefore, we fabricated hibiscus mucilage polymer from *Hibiscus rosa sinensis* leaves, which is applied for second-degree burn and excision wound healing.

As mentioned earlier, microorganisms are another barrier to the wound-healing process. The *Staphylococcus aureus, Pseudomonas aeruginosa, Proteus mirabilis, Escherichia coli, Corynebacterium* spp, etc, bacteria have been grown on the wounded tissue and are delaying the wound healing process. As previously reported most of the articles have used either chemically synthesized vehicles or drugs for treating wound infection (Liu *et al* 2020), therefore, we developed a green silver nanoparticle encapsulated mucilage microsphere for chronic wounds. The green silver nanoparticle was synthesized using hibiscus leaves and it was encapsulated with hibiscus leaves mucilage polymer and it finally formed the HM@GSNP microsphere. The synthesized microsphere was applied against MARSA (methicillin-resistant *Staphylococcus aureus*) infected second-degree burn or excision wound. Since microspheres have a large surface area and small particle sizes, which boost their bioavailability and absorption rate, they are often utilized in the drug delivery carrier.

Our all synthesized products are biocompatible, biodegradable, cheap, facile, and less time-consuming process; it applied topically as well as it is suitable for biomedical applications in the near future.

The major objectives of my thesis are as follows

➢ To evaluate the effects of polyherbal extract loaded hydrogel polymer and applied for excision wound

➢ To evaluate the effect of mucilage biopolymer for excision and second-degree burn wound

➢ To evaluate the effect of microspheres by using nanoparticle and mucilage biopolymer and applied against pathogenic bacteria infected second-degree burn and excision wound.

1.9. The rationale behind the study

Previously reported most the articles have mentioned the single herbal extract effect or bare polyherbal extract effect or developed dressing material using synthetic polymer or encapsulated synthetic drugs into the natural polymer for wound healing therefore, this process is either toxic or highly cost-effective or not properly protect the wound from pathogenic infection. So, in this study, we have fabricated polyherbal extract encapsulated xanthan gum hydrogel for excision wound healing. The xanthan gum was produced by natural polymer xanthan gum powder and cross-linking agent PEG 8000. After that, we focused on fully biopolymeric material because it is more cost-effective compared to xanthan gum hydrogel and it is applied for second-degree burns and excision wounds. Currently, we observed sepsis is a major cause of increasing the mortality rate. So that we have isolated green silver nanoparticles from *Hibiscus rosa sinensis* leaves and at the same time we have developed a green silver nanoparticle loaded hibiscus mucilage microsphere and it applied against antibiotic-resistant pathogenic bacteria infected second degree burn and excision wound.

Therefore in this thesis we have approached the development and therapeutic process of biocompatible, biodegradable natural polymeric materials for acute and chronic wound healing.

Chapter 2

Materials &Methods

2.1. Materials

1. Reagents

The Thermo Fisher Scientific, USA was provided DMEM medium, FBS, Penicillin/streptomycin. The amphotericin-B (anti-fungal), MTT ((3, 4, 5-dimethylthiazol-2-yl)-2, 5-diphenyltetrazolium bromide) dye were purchased from SRL, India. N-acetylcysteine (NAC), xylene, and ethanol were purchased from Merck. Abcam was provided DAB (ab94665), ECL detection reagent, and hematoxylin stain, Luria broth was taken from Hi-Media Laboratories Pvt. Ltd, India.

2. Antibodies

The primary antibodies Akt(9272S), pAkt (4058S), and IL6 (12912T) were bought from Cell Signaling Technology, USA, and Santa Cruz Biotechnology, INC has provided Collagen type I (sc-25974), TGF β1 (sc-52893), IFNγ (sc-8423) primary antibodies and also supplied. Abcam supplied the α SMA (ab-32575), and Bio Bharati Life Science provided GAPDH (BB-AB0060S). The secondary antibodies Alexa Fluor 568 conjugated anti-rabbit IgG (1:150), Alexa Fluor 488 conjugated anti-mouse IgG (1:150), purchased from Life Technologies, USA, and HRP conjugated anti-rabbit IgG (1:25000), and HRP conjugated anti-mouse IgG (1:25000) purchased from SRL, India.

2.2. Methods

1. Physical Characterization of synthesized samples:

The X-ray diffractometer model D8, Bruker AXS, Wisconsin, USA was used for XRD (X-Ray Diffractometer) analysis and measured the data at Cu-kα target employing wavelength of 1.5418å and operating at 35 kV with a scan speed of 1s/step. The FTIR-8400s, Shimadzu, was used for Fourier transform infrared spectroscopy (FTIR) analysis and was done using the wave number range from 400 cm^{-1} to 4000 cm^{-1}. In the case of dry materials, we used KBr

pallets at the ratio of samples to KBr was 1:50. The structure of the synthesized models was measured by FESEM (field emission scanning electron microscopy) or SEM (scanning electron microscopy) or Phase contrast microscopy (Leica ICC50 W). BET (Brunauer–Emmett–Teller) specific surface area and pore size distribution of the polymer was determined by Gas sorption (both adsorption and desorption) technique and it measured by the Quantachrome Autosorb iQ adsorption instrument. The NL-DFT method was used to calculate the pore size distribution from the N_2 isotherm at 77K. (Halder *et al* 2021)

The DTG-60H DTA-TGA instrument was used for TGA and DTA analysis. The hydrodynamic diameter and absorbance intensity of the synthesized samples was analyzed by Dynamic Light Scattering and UV-Vis (Bio-Tech) spectroscopy. The charges of synthesized samples were analyzed by Zetasizer (NanoZS90, Malvern Instruments Ltd., UK).

2. Measuring process of water absorbance capacity

A crucial physical factor in the healing of wounds is swelling study. The synthesized sample was first measured in the needed amount (A_0), dipped into a PBS buffer solution, and incubated at 37 ^{o}C for the necessary period of time based on sample attributes (Seeli *et al*. 2017). After that, the swelled sample was weighed at various points after the extra water had been drained with tissue paper. The following formula was used to figure out the sample's swelling ratio at time t.

Degree of swelling, % = [(A_t − A_0)/A_0] x100

Here, A_t and A_0 are the weights of the samples at time t and zero h respectively.

3. Measuring the process of drug release capacity

The drug release percentage of synthesized materials was analyzed by the incubation process. The drug-loaded vehicle was incubated under the required pH conditions and continuous mechanical shaking conditions. The 200 µl of the solution was collected from the shaking

material for the necessary durations of time and simultaneously added an equal volume of buffer solution was in the incubated samples. The absorbance maxima of the drug and the drug release percentage of the vehicle were measured by UV-Vis spectroscopy (epoch microplate spectrophotometer, USA). The drug loading capacity and drug encapsulation or loading efficiency were analyzed by the following equations (Alle *et al*. 2020).

DLC (%) = {(weight of drug encapsulated in the vehicle / weight of vehicle taken)} x100

DEE or DLE (%) = {(total amount of drug - free drug in supernatant) / (total amount of drug)} x 100

4. Initial Phytochemical testing

The different phytochemicals of polyherbal excipients (*Calendula officinalis*, *Hibiscus rosa sinensis* flower extract) were identified by the phytochemical screening test.

Test for detecting flavonoids

One mL of polyherbal excipient and a few droplets of diluted NaOH were applied for the flavonoid test. When the two were mixed, a reddish color appeared. After that, a few drops of diluted acid were added, and the sample became white. This colour detected that the flavonoid components have been present in the polyherbal extract.

Terpenoids recognition experiment

For this experiment, two mL of polyherbal excipient was mixed with an equivalent amount of chloroform and concentrated hydrogen sulfuric acid, formed the reddish-brown color. However, the fact that the polyherbal extract contains a terpenoids compound.

Reducing sugar detection test

In this experiment, we mixed one mL of polyherbal excipient with two mL of Benedict's reagent and boiled the mixture in a water bath for 3–5 minutes. The brick red color of the sample showed that the polyherbal extract contained reducing sugar.

Analysis for detecting alkaloids

In this experiment, two mL of Wagner's solution was mixed with two mL of polyherbal excipient. Brownish precipitation showed that the polyherbal excipient contained alkaloids.

Analysis for detecting tannins

Tannins were proven to be in the polyherbal extract when 0.1% $FeCl_3$ was mixed with two mL of the excipient. This made the extract turn a brownish-green color.

Test for detecting saponins

In this experiment, we used two mL of polyherbal excipient, and an equal amount of Benedict's solution was mixed together. The bluish-black color of the precipitation showed that saponins were there.

Anthraquinones detection test

Anthraquinones were found in the polyherbal extract after boiling 1 mL of a crude extract with 10% HCl in a water bath and watching it cool. The mixture had been heated and then an equivalent amount of $CHCl_3$ and a few droplets of 10% NH_3 were added. Anthraquinones were found because they caused a rose-pink color to form.

Amino acids detection test

A few droplets of Ninhydrin reagent were put into one mL of polyherbal excipient as well as formed a purple color. It defines the existence of amino acids in the crude excipient.

Glycosides recognition test

Adding one mL of polyherbal excipient to one mL of concentrated H_2SO_4 acid confirmed the existence of glycosides in the crude excipient. The red precipitation mentioned that the glycoside exists in the polyherbal excipient.

In-Vito experiment

5. Minimum inhibitory concentration study

The LD_{50} value of synthesized samples was measured by minimum inhibitory concentration assay. The gram-positive bacteria (Methicillin-resistant *Staphylococcus aureus*) and gram-negative bacteria (*Escherichia coli*) were grown in 4 mL of Luria Broth (LB) medium while being mechanically shaken at 37°C for O/N. On the second day, test tubes containing broth medium were inoculated with bacterial cultures, and various concentrations of synthesized material were added to each tube before being incubated at 37°C with constant mechanical stirring overnight. In the case of MRSA bacteria, methicillin was added to the broth medium. UV-Vis spectroscopy was utilized to determine the bacterial growth at 600 nm.

6. Minimum bactericidal concentration analysis

MBC was utilized to determine the minimal concentration of synthesized particles at this concentration no bacterial growth occurred on agar plates. The MBC values utilized to treat the bacterial cultures were calculated using the MIC values. The bacterial cultures were distributed on sterile agar plates and kept at 37°C for 24 hours. Only a 99.99% reduction in CFU as compared to the untreated growth was considered as MBC value.

7. Agar well diffusion method

The agar well diffusion method was an alternative process for determining the antibacterial activity of the synthesized sample. The desired bacteria were grown in a nutrient broth medium and incubated overnight at 37°C. Thereafter 150 µl of bacteria culture was spread over the agar plate. Wells with a 6.0 mm diameter were created inside the petri dishes and then various concentrations of sample solution were added inside the whole. The sample dosage was chosen according to the results of the MIC value. Further, the petri dish was

incubated overnight at 37°C. The next day had taken an image of Petri dishes and measured the inhibitory zone by using Image J software. In the case of MRSA, methicillin was added to the Petri dish.

8. Bacterial morphology study

The morphology of bacterial cells was investigated with scanning electron microscopy (FSEM, Inspect, F-50, FEI, Netherlands). The bacterial subculture was treated with various concentrations of samples and incubated overnight. The next day, the cells were fixed with 2% paraformaldehyde after being rinsed three times in PBS (pH 7). After that, a drop cast of diluted cell suspension was on a coverslip and vacuum-dry the coverslip, and then it was used for bacterial SEM analysis.

9. Human cell lines and cell culture conditions

The WI-38 cell line was derived from a three-month gestation female fetus lung tissue, while the HaCaT cell line was obtained from adult human skin. WI-38 and HaCaT were grown in DMEM medium and 10% FBS, penicillin (100 U/mL), and streptomycin (100 U/mL) were added into the respective medium. The cells were incubated at 37°C, 5% CO_2, and 95% relative humidity (RH).

10. MTT assay or cytotoxicity study or cell viability study

The required cell lines were seeded (2.5×10^4 cells per well) in 24 well plates and after 18-20 hr incubation the cells were treated with synthesized components at several concentrations, further incubation for 18-20 hr. Next day discard the media, add the fresh solution (5mg/mL), and re-incubate for 3 hrs at 37 °C. Finally, discard the MTT solution, add extraction buffer (Isopropanol, Triton X 100, HCl), and form a formazan crystal violet color, measuring the absorbance at 570 nm by using UV-Vis spectroscopy.

11. Immunocytochemistry and BrdU incorporation assay

The cells were seeded on 18 mm coverslip and kept at 37 ^{o}C, 5% CO_2 for 18 h. The next day the cells were treated with the desired concentration of synthesized samples and incubated for 24h, and then 10 μm BrdU was added and incubated for 1 hr. After that coverslips were rinsed with PBS buffer, and added 4% paraformaldehyde for fixation. After 30 minutes the coverslip was rinsed with PBS and submerged in 0.2% Triton X-100 at 4 ^{o}C, 10 min. for cell permeabilization. The cells were treated with 2N HCl for 45 min and incubated at RT. After that washed with PBS and incubated at RT for one hour with added blocking. The Anti-BrdU mouse monoclonal antibody (BD Biosciences) was diluted into the wash buffer at 1:100 dilutions and added on the coverslip and kept at 4 ^{o}C overnight. The FITC-conjugated goat anti-mouse IgG (SC-2078) was added after PBS washing and kept in dark conditions for 1h. The slides were then rinsed with wash buffer and mounted with DAPI medium. The cells were observed under a fluorescence microscope (Leica, Wetzlar, Germany).

12. Scratch wound assay

The cell lines were plated on a 35 mm dish and kept at 37 °C for 24 hours. After 24 hr we formed a monolayer wounded zone on the 35 mm plate by using 200 μl tips. Cells were then treated with the necessary concentration of the synthesized sample and incubated for required periods at 37°C with 5% CO_2. Every day had taken a picture of the scratched area and measured the gap width by using Image J software.

13. Antioxidant assay

The DCF-DA technique was also used to assess the antioxidant properties of synthesized components. In this experiment, DCFH-DA was used as a ROS probe. The DCFA-DA is a

deacetylated non-fluorescent compound but after entering the cells it becomes highly fluorescent DCF (2´,7´-dichlorofluorescein) in the presence of ROS. The cells were seeded on sterile 18 mm coverslips and incubated at 37 ^{o}C, 5% CO_2. After 18 h N-acetylcysteine (NAC) (5 mM) and required concentration of synthesized components were then applied to the cells on the coverslips, and incubated for the necessary amount of time. The cells were then rinsed with PBS, followed by a 30-minute incubation with 100 μM DCF-DA at 37 °C. The cells were again rinsed in PBS after incubation and examined under a fluorescence microscope (Leica, Wetzlar, Germany).

14. Western blot or Immunoblot study

The cells were seeded on a 60 mm plate and treated with a desired concentration of samples and incubated for 24 hr. After incubation periods the treated cells were used as a lysate. 1X RIPA lysis buffer (ab156034), phosphatase, and protease inhibitors (G Bioscience) were used to prepare whole-cell lysates from the cells. Bradford's reagent was used to estimate the protein concentration. After the addition of 5X protein loading dye, lysates were boiled for 5 min, and an equal amount of protein (100 μg) containing lysates was electrophoresed on a 10% SDS polyacrylamide gel in Tris–glycine buffer (pH 8.8). Polyvinylidene difluoride (PVDF) membrane (Merck) was used to transfer the proteins. 5% non-fat dry milk and 0.05% Tween-20 in 20 mM Tris–Cl, pH 7.6 (TBS-T) was used to block nonspecific binding. TBS-T was used to wash the membrane after incubation with the appropriate primary antibody and then HRP-conjugated secondary antibodies were used to reincubate the membrane. The ECL-detecting solution was used for protein detection and the ImageJ software was used to measure the intensity of each band. The anti-GAPDH antibody was used as a loading control.

In-Vivo experiment

15. Animal experiments

In all these experiments we used about 6–7 weeks old male BALB/c murine model and the weight of these mice was about 25-30 g. The mice were given a pellet with a limited amount of vitamins and libitum-added water. Animals were cared for under the recommendations of the National Institute of Nutrition, Hyderabad, India.

16. Experimental planning for in-vivo tests

The mice were distributed into required groups and each group comprised five mice. After shaving the dorsal hair of mice was cleaned with 70% ethanol. Based on the experiment the 5 mm diameter excision wound or second-degree burn wound was created on the dorsal side by punch biopsy and metal comb respectively. The photograph of the injured region was captured on the desired days and measured the area by using Image J software.

17. Hematoxylin and eosin staining

The fixed tiny sections of wounded tissue underwent the following consecutive procedures: first dehydrated by graded alcohol (30-100%), kept in xylol for 30min for de-alcoholization, then embedded in paraffin (solidification point 60-62°C), subjected to microtome sectioning of thickness 3-4 μm, sections were affixed on glass slides (pre-layered with Mayer's albumin) by heating on hot-plate for 30 sec, deparaffinised with xylene, stained with hematoxylin and eosin and a cover-slip was mounted on each stained sample by DPX. Finally, pictures were acquired using a bright-field optical microscope (Leica dm 2500, Germany).

18. Immunohistochemical analysis

The paraffin-embedded tissue sections were rehydrated using a graded ethanol series of 100%, 95%, 70%, and 50% after being deparaffinized in xylene. The slides were boiled in 10

mM citrate buffer, pH 6.0, to remove the antigen. The sections were cooled and washed with distilled water as well as PBS. For quenching the endogenous peroxidase was used 0.3% H_2O_2 in PBS for 15 min. Then the slides were dipped in PBS + 0.1% Triton X after 10 min. PBS washed. Then the sections were placed in the wet chamber for 1 hr at room temperature after adding Blocking (2% BSA, 0.1% Triton X, PBS). The sections were incubated overnight at 4 °C with Collagen Type 1 and α-SMA primary antibodies and further processed according to the protocol (ab94665). The next day the HRP conjugated secondary antibody was added after a few times washing with PBS + 0.1% Triton X and incubated for 1 h. After incubation, the tissue was 3 times washed with PBS and finally added to DAB strain and incubated for 30 minutes. After 30 minutes add 0.5% $CuSO_4$+ 0.9% NaCl and incubate for a few minutes. After that, the tissue was washed with PBS and added hematoxylin and it was finally dehydrated by graded ethanol series (50 %, 70%, 90%, and 100%) and xylene. The tissue was mounted with a cell mounting medium and observed under a Bright-field microscope (Leica DM2500, Germany). Five microscopic fields of each slide were captured at 40× magnification. The measurements were undertaken exclusively on the edge of the epidermis. The images were analyzed using ImageJ software.

19. Bacteria colony counting method

During a 48-hour post-infection period, mouse tissue was removed from the injured area and stored in a sterile 1 X PBS buffer for thorough washing. After being weighed, the tissue was homogenized in a 1 X PBS buffer using a tissue homogenizer. The homogenate sample was combined with 1X PBS buffer after being centrifuged at 8000 rpm for 8 minutes. After that, 100 μl tissue samples were spread out on methicillin-treated agar plates after the centrifuge tissue had been serially diluted in 1X PBS buffer. The agar plates were then incubated at 37°C for 24 hours to get a bacterial colony and taken images of the culture plates. The Image J. software was used for counting the bacterial colony.

20. RT-PCR

RT-PCR experiments were conducted on the sixth and thirteenth days for bacteria-infected burn mice and on the ninth and seventeenth days for bacteria-infected excision wounded mice tissue. The tissue was then isolated using TRIzol reagent (Invitrogen, Cat. no. 15596-026) after being rinsed with 1X PBS. The RNA was then quantified using a Qubit 4 machine, and 1 μg of RNA from each sample was used to produce cDNA using an iScript cDNA synthesis kit (170889, BIORAD). Real-time PCR was performed from the cDNA samples using Sso Fast Eva Green for hypertrophy marker gene *α-sma* (α-smooth muscle actin), and *ctgf* (connective tissue growth factor). All primers design have been obtained from IDT and the primer sequences are *β-actin* (M)- Forward 5′-CCTCTATGCCAACACAGTGC-3′ Reverse 5′ -CCTGCTTGCTGATCCACATC-3′; *α-sma*(M)- Forward 5'-CTTGGCTATTCCTTCGTGACTAC-3' Reverse 5'-CTGACTCCATCCCAATGAAAGA-3'; and *ctgf* (M)- Forward 5'-TCAAGCTGCCTGGGAAATG-3' Reverse 5'-CAGTTGGCTCGCATCATAGT-3'. All the Gene expression has been normalized against *β actin* gene expression.

21. Statistical analysis

Statistical differences between the groups were calculated by the student t-test method. '*'P <0.05, '**'P <0.01, '***'P <0.001 was considered statistically significant. Error bars represent the means ± SD for all plots. Data analysis was performed by one way ANOVA test using a statistical package of Microsoft Excel Software. Every biological experiment was repeatedly performed minimum two or three times.

Chapter 3

Fabrication and wound healing activity of polyherbal extract loaded hydrogel matrix: An in-vitro and in-vivo study

Fabrication and Wound Healing Activity of Polyherbal Extract loaded Hydrogel Matrix: an In-Vitro and In-Vivo Study

3.1. Introduction

The wound recovery process is intricate and dynamic. Wounds are divided into two broad types acute wounds (large skin injuries, burns) and chronic wounds (diabetic foot ulcers), chronic wounds are a worldwide public health burden (Han and Ceilley 2017). Several wound healing therapies, like plant extract, phytochemicals, and biopolymers have been found in recent years to enhance tissue regeneration (El-aie *et al* 2015). Polymeric biomaterials have the potential to hydrate, protect the wound from microorganisms, and accelerate wound healing. The granulation tissue formation is induced by plant extracts, antibacterial chemicals, or extracellular components in polymeric biomaterials. (Das and Baker 2016, Murray *et al* 2019) The previously reported hydrogel was utilized for wound dressing purposes due to its capacity to absorb the excess amount of exudates, facilitate gas exchange, maintain the moist environment, and release bioactive chemicals. (Jaiswal *et al* 2019) The polymeric materials are synthesized from two sources synthetic and natural polymers. Synthetic polymers have some hazardous effects so currently, most scientists are focused on natural polymers like alginate, gum acacia, chitosan, gelatine, etc. (Sharma *et al* 2015)

Here we used macromolecular polysaccharide xanthan gum, which is isolated from *Xanthomonas campestris* bacteria. Xanthan gum contains citric acid, glucuronic acid, and mannose as well as a β-1,4-glycosidic bond and a side chain of tri-saccharide. Xanthan gum (XG) is a non-toxic, eco-friendly, and cheap natural polysaccharide. It has been used for

various industrial purposes as a stabilizing agent, rheological modifier, etc. (Hu *et al* 2019) It has a distinct chemical structure, excellent porosity, excellent absorbing capacity, and rheological properties, as well as highly stable under different environmental conditions.

In ancient times different types of traditional medicine, including *Curcuma zedoaria, and Aloe vera* extract, have been used for the wound repair process though individually they are not suitable for complex wound management where different types of cells are involved in overlapping phases during healing. Thus polyherbal mixture components are currently being used to promote the cellular activity at different phases. It consists of more than one plant product, such as the polyherbal root extract of *Astragalus propinquus* and *Rehmannia glutinosa* used for antioxidant and angiogenesis in diabetic mice. (Lee *et al* 2015) Thus, additional research into polyherbal plant products is required for effective and side-effect-free therapy for wounds. For effective delivery of healing agent, we explored the polyherbal excipient (ethanolic *Calendula officinalis* flower extract and ethanolic *Hibiscus rosa-sinensis* flower extract) doped xanthan gum hydrogel matrix (X@C-H). We found that the X@C-H hydrogel also aided in the prolonged release of polyherbal extract from the hydrogel matrix. In addition, we noticed that X@C-H biopolymeric hydrogel patches promote proliferation, migration, and epithelialization of WI-38 and HaCaT cell lines more than uncoated herbal extract treated cell lines. In an in-vivo investigation, we observed that X@C-H is more successful in excision wound healing than uncoated excipient (C@H) or X@C, X@H hydrogel (Scheme 3.1). As a result, this biocompatible polyherbal extract encapsulated Xanthan gum hydrogel might be used to transport herbal excipients for excision wound healing.
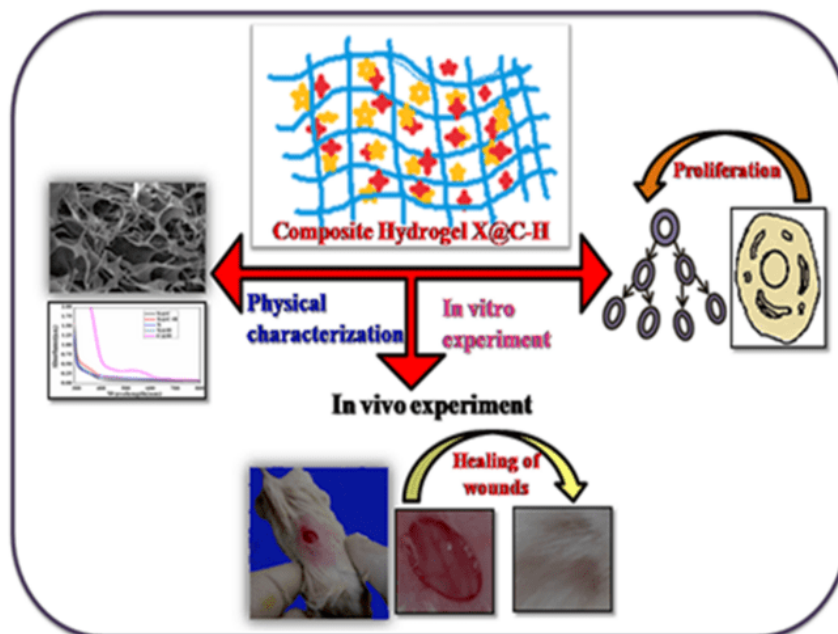
Scheme 3.1: *Graphically represents the objective of our experiment.*

3.2. Plant extract and hydrogel synthesis process

Collection and identification of plant material

Calendula officinalis (family Asteraceae) as well as *Hibiscus rosa-sinensis* (Malvaceae family) flowers were gathered from Burdwan, and Jadavpur University grounds respectively. The Agri Horticultural Society of India, in Kolkata, authenticated both plant samples.

The extraction methods of polyherbal flower

The fresh petals of *C. officinalis* (60g) were collected and dehydrated in the shaded condition. The dry flowers were soaked in 500 mL of 50% ethanol for 5 days at RT and then filtered through Whatman filter paper no. 1 (Merck Millipore). The filtrate portion was dried by lyophilizer and kept at a -20 ^{o}C. (Dinda *et al* 2016)

H. *rosa-sinensis* flowers were dehydrated at RT and crushed with a machine. 500 g of fine flower powder was mixed with 1500 mL of 32% ethanol for 24 hours at room temperature. Then the mixture was filtered with filter paper (Whatman no.1). The filtrate was

lyophilized and kept at -20 ^{o}C. The dry flower extract was used for different *in-vitro* and *in-vivo* experiments. (Shivananda *et al* 2007, Shen *et al* 2017)

The hydrogel preparation process

Initially, 5 mg/mL of Xanthan gum powder (SRL, India) was dissolved in millipore water with constant stirring for 12 hours, then the cross-linking agent PEG-8000 (Hi Media, India) was added. After the complete dissolution of the gum, it transformed into a semi-transparent hydrogel polymer and it was known as X.

The formation process of polyherbal extract encapsulated hydrogel patch:

A drop-by-drop addition of the ethanolic polyherbal flower extract (Calendula and Hibiscus extract adds 40% of the hydrogel vol.) to the hydrogel solution (1:1 w/w) and continuous magnetic stirring for one hour. The polyherbal extract encapsulated xanthan gum hydrogel was subsequently collected and desiccated using the lyophilization technique and it is named as X@C-H. Figure 3.1 depicts the preparation procedures of the hydrogel matrix.
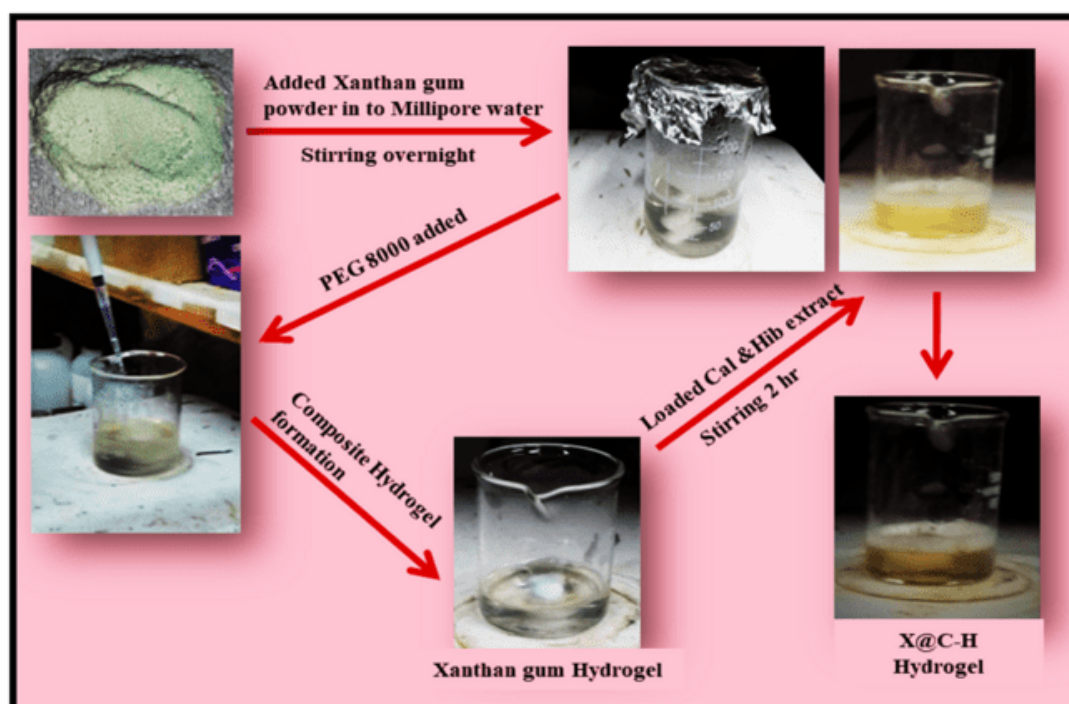
Figure 3.1. *Xanthan gum hydrogel and polyherbal extract loaded hydrogel making process are shown in a schematic.*

3.3. Results and Discussion

Phytochemical compounds screening test

The phytochemical screening was utilized to examine the chemical elements of the combined flower excipient. These chemical elements play a vital function in wound healing. Table 3.1 represents the results of the phytochemical screening test. The polyherbal extract contains alkaloids, flavonoids, terpenoids, saponins, tannins, amino acids, anthraquinones, as well as glycosides. The polyherbal extract created a yellowish-red color in the reducing sugar experimental test, while the Benedict reagent test revealed that the brick-red color formed during the presence of reducing sugar. The dextrose sugar was used as a positive control for reducing sugar test that it produced a brick-red color thus polyherbal extract contained low amount of reducing sugar. It was previously reported that Calendula and Hibiscus flower extracts contain major flavonoids like rutin, quercetin, and gallic acid respectively (Dinda *et al*. 2016; Purushothaman *et al*. 2016) which are responsible for the excessive growth of fibroblast. Therefore, this polyherbal extract may be suitable for wound therapy.

Table3. 1. Phytochemical screening of polyherbal ethanolic extract

PHYTOCHEMICALS	RESULT
Flavonoids	+
Alkaloids	+
Reducing sugars	+ (few %)
Terpenoids	+
Tannins	+
Saponins	+
Anthraquinones	+
Amino acids	+
Glycosides	+

Physical properties of the hydrogel matrix

The XRD (X-Ray Diffractometer) structure of pure xanthan gum powder (XG) revealed no diffraction maxima, so it was amorphous nature (Mohsin et al. 2018) (Figure 3.2b), while the cross-linking agent PEG 8000 revealed diffraction maxima of 19.1 and 23.2 degrees so, it was semi-crystalline nature (Figure 3.2b) (Özdemir Dinç and Güner 2017). The samples X (bare hydrogel), X@C (Calendula loaded hydrogel), and X@H (Hibiscus loaded hydrogel) had diffraction peaks at 19.1 and 23.2 degrees, respectively, while the polyherbal doped hydrogel sample the diffraction peaks at 19.1, 23.2, and 31 degrees (Figure3.2. a). As a result, our synthesized X contains two diffraction lines at 19 and 23.33 degrees, which was identical to PEG 8000, forming a hydrogel matrix. The 19.1 and 23.2 degrees diffraction lines mentioned that the X@H, X@C, and X@C-H are semi-crystalline structures. (Sung et al 2010)

Figures 3.2c and d show the FTIR structure of our synthesized materials. When Xanthan gum was mixed with the PEG8000 solution, it was created X hydrogel. The hydrogel's FTIR spectrum exhibits unique properties, confirming the interaction between the two polymers and the formation of the hydrogel. The first highlighted area is the 3600-3000 cm^{-1} range of the -OH group stretching vibration. The -OH group signal emerges at 3478 cm^{-1} in PEG, 3256 cm^{-1} in Xanthan gum (XG), and 3312 cm^{-1} in X hydrogel. The 3256-3478 cm^{-1} ranges of peak detecting the -OH group of stretching vibration, showing the interaction between XG and PEG molecular chains, and increased gelling properties. The second is the C-H group stretching vibration, which was found in the 2500-3000 cm^{-1} range. The C-H group signal emerges at 2885 cm^{-1} in PEG, 2913 cm^{-1} in XG, and 2893 cm^{-1} in X. The hydrogel indications suggest that the XG concentration was greater. A distinctive absorption

signal occurs for pure PEG at 537cm^{-1}, 862cm^{-1}, 1116cm^{-1}, and 1476 cm^{-1} for C-O-C, CH$_2$, C-O, and CH$_2$ stretching, respectively (Ofokansi *et al*. 2016), and for pure XG at 1017cm^{-1}, 1394cm^{-1}, and 1644 cm^{-1} for COO-, COO-, and C$_2$H$_3$O stretching, respectively (Zhang et al. 2011; Faria et al. 2019). Other absorbance peaks at 1110 cm^{-1} (C-O stretching), 1070 cm^{-1} (C-O stretching), and 1608 cm^{-1} (C=C stretching) were found in the case of the naked hydrogel, showing its purity (Figure 3.2c). In Figure 3.2.c 1043cm^{-1}, 1533cm^{-1}, and 3010 cm-1 bands of X@C-H hydrogel, was indicated appropriate poly-herbal excipient incorporation. Furthermore, the 1043 cm^{-1} FTIR peak corresponds to the polysaccharide C-O valence vibration (Mak et al 2013), whereas the 1533 cm^{-1}and 3010 cm^{-1} FTIR peaks were due to the C-OH and -OH vibrations, respectively (Al-MussawiandAl-Hussani, 2019). This -OH vibration might be caused by the absorbed water in the hydrogel sample. In poly-herbal excipient doped hydrogel, C-OH and C-H bonds were formed at 1643 and 2130 cm^{-1} (Mak *et al* 2013, Azizi et al 2018).

The UV-Vis spectrophotometer was used to record the absorption spectra. Figure 3.2e shows that the undoped hydrogel sample had no clear absorption maximum. However, the poly-herbal extract doped hydrogel had a broad absorption maximum at around 352 nm. This corresponds to the n- π* transition of the herbal excipients, which shows that the doping was successful. The XRD & FTIR results also suggested the successful encapsulation of the dopants in the hydrogel.

Figures 3.2f and 3.2 g show that the plant excipient-doped hydrogel sample had a more porous structure than the bare vehicle sample. The doped hydrogel is also porous and less agglomerate in nature. It is quite interesting our synthesized doped sample has an exfoliated microstructure, which suggests that the sample is more porous and has less

clumping, giving it a better attachment probability to the substrate like in contact with wound. DLS found that the hydrodynamic diameter of X (undoped) hydrogel was 20.144 d.nm, while the corresponding value for X@C-H was 1596 d.nm with a Poly-Dispersity Index (P.D.I) of 0.64 (Figure3.2h). Also, the pure xanthan gum hydrogel had a surface charge of 0.136 mv, which was positive and pretty low to be stable enough. However, polyherbal excipient-loaded hydrogel becomes negative (-27.7 mV) and very stable. It was interesting that the architecture of the hydrogel matrix was changed after poly-herbal excipients were added to a hydrogel patch. The doped sample have a stronger negative surface charge and a lower poly-dispersity index (0.64), which shows that the extract-encapsulated hydrogel makes a homogeneous solution that could be useful for any biological application.

The swelling properties of hydrogel were used to evaluate its drug-release capability. In this experiment, we used two pH, pH 7.5 and pH 5.4. After 24 hours, the weight of bare hydrogel was increased (Figure 3.2i), and the swelled hydrogel matrix structure was better at pH 7.5 than pH 5.4. The huge surface area of the hydrogel patch accounts for the great drug loading capacity. At the same time, high water absorption capacity is another important part of wound healing materials.
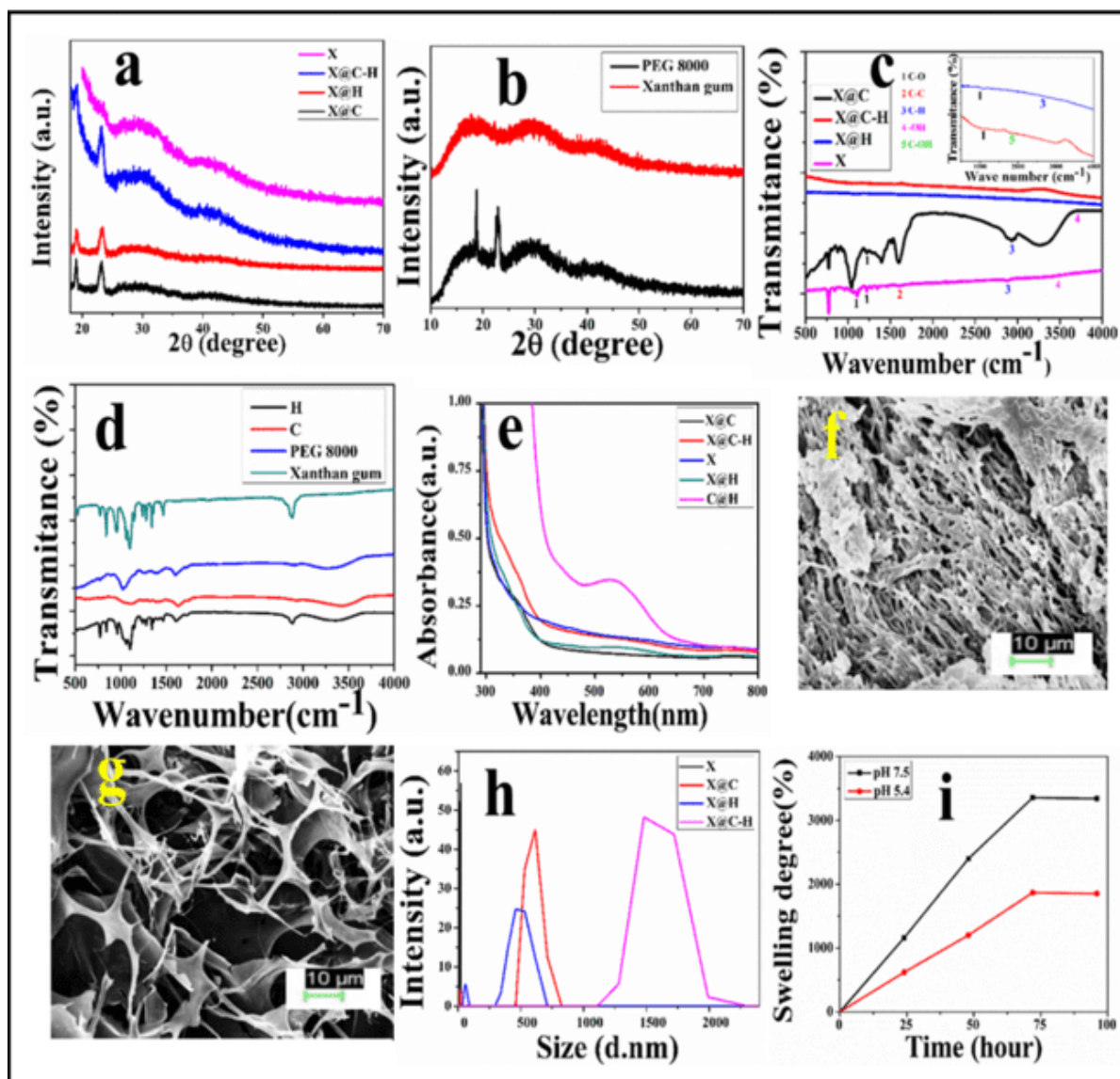
Figure 3.2. *Biophysical properties of synthesized hydrogel (a) XRD of doped and undoped samples; (b) XRD of Xanthan gum and PEG 8000; (c) FTIR spectroscopy of doped and undoped samples; (d) FTIR spectroscopy of Hibiscus extract, Calendula extract, Xanthan gum, and PEG 8000; (e) UV-VIS spectroscopy; (f-g) FESEM images of X and X@C-H respectively; (h) DLS; (i) swelling ratio.*

Evaluation of the stability of hydrogel patches:

The thermal stability of the hydrogel patch was also tested using the DTA-TGA method, demonstrating its stability up to 200°C. The DTA-TGA instrument was used to assess the temperature-dependent mass loss and differential thermograms while maintaining a heating

rate of 10^oC/min in the nitrogen atmosphere (flow rate 50 cc/min). It was noticed that the hydrogel dehydrates around 60-70 ^{o}C, however, no mass loss was detected in this area. Aside from that, another significant thermal transition occurs around 190 ^{o}C, showing the excellent stability of the hydrogel sample, and the highly fragile structure which must be maintained under correct ambient conditions (Figures 3.3a and 3.2. b). TGA measurements allow us to determine the softening and phase formation temperatures, which not only indicate the stability of the material but also assist in the design of its storage conditions.

The synthesized sample was tested for structural and chemical stability at three different pH levels (5.3, 7.5, and 9.6). There was no change in their absorbance spectra at varied pH (Figure 3.3. d), and no change in their absorbance spectra with time (Figure 3.3. c). The stability of synthesized samples was unaffected by dissolving them in various buffer solutions (H_2O, PBS, and TBS) at the same time (Figure 3.3. e). Furthermore, pH and time-dependent stabilities study mentioned that the hydrogel is suitable for biological applications.

Drug release property of X@C-H hydrogel

Figure 2.3. f shows the release percentage of polyherbal extract from the hydrogel matrix was measured at different pH (pH 7, 7.5, 8, and 8.5) for a period of 10 h. The amount of released excipient in the hydrogel patch was measured at 540 nm with the help of a spectrophotometer (epoch microplate spectrophotometer, USA). The percentages of DLC and DEE or DLE in the xanthan gum hydrogel patch were determined to be 71% and 85%, respectively. As demonstrated in Figure 3.3. f was approximately 55%, 58%, 70%, and 80% of the polyherbal extract was released from xanthan gum hydrogel at pH 7, 7.5, pH 8, and 8.5, respectively. However, the present results confirmed that the pH-dependent release is significantly more sensitive to alkaline pH (pH 8 or 8.5) than to the normal pH range of 7 or 7.5.
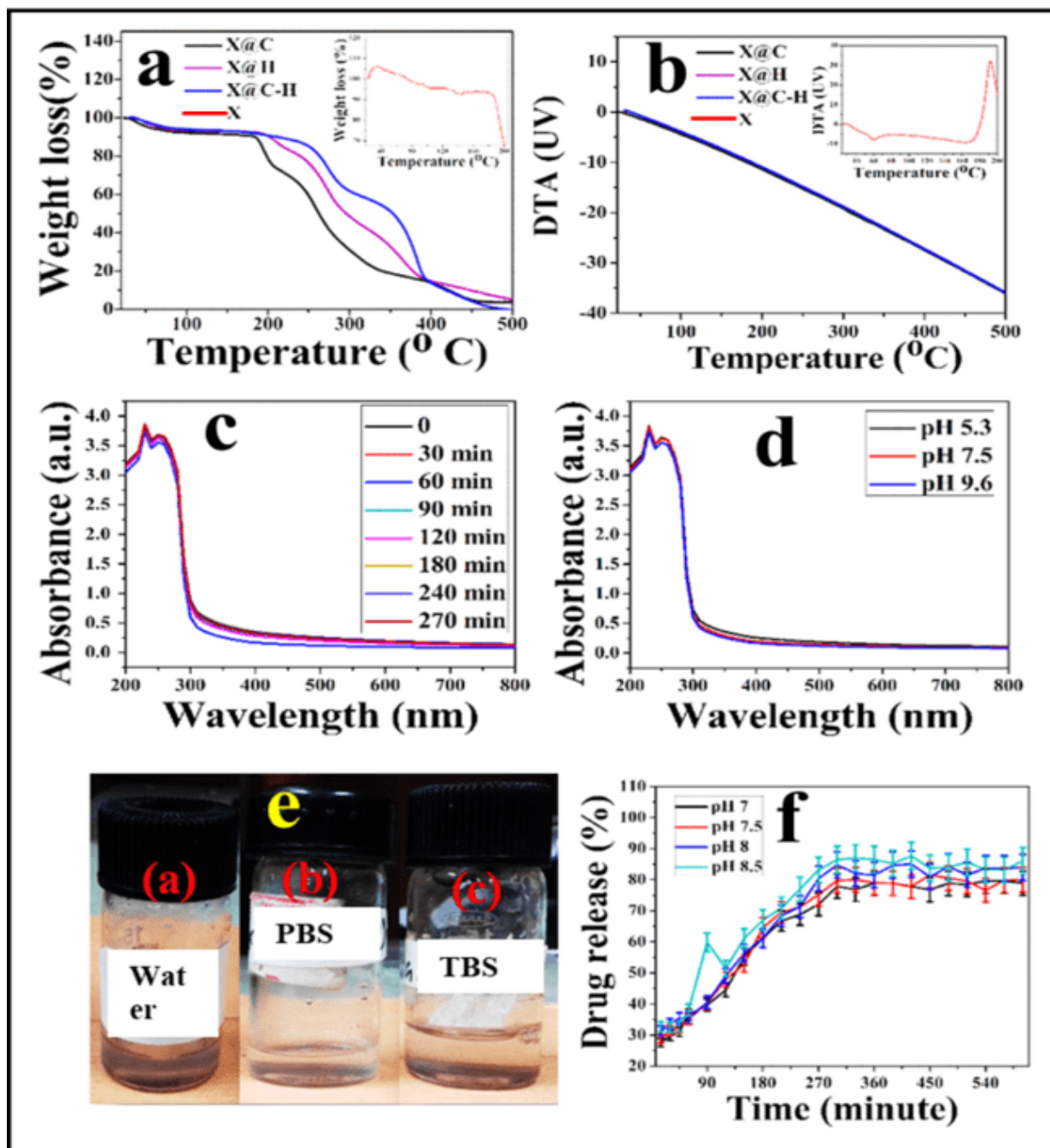
Figure 3. 3. *(a) TGA, and (b) DTA of doped and undoped samples; (c-e) stability study of xanthan gum hydrogel at various conditions (c) on the basis of various time, (d) on the basis of different pH, and (e) images of hydrogel polymer was taken at different buffer solution at 270 mins later; (f) drug release property of polyherbal extract encapsulated hydrogel polymer was measured at different pH.*

Cell viability and cell proliferation studies of hydrogel matrix:

MTT assay was used to measure the proliferation effect of synthesized components on human lung fibroblast cell line WI-38 as well as keratinocyte cell line HaCaT. The cells were seeded in 24 well plates and treated with synthesized materials at different concentrations (0-400µg/mL) for 24hr. In figures3.4a and 3.4b show that X@C-H treated WI-38 and HaCaT cells were multiplied at 200 µg/mL and 400 µg/mL, respectively. We had also found that the bare hydrogel (X) did not kill cells and the X@C-H significantly increased cell growth at dose dependent manner. The result suggested that the polyherbal extract loaded xanthan gum hydrogel are more effective for cell proliferation than the polyherbal extract and single extract loaded hydrogel or free combination of C-H.
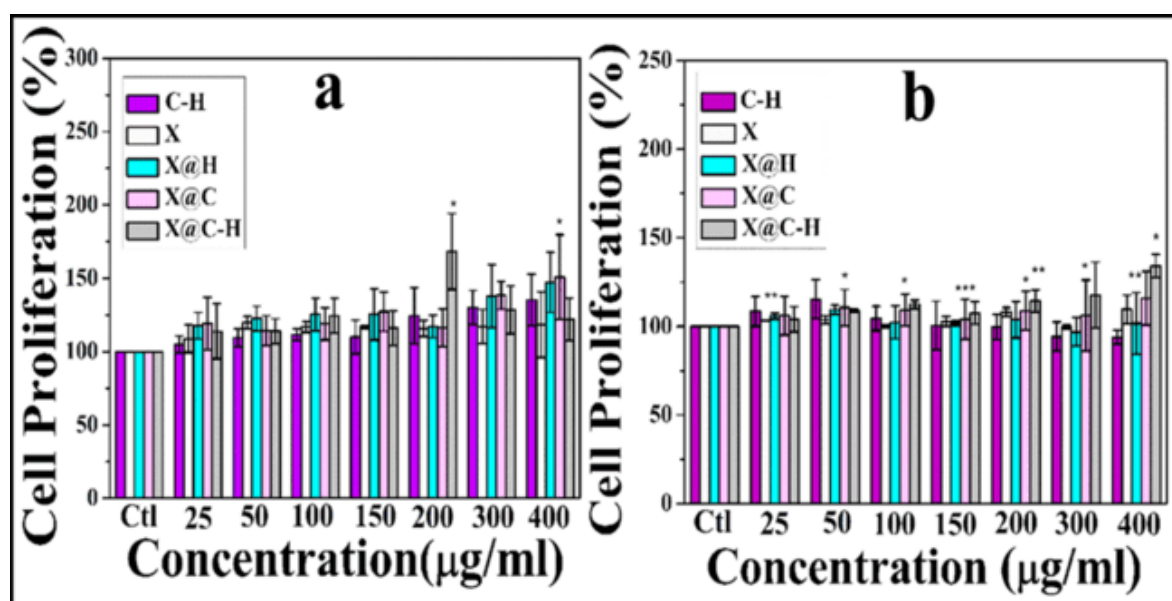
Figure 3.4. *(a-b) Evaluation of C@H (combined extract), X (bare hydrogel), X@C (Calendula loaded hydrogel), and X@H (Hibiscus encapsulated xanthan gum hydrogel) cell cytotoxicity and cell proliferation on human lung fibroblast and keratinocyte cells, respectively. The MTT assays also demonstrate a dose-dependent rise in cell number. All data were shown as the mean ±SD of three different tests, with the statistical significance of the results denoted by the * (P<0.05), ** (P<0.01), and *** (P<0.001).*

Proliferation effect of excipient encapsulated hydrogel was performed by BrdU assay

The proliferation efficacy of the polyherbal extract-loaded hydrogel matrix was measured by BrdU-positive cells. The WI-38 & HaCaT cells were treated with 200μg/mL and 400 μg/mL drug and incubated for 24h. The BrdU-stained cells were looked at under a fluorescence microscope and counted the number of BrdU-positive cells (Figure 3.5. c-d). Figures3.5e and3.5f show that polyherbal loaded hydrogel matrix (X@C-H)treated BrdU-positive cells number is higher (for both the cell lines, 150% of the cells were BrdU-positive) than Calendula loaded hydrogel matrix (X@C), and Hibiscus loaded hydrogel matrix (X@H) treated cells. After the X@C-H hydrogel treatment, we also observed that BrdU-positive fibroblast cell numbers were higher than BrdU-positive keratinocyte cells.

Figure 3.5. *The impact of xanthan gum hydrogel (X), Calendula-loaded hydrogel matrix (X@C), Hibiscus-loaded hydrogel matrix (X@H),and polyherbal loaded*

hydrogel matrix (X@C-H) on cell proliferation was determined by BrdU staining. Figures a and b represent the BrdU staining images. Figures c and d displayed the number of BrdU-positive human lung fibroblast and keratinocyte, respectively. All data were shown as the mean ±SD of three different tests, with the statistical significance of the results denoted by the * (P<0.05), ** (P<0.01), and *** (P<0.001).

Cell migration study of synthesized materials

The cell migration pattern and in-vitro wound recovery efficacy of xanthan gum hydrogel (X), Calendula loaded hydrogel matrix (X@C), Hibiscus loaded hydrogel matrix (X@H), and polyherbal loaded hydrogel matrix (X@C-H)were measured by Scratch assay. In this experiment, we used human lung fibroblast cells (WI-38). The xanthan gum hydrogel (X), Calendula loaded hydrogel matrix (X@C), Hibiscus loaded hydrogel matrix (X@H), and polyherbal loaded hydrogel matrix (X@C-H) (200 μg/mL) were added into the cells and incubated for 24 hours. The scratch area images were captured at 0 h and 24h and the initial (0h) and final (24h) gap width was mentioned in Figures3.6a and3.6b. This result indicated that the X@C-H (polyherbal extract-encapsulated hydrogel) patch enhanced the cell migration process compared to other treated cells.
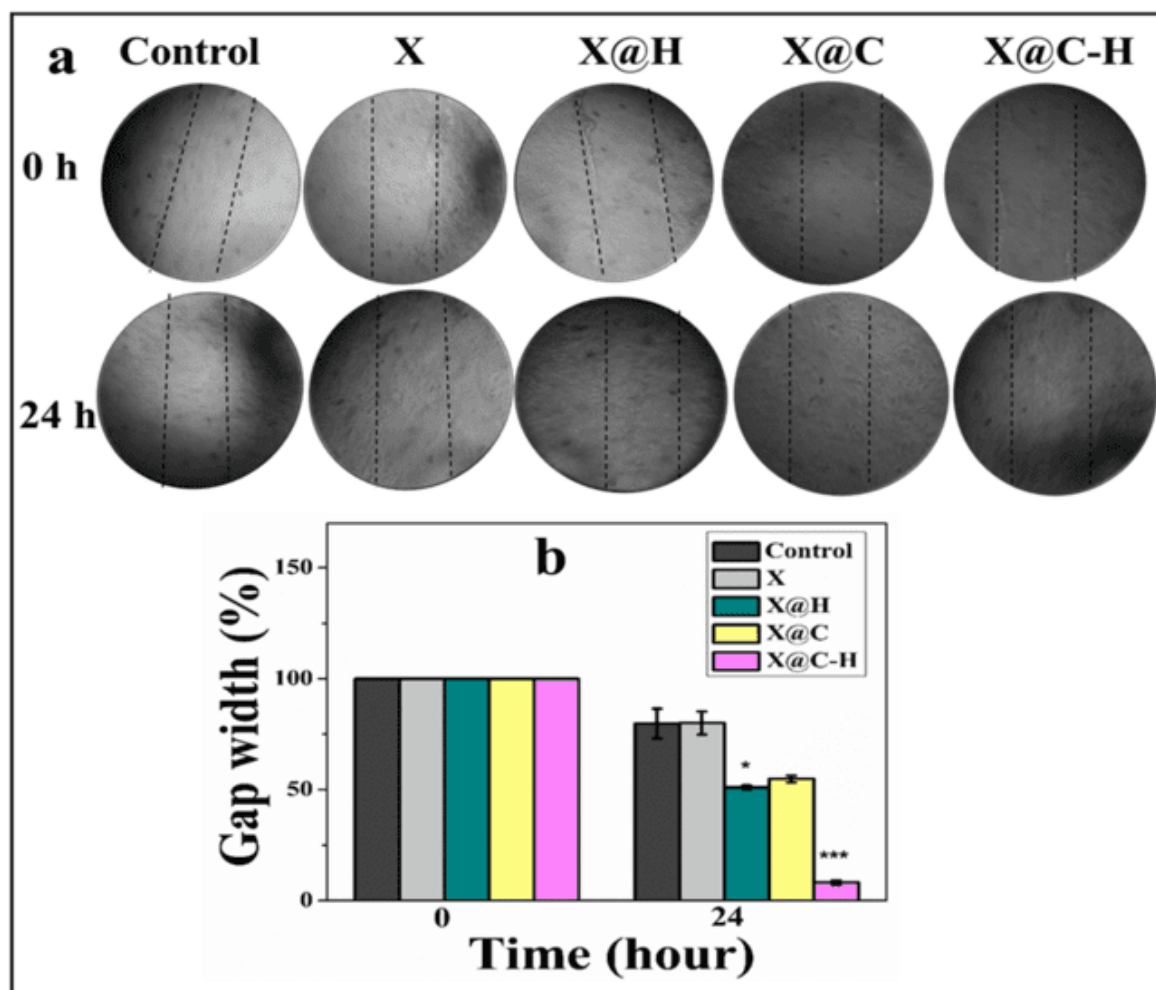
Figure 3.6. *(a) Scratch area was taken with a phase-contrast microscope (10X) at 0hr and 24hr. (b) The migration of treated and untreated cells was measured with ImageJ software, and the percentage of gap width was calculated at different time points, where * (P<0.05) and *** (P<0.001) are statistically significant.*

Immunoblot assay

The intensity of Akt and pAkt protein was then examined on human lung fibroblast cell line (WI-38) as well as keratinocyte cell line (HaCaT) after treatment with xanthan gum hydrogel (X), Calendula loaded hydrogel matrix (X@C), Hibiscus loaded hydrogel matrix (X@H) and polyherbal loaded hydrogel matrix (X@C-H). Here we have applied primary antibody pAkt (Ser 473), total Akt, and GAPDH as a loading control. The pAkt protein intensity is shown in Figure 3.7 a, c and the quantification values are demonstrated in Figure 3.7 b, d. The

expression of pAkt protein for both the cell lines increased in the presence of polyherbal loaded hydrogel matrix (X@C-H) compared to xanthan gum hydrogel (X), Calendula loaded hydrogel matrix (X@C), and Hibiscus loaded hydrogel matrix(X@H) treated cells. Thus X@C-H treatment activates the PI3K pathway and thus promotes the wound healing process by stimulating cell growth. (Dinda *et al* 2015)
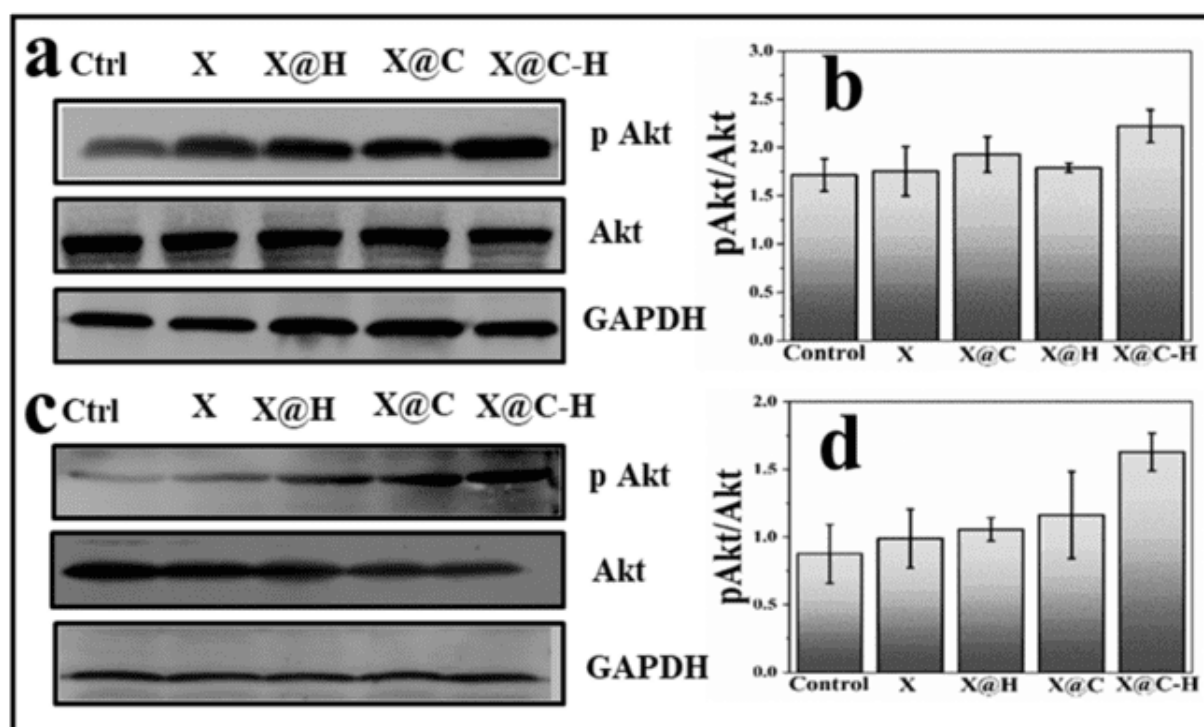
Figure 3.7: *Investigation of Akt (MW 60 kDa) and pAkt protein (MW 60 kDa) in the interaction to xanthan gum hydrogel (X), Calendula loaded hydrogel matrix (X@C), Hibiscus loaded hydrogel matrix (X@H) and polyherbal loaded hydrogel matrix (X@C-H)by Western blot. This suggests that pAkt protein expression goes up when the X@C-H hydrogel patch is applied to human lung fibroblast as well as human keratinocyte cell lines, as shown in (a-b) for human lung fibroblast and (c-d) for keratinocyte cell. The protein intensity was measured using ImageJ software for (b) WI-38 and (d) HaCaT. All results were given as the mean ±SD of three separate tests.*

In vivo experiment

Estimation of excision wound area on the male BALB/c mouse model.

In this experiment, we used male BALB/c mice, and the mice were split into five groups, and every group comprised five mice. Group 1: untreated. Group 2: treated with X hydrogel patches. Group 3: treated with X@C hydrogel patches. Group 4: treated with X@H patches. Group 5: treated with X@C-H patches. The excision wound-created mice (groups 2, 3, 4, and 5) were treated with the same amount of drug (20 mg/kg b.w) for 12 days, every three days intervals we also took images. The mice were sacrificed on the 6th, $9^{th,}$ and 12th days and tissue was used for histological analysis. In Figure 3.8a we observed that the polyherbal extract encapsulated hydrogel treated group showed a better effect on 9 days, compared to xanthan gum hydrogel (X), Calendula loaded hydrogel matrix (X@C), and Hibiscus loaded hydrogel matrix (X@H) -treated group. The size of the wound area was estimated using ImageJ software. The polyherbal loaded hydrogel matrix (X@C-H) treated groups of mice completed the wound repair process on 12th day (Figure 3.8b). The outcomes showed that applying undoped hydrogel did not have any harmful effects on the mice, and neither it encourage the re-epithelialization process of the epidermis. However after 9 days of treatment with X@C-H hydrogel, there was a lot of re-epithelialization, and hair follicle formation which could be seen on the tissue of the dermal sheath. Also, unlike the other groups, they didn't have any scars or hair loss. Thus, our synthesized polyherbal loaded hydrogel matrix successfully delivered the loaded drug to wounds for promoting healing.

Histological analysis of wounded tissue

In histological analysis, eosin and hematoxylin were used to visualize the changes in tissue morphology with the progression of wound healing in response to the application of various hydrogel forms, s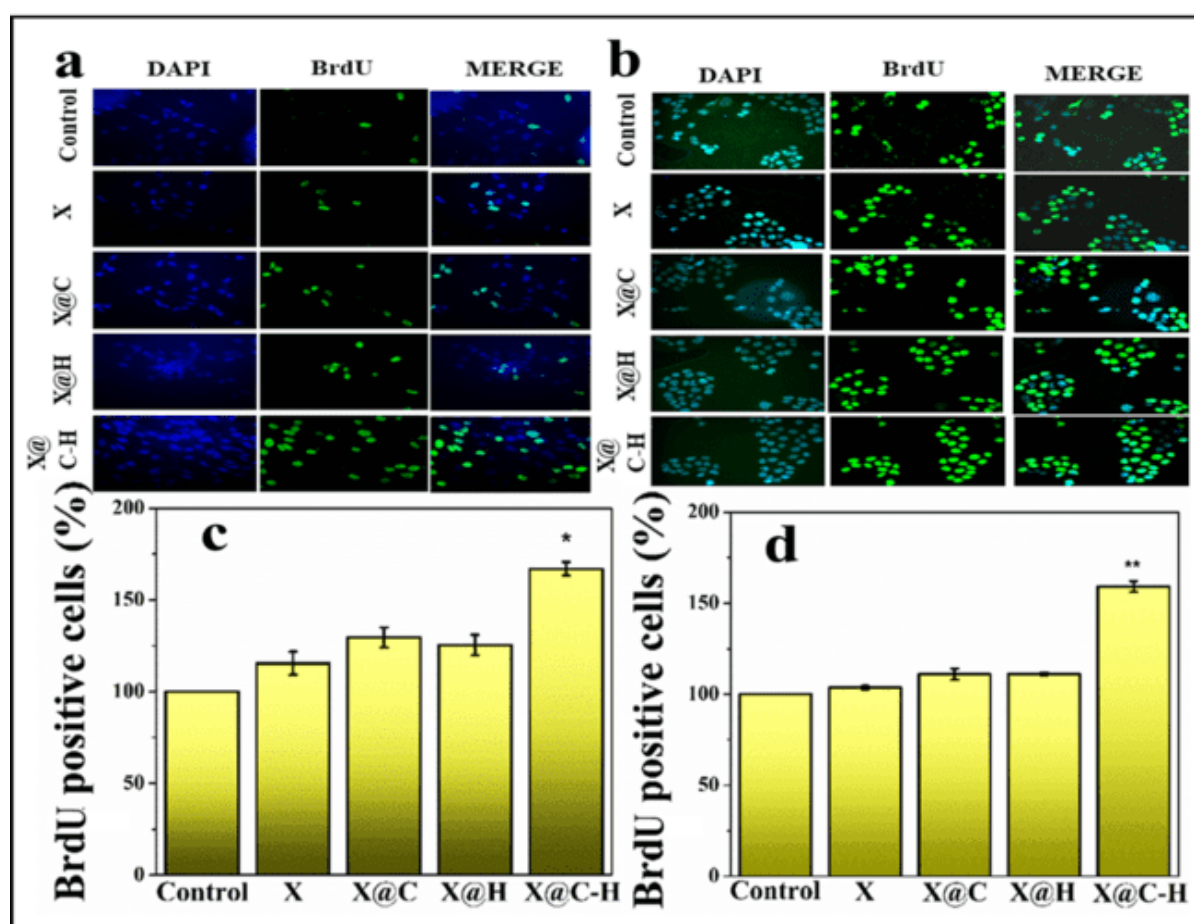uch as xanthan gum hydrogel (X), Calendula loaded hydrogel matrix (X@C), Hibiscus loaded hydrogel matrix (X@H) and polyherbal loaded hydrogel matrix (X@C-H) for different time intervals. The X@C-H treated mice developed complete granulation tissue and underwent regeneration of the epidermis within six days, while Calendula-loaded hydrogel matrix (X@C), and Hibiscus-loaded hydrogel matrix (X@H) treated mice developed granulation tissue on 12thday. However, in the untreated and bare hydrogel application groups were slowly developed the granulation tissue layers. On day 12, the wound re-epithelialization process was completed in animals treated with X@C-H compared to animals treated with xanthan gum hydrogel (X), Calendula loaded hydrogel matrix (X@C), Hibiscus loaded hydrogel matrix (X@H), in which wound re-epithelialization was incomplete (Figure 3.8. c). Therefore, the polyherbal extract encapsulated hydrogel demonstrated stronger wound healing abilities compared to other groups.
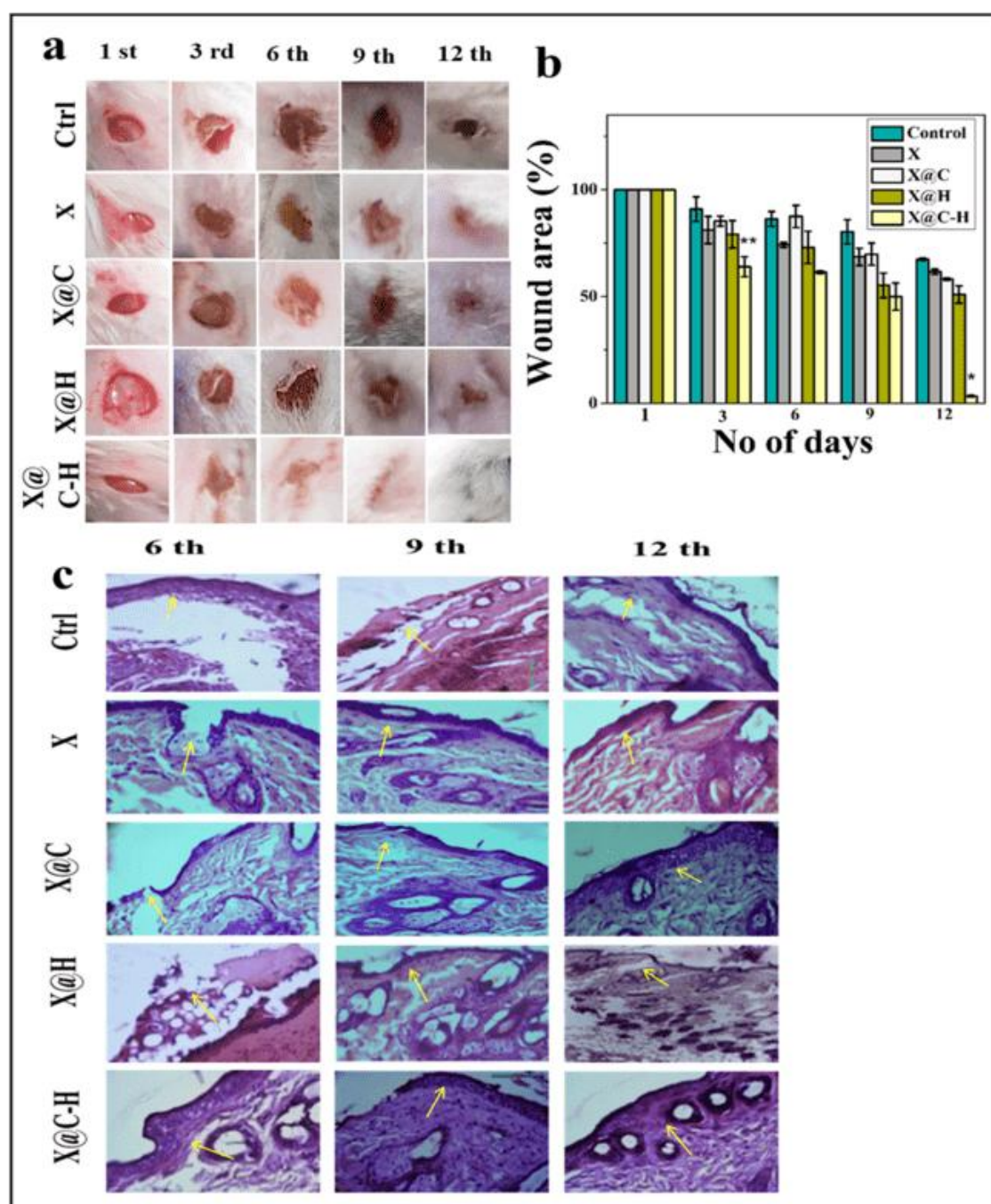
Figure 3.8. *Diagrammatic depiction of in vivo experiments (a) Excisional wounds of untreated and treated mice were monitored on 1, 3, 6, 9, and 12 days using a digital camera (Sony Cyber-shot DSC-WX80); (b) The wound areas were calculated using ImageJ software and expressed as a percentage of the initial wound area versus the number of days post-wounding. Results were presented as mean ±SD, with * (P<0.05) and ** (P<0.01) indicating statistical significance in comparison to the control group, (c) Histological study of tissue from the wounds of treated and untreated mice on days 6, 9, and 12 after the wounds were made. Original magnification 40X, scale bar-100μm.*

3.4. Conclusion

Taking into consideration of above mention experiments we can conclude that our synthesized hydrogel matrix is biocompatible, biodegradable, and a promising biomaterial for drug-delivering agents. This hydrogel stimulated the water absorption, drug loading as well as sustained drug release ability due to the presence of a large number of carboxyl groups. *Calendula* flower is used for burn and ulcer wound treatment as well as *Hibiscus* flower is used for incision, excision, dead space wound model, and antibacterial purposes. So, we have used polyherbal extract because they act at different stages of wound healing.. According to the findings of our in vitro investigation, X@C-H has more potential for wound healing than the bare herbal excipients Calendula and Hibiscus. The undoped hydrogel demonstrates high biocompatibility as we demonstrated in vivo and in vitro experiments. Further, we noticed that the drug release ability of xanthan gum hydrogel is moderately high at pH 8.5 (pH of the wounded area varies from 8-8.5) than at lower pH of 7, 7.5, and 8**.** Additionally, many more herbal excipients with defined activities on wounds can be loaded with this cheap, biocompatible matrix to address complicated wounds like diabetic or burn wounds. In light of these, this biocompatible, cheap xanthan gum hydrogel can become a very successful delivery system for a variety of herbal excipients or drugs in the near future.

Chapter 4

Hibiscus Mucilage Polymer: Natural Fabrication & Innovative Approaches in the Treatment of Second-Degree Burns, and Excision Wounds

Hibiscus Mucilage Polymer: Fabrication, Characterization & Innovative Approaches in the Treatment of Second-Degree Burns, and Excision Wounds

4.1. Introduction

According to WHO reports, around 11 million individuals have suffered burns, and out of those 1,80,000 deaths occurred from sepsis. (Eming *et al* 2014)The normal process of wound healing is delayed due to deep cutting (generally reported by burn wounds) and microbial infections. The delayed healing results in post-surgical problems, persistent ulcers, tissue malfunction, neurodegeneration, and precancerous lesions. (Bombin *et al* 2020) Burn wound is a type of painful injury that may happen in different ways (thermally, chemically, electrically, or by stitches) and such incidences play an impact on wound-mediated global mortality because of their diversity, severity, and fatalities.(Kalantari *et al* 2020) Therefore, the proper wound healing material is urgently needed to reduce the mortality rate and materials should have maintained the following characteristics: 1) could improve the healing process (Singh *et al* 2022), 2) deliver a moist environment to the wound site, 3) provide sufficient gas exchange permeability, 4) increase absorption capacity to absorb wound exudate, 5) reduce pain and healing time, 6) promote antibacterial activity, 7) decrease toxic effects, and 8) stimulate re-epithelialization process. (Moholkar *et al* 2021)

Wound dressing or healing materials are available in both synthetic and natural forms. Synthetic wound dressing materials are usually made of PEG, PVA, PLGA, and hydrocolloids and natural dressing materials are made up of honey, aloe vera, alginate, plantains etc.(Li *et al* 2021)In recent years, some scientists have used plant-derived polymers

for diverse pharmaceutical applications, such as diluents, binders, disintegrant in tablets etc. (Kaleemullah *et al* 2017) (Tyagi *et al* 2015; Bahadur *et al* 2018)

In various research studies, the *Hibiscus rosa sinensis* plant-derived mucilage has been demonstrated as a delivery vehicle or as the main therapeutic to treat a wide range of ailments including sore throats, stomach problems, and skin infections. (Vignesh *et al* 2018) Additionally, it is also used as a natural remedy for reducing fever and inflammation. As reported previously hibiscus mucilage contains various types of phytochemicals that promote wound healing, including reducing sugar, flavonoids, and acidic polysaccharides (27% Galactosides, 24% L Rhamnose, 19% D-galacturonic acid, D-galactose, Glucuronic acids, etc.).(Kassakul *et al* 2014; Vignesh *et al* 2018; Jani *et al* 2008; Bakr *et al* 2021; Vignesh *et al* 2018). But therapeutic potential and wound healing activity of pure hibiscus mucilage polymer has not been reported earlier. Here we isolated the pure hibiscus mucilage polymer and tested in murine model. The result demonstrated a significant improvement in wound healing for both burn and excision wound. Thus mucilage polymer may be a promising alternative for the treatment of excision and second-degree burn wounds. The study also assessed the efficacy of the hibiscus mucilage polymer for wound healing applications by measuring cell proliferation, cell migration, antioxidant effects, and anti-inflammatory effects (Scheme 4.1). The results of this study also suggested that the HM polymer is a viable option for use in clinical translation.
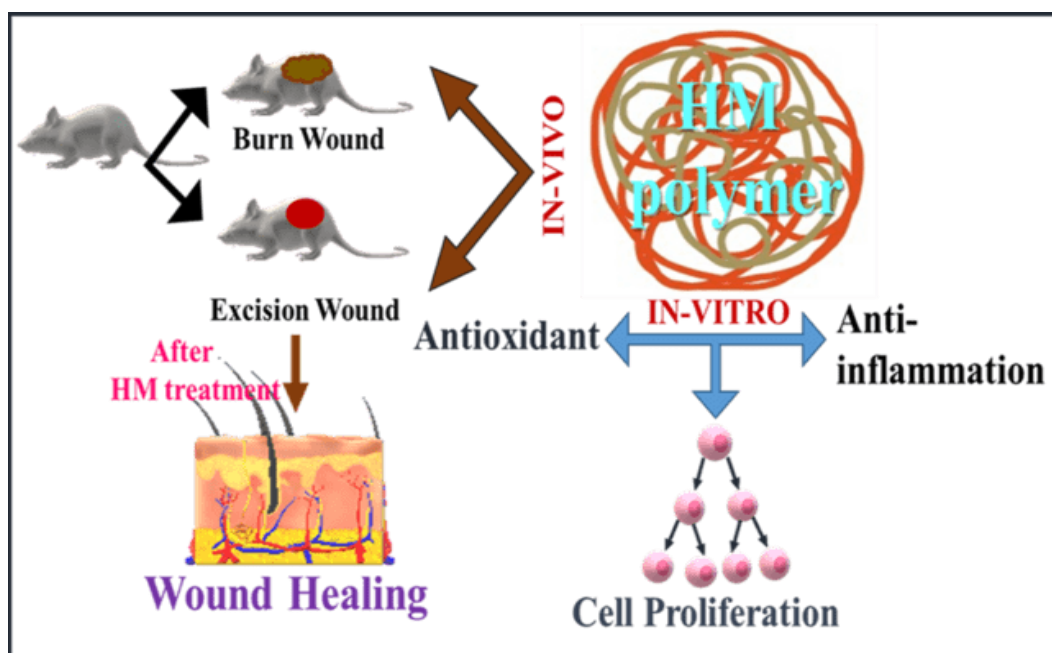
Scheme 4.1. *Schematically represents the objectives of our study*

4.2. Biopolymer fabrication process

Plant material collection

The young and fresh *Hibiscus rosa sinensis* leaves were taken from the Jadavpur University grounds in Kolkata, India. The leaves were verified and authenticated by the Agri-horticultural Society of India.

Synthesis of Hibiscus mucilage polymer

The leaves of *Hibiscus rosa sinensis* were carefully washed with distilled water, and after that the dry leaves powder (40 gm) put in 500 mL of deionized water, and mixed for 4 to 5 hours. The leaves were then mashed and boiled for a few minutes and filtrated with a cotton cloth. Acetone was used for the purification of extracted mucilage and the precipitated portion was dried in a hot air oven at 40 °C. HM is the name for the dried sample and it is stored at 27-30 °C for six months. The process of synthesis is given in Figure 4.1.

Figure4.1. *Diagram represent the fabrication process of Hibiscus mucilage polymer*

4.3. Results and Discussion

Biophysical properties of Hibiscus mucilage polymer

The biophysical properties (XRD, FTIR, UV-Vis, DLS, Zeta potential, SEM, BET and Swelling ratio) of HM polymer is shown in Figure 4.2.

The X-ray diffractometer is used for analysis the nature of polymer. The distinct diffraction maxima of HM polymer indicate that it was amorphous in nature. Figure 4.2. a depicts the XRD pattern of a polymeric mucilage.

The chemical structure and functional groups of mucilage were assessed through the FTIR analysis. The distinct absorption signal of mucilage polymer was found to be present at 1235.56 cm^{-1}, 2160.71 cm^{-1}, and 2934.44 cm^{-1}, corresponding to the C-O bend (aromatic),

C≡C stretch, and C-H stretch respectively (Vignesh *et al* 2018). In addition, mucilage polymer exhibited significant absorption peaks at 770.72 cm^{-1}, 1598.36 cm^{-1}, and 1398.82 cm^{-1} corresponding to the chloride C-Cl, N-H bending, N=O (Nitro R-NO$_2$) respectively. Furthermore, the C-H and C=O (aldehyde) stretching vibration was seen at 2934.44 cm^{-1} and 1737.18 cm^{-1} for the carbohydrate group (Hssaini *et al.*, 2022) and flavonoids group respectively (Oliveira *et al* 2016). On the other hand, C=O (aldehyde) stretching is an indicative band of the amorphous structure of the polymer (Guo *et al.*, 2010). However, for C-O bending, also known as alcohol, ether, ester, anhydride, and carboxylic acid, the strong absorption peaks at 1229.24 cm^{-1} was observed. Strong, pointed peaks at 1036.01 cm^{-1} were most likely attributed to the C-OH group and C-O stretching in the structure of the phenol and carbohydrates. Most likely, the C-H, O-H, and NH$_3$ groups also known as carbohydrates, carboxylic acids, free amino acids, and phenolic compounds were responsible for the absorbance region between 3,000 and 2,800 cm^{-1} (Hssaini *et al* 2022), whereas the polysaccharides were associated with the C-H and O-H stretching between 2900-3380 cm^{-1} absorbance Figure 4.2 b demonstrates this outcome. It was reported that carbohydrates provide support for wound healing phases (Barchitta *et al* 2019) and additionally, the flavonoid and phenolic groups enhance the second-degree burn and excision wound healing process (Ramamoorthy *et al* 2023).

After the complete dissolution of the polymer in water, its absorbance was measured by using UV-Vis spectroscopy. Figure 4.2 c demonstrates that our isolated HM polymer exhibited a broad-spectrum absorbance at 336.14 nm.

DLS estimated the polymer's hydrodynamic size to be 1069 d.nm, and the Poly-Dispersity Index (P.D.I) value was 1 (Figure 4.2. d). Also, the pure polymer had a surface charge of -2.68 mV, which was negative and made it very stable against amalgamation.

The SEM result indicated that our synthesized Hibiscus mucilage exhibits an agglomeration structure. The agglomeration structure was made up of tiny pieces that were closely bound together. The agglomerate structure size and shape varied depending on the sample preparation process. (Figure 4.2. e).According to the examination of the pore size distribution using N_2 sorption data at 77K and non-local density function theory (NL-DFT), it was determined that the BET surface area was 25.447 m²/g and the average pore width of the HM mucilage polymer was 31.69 Å. However, the HM structure formed a mesoporous nature that would be perfect for managing wounds (Figure 4.2. f, & g). The sample's structure suggested that it may have produced a porous polymer, which may be perfect for managing wounds

The absorption characteristic of HM polymer was assessed by swelling ratio. The absorbance percentage of the HM polymer was 90% after 6 hours, and it stayed up to 24 hours (Figure 4.2. h), moreover, it maintained the structure at pH 7.5. Therefore, exudate absorption from the damaged region is the most critical function for initiating the wound healing process and thus the swelling ratio analysis is the most important attribute for wound healing agents.(Ruffo *et al* 2022; Lu *et al* 2023).
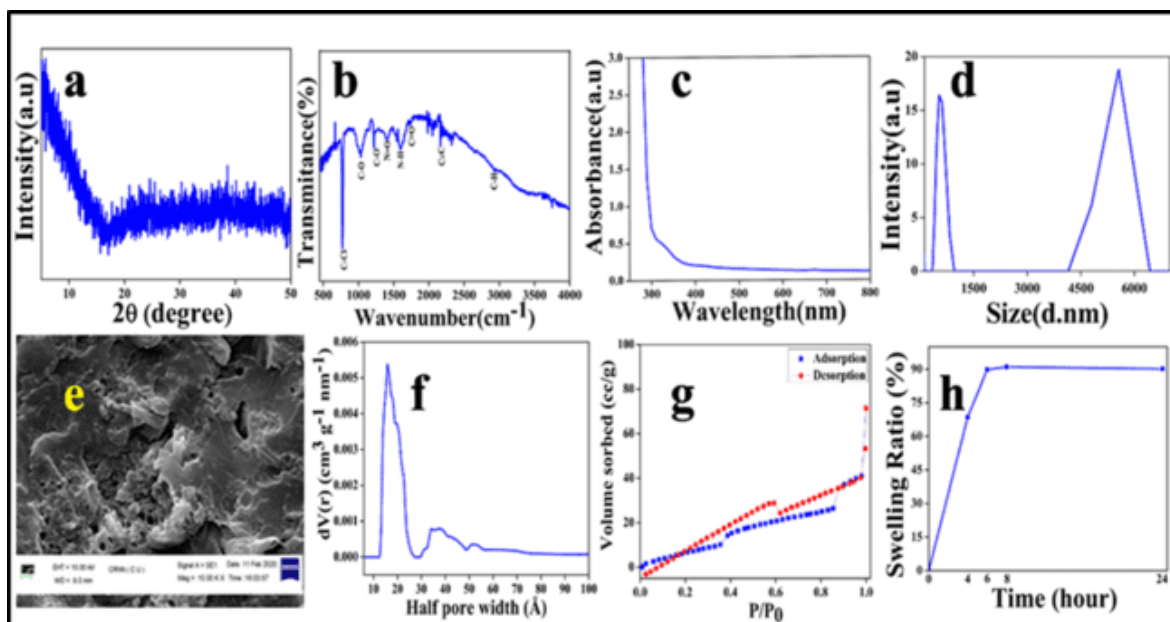
Figure4.2. *Physical characterization of hibiscus mucilage polymer (a) XRD (b) FTIR spectroscopy (c) UV-Vis spectroscopy, (d) DLS, (e) SEM images, (f) NL-DFT pore size distribution curve of HM polymer is obtained from the N_2 isotherm, (g) N_2 adsorption-desorption isotherms and (h) Swelling ratio.*

Cell viability and Cell proliferation efficacy of HM polymer was studied by MTT assay

The cellular metabolic activity was measured by the standard MTT assay in the presence of HM polymer in human lung fibroblast WI-38 and keratinocyte cell lines HaCaT. The cells were treated with various concentrations (0, 40, 60, 80, 100, 120, 140, and 160 µg/mL) of HM polymer and incubated for 24h at 37 ^{O}C, 5% CO_2. The cellular viability rate of HM polymer-treated WI-38 and HaCaT cell lines was 100% and additionally, it also helped for cellular proliferation at about 40% and 50% higher rates at 100 µg/mL and 120 µg/mL respectively, compared to untreated cells under the same conditions (Figure 4.3 a). Therefore, the MTT result suggest that HM is a biocompatible polymer and simultaneously it also helped for further in-vitro and in-vivo assessment.

Cell migration properties of HM polymer were observed by Scratch wound assay

The cellular migratory capability was detected by the scratch-wound assay. The WI-38 cell was treated with HM polymer at a concentration of 100 μg/mL and in the HaCaT cell line the HM polymer was added at 120 μg/mL concentration and the cells were incubated for 24 hours at 37 °C with 5% CO_2. We observed that the WI-38 and HaCaT covered the created scratch wound area by 80% and 90% when treated with HM polymer compared to untreated cells (Figure 4.3 b-e). The result also reported that after the treatment of HM polymer the HaCaT cell line was more effective compared to WI-38. In practical the keratinocyte play an important part in repairing the epidermal fence. (Ter Horst *et al* 2018)

Proliferative effect of HM-treated cells was assessed by BrdU assay:

BrdU is a thymidine analog, it integrated into the DNA of the newly dividing cells and thus BrdU incorporation an indicative of replicative capacity of cells The WI-38 and HaCaT cells were seeded on the coverslips and treated with 100 μg/mL and 120 μg/mL HM polymer respectively. The cell proliferation percentage of the HM-treated WI-38 and HaCaT cell lines was found to be 10% and 5% higher (Figure 4.3. f-h) than that of the untreated cells, respectively. The BrdU-positive cells were followed by fluorescence microscopy.
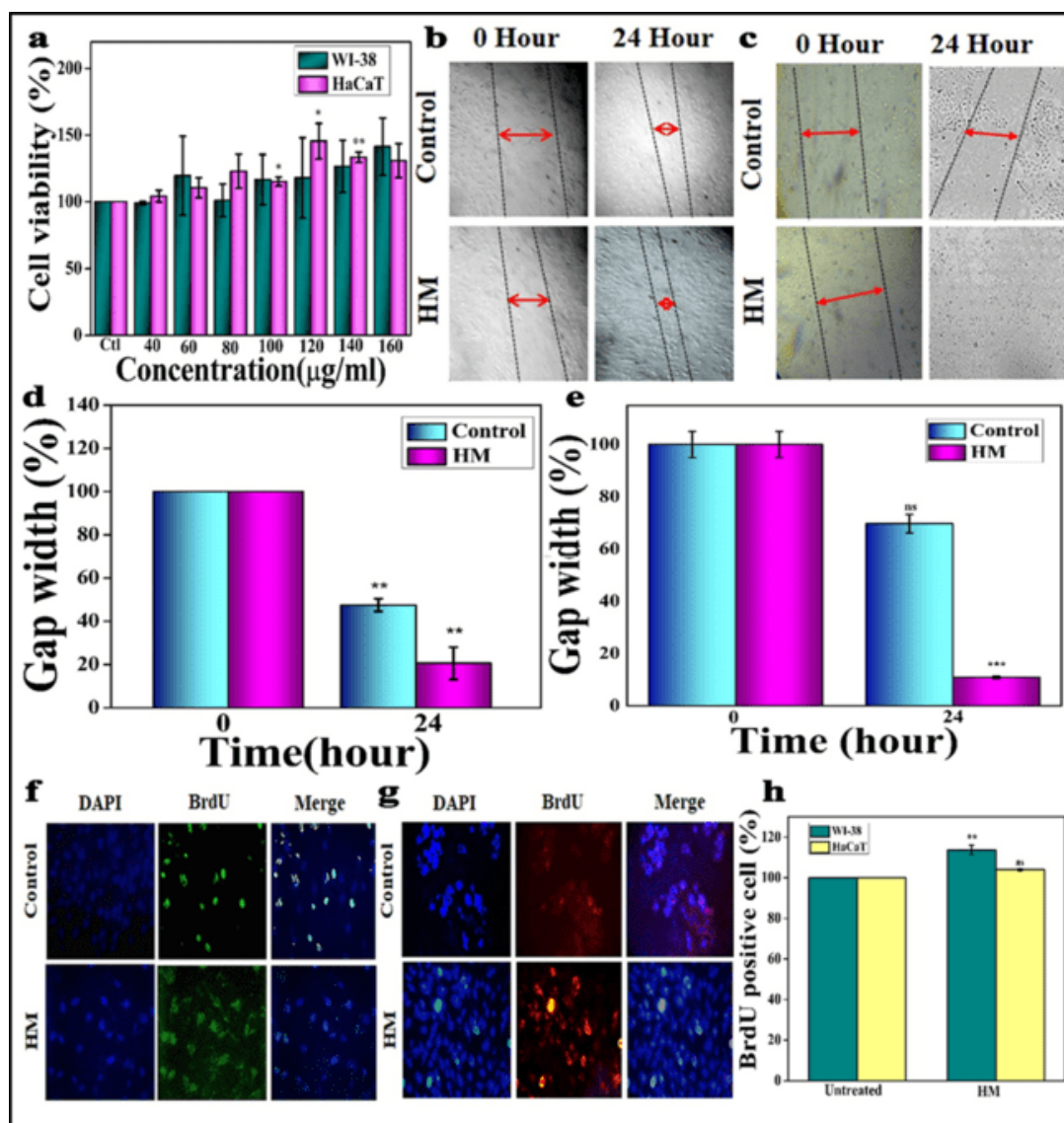
Figure 4.3. *Assessment of cytotoxicity and cell proliferation effect of HM polymer by MTT assay; The MTT assay results were expressed as mean ±SD of three independent experiments, where, * (P<0.05), ** (P<0.01), and *** (P<0.001). (b-c) Determination of cell migratory efficiency by scratch wound assay; (d-e) Quantitative representation of cell migratory efficiency in terms of 'Gap width'; (a & c) for WI-38 cell line and (b & d) for HaCaT cell line. The Scratch wound assay results were expressed as mean ±SD of three independent experiments, where, (* (P<0.05), ** (P<0.01), and *** (P<0.001). The de-novo synthesized DNA was assessed by BrdU staining assay. The WI-38 and HaCaT cell images of BrdU staining were shown in Figures f & g respectively. The quantitative estimation of BrdU positive WI-38 and HaCaT cells was shown in the respective figure h, where BrdU assay results were expressed as mean ±SD of three independent experiments, where, ** (P<0.01).*

Antioxidant activity of HM polymer was assessed by ROS scavenging assay

Wound healing is compromised in oxidative stressed conditions due to the over-expression of reactive oxygen species (ROS). As a result, antioxidants control oxidative stress and hasten the healing of wounds. HM polymer was applied to the WI-38 and HaCaT cell lines, and the ROS reduction rate was determined by the DCF-DA technique. The cells were treated separately with 5 mM of N-acetyl cysteine (NAC) or 100 µg/mL of HM for WI-38 cells, and 120 µg/mL for HaCaT cells, and incubated for 24 h. In this case, NAC acted as a positive control and conventionally it is used at a concentration of 5mM. In the WI-38 and HaCaT cell lines, the ROS intensity in NAC-treated cells was reduced by 0.1 and 0.2 folds, respectively, compared to untreated cells. On the other hand, HM-treated cell lines showed a 0.5 and 0.4 folds reduction in ROS intensity, respectively (Figure 4.4). Therefore, this result suggested that HM polymer shows greater antioxidant capabilities than the well-known antioxidant drug NAC. In the case of wound healing process, the low amounts of ROS production are shown better effect because they protect tissues from infection and cells to stay alive. (Schieber et al 2014)
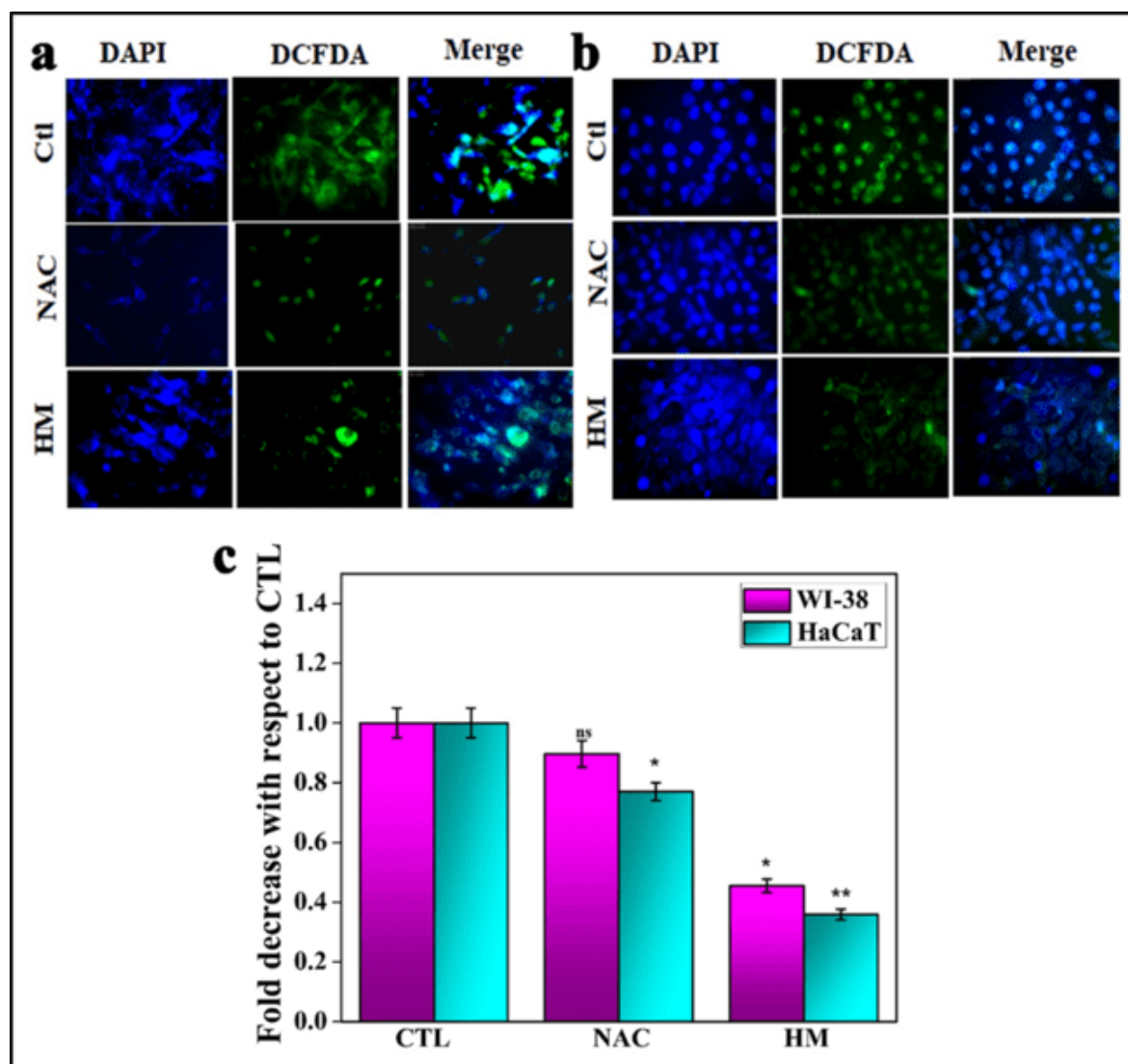
Figure 4.4. *In the antioxidant activity determined by ROS assay in (d) WI-38 and (e) in HaCaT cell line; (f) the quantitative estimation of ROS negative cells, where mean ±SD was calculated by three independent experiments (* (P<0.05), ** (P<0.01)).*

Immunoblot analysis

In this experiment, the various concentrations of cell lysate were selected based on a cell proliferation assay. We have used the primary antibodies Akt (1:1000, rabbit monoclonal, Cell signaling, USA), pAkt (Ser 473) (1:1000, rabbit polyclonal; Cell signalling, USA), TGFβ1 (1:1000, mouse monoclonal, Santacruz biotechnology, USA), IFN-γ (1:1000, mouse

monoclonal; Santacruz biotechnology, USA), and GAPDH as loading control (1:1000, rabbit monoclonal; Biobharati LifeScience, India). In Figures 4.5 a and c, the relative levels of the proteins pAkt (Ser 473), TGF-β1, and IFNγ were 74%, and 114%; 83%, and 106%; 128%, and 95%; respectively, at a concentration of 60 μg/mL, and 100 μg/mL of HM treatment compared to WI-38 cells that had not been treated with HM. Compared to untreated cells, the level of pAkt (Ser 473) was 121% and 137%, TGFβ1 was 101% and 152%, and IFNγ was 114% and 43% in the HaCaT cell line when HM was used at 80 g/mL and 120 g/mL (Figure 3.5. b, 3.5. d).Since the HM polymer has anti-inflammatory properties, it reduced IFN-γ intensity when present in high concentrations. The pAkt (Ser 473) protein is present in the PI3K pathway, and the phosphoinositide 3-kinase (PI3K)/protein kinase B (Akt) signaling pathway regulates angiogenesis, metabolism, cell proliferation, differentiation, and migration in the HaCaT cell line. (Teng *et al* 2021) IFNγ is a pro-inflammatory cytokine that is released during the inflammatory phase; at higher doses, it degrades the microorganisms and promotes cellular proliferation, migration, and invasion (Krzyszczyk *et al* 2018), but its long-term effects can delay wound healing and increase the risk of infection.(Liu *et al* 2020)This result also suggested that the HM polymer upregulates anti-inflammatory activity, pAkt protein expression, and TGFβ1 pathway so, it is suitable for various wound healing applications.
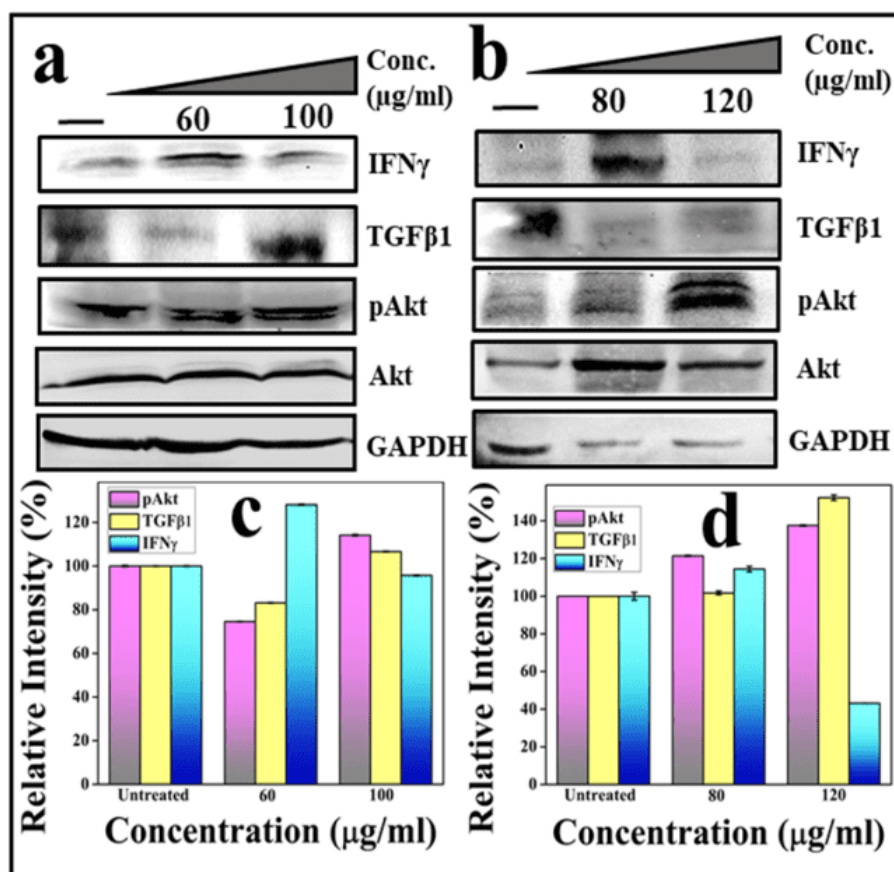
Figure 4.5. *The expression of the proteins including GAPDH (MW 37 KDa), Akt (MW 60 KDa), pAkt (Ser 473) (MW 60 KDa), TGFβ1 (MW 13 KDa), and IFNγ (MW 21KDa) were assessed by western blot analysis (a) WI-38 cell line and (b) HaCaT cell line at various concentrations; (c) and (d) graphically represents the relative intensities of the proteins in WI-38 and HaCaT cell line respectively. The relative intensities of those proteins were measured by ImageJ software.*

In vivo experiment

In this experiment we used male BALB/c mice; the mice were separated into six groups, each with five mice. Excision wounds were divided into three categories, and burn wounds were also divided into three groups. The treatment process is represented in Table 4.1. On days one, three, six, and eleven, the mice with excision wounds were observed, and one, three, and six days mice was treated with silverex and HM polymer. On days one, three, six, and eight the second-degree burn wounds mice were treated, and days one, three, six, eight, and eleven

were used to capture the photographs. All tests were conducted under the supervision of the animals and in accordance with the Institutional Animal Ethics Committee (IAEC) of the University of Kalyani's rules and those of the Committee for the Purpose of Control and Supervision of Experimental Animals (CPCSEA), which is a committee under the Government of India.

Table 4.1. Treatment process of excision and second-degree burn wound

Group No	Treatment process (Excision wound)	Treatment process (Burn wound)
Group 1	excision wound + untreated	burn wound + untreated
Group 2	excision wound + placebo (Silverex Ionic Gel)	burn wound + placebo (Silverex Ionic Gel)
Group 3	excision wound + HM treated	burn wound + HM treated

Measurement of excision and second-degree burn wound area in male BALB/c murine model

In BALB/c male mice, the created excision and second-degree burn wounds were treated with HM polymer at 8 mg/kg body weight in both cases. The wound areas in both cases were substantially reduced with HM treatment (Figures 4.6 a, b) at every treatment time compared to the placebo (silverex ionic gel treatment) or untreated group.. The quantitative analysis of the wound healing capability of HM treated, placebo and untreated control has been demonstrated in Figures 4.6 c and d. Moreover this result suggest that our synthesized HM polymer is a suitable component for excision and second degree burn wound healing compared to the well known wound healing gel-Silverex ionic gel.
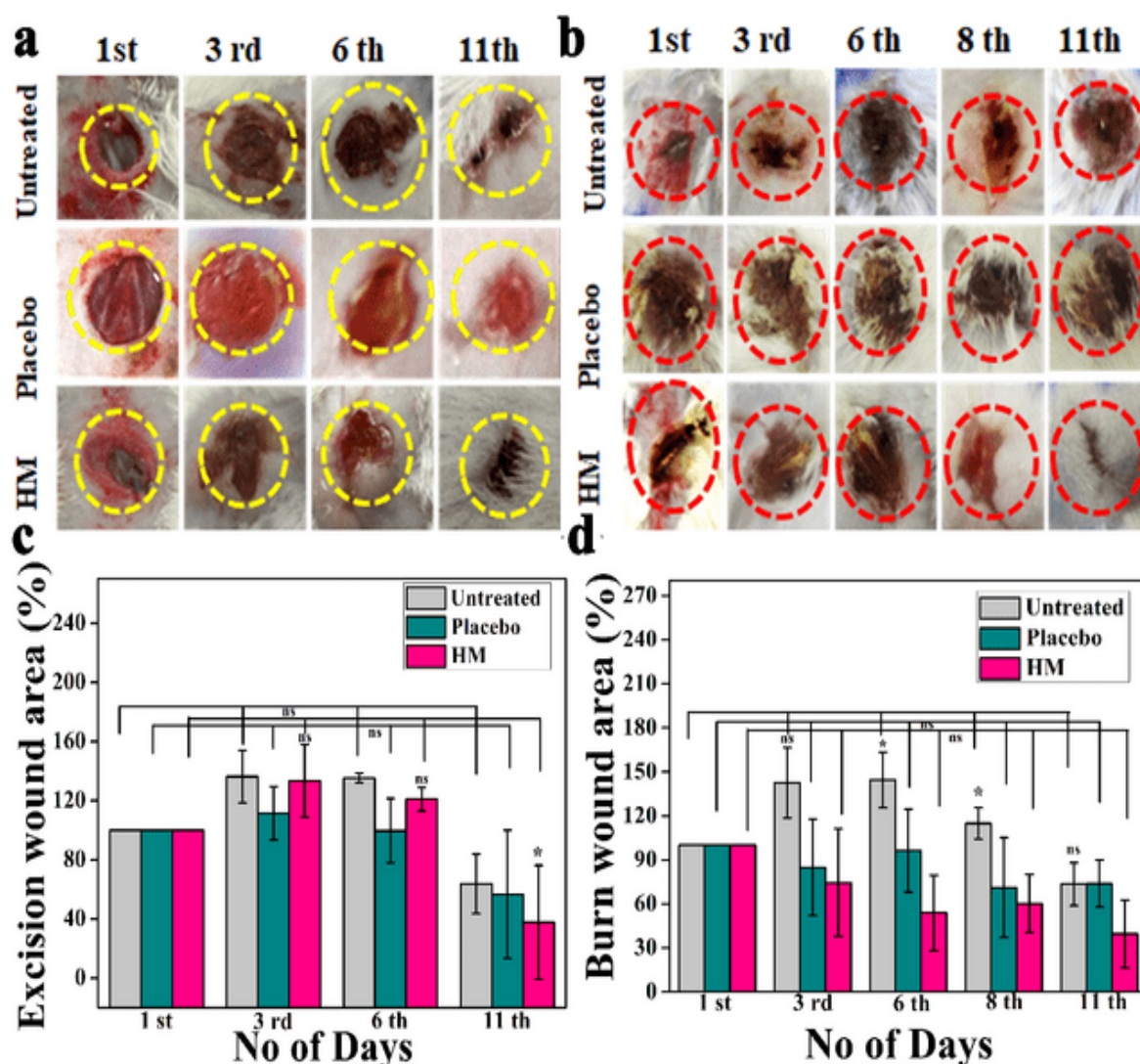
Figure 4.6. *In male BALB/c mice wounds were created on the dorsal surface of the skin (a) excision wound, (b) second-degree burn wound; and c-d were the quantitative estimation of excision and burn wound area respectively, where * is P<0.05) wound area was measured by ImageJ software.*

Histological analysis of excision and second degree burn wounded tissue:

Histological analysis revealed many cell types that are involved in the coordination of the wound healing process. On the sixth day of the HM and placebo group, it was seen that the epidermis (white arrow) in the excision wound (Figure 4.7 a) was recovering, while on the eleventh day of untreated, the epidermis was beginning to do so. In the instance of burn wounds (Figure 4.7 b), HM treatment encouraged the repair of the injured epidermis (White

arrow) by the sixth day; Placebo and untreated showed no indications of epidermal recovery by the eleventh day.

Neutrophils or WBC increase during the subsequent inflammatory stage to eliminate necrotic tissue and pathogens by phagocytosis, while also releasing ROS, antimicrobial peptides, and proteolytic enzymes. (De Oliveira *et al* 2016) On the third day of HM treatment, inflammatory signs (yellow arrow) were seen to be reduced in both types of wounds (Figure 4.7), whereas in the placebo group, inflammation had been prolonged to the sixth day in burn wounds but limited to the third day in cases of excision wounds. For untreated excision wounds that were increased, neutrophil infiltration from the third to the sixth day after damage, but for burn wounds, inflammation begins on the sixth day and extends until the eleventh. The prolonged inflammation stimulates tissue damage and reduces the recovery process.

A proliferative step known as the third phase of healing occurs when keratinocytes, fibroblasts, macrophages, and endothelial cells are heavily activated in order to direct wound closure, matrix deposition, and angiogenesis.(Tonnesen *et al* 2000) A new blood vessel (red arrow) develops as a result of endothelial cell activation, which occurs on the sixth day in each group of mice. However, in the untreated and placebo groups, angiogenesis continued on the eleventh day, whereas after HM treatment, this process was finished on the sixth day in both groups of mice (burn and excision).

Matrix remodeling, the last stage of wound healing, includes the whole range of damage reactions, starting with the initial deposition of a fibrin clot and ending with a mature scar that is abundant in collagen type 1. Granulation tissue's (black arrow) growth marked the beginning of scar formation. In the burn wound, HM treatment and silverex treatment (placebo) accelerated the process of granulation tissue development within the 3rd day and 6th day, respectively, and it was continued to the 11th day, but in the untreated group, the

granulation tissue was not developed. In the excision wound, granulation tissue started to develop on the 6th day and continued on the 11th day of HM treatment, but the granulation tissue was not developed in the silverex (placebo) and untreated mice.

Collagen type I, which resurfaces the wound with the growth of hair follicles (sky arrow), replaces collagen type III of granulation tissue as healing advances. On the third day of HM treatment, hair follicles began to form in burn and excision wounds. Silverex-treated (placebo) excision and burn wounds accelerated hair follicle formation on the sixth and eleventh days, respectively. In both cases, untreated groups began developing hair follicles on the eleventh day.
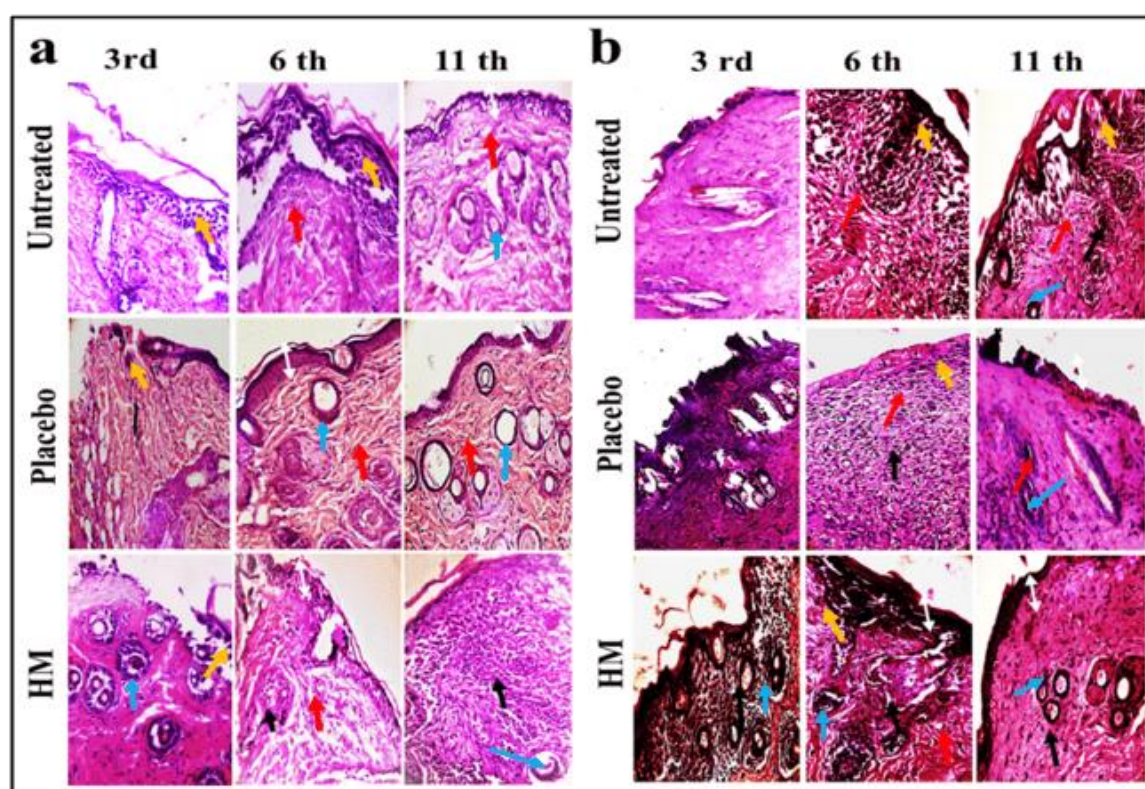
Figure 4.7. *Histopathological features of wounded murine tissue (a) excision wounded mice tissue and (b) second-degree burn wounded mice tissue. Where the white arrow-epidermis, yellow arrow- neutrophil infiltration, red arrow- blood vessel, black arrow-granulation tissue and sky-blue arrow- hair follicles*

The α-SMA and Type 1 collagen protein levels of wounded tissue was estimated by immunohistochemistry

The expression of α-SMA and collagen type 1 protein in the post-wounded tissue region identifies the production of neo-connective tissue (activated fibroblast), differentiation of fibroblast into myofibroblast, and the formation of new blood vessels at the wound site..In the excision wound from the sixth (sky blue bar) to the eleventh (brown bar) day of treatment, the expression of α-SMA increased from 12% to 28% in excision wounds for the untreated group, 12% to 15% for the silverex treatment (placebo), and 48% to 55% for the HM treatment, whereas in most of the cases, the expression of collagen type 1 decreased from 6th to 11 th day at 22% to 2%, 2% to 8%, and 32% to 20% in untreated, placebo control, and HM-treated respectively (Figure 4.8. a, b).

In the case of burn wound (Figure 4.8. c), within the 6th (green) to 11th (purple) days of the treatment regimen, the expression level of α-SMA was changed from 18–68%, 65–62%, and 70–35% in untreated, silverex (placebo), and HM-treated tissues, respectively. Similarly, the percentage of collagen type 1 was changed from 32-40%, 28–31%, and 48–25% for untreated, placebo control, and HM-treated mice, respectively.

The α-SMA protein exhibited a progressive decline, which is associated with scar formation. Conversely, the presence of collagen type 1 protein and the growth of hair follicles are indicative of scar maturation. Collagen, being the principal component of connective tissue, plays a crucial role in the process of wound healing by serving as the fundamental structural framework for tissue remodeling. This remodeling process ultimately leads to an enhancement in the strength of the wound. (Schultz *et al* 2011) Therefore, the HM therapy elevated the expression of α-SMA in excision wounds by the eleventh day and raised the amount of collagen type 1 in both kinds of wounds on day 6 when HM therapy was applied.

Moreover, on the 11th day, excision wounds reduced the scar formation process and closed the wound area whereas in the case of burn wounds the scar maturation was nearly complete.
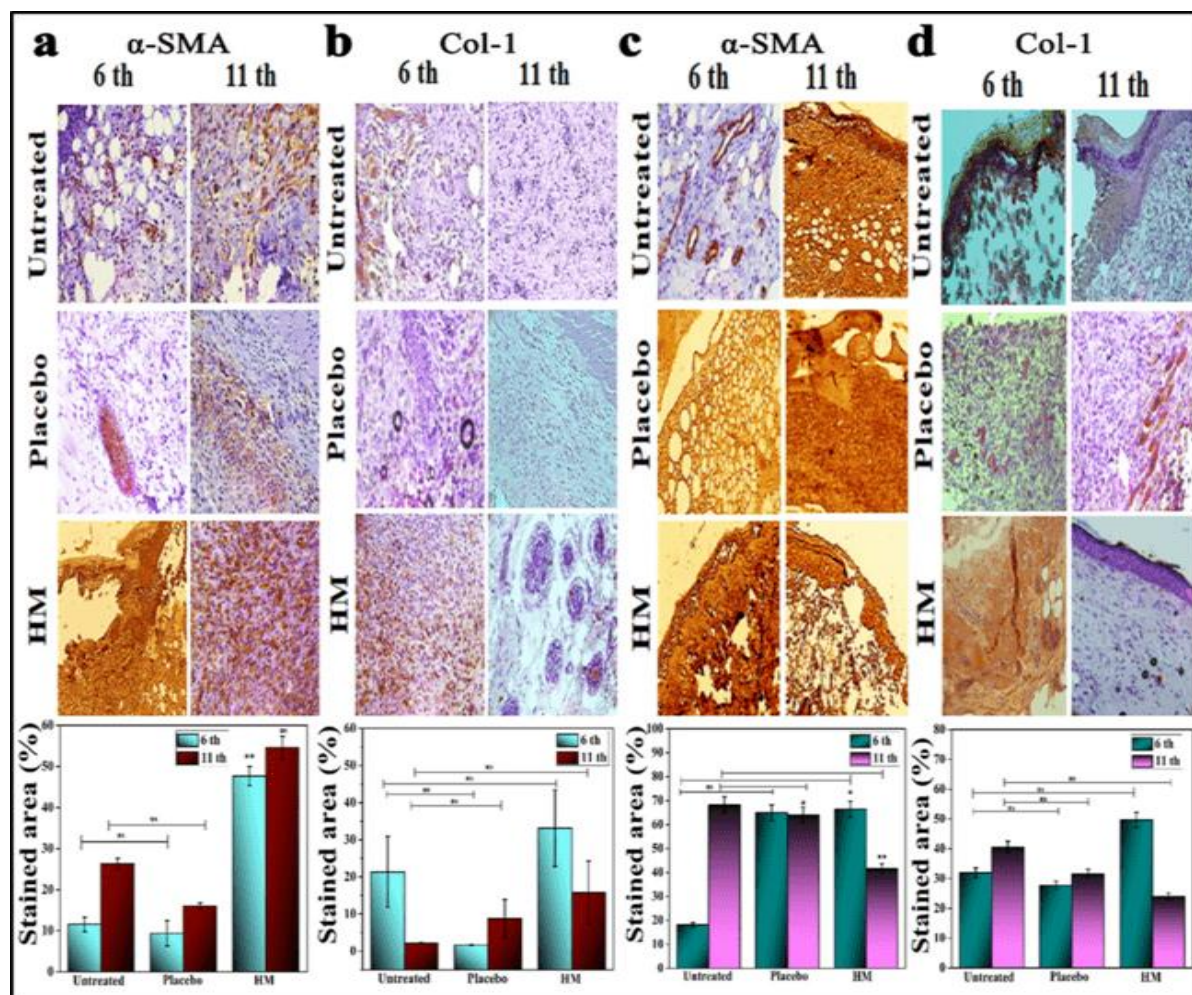
Figure 4.8. *Immunostaining was performed with anti-α-SMA (rabbit, Abcam, 1:200) and anti-Type 1 Collagen (goat, Santa Cruz Biotechnology, 1:50) as primary antibodies and horseradish peroxidase (HRP)-conjugated anti-IgG as a secondary antibody. The images were taken in 40 X magnification, the scale bar is 50 μm. (a-b) Immunostaining of excision wound tissue; (c-d) Immunostaining of burn wound tissue; Quantitative representation of the stained area in murine tissue in the 6th and 11th days of treatment for α-SMA and collagen type I in excision and burn wounds, respectively. The positively stained areas were calculated using ImageJ software and expressed as %. Results were expressed as mean ± SD, * (P < 0.05) and ** (P < 0.01) in comparison to untreated.*

4.4. Conclusion

In conclusion, our findings indicated that the hibiscus mucilage polymer (HM) is a biocompatible compound with the potential to exhibit antioxidant, anti-inflammatory, and cellular proliferative capabilities. In the murine model, HM polymer is also found to be effective for excision and second-degree burn wound healing and management. In addition, the polymer is harmLess to the environment and has low production costs. Therefore, it could be utilized as a desirable substance with potential biomedical applications for wound management.

Chapter 5

Fabrication process of Green Silver Nanoparticle Embedded Mucilage Microsphere and Applied Against Highly Pathogenic Bacteria Infected Second-Degree Burn and Excision Wound

Fabrication process of Green Silver Nanoparticle Embedded Mucilage Microsphere and Applied Against Highly Pathogenic Bacteria Infected Second-Degree Burn and Excision Wounds

5.1. Introduction

Burn and excision wound patients have higher rates of morbidity and mortality due to microbial infections, especially by numerous drug-resistant micro-organisms. WHO reports indicate that fifty percent of patients are infected with antibiotic-resistant bacteria.(World Health Organization, 2022) Most of the injured area is infected by different pathogenic bacteria like *Pseudomonas aeruginosa* (17%), *Staphylococcus aureus* (37%), *Proteus mirabilis* (10%), *Corynebacterium* spp. (5%) and *Escherichia coli* (6%) etc. and it entered into deeper regions of the skin and formed biofilm on the upper surface of the wounded portion (Bruna *et al*, 2021) causing bacteremia or sepsis (Elkordy *et al*, 2021). Treatment of burn wounds in a clinic may be difficult since they are prone to bacterial infections and often have a lot of exudates, while effective wound care management is a crucial component of quick wound healing. Various type of chemical, herbal drugs, nanoparticles (like zinc, zinc oxide, silver, titanium dioxide, and zeolite), and antibiotic has been used for the regeneration of injured tissue but these components may have some hazardous side effects. Therefore, recently some scientists are focused on natural polymer-coated nanoparticle formation to prevent infection in wound. (Mukherjee *et al*, 2019)

In the last few years, some researchers have used mucilage biopolymers in various forms like microspheres, gel, tablets etc.(Okunlola *et al*, 2020) Microspheres are free-flowing, 1–1000 µm ranges spherical particles, consisting of natural or synthetic polymers. The small-size

particles are efficient for drug loading, controlled release, and targeted delivery process. (Akin-Ajani *et al*, 2022).

For the last few decades, nanoparticles have been demonstrating a huge potential in transforming biologically active substances with limited absorbance, solubility, or higher labiality into effective and deliverable drugs with prolonged circulation. In recent years, NPs are being extensively used in drug delivery to assess the potential antimicrobial, anticancer and antioxidant properties of various biomolecules like drugs and growth factors. (Aguilar, Z., 2012) Depending on the constituents, NPs are broadly divided into two main groups- organic and inorganic. (Lu *et al*. 2016) Bio-nanoparticles can be synthesized via synthetic routes or by "Green Synthesis" which in simpler words means producing bio-nanoparticles with the help of microorganisms, fungi, and plant extracts. (Jha *et al*. 2009) In our study, we have achieved a green synthesis of silver nanoparticles (GSNPs) from the leaves of *Hibiscus rosa-sinensis* plant.

The goal of our study is to synthesize green silver nanoparticle encapsulated hibiscus mucilage microsphere (HMMS@GSNP), against MRSA-infected (Methicillin-resistant *Staphylococcus aureus*) second-degree burn and excision wounds. Both the green silver nanoparticles (GSNP) and the mucilage polymer (HMMS) are synthesized from *Hibiscus rosa-sinensis* leaves. Henceforth, our synthesized HMMS@GSNP microsphere was biocompatible, biodegradable, sustained drug release properties, and additionally it can stimulate anti-inflammation, proliferation, migration, anti-oxidant activity, and simultaneously promote healing process in pathogenic bacteria-infected burn and excision wound (Scheme 5.1).
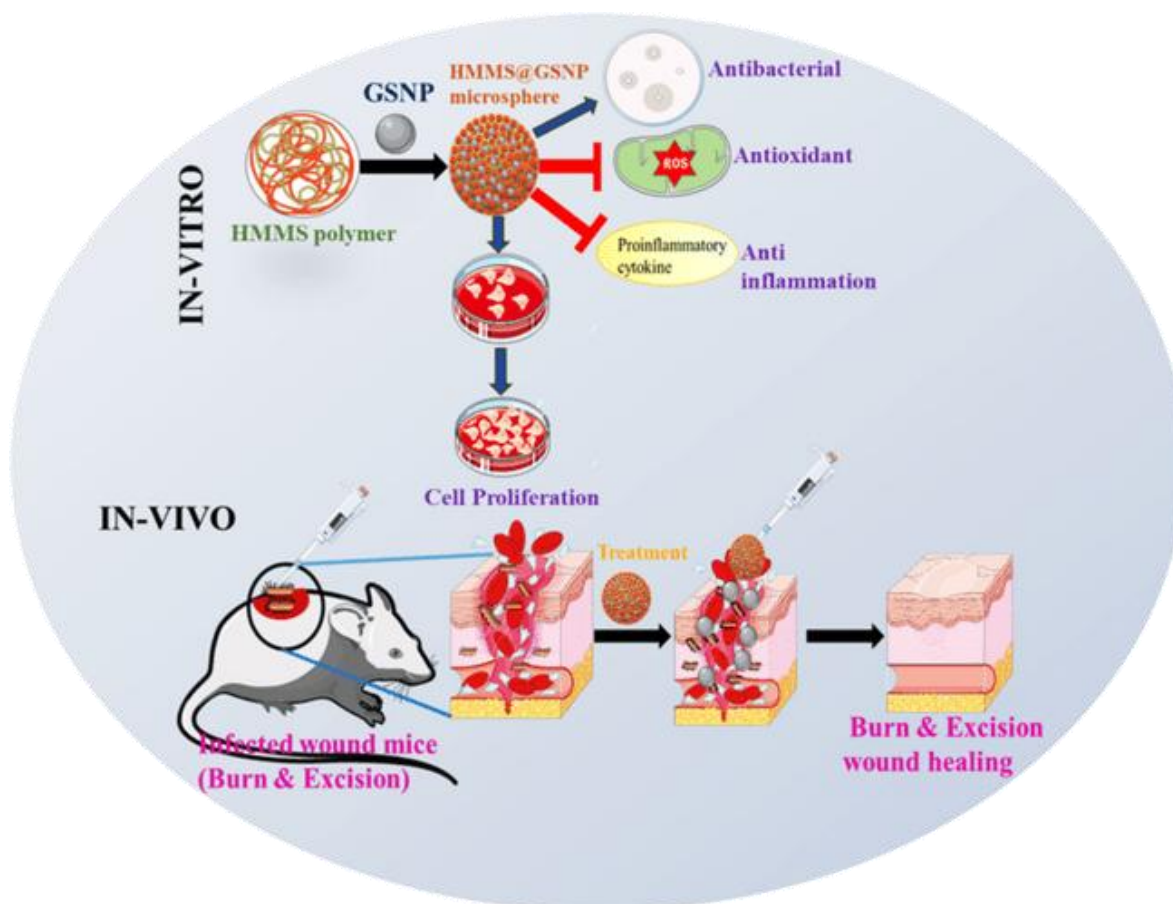
Scheme 5.1. *Graphical abstract of our work*

5.2. Fabrication process of mucilage microsphere encapsulated GSNP

Plant materials collection and authentication

The *Hibiscus rosa sinensis* leaves were taken from the Jadavpur University campus in Kolkata, and authenticated by the Agri-horticultural Society of India, Kolkata.

Preparation process of Green silver nanoparticle (GSNP):

Hibiscus rosa-sinensis leaves were picked while still green and young, washed, and air-dried at room temperature. The dried leaves powdered (1 gm) were dissolved in distilled water (100 mL) after that powdered aqueous solution was boiled for 5 minutes. The aqueous powder solution was strained by Whatman filter paper 1. To make the GSNP suspension, the

leaf extract was heated to 90 degrees Celsius in a water bath while the 1.7 mM $AgNO_3$ solution was added drop by drop until the mixture turned brown, and then centrifuged at 9000 revolutions per minute for 25 minutes. Once the particle had been collected and dried at 45 to 50 degrees Celsius before the supernatant was discarded.

The development process of mucilage polymer (HMMS):

After washing thoroughly with distilled water, we macerated the leaves (40 gm) of the *Hibiscus rosa sinensis* in deionized water (500 mL), stirred constantly for 45 minutes, and then boiled for a few minutes. A muslin cloth was used to filter the concentrated hibiscus solution. After being extracted, the mucilage was cleaned using acetone and then dried using a hot air oven.

A method for creating Mucilage microspheres encapsulated GSNP (HMMS@GSNP)

5 mg of HMMS polymer was mixed into 1 mL of water while being constantly stirred for 6 h. The HMMS solution was then mixed with 2 mg of GSNP and left to stir for 2 hours. The mixture was then lyophilized or dried at 45 $^{\circ}$C to remove the excess water and stored at room temperature. Figure 5.1 depicts the preparation process of the HMMS@GSNP microsphere.
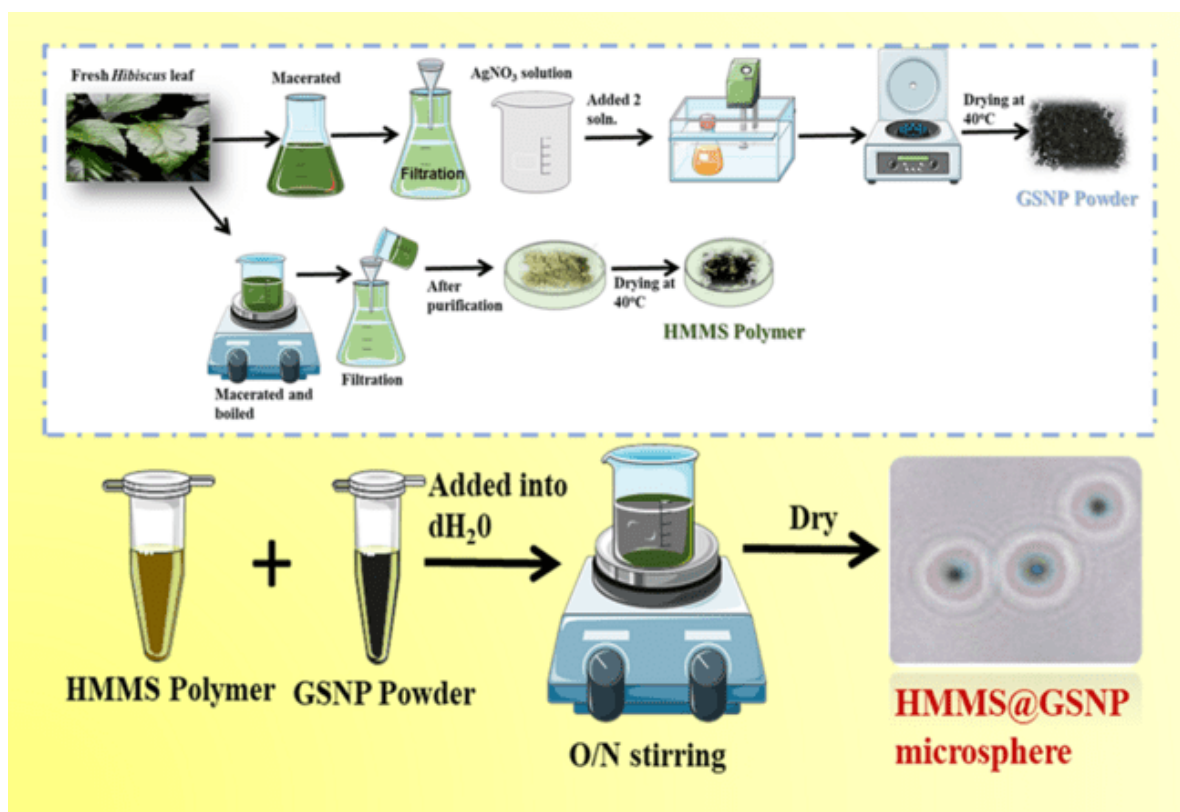
Figure 5.1. *Fabrication process of HMMS, GSNP, and HMMS@GSNP microsphere.*

5.3. Results and Discussion

Biophysical properties

The XRD (X-Ray Diffractometer) patterns of Hibiscus mucilage polymer (HMMS) showed no diffraction maxima, but GSNP showed diffraction maxima at 27.56, 32.06, 38.04, and 46.16 degrees. At 24.23 degrees, HMMS@GSNP showed a slight hump, and at 27.86, 32.36, 46.26, 54.88, and 57.33 degrees, respectively, absorbance maxima were seen. In HMMS@GSNP, the HMMS and GSNP distinctive peaks were visible. This means that HMMS has an amorphous nature, GSNP has a crystalline structure, and HMMS@GSNP has a semi-crystalline nature based on the XRD pattern (Figure 5.2. a).

We employed UV-Vis spectroscopy to verify the doping of the GSNP. Figure 5.2 b illustrates the broad-spectrum absorbance of the undoped mucilage polymer at 332.35 nm, the

absorbance maxima of the GSNP at 450 nm, and the broad absorption maximum of the GSNP-doped mucilage polymer at about 441 nm. This result indicated that GSNP doping into the mucilage polymer matrix had been carried out satisfactorily.

HMMS, GSNP, and HMMS@GSNP may all be differentiated from one another by the FTIR technique, which is a helpful tool. The C-H bond (vinyl, mono substituted alkenes), C-O bond (ethers, aromatic), C-N bond, and C-H bond (alkyl, methyl) bonds for the HMMS polymer were observed at 1022.60, 1417, 1600, and 3302 cm^{-1}, respectively. According to (-CN- stretching of amines) (Valli *et al*, 2012), GSNP showed absorbance peaks at 1576 cm^{-1} and 1010 cm^{-1}, as well as 1305 cm^{-1} (C-O stretching) (Philip *et al*, 2010). The absorbance peaks in HMMS@GSNP were noted at 1028 cm^{-1}, 1600 cm^{-1}, and 3297 cm^{-1}. The GSNP doped microsphere showed an additional absorbance band at 3297 cm^{-1}, which may indicate -OH stretching (Figure 5.2c). The XRD and FTIR data show that the dopants were properly incorporated into the sample.

The swelling ratio (Figure 5.2 d) was used to compare the water absorbance capacity of HMMS@GSNP to that of the undoped mucilage polymer (HMMS). As seen, GSNP was released from the HMMS polymer with control release manner. At pH 7.5 (normal skin pH), the release profile of GSNP-encapsulated HMMS was assessed, and the release profile was monitored every two hours for 22 hours (Figure 5.2. e). Drug encapsulation efficiency (DEE) and DLC (Drug loading capacity) percentages of mucilage polymer were determined to be 60% and 80%, respectively. The highly significant surface area of the HMMS polymer is revealed by the excellent drug loading capacity. In the first two hours, about 18% of the drug was released; the remaining 20% were released after that.

The thermal stability of HMMS and HMMS@GSNP was tested using the DTA-TGA technique, revealing the polymer's stability up to 500 $^{\circ}$C. To verify their storage and usage,

the polymer's thermal stability has been examined (Figure 5.2 f and g). The DTA-TGA instrument was used to analyze the temperature-dependent mass loss and differential thermograms while maintaining a heating rate of 10 ^{o}C per minute in a nitrogen atmosphere (flow rate of 50 cc/min). It was found that the undoped sample (HMMS) displayed a thermal transition at 100 ^{o}C. In addition, HMMS@GSNP revealed a significant thermal transition at 300 ^{o}C, indicating that it is exceptionally stable at such high temperatures. This would undoubtedly make this sample suitable for use in biological applications.

FESEM and phase contrast microscopy were used to examine the morphology of the synthesized materials. Inspect-F50, FEI instrument was used for FESEM analysis. The microscopic image of green silver nanoparticle encapsulated mucilage polymer (HMMS@GSNP) revealed a more exfoliated microsphere structure compared to pristine mucilage polymer. The undoped polymer (HMMS) was an agglomeration in nature (Figure 5.2. i), the GSNP was spherical and hexagonal shape (Figure 5.2. h), the doped polymer exhibits a spherical and porous shape as well (Figure 5.2 j). The size range of GSNP was 8.40 to 23 nm. The size range was narrowed by the addition of GSNP to the polymer, which also increased sample porosity, decreased agglomeration, and created a microsphere-like structure. All of these characteristics offer a wound substrate a better chance of adhesion. The size range of the phase contrast microscopic pictures of the HMMS@GSNP microsphere was 400-450 μm, and Figure 4.2 k displayed the size distribution of the histogram graph.

According to DLS measurements, the hydrodynamic diameter of pure mucilage polymer was 5545 d.nm, while the hydrodynamic diameter of GSNP conjugated polymer (HMMS@GSNP) was 3200 nm with a polydispersity index (P.D.I) of 0.381. The GSNP had a PDI value of 0.299 and a hydrodynamic size of 191.5 d.nm. In addition, the GSNP surface charge was -38.5 mV and the pure mucilage polymer's surface charge was 2.68 mV. A

persistent microsphere with a surface charge of 33.1 mV was produced by doping with GSNP

in HMMS, though. Therefore, a better chance of attachment to the wound surface was

provided by the spherical and porous structure. The doped sample creates a homogeneous

solution that is appropriate for any biological application and shows an elevated microsphere

surface charge.
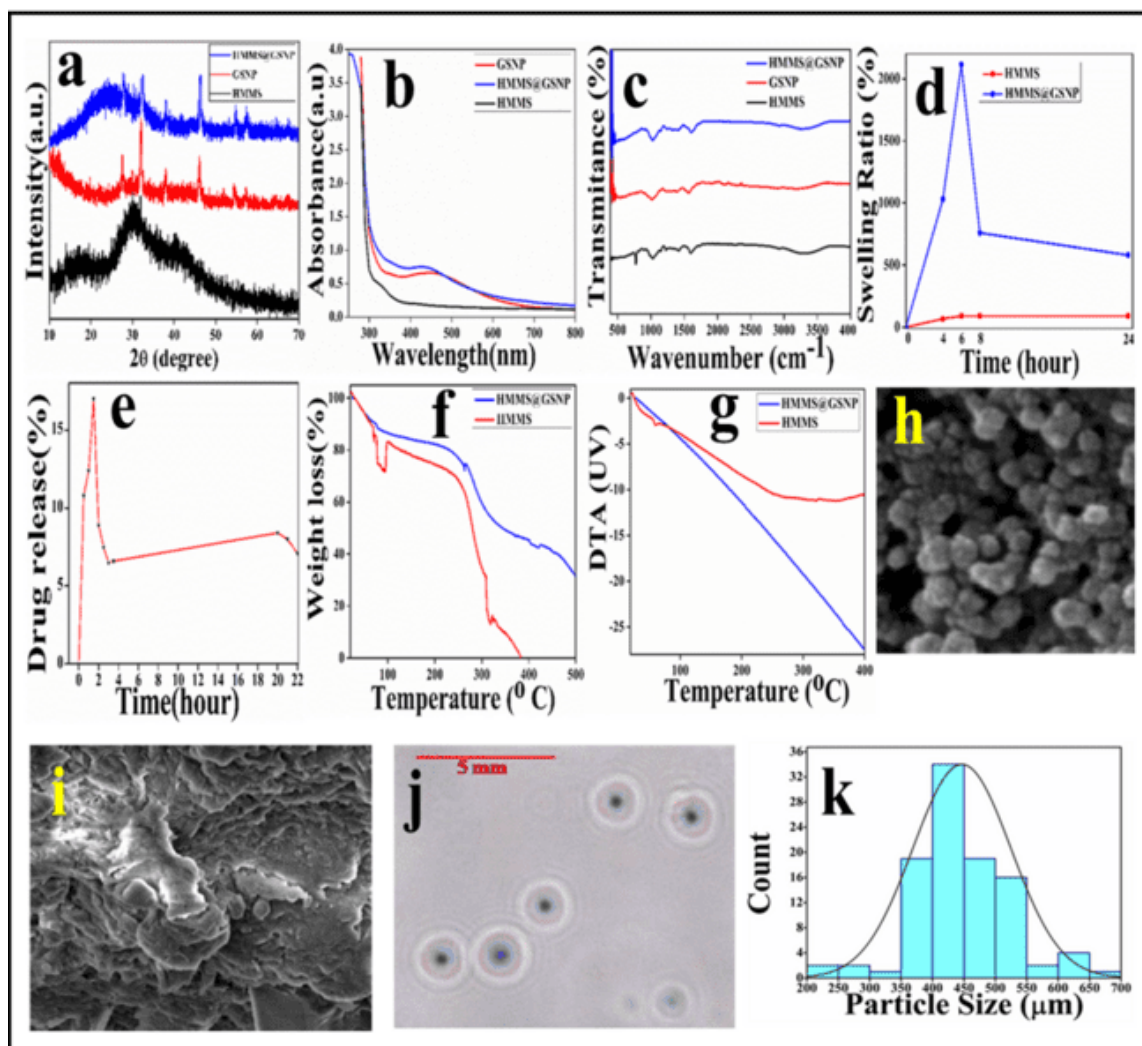
Figure 5.2. *Biophysical properties of synthesized materials, (a) XRD of HMMS, GSNP, HMMS@GSNP; (b) UV-VIS spectroscopy of HMMS, GSNP, HMMS@GSNP; (C) FTIR spectroscopy of HMMS, GSNP, HMMS@GSNP; (d) Swelling ratio of HMMS and HMMS@GSNP at pH 7.5, (e) Drug release property of HMMS@GSNP (f) TGA, and (g) DTA of HMMS, HMMS@GSNP (h-i)FESEM images of GSNP and HMMS respectively; (j-k) Phase contrast microscopic images and histogram of HMMS@GSNP.*

Antibacterial activity:

The MIC assay was used to establish the minimal inhibitory concentration of microorganisms. Gram-negative *E. coli* and gram-positive methicillin-resistant *S. aureus* were employed in the aforementioned case. The bacteria were exposed to varied concentrations of HMMS, GSNP, and HMMS@GSNP. It was discovered that HMMS had no impact on either gram-positive or gram-negative bacteria. Gram-negative and gram-positive bacteria treated with GSNP had IC_{50} values of 30 and 70 μg/mL, respectively, while GSNP-encapsulated HMMS microsphere demonstrated IC_{50} values of 12 and 15 μg/mL, which were more effective than GSNP. This result has shown in Figure 5.3 a, b.

We also measured the MBC values of *E. coli* and *S. aureus* bacteria that had been exposed to GSNP and HMMS@GSNP. GSNP-treated *E. coli-DH5α* and methicillin-resistant S. aureus had bactericidal concentrations of 40 and 80 μg/mL, respectively, whereas HMMS@GSNP-treated *E. coli* and *S. aureus* had bactericidal concentrations of 30 and 50 μg/mL, respectively. The results are depicted in Table 5.1.

Table 5.1: Minimum inhibitory concentration, Minimum bactericidal concentration, and their ratio after HMMS@GSNP microsphere treatment against *E.coli* and *S. aureus* (MRSA).

Strains	MIC (μg/mL)	MBC (μg/mL)	MBC / MIC
E. coli DH5α	12 μg/mL	30 μg/mL	2.5
MRSA	15 μg/mL	50 μg/mL	3.3

The agar well diffusion method was used to calculate the zone of inhibition area.When treated with GSNP, the maximum inhibitory zone areas against Methicillin-resistant S. aureus and E. coli-DH5α were 27 mm at 150 μg/ mL and 25 mm at 300 μg/ mL, respectively.

However, when treated with HMMS@GSNP, the corresponding zone of inhibition was 30 mm at 60 µg/ mL concentration against Methicillin-resistant S. aureus bacteria and 45 mm at 150 µg/ mL(Figure 5.3. c, d).

The silver nanoparticle has been utilized to treat a variety of bacterial strains with broad-spectrum antibacterial action, but it does not prevent bacterial infection at the wound site. (Bruna *et al*, 2021)Antibacterial, anti-inflammatory, and wound-healing characteristics should all be present in advanced wound dressing materials. The findings of the MIC, MBC, and Agar-well diffusion results showed that the HMMS-incorporated GSNP microsphere had a better effect than the untreated, HMMS, and GSNP-treated bacteria.

The morphological structure of the bacterial sample after exposure to GSNP, HMM, and HMM@GSNP was obtained using the SEM. We observed that excessive membrane damage after treatment which is perhaps responsible for bacterial cell death. HMMS did not exhibit any antibacterial effect, while HMMS@GSNP exhibited a stronger antibacterial impact than GSNP at the same period (Figure 5.3. e). According to earlier reports, AgNP stopped bacterial development by cleaving bacterial DNA, damaging cell walls, and disrupting the respiratory enzyme route. (Shaikh *et al*, 2019) Here, the bacterial SEM pictures demonstrated that apart from other damages bacterial membrane damage may be responsible for the development of gram-positive and gram-negative bacteria growth after treatment with HMMS@GSNP.
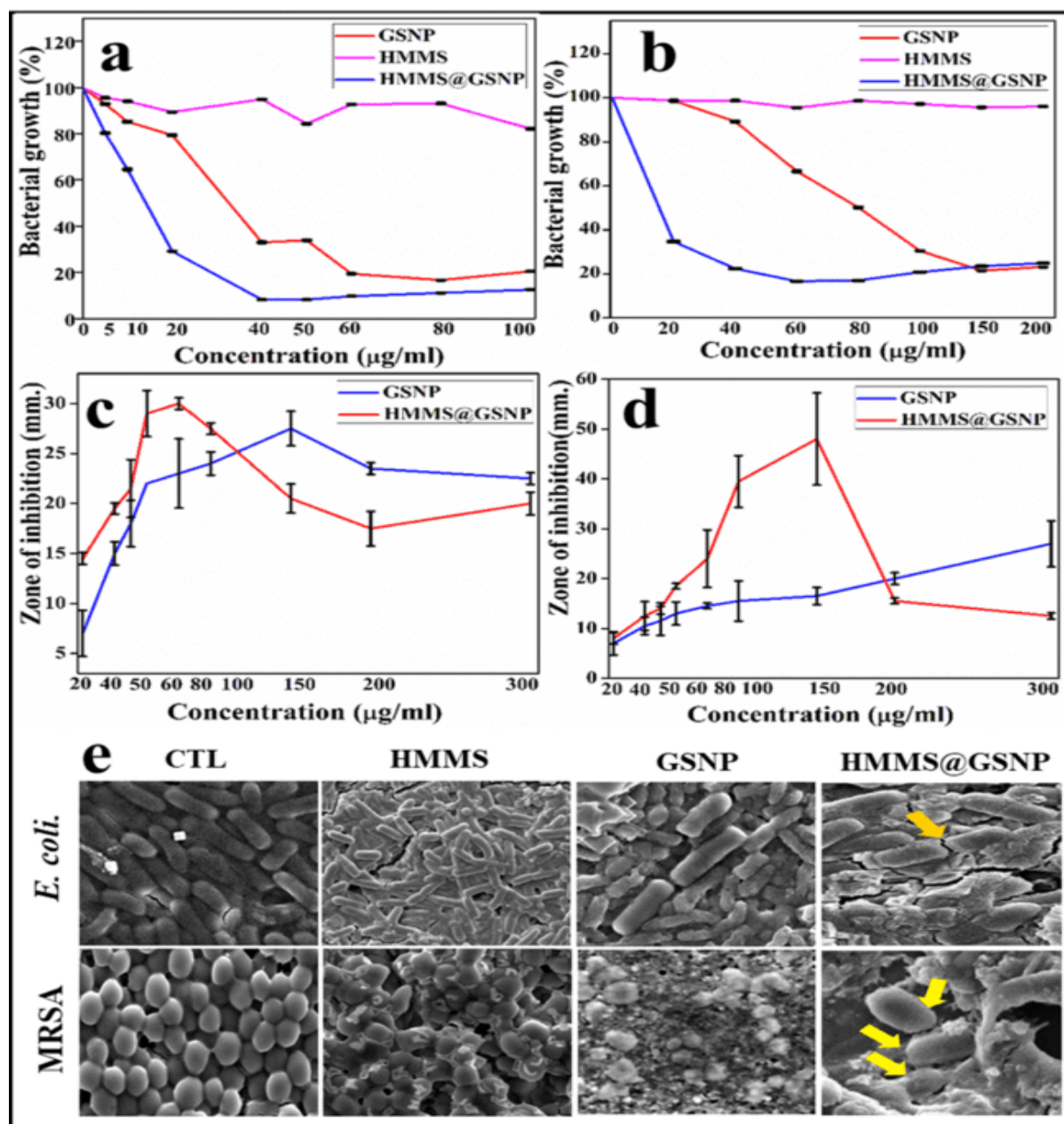
Figure 5.3. *Assessment of antibacterial activity on E. coli and MRSA (a-b) MIC of GSNP, HMMS, and HMMS@GSNP treated E. coli and MRSA bacteria respectively (c-d) Agar well diffusion method of GSNP, and HMMS@GSNP treated E. coli and MRSA bacteria respectively (e) SEM images of GSNP, HMMS, and HMMS@GSNP treated bacteria.*

Estimation of cell proliferation and cytotoxic effect of HMMS, GSNP, and HMMS@GSNP treated human cell lines

By using the MTT assay, the cytotoxicity and proliferative impact of HMMS, GSNP, and HMMS@GSNP were assessed. We noticed that GSNP treatment had harmful effects on the WI-38 and HaCaT cell lines at concentrations of 40 μg/mL and 60 μg/mL, respectively. The HMMS polymer promotes cell growth and has no harmful effects. Additionally, GSNP-doped HMMS polymer boosts cell proliferation (10 μg/mL for WI-38 and 20 μg/mL for HaCaT) while also reducing GSNP's toxicity. The outcome is depicted in Figure 5.4. The GSNP showed some toxic effect on both cell lines in this experiment, but it was comparatively very low from the earlier published article (El-Naggar *et al*, 2017; Potara *et al*, 2015), and it was incorporated in the HMMS polymer that reduced the toxic effect and also helped for cell proliferation in very low concentration.
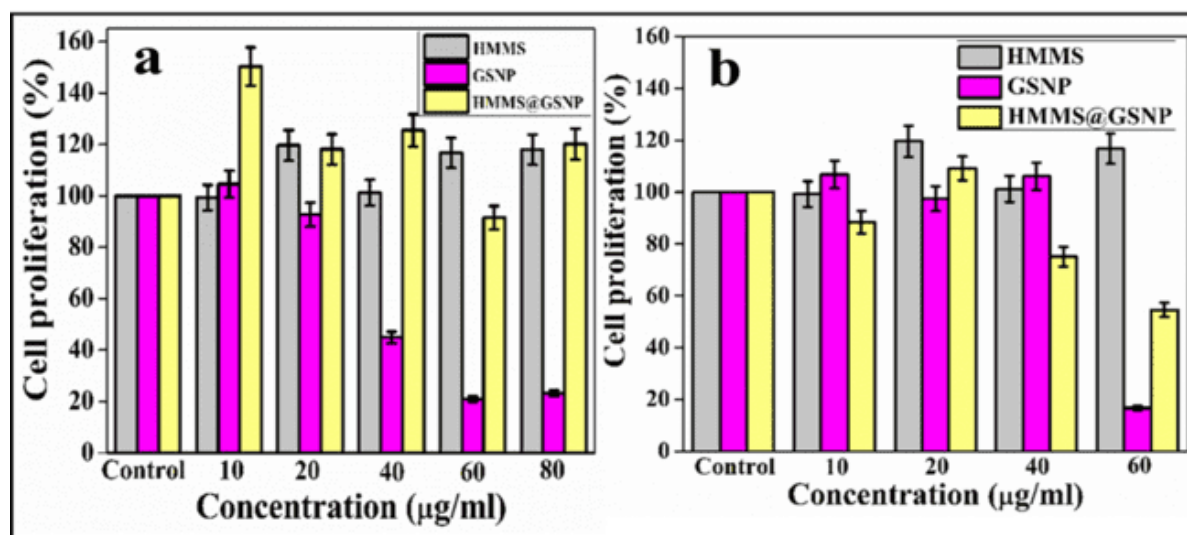
Figure 5.4. *Cell cytotoxicity, and cell proliferation study of GSNP, HMMS and HMMS@GSNP treated human lung fibroblast and keratinocyte cell lines (a-b) MTT assays on WI-38 and HaCaT cells respectively. The MTT assay results were expressed as mean ±SD of three independent experiments and where * (P<0.05), ** (P<0.01), and *** (P<0.001).*

Cell migration study

The cell migration study was conducted after 24 and 48 hours of treatment using the scratch wound assay. Figure 5.5 demonstrates that after 24 hours the GSNP, HMMS, and HMMS@GSNP microsphere promoted WI-38 migration. After 48 hours, we noticed that only the scratch wound area treated with the HMMS@GSNP microsphere had fully recovered, while the GSNP and HMMS-treated wound areas had recovered 90% and 80%, respectively, in comparison to the untreated wound (Figure 5.5 c). The wound region was also healed by the HMMS@GSNP-treated HaCaT cell line after 48 hours (Figure 5.5 d, b). However, after 48 hr the repaired wound areas were 25%, 60%, and 80%, respectively, for untreated, GSNP, and HMMS-treated HaCaT cells (Figure 5.5d). Therefore, HMMS@GSNP treated WI-38 and HaCaT cell lines more effectively promoted cell migration than the other treated groups.
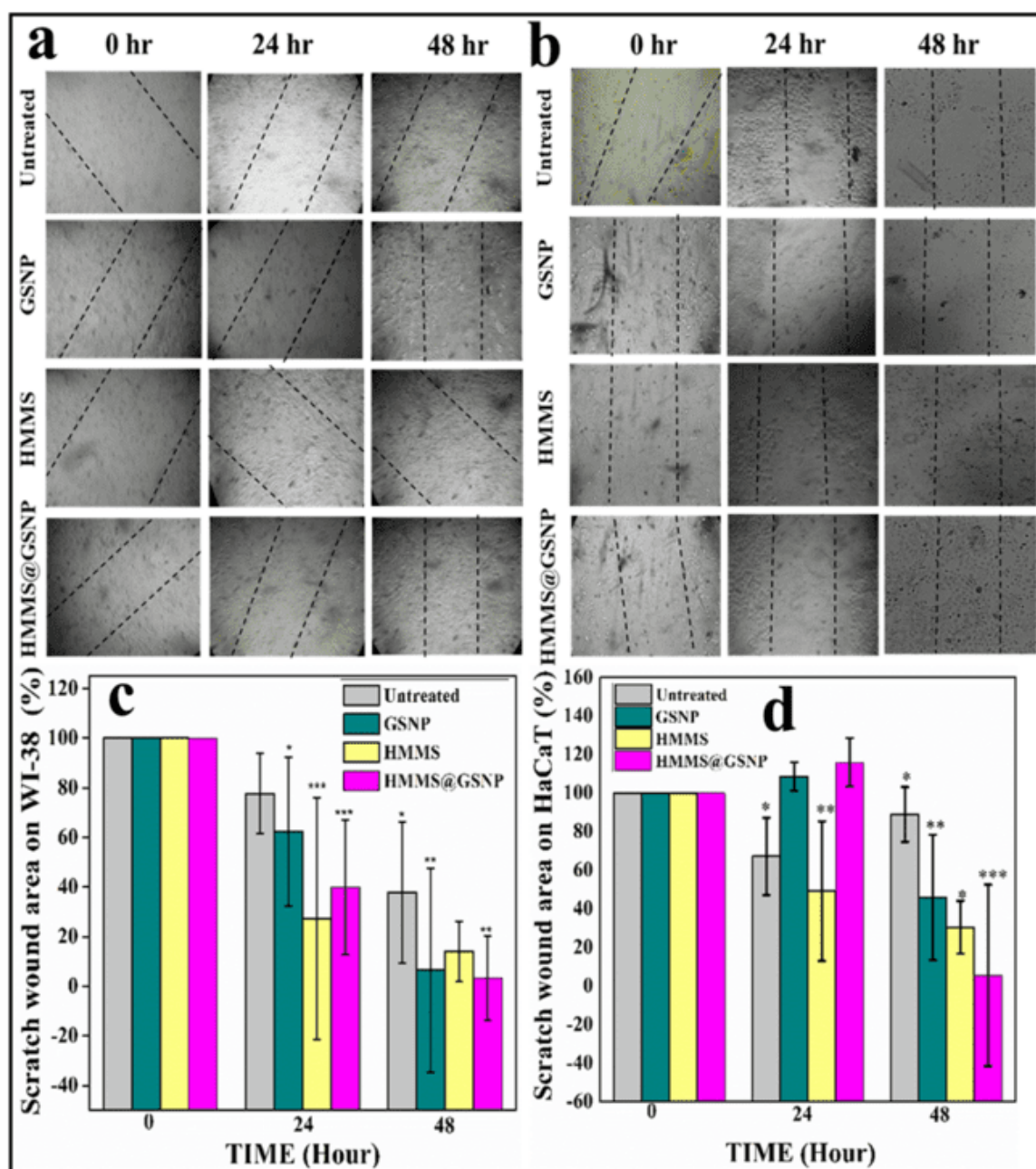
Figure 5.5. *Cell migration study of GSNP, HMMS and HMMS@GSNP treated human lung fibroblast and keratinocyte cell lines (a-b) The pictorial images of Scratch wound area of GSNP, HMMS and HMMS@GSNP treated human lung fibroblast and keratinocyte cell lines at 0, 24 and 48 hours respectively. The recovery percentage of scratch wound area of WI-38 and HaCaT was shown in c-d respectively. The scratch wound assay results were expressed as mean ±SD of three independent experiments and where * (P<0.05), ** (P<0.01), and *** (P<0.001).*

Antioxidant activity

We employed the human keratinocyte cell line HaCaT and the human lung fibroblast cell line WI-38, which have been treated with NAC, GSNP, HMMS, and HMMS@GSNP, for the ROS scavenging experiment,. In contrast, the ROS intensity of cells treated with NAC, HMMS, and GSNP was 0.82, 0.49, and 1.81 fold for the WI-38 cell line (Figure 5.6 a, e) and 0.73, 0.33, and 0.85 fold for the HaCaT cell line (Figure 5.6 b, e). We found that the ROS intensity decreased 0.7 and 0.8 fold on HMMS@GSNP treated WI-38 and HaCaT cells (Figure 5.6 e).According to this finding, our synthesized HMMS@GSNP microsphere performed better than NAC which was used (5 mM). Since oxidative stress causes inflammation, inhibits angiogenesis, and impairs endothelial function, the generation of antioxidants is a crucial component in wound healing. (Ter Horst *et al*, 2018) According to earlier research, damage to mitochondrial DNA for ROS production via the Sirt3 signaling pathway was the primary cause of endothelial cell dysfunction.(Amini-Nik *et al*, 2018) In both the cell lines' antioxidant characteristics was stimulated by HMMS@GSNP microsphere, although the keratinocyte cell line displayed more antioxidant property after treatment (Figure 5.6 e).The replacement of the damaged ECM and the restoration of injured tissue are two primary functions of the proliferation phase that are mostly carried out by keratinocytes and fibroblasts.

Cell proliferation by BrdU assay

By counting BrdU-positive cells, the effect of the HMMS@GSNP microsphere on the proliferation of WI-38 and HaCaT cells was further examined. Cells were BrdU-labeled and then counted for BrdU-positive cells under a fluorescence microscope. Figure 5.6. c, d, f shows that HMMS@GSNP has more BrdU-positive cells than GSNP and HMMS-treated cells (172% of cells for WI-38 cell lines and 273% for HaCaT cell lines).
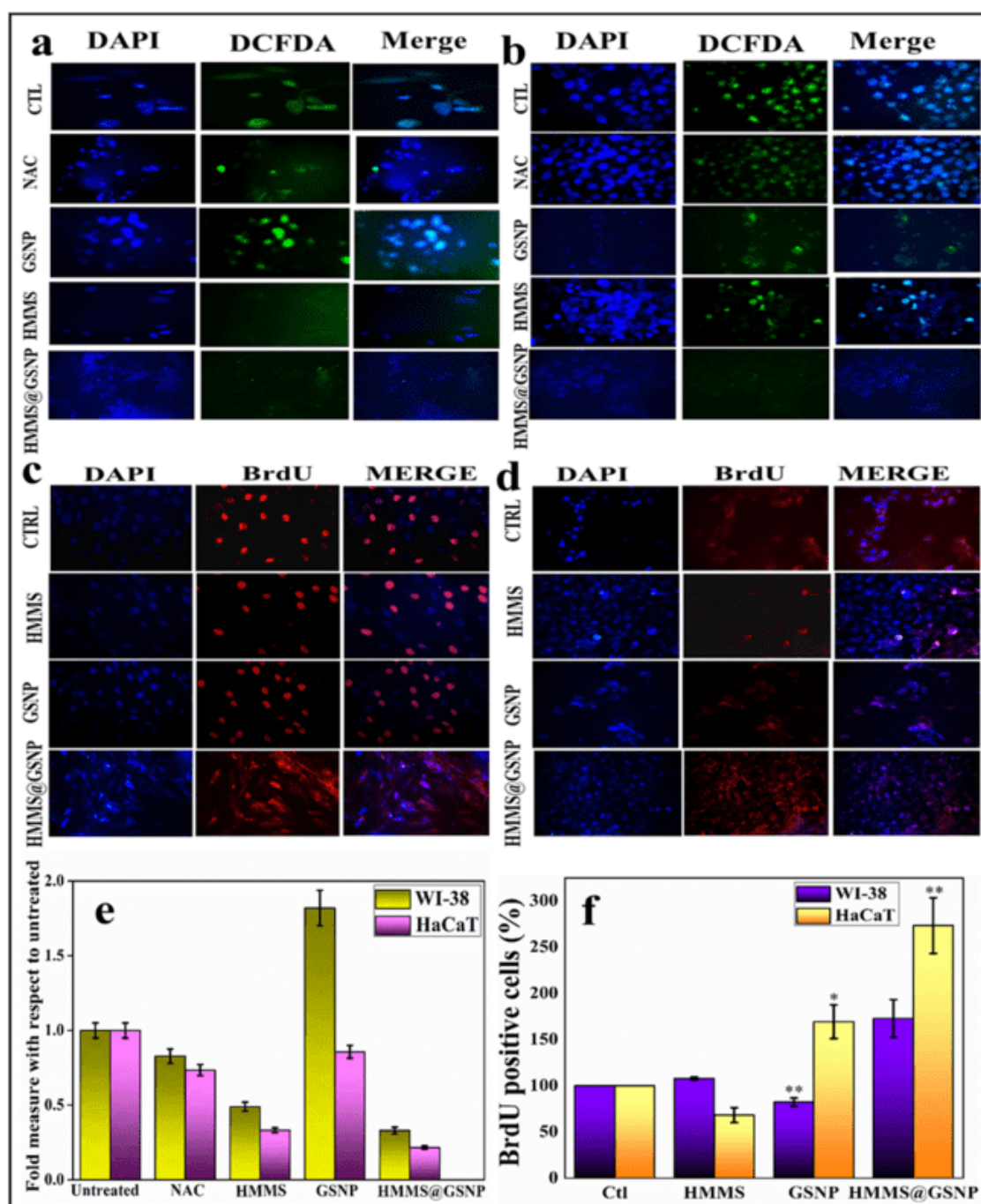
Figure 5.6. *The antioxidant properties of NAC, GSNP, HMMS, HMMS@GSNP treated WI-38 and HaCaT cell lines were shown in figures a & b respectively and the quantitative analysis was shown in figure e; Effect of HMMS, GSNP, and HMMS@GSNP treated cell proliferation were determined by BrdU staining assay treatment with/without extract in WI-38 and HaCaT cell lines for 24h and labeled with 10-μM BrdU before immunocytochemical analysis. The representative images of BrdU staining are shown in Figures c and D respectively. The quantitative estimation of BrdU positive WI-38 and HaCaT cells was shown in the respective Figures f, where * (P<0.05) and ** (P<0.01).*

Immunoblot analysis

In this experiment, the western blot analysis was utilized to identify the signaling proteins related to the wound healing process. The production of ECM elements like collagen I and fibronectin, fibroblast proliferation, myofibroblastic phenotypic differentiation, and wound contracture are all influenced by TGF-β1 (Nikpasand *et al.* 2019). The bacterial infection enhanced tissue inflammation, slowed the healing process, and accelerated scar formation. Therefore, the immune cell fights off germs, clears away cell debris, and secretes several pro-inflammatory cytokines like TNF-α, IL-6, and IL-1β, however, prolonged cytokine secretion slows the process of healing.(Huang *et al*, 2022). In both the cell lines treated with HMM@GSNP, the level of pAkt (Ser 473) increased following treatment, indicating cellular growth. IFN-γ, pAkt, and TGF-β1 protein expression levels and intensities in HMMS@GSNP-treated WI-38 cell lines were quantified and are shown in Figures 5.7 a and b, respectively, as compared to the untreated control. When compared to the untreated control, the IFN-γ, pAkt, and TGF-β1 protein intensities in the HMMS@GSNP-treated HaCaT cell line were 58.42%, 141.89%, and 105.85%, respectively. (Figures 5.7c & 5.7d). We found that HMMS@GSNP upregulated the expression of pAkt and TGF-β1 for both cell lines compared to GSNP, HMM, and untreated cells while down-regulating the expression of the pro-inflammatory cytokine IFN-γ.
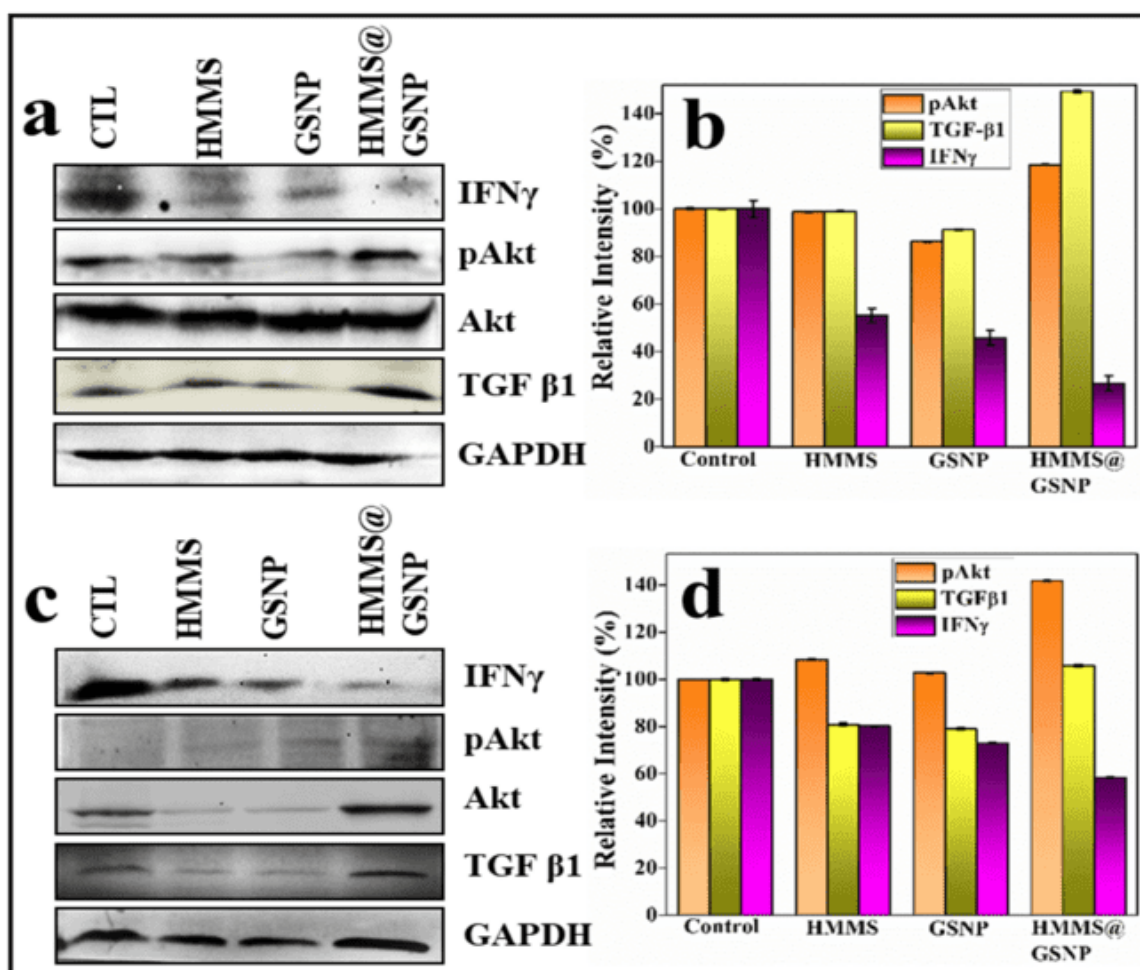
Figure 5.7. *Western blot analysis of Akt (MW 60 kDa) and pAkt (MW 60 kDa), IFNγ (MW 25 kDa), TGFβ1 (MW 13 kDa) protein in response to HMMS, GSNP and HMMS@GSNP. This suggests the upregulation of pAkt and TGFβ1 protein expression upon delivery of HMMS@GSNP microsphere in fibroblast and keratinocyte cell lines shown in (a) for WI-38 and (b) for HaCaT; (c-d) represents the band intensity of WI-38 and HaCaT cell line. The protein intensity was quantified using ImageJ software.*

In vivo experiment

In this experiment all male BALB/c mice were randomly divided into two main groups (1) Bacteria-infected second-degree burn wound, (2) Bacteria-infected excision wound, and each group was divided into six subgroups and each group contained five mice. The treatment process is mentioned in Table 5.2.A. 5mm diameter excision wound was made on the dorsal

surface by punch biopsy, and a second-degree burn was created on the surface with the aid of a metal comb. The second-degree burn and excision wound area were infected by methicillin-resistant *Staphylococcus aureus* pathogenic bacteria (5×10^8 ratio). The bacteria were injected in the burn wound mice on the first and third days, and in the excision wound area on the first and sixth days. Bacterial colony counting techniques were used to calculate the rate of bacterial infection. Bacteria-injected excision wound mice were treated on days 9, 13, and 17, while bacteria-infected burn wound mice were treated on days 6, 10, 13, and 16. The Committee for the Purpose of Control and Supervision of Experimental Animals (CPCSEA), Government of India, provided guidelines for the conduct of animal studies and as approved by the Institutional Animal Ethics Committee (IAEC), Department of Zoology, University of Kalyani. The tissue sample was used for histological analysis, immunoblot analysis, and real-time PCR.

Table 5.2. The treatment process of MRSA-infected burn and excision wound

Groups	Treatment Process (infected excision wound)	Treatment Process (infected burn wound)
Group 1	excision wound + bacteria injected + untreated	burn wound + bacteria injected+ untreated
Group 2	excision wound + bacteria injected + Silverex ionic gel treated (Placebo)	burn wound + bacteria injected + Silverex ionic gel treated (Placebo)
Group 3	excision wound + bacteria injected + AgNO$_3$ treated	burn wound + bacteria injected +AgNO$_3$ treated
Group 4	excision wound + bacteria injected + HMMS treated	burn wound + bacteria injected + HMMS treated
Group 5	excision wound + bacteria injected + GSNP treated	burn wound + bacteria injected + GSNP treated
Group 6	excision wound + bacteria injected + HMMS@GSNP treated	burn wound + bacteria injected + HMMS@GSNP treated

Quantification of the wounded area

The MRSA-infected (treated 5×10^8 ratio) second–degree burns and excision wounds were created on the dorsal surface of the male BALB/c mice. We observed, on the 6th day the second-degree burn wound mice, and on the 9th day, the excision wound mice started inflammation respectively. The initial treatment began in the mouse groups that followed excision and burn wounds on the ninth and sixth days, respectively (Figure 5.8 a). The mice were given treatments in both cases that included silverex ionic gel (placebo), $AgNO_3$, HMMS, GSNP, and HMMS@GSNP. The silverex ionic gel and $AgNO_3$ are each recognized as antibacterial medications and wound care ointments, respectively. In comparison to untreated, placebo, $AgNO_3$, HMMS, and GSNP-treated mice, the wounded areas of HMMS@GSNP-treated mice with burn and excision wounds recover gradually as shown in in Figures 5.8 b and c. On the 20th day, HMMS@GSNP treated excision wound mice had recovered wound area at 66%, while the burn wound area had recovered at 83% and no scar formation was observed. The second-degree burn and excision wound recovery result was quantitatively represented in Figure 5.8 d and e respectively.
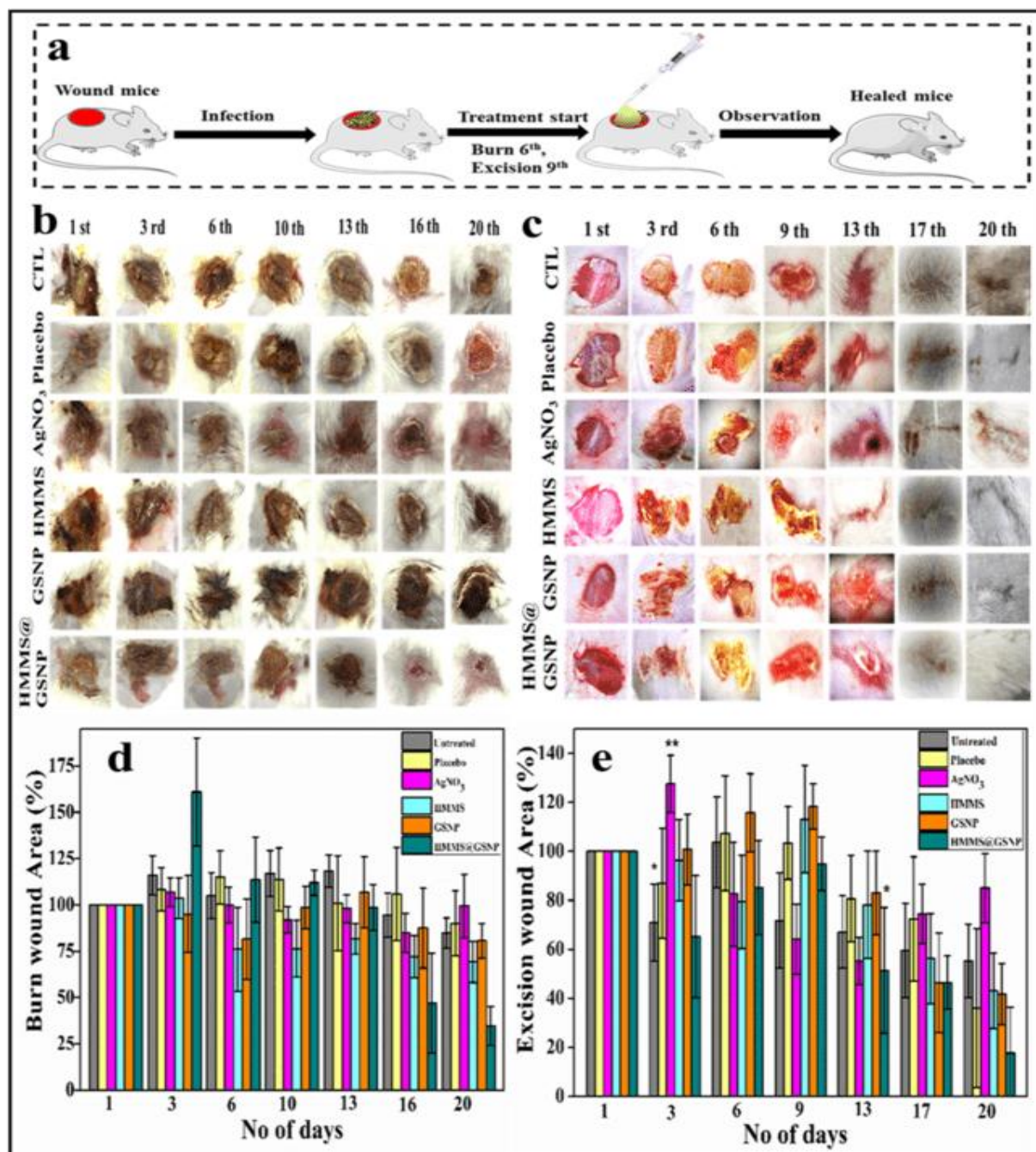
Figure 5.8. *In vivo experiment of MRSA infected second-degree burn and excision wound (a) experimental design of in-vivo experiment;(b-c) Pictorial representation burn and Excisional wounds of untreated and treated mice were monitored on various days and the corresponding images were taken with a digital camera (Sony Cyber-shot DSC-WX80); (d-e) quantitatively represent the second-degree burn and excision wound area respectively, where * (P<0.05) and ** (P<0.01).*

Histological analysis of burn and excision wound treated tissue

Figures 5.9 a and b depict the histological examination of MRSA-infected second-degree burn and excision wound tissue, respectively. Hematoxylin and eosin staining were used to determine the morphological modifications or progression of the injured area following treatment with the synthesized component. The wound repair process is differentiated into four phases, hemostasis, inflammation, proliferation, and maturation. In the first phase recovered epidermis and developed fibrin; in the inflammation phase neutrophil, monocytes developed and removed necrotic tissue and pathogen; in the proliferation phase started re-epithelialization, collagen synthesis, angiogenesis, hair follicle, and extracellular matrix formation; and in the last phase stated collagen remodeling and vascular maturation, regression.(Schultz *et al*, 2011)

The HMMS@GSNP-treated burn and excision wounds mice removed debris and necrotic tissue from the wound surface area on days 13 and 17, respectively. They also formed blood vessels, a thin layer of epidermis, and reduced the inflammatory component, as shown in Figs. 5.9 a and b. Compared to the HMMS@GSNP treated group, the mice in the placebo, AgNO$_3$ treated, HMMS treated, and GSNP treated groups all developed tissue very slowly. In contrast to other groups of mice, the HMMS@GSNP-treated post-infected burn and excision wound mice completed the reepithelialization process by day 20 and hair follicles appeared in the wound area.
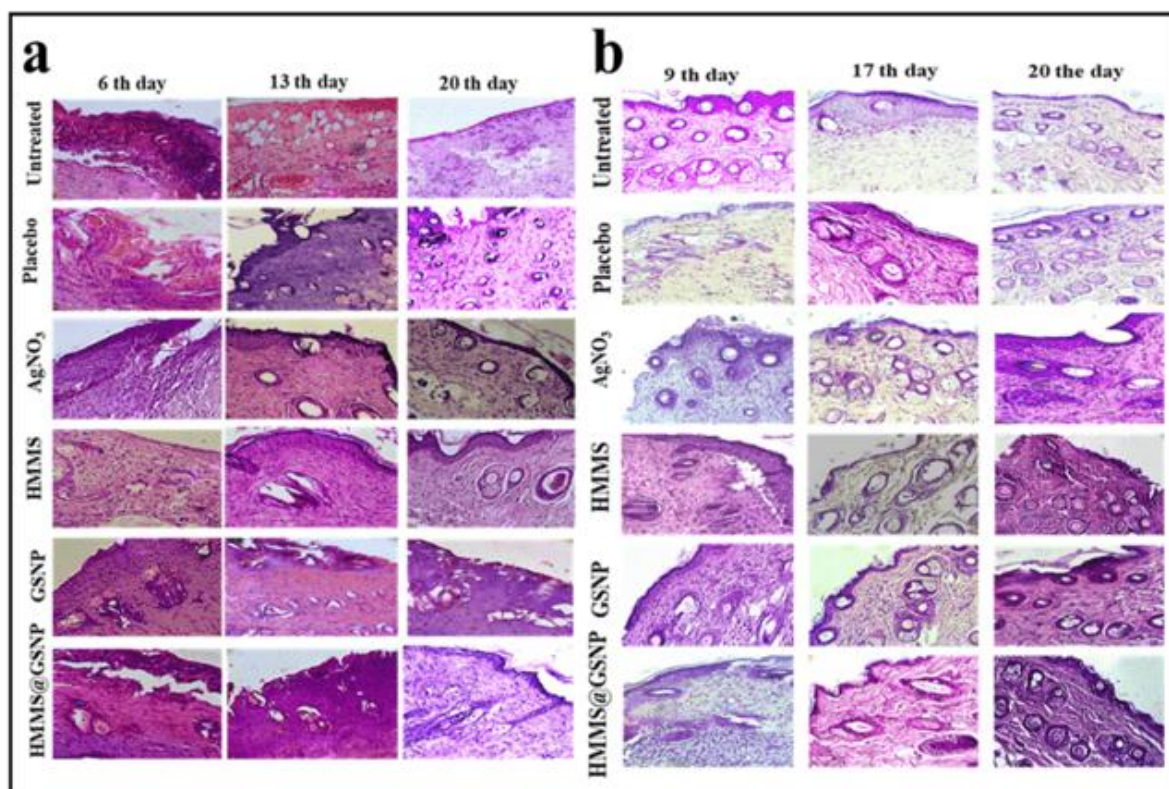
Figure 5.9. *a and b represent the histological images of second-degree burn and excision wounds respectively*.

Bacterial colony count of infected mice

According to recent reports, methicillin-resistant *S. aureus* (MRSA) bacteria are present in more than 37% of acute and chronic wounds.(Siddiqui *et al*, 2018) Therefore, we examined the impact of the HMMS@GSNP microsphere on mice with second-degree burns and excision wounds that were infected with MRSA. Treatment for mice with second-degree burn wounds began on the sixth day following infection, while for mice with excision wounds, treatment began on the ninth day. Our findings showed that the number of live bacteria in burn-infected mice treated with HMMS@GSNP was much lower than in control groups. After 20 days, the HMMS@GSNP microsphere in burn wounds reduced bacterial growth by close to 40%, but other groups did not (table 5.2 a). Table 5.2. b demonstrates that after 20 days, the HMMS@GSNP treated MARSA-infected excision wound mice suppressed

bacterial growth by 75%, in contrast to less than 30% inhibition in the other groups (untreated, placebo, AgNO$_3$, HMMS, and GSNP).The result of our investigation revealed that mice treated with HMMS@GSNP microsphere at a dose of 8 mg/kg body weight had less viable bacterial growth than mice in other groups.

Table 5.2: Bacterial colony count on post-infected excision and second-degree burn wound mice

(a) Number of Bacterial colonies on second-degree burn wound mice

GROUPS	No of Bacterial Colony [Log (CFU/mL)]		
	6th day	13th day	20th day
Untreated	15.45±0	15.69±0	15.74±0
Silverex (Placebo)	10.52±2.70	11.63±2.22	11.58±2.27
AgNO$_3$	5.71±5.33	4.93±5.89	4.73±6.02
HMMS	10.76±2.5	10.55±2.82***	15.51±0.13**
GSNP	13.41±1.12***	15.93±0.13**	15.02±0.39***
HMMS@GSNP	16.54±0.61**	13.03±1.53***	10.3±2.98***

(b) Number of Bacterial colonies on excision wound mice

GROUPS	No of Bacterial Colony [Log (CFU/mL)]		
	9th day	17th day	20th day
Untreated	17.11±0	16.96±0	15.83±0
Silverex (Placebo)	24±4**	24.61±4.5	16.30±0.2
AgNO$_3$	16.31±0.4***	16.70±0	16.82±0.58
HMMS	15.97±0.65	13.84±2.9	16.52±0.40*
GSNP	16.05±0.6**	16.61±0.04**	16.24±0.26
HMMS@GSNP	23.84±3.88	16.84±0.09	6.01±0.14

Western blot analysis of infected mice tissue

The expression of pro-inflammatory cytokines including IL-6, IFN-λ, IL8, TNF-α, IL-1β, etc. increased after methicillin-resistant *Staphylococcus aureus* bacteria entered the damaged area.(Chen *et al*, 2022) Therefore, we investigated whether the male BALB/c mice with excision and burn wounds after infection could modulate the expression of pro-inflammatory cytokines and increase wound healing responsive proteins. Here, tissue was obtained for investigation from mice with burn wounds at the 6th and 20th days (Figure 5.10. a, b); and mice with excision wounds at the 9th and 20th days (Figure 5.10 c, d). We observed that HMMS@GSNP microsphere-treated post-infected burn wound mice formed 102% pAkt (Ser 473) protein, TGF-β1 118.86%, IL-6 70.80%, and 117.74% Collagen Type-1 protein on day 20 th compared to untreated control (Figure 5.10 b)as well as on the same day post-infected excision wound mice formed 132.39% pAkt (Ser 473), 141.47% TGF-β1, 80.41% IL-6, and 127.91% Collagen Type-1 protein compared to untreated control (Figure 5.10 d). Figure 5.10 shows the outcomes in both situations, showing that the HMMS@GSNP microsphere had superior anti-inflammatory, PI3K pathway, TGF-β1 pathway, and Type 1 Collagen production effects compared to the other mouse groups
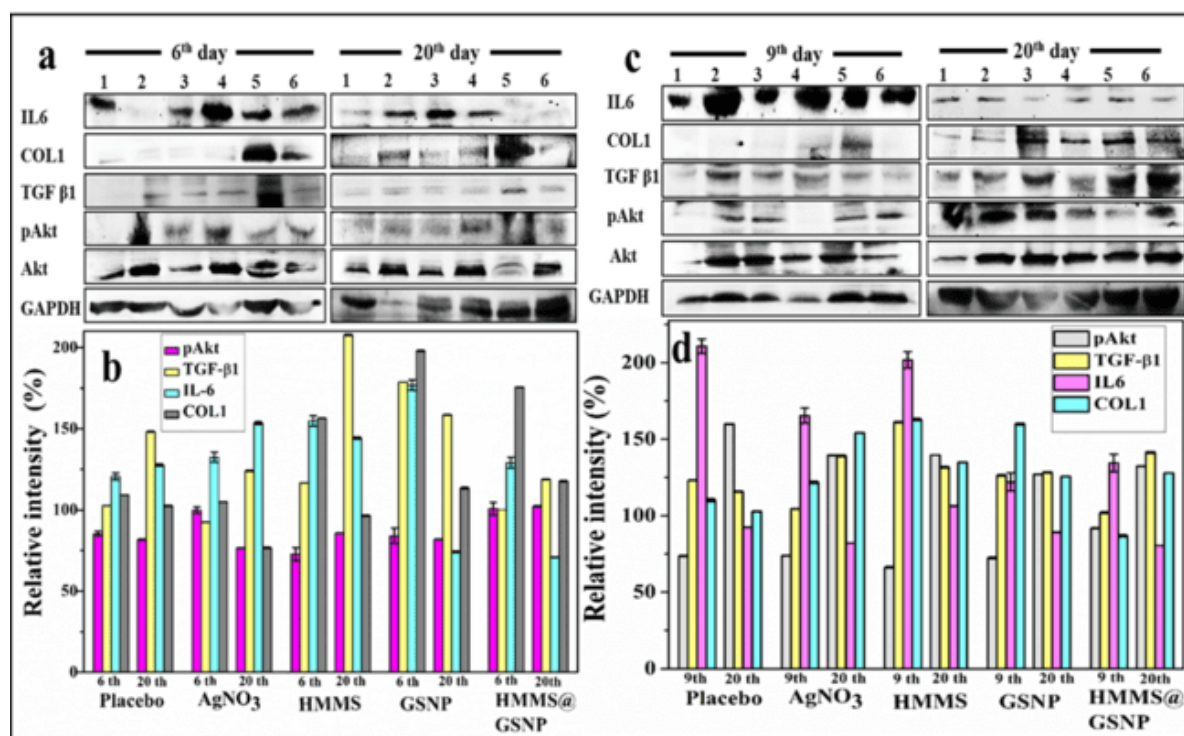
Figure 5.10. *Western blot analysis of post-infected burn and excision wound mice. (a, d) represent the Akt (MW 60 kDa) and pAkt (MW 60 kDa), IL6 (MW 21 kDa), TGFβ1 (MW 13 kDa), COL1(MW 210 kDa) protein expression of burn and excision wound infected mice respectively; (b, d) relative the band intensity of post infected burn and excision mice tissue was represented graphically; The proteins intensity was quantified using ImageJ software. Here lane 1-untreated, 2- Silverex gel treated, 3-AgNO₃ treated, 4- HMMS treated, 5- GSNP treated, and 6- HMMS@GSNP treated.*

The *α-sma* and *ctgf* gene expression by RT-PCR

The results of *α-sma* and *ctgf* gene expression on various days of burn and excision wound tissue are shown in Figure 5.11. We evaluated the gene level between the pre-treatment and post-treatment wound tissue in both cases on the 6th and 9th day using pre-treatment and post-infected burn and excision wound tissue. According to our research, HMMS@GSNP-treated burn and excision animals had considerably higher levels of α-*sma* mRNA expression than the untreated, placebo, AgNO₃, HMMS, and GSNP-treated groups (Figures 5.11 a and c). Figure 5.11 b demonstrates a significant increase in *ctgf* gene expression on day 16 in

mice with burn wounds treated with HMMS@GSNP microspheres compared to untreated mice on day 6. When compared to other groups, the HMMS@GSNP microsphere increased *ctgf* gene expression levels (17th day) in the excision wound case (Figure 5.11 d). This findings revealed that the HMMS@GSNP microsphere was more successful in upregulating the expression of the α-*sma* and *ctgf* genes in excision wound mice treated with the microsphere than in infected burn wound animals. Further research into the literature revealed that the *ctgf* and α-*sma* genes increased the growth of granulation tissue and speed up the healing process. (Mathew-Steiner *et al*, 2021)
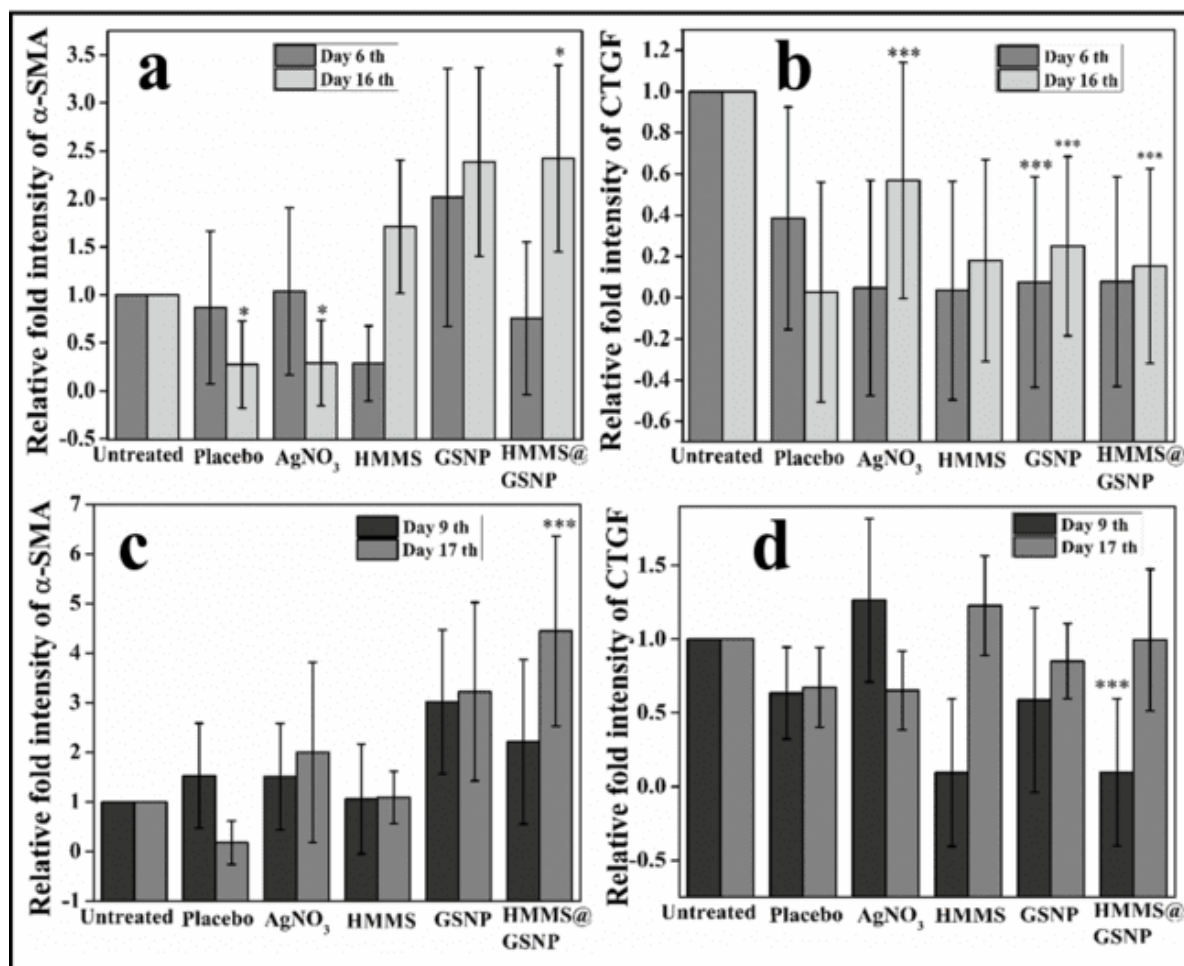
Figure 5.11. *RT-PCR analysis of Silverex (placebo), AgNO3, HMMS, GSNP, and HMMS@GSNP treated post infected burn and excision wound mice tissue (a-b) α-smaand ctgf gene expression of post infected burn mice respectively; (d-e) α-SMA and CTGF gene expression of post infected excision mice respectively; here * (P < 0.05) and ** (P < 0.01), *** (P < 0.001)*

5.4. Conclusion

To sum up, our results suggest that the HMMS@GSNP microsphere is a biocompatible, biodegradable, cost-effective material and additionally, it also helps for sustained drug release. As mentioned, these materials show antibacterial, anti-inflammation, antioxidant, and proliferation activities. The HMMS@GSNP microsphere activates the PI3K pathway as seen by the upregulation of pAkt (Ser 473) in Figure 5.7 and 5.10 Additionally, this material upregulates TGF-β1, Collage type I protein expression which plays an important role like granulassion tissue formation, and differentiation of fibroblasts to myofibroblasts in wounded region. , Further, this material downregulates the expression of pro-inflammatory cytokine IL6 and IFN-γ expression however, reduce the inflammation periods and stimulates the fast healing process. In the in-vivo experiment, we also noticed that the HMMS@GSNP microsphere also helped for angiogenesis, granulation tissue formation, re-epithelialization process, hair follicle formation, inhibited antibiotic-resistant bacterial growth, and reduced scar formation at the same time it also increased the expression of mRNA responsible gene *α-sma* and *ctgf* in pathogenic bacteria infected second-degree burn and excision wound. Thus HMMS@GSNP microsphere is a suitable material for pathogen-infected burn and excision wound healing so, may be used for chronic wound healing or other biomedical applications.

Chapter 6

General Conclusion

Wound healing is a complex series of events that encompasses various cellular and molecular processes to restore the structural and functional integrity of the affected tissue. The wounded portion is infected by numerous gram-positive and gram-negative bacteria like Methicillin-resistant *Staphylococcus aureus*, *Streptococcus pyogenes*, *Pseudomonas aeruginosa*, *Enterococcus faecalis*, *Escherichia coli*, etc. In ancient times different types of herbal extract were used for wound healing though standard procedure for preparation is not available due to lack of research. The proper evaluation of such herbals blended with modern scientific approaches may make them more attractive and effective for treatment. Moreover, their evaluation for cytotoxicity, bioavailability, and delivery needs to be investigated. In the 19 to 20th centuries, different types of synthetic polymers like PLGA, PEG, and PVA, like polylactic acid (PLA) and polyglycolic acid (PGA), etc have been used for wound dressing and wound care management but these polymers have some hazardous effects. Therefore, in the late 20th century to present the various polymers, scientists moved on to natural and bioactive polymer-based materials (like gum acacia, guar gum, chitosan, xanthan gum, etc.) for tissue engineering and wound healing. These materials often incorporate bioactive agents, growth factors, or antimicrobial agents to enhance wound healing and prevent infections. Most natural polymers are biocompatible, biodegradable, have high water absorbance capacity, and are water-soluble. Recently some scientists have been focussing on biopolymeric materials, like mucilage. Mucilage is used in the pharmaceutical industry, food industry, etc. In the 21st century, some scientists started exploring the potential of nanoparticles as drug delivery systems to enhance the efficacy of topical wound treatments. This included nanoparticles made from various materials such as metals (e.g., silver, gold), polymers, lipids, and inorganic materials. Nanoparticles can inhibit bacterial growth, increase the anti-inflammation promotion of tissue regeneration, and accelerate wound closure. On the other hand, a few nanoparticles have adverse effects like toxicity, short half-life period, less

water solubility etc. During this period, researchers have focused on advancements in polymer and nanoparticle synthesis techniques, increasing their properties, to enhance their performance and address various types of wound healing challenges.

In this thesis, we have synthesized three types of wound healing materials - polyhedral excipient loaded xanthan gum hydrogel (X@C-H), hibiscus mucilage polymer (HM polymer), and green silver nanoparticle encapsulated hibiscus mucilage microsphere (HMMS@GSNP microsphere). The X@C-H hydrogel, HM polymer, and HMMS@GSNP microsphere have been used for excision wound healing; second-degree burn and excision wound healing; and against pathogenic bacteria-infected second-degree burn and excision wound healing respectively. In the in vitro experiment, we used a human lung fibroblast cell line and a human keratinocyte cell line as well as in the in-vivo experiment we used male BALB/c mice. The physicochemical properties of all these materials were characterized by UV-Vis spectroscopy, DLS, ZETA Potential, swelling ratio, XRD, FTIR, etc.

In X@C-H hydrogel we have used polyherbal extract (*Calendula officinalis* and *Hibiscus rosa sinensis* flower extract) because polyherbal extract is used for multiple aspects of wound healing, such as inflammation, infection, and tissue regeneration; decreased toxic effect compared to single herbal extract. The polyherbal extracts contain the phytochemicals of flavonoids, terpenoids, alkaloids, saponins, tannins, anthraquinones, amino acids as well as glycosides. In xanthan gum hydrogel the water absorption capacity was more than 3000% at 75 hr and drug release percentage was 55% (pH 7), 58% (pH 7.5), 70% (pH 8), and 80% (pH 8.5) within 10hr. It is another important characteristic of wound healing activity. In an in-vitro experiment, the MTT assay, cell proliferation assay, and cell migration assay were suggested that X@C-H hydrogel exposed a better effect than the single excipient loaded hydrogel (X@C, X@H), X, and untreated group. We also found that phosphorylation of Akt

percentage was better in polyherbal excipient-loaded hydrogel compared to X, X@C, X@H, and untreated cells. In the in-vivo test, we also observed that after 9 days of treatment with X@C-H hydrogel, the excision wounded portion started re-epithelialization, and hair follicle formation process and decreased scar but not found in other groups of mice. So, all these findings suggested that X@C-H hydrogel is biocompatible, biodegradable, and carries out all kinds of excision wound healing properties. In the future more herbal products may be loaded and tested for better activity.

In yet another search for the potential of second-degree burn and excision wound healing attributions of hibiscus mucilage polymer (HM polymer). The HM polymer was synthesized from Hibiscus *rosa- sinensis* leaves and during the literature survey we noticed that most scientists used the leaves for diluents, binders, disintegrants in tablets, thickeners in oral liquids, protective colloids in suspensions, etc. One step further we used it for topical application of burn and excision wound treatment. The HM polymer stimulated cell proliferation, migration, and antioxidant activity of WI-38 and HaCaT cell lines. Simultaneously this polymer also promoted the expression of PI3K, TGF-β1 signaling pathway, and anti-inflammation activity. Furthermore, to evaluate the potentiality of HM polymer in an in-vivo mice model, on the dorsal portion of skin were created second-degree burns and excision wounds by metal comb and punch biopsy respectively. It was observed that the HM polymer treated second-degree burn and excision wound healing group of mice formed collagen type I, α-SMA protein, granulation tissue formation, endothelial cell development, hair follicle formation, and start re-epithelialization process faster compared to the negative control and placebo groups. Therefore, our synthesized HM polymer is another successful wound-healing material.

After that, we used hibiscus mucilage polymer for the drug-delivery carrier (HMMS) for the major focus on the pathogen-infected second-degree burn and excision wound healing. In this experiment, we doped green silver nanoparticle (GSNP) into the HMMS polymer and it formed the HMMS@GSNP microsphere. The HMMS polymer and GSNP both were synthesized from *Hibiscus rosa sinensis* leaves. We observed that the uncoated nanoparticles showed some toxic effects but HMMS-encapsulated GSNP are less toxic and at the same time showed increased antibacterial activity. In the antibacterial experiment, we used *Escherichia coli* and methicillin-resistant *Staphylococcus aureus* (gram-positive bacteria) bacteria and observed HMMS@GSNP inhibited bacterial growth at very low concentrations compared to uncoated GSNP. This is likely due to extended release of Nanoparticles from the HMMS@GSNP. The cytotoxicity of HMMS, GSNP and HMMS@GSNP was evaluated on WI-38 and HaCaT cell lines. The HMMS@GSNP induced proliferation, migration and antioxidant activity on WI-38 and HaCaT cell lines. We also observed the HMMS@GSNP stimulated PI3K, TGF-β1 signaling pathway, and anti-inflammatory protein activity on human cell lines. Now to evaluate the potentiality of this microsphere in an in-vivo mice model, the second-degree burn and excision wound-created mice were infected with methicillin-resistant *Staphylococcus aureus* bacteria. The HM@GSNP treated burn wound infected mice recovered 66% wound and infection recovered 80% on 20 th day compared to untreated, placebo AgNO$_3$, HMMS, and GSNP treated mice. Similarly, HM@GSNP treated excision wound-infected mice 82% of wounds recovered, and 87% bacterial infection reduced on 20th days compared to other groups. The immunoblot and RT-PCR analysis suggested that the HMMS@GSNP microsphere gradually downregulated the expression of IL6 and TNF-α cytokines and upregulated the expression of pAkt (Ser 473) protein, TGF-β1 pathway, collagen type-1 protein and *ctgf*, *α-sma* gene expression compared to others group. Histological tissue sections were also suggested that

HMMS@GSNP-treated mice developed blood vessels, granulation tissue, hair follicles and start the re-epithelization process. But it was also unlike in other groups of mice.

Thus our synthesized materials are cheap, less time-consuming, biocompatible, and biodegradable. Our synthesized polyherbal extract encapsulated xanthan gum hydrogel and hibiscus mucilage polymer equally promote acute wound healing and the green silver nanoparticle encapsulated hibiscus mucilage microsphere stimulates chronic wound healing process where bacterial infection is common.
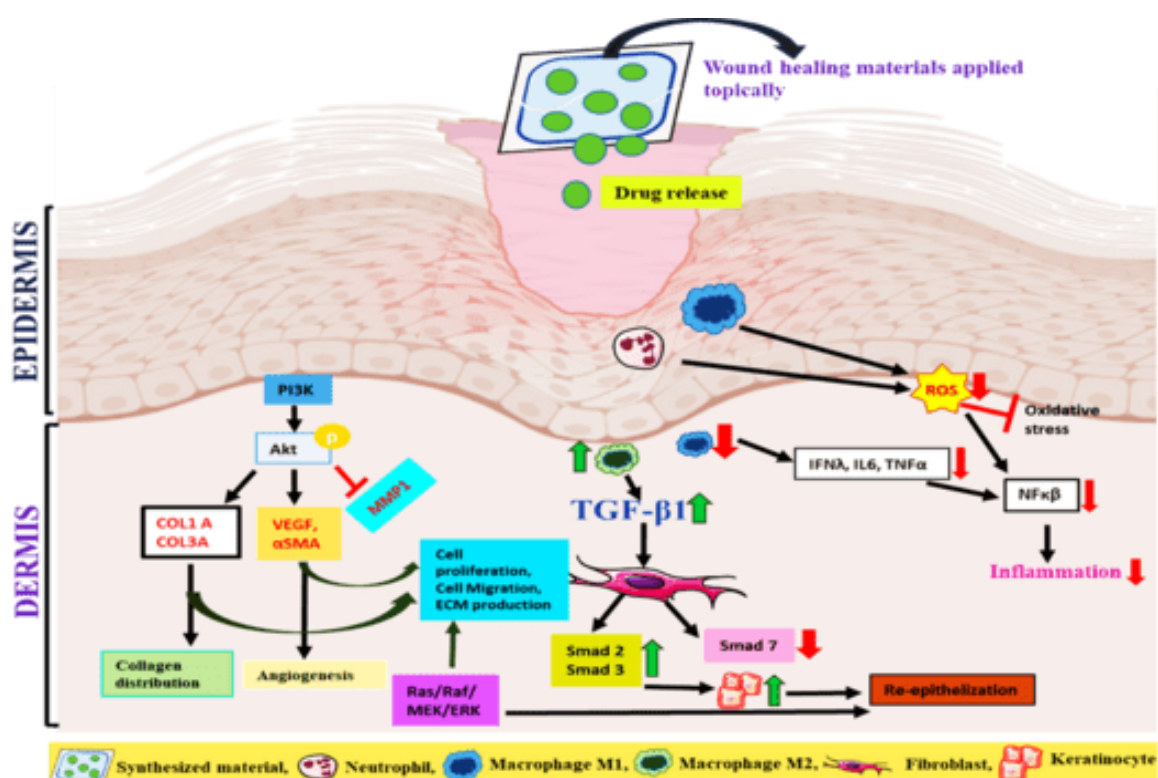
Graphical Abstract

References

Akin-Ajani, O. D., Hassan, T. M., & Odeku, O. A. (2022). Talinum triangulare (Jacq.) Willd. mucilage and pectin in the formulation of ibuprofen microspheres. Polymers in Medicine, 52(2), 83-92.

Alle M, Kim TH, Park SH, Lee SH, Kim JC (2020) Doxorubicin-carboxymethyl xanthan gum capped gold nanoparticles: microwave synthesis, characterization, and anti-cancer activity. Carbohydr Polym 229:115511.

Al-Mussawi ZK, Al-Hussani IM (2019) Phytochemical Study of Calendula officinalis Plant by Used Gc-Ms and FTIR Techniques. Plant Arch. 19(1): 845-851.

Amini-Nik, S., Yousuf, Y., & Jeschke, M. G. (2018). Scar management in burn injuries using drug delivery and molecular signaling: current treatments and future directions. Advanced drug delivery reviews, 123, 135-154.

Azizi M, Azimzadeh M, Afzali M, Alafzadeh M, Mirhosseini MSH (2018) Characterization and optimization of using calendula offlcinalis extract in fabrication of polycaprolactone-gelatinelectrospun nanofibers for wound dressing applications. Adv Mater Process. 6(2): 34-46.

Bahadur, S., Roy, A., Baghel, P., Choudhury, A., Saha, S., & Chanda, R., (2018) Formulation and evaluation of glipizide tablets utilizing Hibiscus rosasinensis leaves mucilage. Indonesian Journal of Pharmacy, 29(1), 23

Bakr, R. O., Amer, R. I., Attia, D., Abdelhafez, M. M., Al-Mokaddem, A. K., El-Gendy, A. E. N. G., ... & Gad, S. S. (2021) In-vivo wound healing activity of a novel composite sponge loaded with mucilage and lipoidal matter of Hibiscus species. Biomedicine & Pharmacotherapy, 135, 111225

Barchitta, M., Maugeri, A., Favara, G., Magnano San Lio, R., Evola, G., Agodi, A., & Basile, G. (2019). Nutrition and wound healing: An overview focusing on the beneficial effects of curcumin. International journal of molecular sciences, 20(5), 1119.

Bhoyar, S. D., Malhotra, K., & Madke, B. (2023). Dressing Materials: A Comprehensive Review. Journal of cutaneous and aesthetic surgery, 16(2), 81–89. https://doi.org/10.4103/JCAS.JCAS_163_22

Bombin, A. D. J., Dunne, N. J., & McCarthy, H. O. (2020). Electrospinning of natural polymers for the production of nanofibres for wound healing applications. Materials Science and Engineering: C, 114, 110994.

Bruna, T., Maldonado-Bravo, F., Jara, P., & Caro, N. (2021). Silver nanoparticles and their antibacterial applications. International Journal of Molecular Sciences, 22(13), 7202.

Budovsky, A., Yarmolinsky, L., & Ben-Shabat, S. (2016). Effect of poly-herbal preparations on wound healing. Wound Repair and Regeneration, 24(1), 196-197.

Cai, Y., Chen, Y., Hong, X., Liu, Z., & Yuan, W. (2013). Porous microsphere and its applications. International journal of nanomedicine, 1111-1120.

Chen, H., Zhang, J., He, Y., Lv, Z., Liang, Z., Chen, J., Li, P., Liu, J., Yang, H., Tao, A., & Liu, X. (2022). Exploring the Role of Staphylococcus aureus in Inflammatory Diseases. Toxins, 14(7), 464. https://doi.org/10.3390/toxins14070464

Chen, X., Martin, B. D., Neubauer, T. K., Linhardt, R. J., Dordick, J. S., & Rethwisch, D. G. (1995). Enzymatic and chemoenzymatic approaches to synthesis of sugar-based polymer and hydrogels. Carbohydrate polymers, 28(1), 15-21.

Choi, J. S., Kim, D. W., Kim, D. S., Kim, J. O., Yong, C. S., Cho, K. H., ... & Choi, H. G. (2016). Novel neomycin sulfate-loaded hydrogel dressing with enhanced physical dressing properties and wound-curing effect. Drug delivery, 23(8), 2806-2812.

Das S, & Baker AB (2016) Biomaterials and nanotherapeutics for enhancing skin wound healing, Front. Bioeng. Biotechnol, 4, 82.

De Oliveira, S., Rosowski, E. E., & Huttenlocher, A. (2016) Neutrophil migration in infection and wound repair: going forward in reverse. Nature Reviews Immunology, 16(6), 378-391

Dev, S. K., Choudhury, P. K., Srivastava, R., & Sharma, M. (2019). Antimicrobial, anti-inflammatory and wound healing activity of polyherbal formulation. Biomedicine & Pharmacotherapy, 111, 555-567.

Dhadde, G. S., Mali, H. S., Raut, I. D., Nitalikar, M. M., & Bhutkar, M. A. (2021). A review on microspheres: Types, method of preparation, characterization and application. Asian Journal of Pharmacy and Technology, 11(2), 149-155.

Dinda M, Mazumdar S, Das S, Ganguly D, Dasgupta UB, Dutta A, Karmakar P (2016) The water fraction of Calendula officinalishydroethanol extract stimulates in vitro and in vivo proliferation of dermal fibroblasts in wound healing. Phytother Res 30(10): 1696-1707

Dinda M, Dasgupta U, Singh N, Bhattacharyya D, Karmakar P (2015) PI3K-mediated proliferation of fibroblasts by Calendula officinalis tincture: implication in wound healing. Phytother. Res 29(4): 607-616.

Dubey, S., & Dixit, A. K. (2023). Preclinical evidence of polyherbal formulations on wound healing: A systematic review on research trends and perspectives. Journal of Ayurveda and Integrative Medicine, 14(2), 100688.

Elkordy, A. A., Haj-Ahmad, R. R., Awaad, A. S., & Zaki, R. M. (2021). An overview on natural product drug formulations from conventional medicines to nanomedicines: Past, present and future. Journal of Drug Delivery Science and Technology, 63, 102459.

El-Naggar, N. E. A., Hussein, M. H., & El-Sawah, A. A. (2017). Bio-fabrication of silver nanoparticles by phycocyanin, characterization, in vitro anticancer activity against breast cancer cell line and in vivo cytotxicity. Scientific reports, 7(1), 10844.

El-Refaie WM, Elnaggar YSR, El-Massik MA, Abdallah YO (2015) Novel curcumin-loaded gel-core hyaluosomes with promising burn-wound healing potential: development, in-vitro appraisal and in-vivo studies. Int.J.Pharm 486(1-2): 88-98.

Eming, S. A., Martin, P., & Tomic-Canic, M. (2014). Wound repair and regeneration: mechanisms, signaling, and translation. Science translational medicine, 6(265), 265sr6-265sr6.

Fahimi, S., Abdollahi, M., Mortazavi, S. A., Hajimehdipoor, H., Abdolghaffari, A. H., & Rezvanfar, M. A. (2015). Wound healing activity of a traditionally used poly herbal product in a burn wound model in rats. Iranian Red Crescent Medical Journal, 17(9).

Faria S, De Oliveira Petkowicz CL, De Morais SAL, Terrones MGH, De Resende MM, De Franca FP, Cardoso VL (2011) Characterization of xanthan gum produced from sugar cane broth. CarbohydrPolym 86(2): 469-476.

Fazal, T., Murtaza, B. N., Shah, M., Iqbal, S., Rehman, M. U., Jaber, F., ... & Ibrahium, H. A. (2023). Recent developments in natural biopolymer based drug delivery systems. RSC advances, 13(33), 23087-23121.

Fu, X., & Li, H. (2009). Mesenchymal stem cells and skin wound repair and regeneration: possibilities and questions. Cell and tissue research, 335(2), 317-321.

Ganguly, S., Das, P., & Das, N. C. (2020). Characterization tools and techniques of hydrogels. In Hydrogels Based on Natural Polymers (pp. 481-517). Elsevier.

Gauglitz, G. G., Korting, H. C., Pavicic, T., Ruzicka, T., & Jeschke, M. G. (2011). Hypertrophic scarring and keloids: pathomechanisms and current and emerging treatment strategies. Molecular medicine (Cambridge, Mass.), 17(1-2), 113–125. https://doi.org/10.2119/molmed.2009.00153

Guo, L., Sato, H., Hashimoto, T., & Ozaki, Y. (2010). FTIR study on hydrogen-bonding interactions in biodegradable polymer blends of poly (3-hydroxybutyrate) and poly (4-vinylphenol). Macromolecules, 43(8), 3897-3902.

Guo, S., & Dipietro, L. A. (2010). Factors affecting wound healing. Journal of dental research, 89(3), 219–229. https://doi.org/10.1177/0022034509359125

Gurtner, G. C., Werner, S., Barrandon, Y., & Longaker, M. T. (2008). Wound repair and regeneration. Nature, 453(7193), 314-321.

Halder, A., Maiti, A., Dinda, S., Bhattacharya, B., & Ghoshal, D. (2021). Unraveling the Role of Structural Dynamism in Metal Organic Frameworks (MOF) for Excited-State Intramolecular Proton Transfer (ESIPT) Driven Water Sensing. Crystal Growth & Design, 21(11), 6110-6118.

Hamad, A., & Hartanti, D. (2023, June). Effects of extraction time on total phenolic and flavonoid contents and antioxidant activities of a polyherbal drink. In IOP Conference Series: Earth and Environmental Science (Vol. 1200, No. 1, p. 012047). IOP Publishing.

Hamidi, M., Azadi, A., & Rafiei, P. (2008). Hydrogel nanoparticles in drug delivery. Advanced drug delivery reviews, 60(15), 1638-1649.

Han G, Ceilley R (2017) Chronic wound healing: a review of current management and treatments. Adv. ther 34: 599–610.

Herman, T. F., & Bordoni, B. (2020). Wound classification.

Hssaini, L., Razouk, R., & Bouslihim, Y. (2022). Rapid prediction of fig phenolic acids and flavonoids using mid-infrared spectroscopy combined with partial least square regression. Frontiers in Plant Science, 13, 429.

Hu X, Wang K, Yu M, He P, Qiao H, Zhang H, Wang Z (2019) Characterization and Antioxidant Activity of a Low-Molecular-Weight Xanthan Gum. Biomolecules 9(11): 730.

Huang, Y., Bai, L., Yang, Y., Yin, Z., & Guo, B. (2022). Biodegradable gelatin/silver nanoparticle composite cryogel with excellent antibacterial and antibiofilm activity and hemostasis for Pseudomonas aeruginosa-infected burn wound healing. Journal of Colloid and Interface Science, 608, 2278-2289.

Jaiswal L, Shankar S, Rhim JW (2019) Carrageenan-based functional hydrogel film reinforced with sulfur nanoparticles and grapefruit seed extract for wound healing application. Carbohydr.Polym 224: 115191.

Jani, G. K., & Shah, D. P. (2008) Evaluation of mucilage of Hibiscus rosasinensis Linn as rate controlling matrix for sustained release of diclofenac. Drug development and industrial pharmacy, 34(8), 807-816

Jin S. G. (2022). Production and Application of Biomaterials Based on Polyvinyl alcohol (PVA) as Wound Dressing. Chemistry, an Asian journal, 17(21), e202200595. https://doi.org/10.1002/asia.202200595

Kaihara, S., Matsumura, S., & Fisher, J. P. (2008). Synthesis and characterization of cyclic acetal based degradable hydrogels. European journal of pharmaceutics and biopharmaceutics, 68(1), 67-73.

Kalantari, K., Mostafavi, E., Saleh, B., Soltantabar, P., & Webster, T. J. (2020) Chitosan/PVA hydrogels incorporated with green synthesized cerium oxide nanoparticles for wound healing applications. European Polymer Journal, 134, 109853

Kaleemullah, M., Jiyauddin, K., Thiban, E., Rasha, S., Al-Dhalli, S., Budiasih, S., ...& Eddy, Y. (2017) Development and evaluation of Ketoprofen sustained release matrix tablet using Hibiscus rosa-sinensis leaves mucilage. Saudi pharmaceutical journal, 25(5), 770-779

Kashyap, N. K. M. R. K. N., Kumar, N., & Kumar, M. R. (2005). Hydrogels for pharmaceutical and biomedical applications. Critical Reviews™ in Therapeutic Drug Carrier Systems, 22(2).

Kassakul, W., Praznik, W., Viernstein, H., Hongwiset, D., Phrutivorapongkul, A., &Leelapornpisid, P. (2014) Characterization of the mucilages extracted from hibiscus rosa-sinensislinn and hibiscus mutabilislinn and their skin moisturizing effect. Int J Pharm PharmSci, 6(11), 453-7

Kassem, I. A., Ashaolu, T. J., Kamel, R., Elkasabgy, N. A., Afifi, S. M., & Farag, M. A. (2021). Mucilage as a functional food hydrocolloid: Ongoing and potential applications in prebiotics and nutraceuticals. Food & function, 12(11), 4738-4748.

Kolhe, S., Kasar, T., Dhole, S. N., & Upadhye, M. (2014). Extraction of mucilage and its comparative evaluation as a binder. American Journal of Advanced Drug Delivery, 2(3), 330-343.

Krzyszczyk, P., Schloss, R., Palmer, A., & Berthiaume, F. (2018) The Role of Macrophages in Acute and Chronic Wound Healing and Interventions to Promote Pro-wound Healing Phenotypes. Frontiers in physiology, 9, 419 https://doi.org/10.3389/fphys.2018.00419

Lai, W. F., & Rogach, A. L. (2017). Hydrogel-based materials for delivery of herbal medicines. ACS applied materials & interfaces, 9(13), 11309-11320.

Landén, N. X., Li, D., & Ståhle, M. (2016). Transition from inflammation to proliferation: a critical step during wound healing. Cellular and molecular life sciences : CMLS, 73(20), 3861–3885. https://doi.org/10.1007/s00018-016-2268-0

LaPelusa, A., & Dave, H. D. (2019). Physiology, hemostasis.

Lee K, Lee B, Lee MH, Kim B, Chinannai KS, Ham I, Choi HY (2015) Effect of Ampelopsis Radix on wound healing in scalded rats. BMC Complement Altern Med. 15(1): 1-9.

Lengyel, M., Kállai-Szabó, N., Antal, V., Laki, A. J., & Antal, I. (2019). Microparticles, Microspheres, and Microcapsules for Advanced Drug Delivery. Scientia Pharmaceutica, 87(3), 20. MDPI AG. Retrieved from http://dx.doi.org/10.3390/scipharm87030020

Li, H., & Wang, F. (2021).Core-shell chitosan microsphere with antimicrobial and vascularized functions for promoting skin wound healing. Materials & Design, 204, 109683

Liu, W., Ou-Yang, W., Zhang, C., Wang, Q., Pan, X., Huang, P., ... & Wang, W. (2020). Synthetic polymeric antibacterial hydrogel for methicillin-resistant staphylococcus aureus-infected wound healing: nanoantimicrobial self-assembly, drug-and cytokine-free strategy. ACS nano, 14(10), 12905-12917.

Liu, W., Yu, M., Xie, D., Wang, L., Ye, C., Zhu, Q., ...& Yang, L (2020) Melatonin-stimulated MSC-derived exosomes improve diabetic wound healing through regulating macrophage M1 and M2 polarization by targeting the PTEN/AKT pathway. Stem cell research & therapy, 11, 1-15

Lu, J., Fan, X., Hu, J., Li, J., Rong, J., Wang, W., ... & Chen, Y. (2023). Construction and function of robust and moist bilayer chitosan-based hydrogel wound dressing. Materials & Design, 226, 111604.

Mahale, M. M., & Saudagar, R. B. (2019). Microsphere: a review. Journal of drug delivery and therapeutics, 9(3-s), 854-856.

Mak YW, Chuah LO, Ahmad R, Bhat R (2013) Antioxidant and antibacterial activities of hibiscus (Hibiscus rosa-sinensis L.) and Cassia (Senna bicapsularis L.) flower extracts. J King Saud Univ-Sci. 25(4): 275-282.

Mathew-Steiner, S. S., Roy, S., & Sen, C. K. (2021). Collagen in wound healing. Bioengineering, 8(5), 63.

Mekkawy, A. I., El-Mokhtar, M. A., El-Shanawany, S. M., & Ibrahim, E. H. (2016). Silver nanoparticles-loaded hydrogels, a potential treatment for resistant bacterial infection and wound healing: A review. British Journal of Pharmaceutical Research, 14(2), 1-19.

Michalik, L., Desvergne, B., Tan, N. S., Basu-Modak, S., Escher, P., Rieusset, J., ... & Wahli, W. (2001). Impaired skin wound healing in peroxisome proliferator–activated receptor (PPAR) α and PPAR β mutant mice. The Journal of cell biology, 154(4), 799-814.

Moholkar, D. N., Sadalage, P. S., Peixoto, D., Paiva-Santos, A. C., &Pawar, K. D. (2021) Recent advances in biopolymer-based formulations for wound healing applications. Eur. Polym. J, 160, 110784

Mohsin A, Zhang K, Hu J, Tariq M, Zaman WQ, Khan IM, Zhuang Y, Guo M (2018) Optimized biosynthesis of xanthan via effective valorization of orange peels using response surface methodology: A kinetic model approach. CarbohydrPolym 181:793-800

Mukherjee, R., Dutta, D., Patra, M., Chatterjee, B., & Basu, T. (2019). Nanonized tetracycline cures deadly diarrheal disease 'shigellosis' in mice, caused by multidrug-resistant Shigella flexneri 2a bacterial infection. Nanomedicine: Nanotechnology, Biology and Medicine, 18, 402-413.

Murray RZ, West ZE, Cowin AJ, &Farrugia BL (2019) Development and use of biomaterials as wound healing therapies, Burns Trauma 7, 2.

Nasir, M. A., Mahammed, N. L., Roshan, S., & Ahmed, M. W. (2016). Wound healing activity of poly herbal formulation in albino rats using excision wound model, incision wound model, dead space wound model and burn wound model. Int. J. Res. Dev. Pharm. L. Sci, 5(2), 2080-2087.

Nguyen, H. M., Ngoc Le, T. T., Nguyen, A. T., Thien Le, H. N., & Pham, T. T. (2023). Biomedical materials for wound dressing: recent advances and applications. RSC advances, 13(8), 5509–5528. https://doi.org/10.1039/d2ra07673j

Niknam, S., Tofighi, Z., Faramarzi, M. A., Abdollahifar, M. A., Sajadi, E., Dinarvand, R., & Toliyat, T. (2021). Polyherbal combination for wound healing: Matricaria chamomilla L. and Punica granatum L. DARU Journal of Pharmaceutical Sciences, 29, 133-145.

Ofokansi KC, Kenechukwu FC, Ezugwu RO, Attama AA (2016) Improved dissolution and anti-inflammatory activity of ibuprofen-polyethylene glycol 8000 solid dispersion systems. Inter J pharm Investing 6(3):139.

Okunlola, A., Odeniyi, M. A., & Arhewoh, M. I. (2020). Microsphere formulations of ambroxol hydrochloride: influence of Okra (Abelmoschus esculentus) mucilage as a sustained release polymer. Progress in biomaterials, 9, 65-80.

Okur, M. E., Karantas, I. D., Şenyiğit, Z., Okur, N. Ü., & Siafaka, P. I. (2020). Recent trends on wound management: New therapeutic choices based on polymeric carriers. Asian Journal of Pharmaceutical Sciences, 15(6), 661-684.

Oliveira, R. N., Mancini, M. C., Oliveira, F. C. S. D., Passos, T. M., Quilty, B., Thiré, R. M. D. S. M., & McGuinness, G. B. (2016). FTIR analysis and quantification of phenols and flavonoids of five commercially available plants extracts used in wound healing. Matéria (Rio de Janeiro), 21, 767-779.

Ozcelik, B. (2016). Degradable hydrogel systems for biomedical applications. In Biosynthetic Polymers for Medical Applications (pp. 173-188). Woodhead Publishing.

ÖzdemirDinç C, Güner A (2017) Solid-State Characterization of Poly (ethylene glycol) Samples Prepared By Solvent Cast Technique, Bulg. Chem. Commun. 49(I): 15-20.

Patel, A. M., Kurbetti, S. M., Savadi, R. V., Thorat, V., Takale, V., & Horkeri, S. (2013). Preparation and evaluation of wound healing activity of new polyherbal formulations in rats. American Journal of Phytomedicine and Clinical Therapeutics, 1(6), 498-506.

Patel, N. R., Patel, D. A., Bharadia, P. D., Pandya, V., & Modi, D. (2011). Microsphere as a novel drug delivery. International Journal of Pharmacy & Life Sciences, 2(8).

Perchyonok, V. T. (2017). Copazan Oral Gel and Wound Healing In Vitro: Assessment of the Functional Biomaterial. EC Dental Science, 14, 185-192.

Philip, D. (2010). Green synthesis of gold and silver nanoparticles using Hibiscus rosa sinensis. Physica E: Low-Dimensional Systems and Nanostructures, 42(5), 1417-1424.

Potara, M., Bawaskar, M., Simon, T., Gaikwad, S., Licarete, E., Ingle, A., ... & Rai, M. (2015). Biosynthesized silver nanoparticles performing as biogenic SERS-nanotags for investigation of C26 colon carcinoma cells. Colloids and Surfaces B: Biointerfaces, 133, 296-303.

Puca, V., Marulli, R. Z., Grande, R., Vitale, I., Niro, A., Molinaro, G., Prezioso, S., Muraro, R., & Di Giovanni, P. (2021). Microbial Species Isolated from Infected Wounds and Antimicrobial Resistance Analysis: Data Emerging from a Three-Years Retrospective Study. Antibiotics (Basel, Switzerland), 10(10), 1162. https://doi.org/10.3390/antibiotics10101162

Purushothaman A, Meenatchi P, Saravanan S, Sundaram R, Saravanan N (2016) Quantification of total phenolic content, HPLC analysis of flavonoids and assessment of antioxidant and anti-haemolytic activities of Hibiscus rosa-sinensis L. flowers in vitro. Int. J Pharma Res Health Sci 4(5): 1342-1350

Ramamoorthy, R., Andra, S., kumar Balu, S., Damiri, F., Andiappan, M., Muthalagu, M., & Berrada, M. (2023). Flavonoids, phenolics, and tannins loaded polycaprolactone nanofibers (NF) for wound dressing applications. *Results in Materials*, *18*, 100407.

Reinke, J. M., & Sorg, H. (2012). Wound repair and regeneration. European surgical research, 49(1), 35-43.

Rezaei, M., Dadgar, Z., Noori-Zadeh, A., Mesbah-Namin, S. A., Pakzad, I., & Davodian, E. (2015). Evaluation of the antibacterial activity of the Althaea officinalis L. leaf extract and its wound healing potency in the rat model of excision wound creation. Avicenna journal of phytomedicine, 5(2), 105–112.

Ruffo, M., Parisi, O. I., Dattilo, M., Patitucci, F., Malivindi, R., Pezzi, V., ... & Puoci, F. (2022). Synthesis and evaluation of wound healing properties of hydro-diab hydrogel loaded with green-synthetized AGNPS: In vitro and in ex vivo studies. Drug Delivery and Translational Research, 12(8), 1881-1894.

Saxena, A. K. (2010). Synthetic biodegradable hydrogel (PleuraSeal) sealant for sealing of lung tissue after thoracoscopic resection. The Journal of thoracic and cardiovascular surgery, 139(2), 496-497.

Schäfer, M., & Werner, S. (2007). Transcriptional control of wound repair. Annu. Rev. Cell Dev. Biol., 23, 69-92.

Schieber, M., & Chandel, N. S. (2014) ROS function in redox signaling and oxidative stress. Current biology: CB, 24(10), R453–R462 https://doi.org/10.1016/j.cub.2014.03.034

Schultz, G. S., Chin, G. A., Moldawer, L., & Diegelmann, R. F. (2011). 23 principles of wound healing. Mechanisms of vascular disease: a reference book for vascular specialists, 423.

Serpico, L., Dello Iacono, S., Cammarano, A., & De Stefano, L. (2023). Recent Advances in Stimuli-Responsive Hydrogel-Based Wound Dressing. Gels, 9(6), 451. MDPI AG. Retrieved from http://dx.doi.org/10.3390/gels9060451

Shaikh, S., Nazam, N., Rizvi, S. M. D., Ahmad, K., Baig, M. H., Lee, E. J., & Choi, I. (2019). Mechanistic insights into the antimicrobial actions of metallic nanoparticles and their implications for multidrug resistance. International journal of molecular sciences, 20(10), 2468.

Sharma R, Kaith BS, Kalia S, Pathania D, Kumar A, Sharma N, Schauer C (2015) Biodegradable and conducting hydrogels based on Guar gum polysaccharide for antibacterial and dye removal applications. J Environ manage 162: 37-45.

Sharma, B. R., Harish, D., Singh, V. P., & Bangar, S. (2006). Septicemia as a cause of death in burns: an autopsy study. Burns, 32(5), 545-549.

Shen HM, Chen C, Jiang JY, Zheng YL, Cai WF, Wang B, Lind Z,Tang L, Wang YH, Shi GG (2017) The N-butyl alcohol extract from Hibiscus rosa-sinensis L. flowers enhances healing potential on rat excisional wounds, J Ethnopharmacol 198(23) : 291-301.

Shivananda Nayak B, Sivachandra Raju S, Orette FA, Chalapathi Rao AV (2007) Effects of Hibiscus rosa sinensis L (Malvaceae) on wound healing activity: a preclinical study in a Sprague Dawley rat. Int. J. Low. Extrem. Wounds 6(2).

Siddiqui, A. H., & Koirala, J. (2018). Methicillin resistant Staphylococcus aureus.

Singh, A., Sharma, P. K., Garg, V. K., & Garg, G. (2010). Hydrogels: A review. Int J Pharm Sci Rev Res, 4(2), 97-105.

Singh, V., Marimuthu, T., Makatini, M. M., & Choonara, Y. E. (2022). Biopolymer-Based Wound Dressings with Biochemical Cues for Cell-Instructive Wound Repair. Polymers, 14(24), 5371.

Snyder, R. J., Driver, V., Fife, C. E., Lantis, J., Peirce, B., Serena, T., & Weir, D. (2011). Using a diagnostic tool to identify elevated protease activity levels in chronic and stalled wounds: a consensus panel discussion. Ostomy/wound management, 57(12), 36-46.

Stashak, T. S., Farstvedt, E., & Othic, A. (2004). Update on wound dressings: indications and best use. Clinical Techniques in Equine Practice, 3(2), 148-163.

Sun, X., Zhang, G., Shi, Q., Tang, B., & Wu, Z. J. (2002). Preparation and characterization of water-swellable natural rubbers. J Appl Polym Sci, 86, 3212-717.

Sung JH, Hwang RM, Kim JO, Lee HJ, Kim JH, Kim YI, Han SS (2010) Gel characterisation and in vivo evaluation of minocycline-loaded wound dressing with enhanced wound healing using polyvinyl alcohol and chitosan. Inter J pharm 392(1-2): 232-240.

Talekar, Y. P., Apte, K. G., Paygude, S. V., Tondare, P. R., & Parab, P. B. (2017). Studies on wound healing potential of polyherbal formulation using in vitro and in vivo assays. Journal of Ayurveda and integrative medicine, 8(2), 73–81. https://doi.org/10.1016/j.jaim.2016.11.007

Tam, J. C. W., Ko, C. H., Lau, K. M., To, M. H., Kwok, H. F., Chan, Y. W., ... & Bik-San Lau, C. (2014). A Chinese 2-herb formula (NF3) promotes hindlimb ischemia-induced neovascularization and wound healing of diabetic rats. Journal of Diabetes and its Complications, 28(4), 436-447.

Teng, Y., Fan, Y., Ma, J., Lu, W., Liu, N., Chen, Y., ... & Tao, X. (2021) The PI3K/Akt pathway: emerging roles in skin homeostasis and a group of non-malignant skin disorders. Cells, 10(5), 1219

Ter Horst, B., Chouhan, G., Moiemen, N. S., & Grover, L. M. (2018) Advances in keratinocyte delivery in burn wound care. Advanced drug delivery reviews, 123, 18-32

Tonnesen, M. G., Feng, X., & Clark, R. A. (2000) Angiogenesis in wound healing. In Journal of investigative dermatology symposium proceedings (Vol. 5, No. 1, pp. 40-46)

Tosif, M. M., Najda, A., Bains, A., Kaushik, R., Dhull, S. B., Chawla, P., & Walasek-Janusz, M. (2021). A Comprehensive Review on Plant-Derived Mucilage: Characterization, Functional Properties, Applications, and Its Utilization for Nanocarrier Fabrication. Polymers, 13(7), 1066. https://doi.org/10.3390/polym13071066

Tyagi, S., Sharma, N., Gupta, S. K., Sharma, A., Bhatnagar, A., Kumar, N., & Kulkarni, G. T (2015) Development and gamma scintigraphical clearance study of novel Hibiscus rosasinensis polysaccharide based mucoadhesive nasal gel of rizatriptan benzoate. Journal of Drug Delivery Science and Technology, 30, 100-106

Valli, J. S., & Vaseeharan, B. (2012). Biosynthesis of silver nanoparticles by Cissus quadrangularis extracts. Materials Letters, 82, 171-173.

Vignesh, R. M., & Nair, B. R. (2018) A study on the antioxidant and antibacterial potential of the mucilage isolated from Hibiscus rosa-sinensis Linn. (Malvaceae). Journal of Pharmacognosy and Phytochemistry, 7(2), 1633-1637

Vignesh, R. M., & Nair, B. R. (2018) Extraction and Characterisation of mucilage from the leaves of Hibiscus rosa-sinensis Linn. (Malvaceae). International Journal of Pharmaceutical Sciences and Research, 6(2), 542-555

Wichterle, O., & Lim, D. (1960). Hydrophilic gels for biological use. Nature, 185(4706), 117-118.

World Health Organization. (2022). Report signals increasing resistance to antibiotics in bacterial infections in humans and need for better data.

Wynn, T. A., & Ramalingam, T. R. (2012). Mechanisms of fibrosis: therapeutic translation for fibrotic disease. Nature medicine, 18(7), 1028–1040. https://doi.org/10.1038/nm.2807

Xiang, J., Shen, L., & Hong, Y. (2020). Status and Future Scope of Hydrogels in Wound Healing: Synthesis, Materials and Evaluation. European Polymer Journal, 109609.

Yang, C., Zhang, Z., Gan, L., Zhang, L., Yang, L., & Wu, P. (2023). Application of Biomedical Microspheres in Wound Healing. International journal of molecular sciences, 24(8), 7319. https://doi.org/10.3390/ijms24087319

Zeng, Z. P., & Jiang, J. G. (2010). Analysis of the adverse reactions induced by natural product-derived drugs. British journal of pharmacology, 159(7), 1374–1391. https://doi.org/10.1111/j.1476-5381.2010.00645.x

Zhang Q, Hu XM, Wu MY, Wang MM, Zhao YY, Li TT (2019) Synthesis and performance characterization of poly (vinyl alcohol)-xanthan gum composite hydrogel. React FunctPolym 136: 34-43.

List of Publications

Thesis related publications

PATENT

- Indian patent: Fabrication of green silver nanoparticle-embedded microsphere and therapeutic activity against bacteria-infected burn and excision wound. **Ishita Saha**, Parimal Karmakar, Sourav Ghosh, Tarakdas Basu; Publication Date: 10/02/2023; Application No.202331006688 A.

PUBLICATIONS

- **Saha, I**., Ghosh S., Mondal A., Roy, S., Basu, T., Sengupta, A., Das, D. & Karmakar, P. (2024). Fabrication and Drug Delivery Process of Green Silver Nanoparticle Embedded Mucilage Microsphere for Pathogenic Bacteria Infected Second-Degree Burn and Excision Wound Healing. *ACS Applied Bio Materials,* https://doi.org/10.1021/acsabm.4c00177

- **Saha, I.,** Ghosh, S., Roy, S., Basu, T., & Karmakar, P. (2024). Facile process of hibiscus mucilage polymer formulation using hibiscus rosa-sinensis leaves to treat second-degree burn and excision wound. Biomedical Materials.

- **Saha, I**., Roy, S., Das, D., Das, S., & Karmakar, P. (2023). Topical effect of polyherbal flowers extract on xanthan gum hydrogel patch—induced wound healing activity in human cell lines and male BALB/c mice. *Biomedical Materials*, *18*(3), 035016.

Other Publications

- Ghosh, B., Roy, S., Bardhan, S., Mondal, D., **Saha, I.**, Ghosh, S., ... & Das, S. (2022). Biocompatible carbon dot decorated α-FeOOH nanohybrid for an effective fluorometric sensing of Cr (VI) in wastewater and living cells. *Journal of Fluorescence*, *32*(4), 1489-1500.

- Bardhan, S., Roy, S., Das, S., **Saha, I**., Mondal, D., Roy, J., ... & Das, S. (2022). Real-time sensitive detection of Cr (VI) in industrial wastewater and living cells using carbon dot decorated natural kyanite nanoparticles. *Spectrochimica Acta Part A: Molecular and Biomolecular Spectroscopy*, *273*, 121061.

- Mohammad, M., **Saha, I**., Pal, K., Karmakar, P., Pandya, P., Gazi, H. A. R., & Islam, M. M. (2022). A comparison on the biochemical activities of Fluorescein disodium, Rose Bengal and Rhodamine 101 in the light of DNA binding, antimicrobial and cytotoxic study. *Journal of Biomolecular Structure and Dynamics*, *40*(20), 9848-9859.

- Roy, S., Bardhan, S., Mondal, D., **Saha, I**., Roy, J., Das, S., ... & Das, S. (2021). Polymeric carbon dot/boehmite nanocomposite made portable sensing device (Kavach) for non-invasive and selective detection of Cr (VI) in wastewater and living cells. *Sensors and Actuators B: Chemical*, *348*, 130662.

- Al Masum, A., Pal, K., **Saha, I**., Ghosh, D., Roy, S., Chowdhury, S. G., ... & Karmakar, P. (2020). Facile synthesis of antibiotic encapsulated biopolymeric okra mucilage nanoparticles: molecular docking, in vitro stability and functional evaluation. *Advances in Natural Sciences: Nanoscience and Nanotechnology*, *11*(2), 025020.

BOOK CHAPTER

- **Saha, I**., Karmakar, P., & Bhattacharya, D. (2023). Fungi-Mediated Fabrication of Copper Nanoparticles and Copper Oxide Nanoparticles, Physical Characterization and Antimicrobial Activity. Mycosynthesis of Nanomaterials: Perspectives and Challenges, 112.

CONFERENCES / PRESENTATIONS

Oral

- India International Science Festival, India: Development Of Biopolymeric Hydrogel Matrix For Delivery Of Herbal Excipient In Chronic Wound. **Saha. I**, Karmakar. P, 2020

Poster

- 3rd International Conference on "Frontiers in Biological Sciences" Organized by the Department of Life Science, NIT Rourkela, India. Fabrication of green silver nanoparticle embedded mucilage microsphere and therapeutic activity against pathogenic bacteria infected second-degree burn and excision wound. **Saha. I**, Karmakar. P, 2023
- International Conference On Molecular & 4th Cesin Symposium: Signaling In Disease Management & Diagnostics. India.Topical Effect of Polyherbal Flower Extract Encapsulated Hydrogel Patch - Induced Cell Proliferation and Wound Healing Activity In Human Cell Lines And Male BALB/C Mice. **Saha. I**, Karmakar. P, 2023
- International Seminar On Emerging Fields of Research In Biotechnology & Biomedicine, India: Fabrication And Wound Healing Activity Of Polyherbal Extract Encapsulated Biopolymeric Xanthan Gum Based Hydrogel Patch: An In-Vitro And In-Vivo Study. **Saha. I**, Karmakar. P, 2022
- BIOCOM, India: Synthesis of Biocompatible and Biodegradable Herbal Excipient Encapsulated Natural Polymeric Gum Acacia Hydrogel for Wound Healing. **Saha. I**, Karmakar. P, 2021
- BIOCOM, India: Development of Biopolymeric Hydrogel Matrix for Delivery Of Herbal Excipient In Chronic Wound. **Saha. I**, Karmakar. P, 2020
- Association Of Indian Universities, New Delhi & Jadavpur University, ANVESHAN 2019-20(East Zone), Development Biocompatible Natural Polymers Advanced Delivery System Of Herbal Excipient. **Saha. I**, Karmakar. P, 2020

- UGC –SAP (DRS II)-Sponsored National Symposium On Modern Perspectives of Research & Development In Biochemistry And Biophysics, India. **Saha. I**, Karmakar. P, 2019

- International Symposium On Frontiers in Development & Molecular Medicine: Models to Insights. India:Development of Biopolymeric Hydrogel Matrix for Delivery of Herbal Excipient In Chronic Wound. **Saha. I**, Karmakar. P, 2019

BEST POSTER AWARDS

- BIOCOM 2021, Best Poster Award (3rd prize), 2021.

- International Seminar On Emerging Fields of Research In Biotechnology & Biomedicine, Best Poster Award (1st prize), 2022.

- 3rd International Conference on "Frontiers in Biological Sciences" Organized by the Department of Life Science, NIT Rourkela, Best Poster Award (3rd prize), 2023.

Biomedical Materials

PAPER

Topical effect of polyherbal flowers extract on xanthan gum hydrogel patch–induced wound healing activity in human cell lines and male BALB/c mice

Ishita Saha[1], Shubham Roy[3], Deepak Das[2], Sukhen Das[3] (ID) and Parimal Karmakar[1,*] (ID)

[1] Department of Life Science and Biotechnology, Jadavpur University, 188, Raja S.C. Mullick Road, Kolkata 700032, West Bengal, India
[2] GLA University, 17 km Stone, NH-2, Mathura—Delhi Road P.O. Chaumuhan, Mathura 281406, U.P., India
[3] Department of Physics, Jadavpur University, 188, Raja S.C. Mullick Road, Kolkata 700032, West Bengal, India
[*] Author to whom any correspondence should be addressed.

E-mail: pkarmakar_28@yahoo.co.in

Abstract

Wound or injury is a breakdown in the skin's protective function as well as damage to the normal tissues. Wound healing is a dynamic and complex phenomenon of replacing injured skin or body tissues. In ancient times the *Calendula officinalis* and *Hibiscus rosa-sinensis* flowers were extensively used by the tribal communities as herbal medicine for various complications including wound healing. But loading and delivery of such herbal medicines are challenging because it maintains their molecular structure against temperature, moisture, and other ambient factors. This study has fabricated xanthan gum (XG) hydrogel through a facile process and encapsulated *C. officinalis* and *H. rosa-sinensis* flower extract. The resulting hydrogel was characterized by different physical methods like x-ray diffractometer, UV–vis spectroscopy, Fourier transform infrared spectroscopy, SEM, dynamic light scattering, electronkinetic potential in colloidal systems (ZETA) potential, thermogravimetric differential thermal analysis (TGA-DTA), etc. The polyherbal extract was phytochemically screened and observed that flavonoids, alkaloids, terpenoids, tannins, saponins, anthraquinones, glycosides, amino acids, and a few percentages of reducing sugar were present in the polyherbal extract. Polyherbal extract encapsulated XG hydrogel (X@C–H) significantly enhanced the proliferation of fibroblast and keratinocyte cell lines in comparison to the bare excipient treated cells as determined by 3-(4, 5-dimethylthiazol-2-Yl)-2, 5-diphenyltetrazolium bromide assay. Also, the proliferation of these cells was confirmed by BrdU assay and enhanced expression of pAkt. In an *in-vivo* study, wound healing activity of BALB/c mice was carried out and we observed that X@C–H hydrogel showed significant result compared to the other groups (untreated, X, X@C, X@H). Henceforth, we conclude that this synthesized biocompatible hydrogel could emerge as a promising carrier of more than one herbal excipients.

1. Introduction

The wound is divided into acute (large skin injuries, burn, etc) and chronic (diabetes foot ulcers) wounds, and chronic wound represents a significant health problem worldwide (Han and Ceilley 2017). Wound healing is a complex step-wise dynamic process that recovered the damaged tissue through four different phases: hemostasis, inflammation, proliferation, and remodeling (Amsden 2015, Alibolandi *et al* 2017). Over the past few years, different types of wound

healing agents including some plant products have been found which are helpful for promoting and regeneration of wounded tissue (El-aie *et al* 2015). Biomaterials are the most important factors for stimulating and promoting wound healing. The damaged tissue is a favorable habitat for microorganisms like *Pseudomonas aeruginosa, Klebsiella pneumonia, Acinetobacter baumannii, Staphylococcus aureus*, and *Enterococcus faecalis*, it reduces the wound healing potential. Polymeric biomaterials can be used to protect the wounded portion from pathogens, hydrate

the wound, and enhanced the wound healing activity. That is why plant extract, antibacterial agents, or extracellular components incorporated in polymeric biomaterials are induced granulation tissue formation in the wounded area (Das and Baker 2016, Murray *et al* 2019). Biomedical research field become an emerging and promising sector for drug delivery systems, through the development of biopolymeric materials from natural sources. Hydrogel is one type of three-dimensional hydrophilic network composed of polymeric chains, it is linked by various physical or chemical bonds like covalent bonds, hydrogen bonds, and van der Waals interactions. Recently hydrogel was used for wound dressing materials because of their excessive water or exudates absorbing capacity, facilitating gas exchange, non-adherence, maintaining a moist environment, and capability of releasing bioactive compounds (Jaiswal *et al* 2019). The hydrogel is an essential homopolymer or utilizes various synthetic monomers for its synthesis such as poly (acrylate acid), poly (ethylene glycol) (PEG), poly (vinyl alcohol) (PVA), etc (Hoare and Kohane 2008). Natural hydrogels have been synthesized from natural sources such as collagen, fibrin, gelatin, agarose, alginate, xanthan, pectin, guar gum, gum arabic, starch, heparin, alginate, chitin, chitosan, etc (Sharma *et al* 2015). Xanthan gum (XG) is a macromolecular polysaccharide; it is isolated from *Xanthomonas campestris*. XG is composed of a β-1, 4-glycosidic bond, and a side chain trisaccharide which contains glucuronic acid, citric acid, and mannose. XG is a biocompatible, biodegradable, cost-effective natural polysaccharide; it is widely used as a thickener, rheological modifier, stabilizer, emulsifier in food, cosmetic, pharmaceutical, textile, and oil recovery industries (Hu *et al* 2019). It also shows a special type of chemical structure, excellent pour ability, thickening, and rheological properties, and is highly stable to heat, acid, and alkali conditions. Hydroxyl groups and carboxyl groups are cross-linked with citric acid and generate ester bonds, forming a chemical hydrogel with a porous structure that renders its high absorbance capacity.

Different types of natural herbal products such as *Aloe vera, Punica granatum* Linn, *Curcuma zedoaria, Azadirachta indica*, etc are already tested for wound healing activity. But molecular pathways associated with a different phase of wound healing and modulation of the factors involved in the signaling by plant products are partially explored. For example, improved vascularization, granulation tissue formation, re-epithelization, and collagen deposition were observed by the extract of *Ampelopsis japonica* (Lee *et al* 2015). PI3K-dependent proliferation and migration of fibroblast were observed by the flower extracts of *Calendula officinalis* (Dinda *et al* 2015). Additionally, in *in-vivo* experiments, it stimulates granulation tissue formation by altering

the expression of α-smooth muscle actin as well as connective tissue growth factor in excisional wounds of BALB/c mice (Dinda *et al* 2016). Thus, different plant products act differentially on the healing process encompassing the promotion of some specific stage. Thus, the use of a polyherbal mixture comprising more than one plant product is necessary. For example, the root of *Astragalus propinquus* and *Rehmannia glutinosa* reduce oxidative stress and induce angiogenesis in diabetic mice (Tam *et al* 2014). In addition to angiogenesis, improving tissue granulation, induces re-epithelialization and collagen synthesis by the herbal mixture of *Alchemilla vulgaris* and *Mimosa tenuiflora* (Choi *et al* 2018). The herbal extract of *Vitex negundo* L. (VN), *Tridax procumbens L.* (TP), and *Emblica officinalis* Gaertn. (EO) promote wound healing by proliferation and migration of fibroblast and keratinocytes at the affected sites (Talekar *et al* 2017). Thus, combinations derived from plant products are needed to explore further for proper management of wounds without any side effects. Moreover, the proper delivery of such agents needs to be explored scientifically.

In such an effort, we have used two herbal flower excipients *C. officinalis* and *Hibiscus rosa-sinensis*. These two are utilized medicinally either in the form of ointments, tinctures, infusions, creams, or liquid extracts. The extract compasses different types of components like polysaccharides, flavonoids, triterpene alcohols, phenol acids, tannins, glycosides, sterols, carotenoids, saponosides, etc. The wound healing activity of Calendula has been documented previously (Khairnar *et al* 2013). A total of 250 species of Hibiscus are widely distributed in tropical and subtropical regions of different countries and have various medicinal properties including antitumor, antihypertensive, and antioxidant properties (Purushothaman *et al* 2016, Shedoeva *et al* 2019). The leaves and flowers promote hair growth and aid in the healing of ulcers (Bhaskar and Nithya 2012). The herbal extracts contain major flavonoid constituents like rutin and quercetin which are suggested to have significant proliferative activities (Almeida *et al* 2015, Doersch and Newell-Rogers 2017). Additionally, for controlled and localized delivery we have synthesized herbal excipient encapsulated XG hydrogel patch and evaluated its physical as well as biological activities. We observed that the synthesized hydrogel polymer also helped with the sustained release of polyherbal excipients from the patch. We also found polyherbal excipient encapsulated biopolymeric hydrogel patch stimulate the proliferation, migration, and epithelization of human lung fibroblast (WI-38) and human keratinocyte (HaCaT) cell lines compared to free herbal excipient treated cells. In an *in-vivo* experiment, we topically applied X, X@C, X@H, and X@C–H hydrogel in an excision wound of BALB/c mice, and observed that X@C–H is more effective in

wound healing compared to a bare excipient or single excipient loaded hydrogel. Thus this biocompatible XG hydrogel is a potential vehicle for the delivery of herbal excipients for wound healing. Studies using hydrogel for the delivery of wound healing agents are limited. One step further we have loaded poly-herbal excipients for successful delivery in wounds and tested their potential *in vivo* experiments.

Our study highlighted the loading of the much-needed polyherbal extract on XG hydrogel, and through *in vitro* and *in vivo* studies we demonstrated the efficacy of such synthesized materials in wound healing. Reports are available about the loading of a single herbal product in hydrogel and only *in vivo* studies were conducted (Rubio-Elizalde *et al* 2019, Elegbede *et al* 2020, Wang *et al* 2020, Najafpour *et al* 2022, Rathod *et al* 2022). Additionally, the thermally stable, smaller size, and sustained release of hydrogel make it an ideal delivery agent for wound healing, particularly polyherbal excipients.

2. Materials and methods

XG (approx. MW 300 kDa), MTT (3-(4, 5-dimethylthiazol-2-Yl)-2, 5-diphenyltetrazolium bromide), phosphate buffer saline (PBS) and sodium dodecyl sulfate, were purchased from SRL, India. PEG 8000 (HI Media, India) and Absolute ethyl acetate obtained from Merck. Dulbecco's modified eagle's medium (DMEM) F12, DMEM, fetal bovine serum (FBS), and antibiotics were purchased from Thermo Fisher Scientific (Waltham, MA, USA). BrdU (5-Bromo $-2'$-deoxyuridine) was purchased from Sigma-Aldrich, (St. Louis, MO, USA) and Vectashield mounting medium containing4′6-diamidino-2-phenylindole (DAPI) was obtained from Vector Laboratories, Inc. (CA, USA). Primary antibodies pAkt Ser-473 (1:1000, rabbit polyclonal, Santacruz biotechnology, USA), GAPDH (1:2000, mouse monoclonal, cell signaling, USA), Akt (1:1000, rabbit monoclonal, cell signaling, USA). Anti-rabbit, anti-mouse HRP-linked, and mouse anti-BrdU antibodies were purchased from Abcam, UK. The acrylamide solution was purchased from Bio-Rad (California). Deionized water was used throughout the experiment with a conductivity of less than 18 mω.

2.1. Plant material collection and authentication
The *C. officinalis* (family Asteraceae) flowers were collected from Burdwan, India, and *H. rosa-sinensis* (family Malvaceae, red color flower) flowers were collected from Jadavpur university campus, Kolkata, India. Both plant materials were authenticated by the Agri horticultural society of India, Kolkata.

2.2. The extraction process of *C. officinalis* and *H. rosa-sinensis* flowers
The fresh petal of *C. officinalis* flowers (60 g) was collected and shade dried. The dry flowers were macerated in 50% ethanol (500 ml) for 5 d at room temperature and filtered through Whatman filter paper no 1 (Merck Millipore). The filtrate was lyophilized and stored at $-20\,^{\circ}$C (Dinda *et al* 2016).

H. rosa-sinensis, flowers were shade-dried at room temperature and crushed by a mechanical grinder. The 500 g of fine flower powder was suspended in 1500 ml of 32% ethanol for 24 h at room temperature. The mixture was filtered by filter paper (Whatman no: 1). The filtrate was lyophilized and stored at $-20\,^{\circ}$C of the final ethanol-free clear residue was used for the study (Shivananda *et al* 2007, Shen *et al* 2017).

2.3. Preliminary phytochemical screening
The phytochemical screening test was used to detect the phytochemicals (flavonoids, terpenoids, reducing sugar, alkaloids, tannins, saponins, anthraquinones, and amino acids) in polyherbal extract (Khan *et al* 2021).

2.4. Flavonoids detection test
For the flavonoid test, we used 1 ml polyherbal extract and a few drops of dilute sodium hydroxide, after mixing it formed yellowish color. After that added a few drops of dilute acid and it becomes a colorless sample indicating the existence of flavonoid components in the polyherbal extract.

2.5. Terpenoids detection test
For the terpenoid test an equal volume of chloroform and concentrated hydrogen sulfuric acid was added within the 2 ml of polyherbal extract. The formation of reddish-brown color and mentioned the presence of a terpenoids compound in the polyherbal extract.

2.6. Reducing sugar detection test
The reducing sugar was detected by Benedict's reagents. Here we used 1 ml polyherbal extract and mixed it with 2 ml Benedict's reagent, and boiled it for 3–5 min in a water bath. The brick red color sample indicated the presence of reducing sugar in the polyherbal extract.

2.7. Alkaloids detection test
For the alkaloids detection test, 2 ml of Wagner's reagent was added to 2 ml of polyherbal ethanolic extract, and the formation of brownish precipitation, confirmed the presence of alkaloids in the polyherbal extract.

2.8. Tannins detection test
The presence of tannins in the polyherbal extract was confirmed by the formation of brownish-green color with the addition of 0.1% ferric chloride to 2 ml of polyherbal extract.

2.9. Saponins detection test
For the saponins detection test, 2 ml polyherbal extract was added with the same volume of Benedict's

reagent. The presence of saponins was confirmed by bluish-black color precipitation.

2.10. Anthraquinones detection test

The presence of anthraquinones in the polyherbal extract was confirmed by the 1 ml crude extract and 10% hydrogen chloride was boiled in a water bath and allowed to cool. Then an equal volume of chloroform and a few drops of 10% ammonia were added subsequently and heated. The formation of a rose-pink color showed the presence of anthraquinones.

2.11. Amino acids detection test

For the amino acid detection test, 1 ml polyherbal extract was added with a few drops of Ninhydrin reagent. The formation of purple color indicates the presence of amino acids in the polyherbal extract.

2.12. Glycosides detection test

The presence of glycosides in the polyherbal extract was confirmed by the 1 ml polyherbal extract added with 1 ml concentrated sulfuric acid. The formation of reddish color precipitation and indicates the presence of glycosides in the polyherbal extract.

2.13. Synthesis of hydrogel

2.13.1. XG hydrogel synthesis

Initially, XG powder (SRL, India) (5 mg ml^{-1}) was dissolved in millipore water under vigorous stirring for 12 h followed by the addition of the cross-linking agent PEG-8000 (Hi Media, India). The solution turned into a semi-transparent gel after the complete dissolution of the gum and was named X.

2.13.2. Herbal excipient loaded hydrogel patch formation

The drug solution was added dropwise into the dissolved polymeric solution and continued stirring for 1 h. Finally, the polyhedral extract loaded XG hydrogel (X@C–H) was collected and dried by lyophilization technique.

2.13.3. Characterization of the hydrogel patch

The x-ray diffractometer (XRD) patterns of the hydrogel patch samples were recorded by XRD model D8, Bruker AXS, Wisconsin, USA, using Cu-kα target employing wavelength of 1.5418 å and operating at 35 kV with a scan speed of 1 s/step. In the case of field emission scanning electron microscopy (FESEM) and Fourier transform infrared spectroscopy (FTIR) measurements, the dry hydrogel powder was prepared by employing the lyophilization technique. In the case of FESEM, the dry powder was then cast on carbon grids and sputtered coated by using gold plasma. The FESEM was employed for the morphological study of hydrogel patches using Inspect f50 (Fei, Netherlands). The FTIR study was done using FTIR-8400s, Shimadzu, in the wave number range from 400 cm^{-1} to 4000 cm^{-1}. The samples

were prepared by mixing dried hydrogel powder with KBr. In this case, the samples to KBr ratio was maintained at 1:50. The mixed powder was then pressed by using a hydraulic press system. A pure KBr pallet was also prepared for baseline correction during the measurement. The TGA and DTA study was done using the DTG-60H DTA-TGA instrument. UV–Vis (Bio-Tech) was used for measured the absorbance intensity. The average particle size distribution and diameter of hydrogel were measured by dynamic light scattering (DLS). In the case of DLS, all the samples were initially immersed in distilled water maintaining a concentration of 5 mg ml^{-1}. Then the samples were further exposed to ultrasound for 30 min. Such vigorous ultrasound readily prepared a hydrogel solution of the respective sample. The charges of the hydrogel were also measured by the Zetasizer (NanoZS90, Malvern instruments Ltd, UK).

2.13.4. Swelling studies

The swelling characteristics of XG hydrogel (5 mg ml^{-1}) were measured in a buffer solution of various pH (pH 5.4 and 7.4) at 37 °C using a standard protocol (Seeli and Prabaharan 2017). The dry hydrogel (S_0) was weight precisely and submerged in a petri dish containing buffer solutions and incubated for 24 h. The weight of the swollen hydrogel (S_t) at different times was measured after removing excess water with tissue paper. The swelling ratio of the hydrogel at time t was determined using the following formula,

$$\text{Degree of swelling}, \% = \left[(S_t - S_0) / S_0 \right] \times 100$$

where S_t and S_0 are the weights of the hydrogel at time t and 0 h respectively.

2.13.5. Drug release study

In vitro study of drug release, was performed from a polyherbal encapsulated XG hydrogel patch at four different pH (7, 7.5, 8, and 8.5) for a period of 10 h. The percentage of encapsulated excipient of the hydrogel patch was calculated by absorbance maxima of herbal excipient solution at 540 nm using a spectrophotometer (epoch microplate spectrophotometer, USA). The DLC (drug loading capacity) and DEE (drug encapsulation efficiency) were calculated by the following equations (Alle *et al* 2020),

$$\text{DLC} (\%) = \left\{ (\text{weight of drug encapsulated in hydrogel} / \right.$$
$$\left. \text{weight of hydrogel taken}) \right\} \times 100$$

$$\text{DEE} (\%) = \left\{ (\text{total amount of drug} \right.$$
$$- \text{free drug in supernatant}) /$$
$$\left. (\text{total amount of drug}) \right\} \times 100.$$

2.13.6. Fibroblast cell culture

Human lung fibroblast cell lines WI-38 and human keratinocyte cell line HaCaT were cultured in DMEM

and DMEM F12 medium (Thermo Fisher Scientific (Waltham, MA, USA)) respectively with 5% FBS (Thermo Fisher Scientific), penicillin/streptomycin (100 units/ml), amphotericin-B (anti-fungal) and incubated at 37 °C, and 5% CO_2 (Heraeus, Thermo Scientific, MA, USA).

2.13.7. Cell proliferation assay

Fibroblast cells WI-38 and HaCaT were seeded at a density of 2.5×10^4 cells per well in 24 well plates and exposed to XG hydrogel loaded with excipients at different concentrations (0–400 μg ml^{-1}) for 24 h. The MTT assay method was performed using a standard protocol (Al Masum *et al* 2020).

2.13.8. Immunocytochemistry and BrdU incorporation assay

WI-38 and HaCaT cells were grown in respective mediums with 10% FBS in a coverslip placed in a 35 mm culture plate. The cells were treated with 200 μg ml^{-1} drug for WI-38 and 400 μg ml^{-1} for the HaCaT cell line and incubated for 24 h, and then 10 μm BrdU was added and incubated for 1 h for immunocytochemical analysis. Coverslips were washed in PBS, fixation with 4% paraformaldehyde for 30 min and permeabilized by 0.2% Triton X-100 at 4 °C for 10 min. The cells were treated with 2 N HCl for 30 min at room temperature. The 5% FBS was used for blocking and stayed for 1 h at room temperature. The cells were incubated with mouse monoclonal Anti-BrdU antibody (BD 44) at 1:100 dilutions in wash buffer and incubated at 4 °C for overnight. After washing, cells were incubated with fluorescein isothiocyanate (FITC)-conjugated goat anti-mouse IgG (SC-2078) at 1:200 dilutions at room temperature in dark conditions for 1 h. The slides were then washed and mounted with a mounting medium containing DAPI. The cells were examined under a fluorescence microscope (Leica, Wetzlar, Germany). Each analysis was performed at least three times (Dinda *et al* 2015).

2.13.9. Scratch assay

The lung fibroblast cell line (WI-38) was seeded in a 35 mm plate and incubated for 24 h at 37 °C. Then, cells were treated with 200 μg ml^{-1} of the drug (X, X@C, X@H, X@C–H) and incubated for 24 h at 37 °C with 5% CO_2. The same field of the wounded zone was photographed after 24 h time points. Scratch assay was done as per the method reported earlier (Dinda *et al* 2016).

2.13.10. Western blot analysis

After incubation with drugs, cell lysate was prepared followed by western blot analysis using a standard protocol (Dinda *et al* 2015). Here we have used primary antibody Akt (1:1000, rabbit monoclonal, Cell signaling, USA), pAkt (Ser 473) (1:1000, rabbit polyclonal, Santacruz biotechnology, USA), and

GAPDH (1:2000, mouse monoclonal, Cell signaling, USA). GAPDH was used as the loading control.

2.13.11. Animal experiments

We used about 25–30 g male BALB/c mice with a minimum of 6–7 weeks old, for the experiments. The mice were fed a restricted vitamin-rich pellet diet and libitum-added water. Animals were maintained according to the guidelines of the National Institute of Nutrition, Hyderabad, India.

2.13.12. Experimental design of in-vivo experiments

The mice were divided into five groups each containing five animals Group 1: excision wound created mice (untreated), Group 2: excision wound created and applied with X hydrogel patch, Group 3: excision wound created and applied with X@C hydrogel patch, Group 4: excision wound created and applied with X@H hydrogel patch, Group 5: excision wound created and applied with X@C–H hydrogel patch.

All the mice of groups 2, 3, 4, and 5 were applied with the same dose rate for 12 d at an interval of 3 d. The dorsal hair of mice was cleaned and shaved with 70% ethanol. One full-thickness excisional wound on the side of the dorsal midline was created by a 5 mm diameter of a punch biopsy. The image of the wound region was taken on 1, 3, 6, 9, and 12 d.

2.13.13. Hematoxylin and eosin staining

Hematoxylin dye is used for staining basophilic structures, nucleic acid-containing molecules like chromatin, ribosomes, and cytoplasmic areas rich in ribonucleic acid (RNA), which are given a blue-purple contrast. Basic components such as muscle, red blood cell (RBC)s, collagen, and cytoplasm are counterstained by acidic eosin in different shades of red, pink, and orange color. All tissues were sectioned into 4 mm sizes and paraffinized. The sections were washed three times with xylene for deparaffinized and rehydrated with ethanol. The section was followed by staining with hematoxylin for 5 min and washed with tap water. Next, the slides dip in 0.5% acid alcohol and are washed three times in distilled water. The blueing agent was used for 1 min and the slides were washed three times in distilled water. The counterstain alcoholic eosin was used for 1 min (Dinda *et al* 2016). The slides were then dehydrated through a graded ethanol series, cleared in xylene, and mounted with coverslips. The hematoxylin and eosin-stained slides were observed by a bright-field optical microscope (Leica dm 2500, Germany).

3. Results

3.1. Phytochemical screening

The phytochemical screening was used for the observation of chemical constituents of polyherbal flower extract (*C. officinalis* and *H. rosa-sinensis*). These chemical constituents play an important role in

Table 1. Phytochemical screening of polyherbal ethanolic extract.

Phytochemicals	Result
Flavonoids	+
Alkaloids	+
Reducing sugars	+ (few %)
Terpenoids	+
Tannins	+
Saponins	+
Anthraquinones	+
Amino acids	+
Glycosides	+

wound healing. Table 1 summarized the result of the phytochemical screening test. The flavonoids, alkaloids, terpenoids, tannins, saponins, anthraquinones, glycosides, and amino acids are present in the polyherbal extract (supplementary figure S4). In the reducing sugar experimental test, we observed that the polyherbal extract formed yellowish-red color but the Benedict reagent test mentioned that reducing sugar formed a brick-red color. Here we have used dextrose sugar as a positive control of reducing sugar test and found that it formed a brick-red color. That is why this result indicates, the reducing sugar percentage is low of our synthesized polyherbal extract. (supplementary figures S4(B) and (C)). This polyherbal extract can be utilized for wound healing activity because it is made up of a medicinal compound and is highly therapeutic which plays a crucial role against wound infection and induce wound tissue regeneration.

3.2. Synthesized biopolymeric hydrogel patch
The synthesis process of the hydrogel patch is very facile, it is shown in figure 1.

3.3. Physical characteristics of the synthesized hydrogel samples
The XRD patterns of pure XG powder did not find diffraction maxima but cross-linking agent PEG 8000 was showing diffraction maxima of 19.1° and 23.2° (supplementary figure S2(b)). The samples X, X@C, and X@H was showing diffraction peaks at 19.1° and 23.2° whereas, diffraction peaks centered at 19.1°, 23.2° and 31° have been found in the case of the doped hydrogel sample (figure 2(a)). The absence of any sharp diffraction line in XRD indicates an amorphous pattern of the pure XG powder (Mohsin *et al* 2018) and PEG 8000 shows two sharp peaks at 19° and 23.33°, it is semi-crystalline type (Özdemir Dinç and Güner 2017). Therefore, X also carries two diffraction lines at 19° and 23.33° which is similar to PEG 8000 so it is formed a hydrogel. The herbal excipient doped samples X@C, X@H, and X@C–H show diffraction lines at 19.1° and 23.2° revealing the semi-crystalline nature (Sung *et al* 2010).

In FTIR study is shown in figure 2(b) and supplementary figure S1(a). The XG is added to the PEG 8000 solution, and it is formed X hydrogel. The FTIR spectrum of the hydrogel shows special characteristics, that confirms the interaction between the two polymers and forms hydrogel. The 3600–3000 cm^{-1} region mentioned –OH group stretching vibration which is the first featured. In the case of PEG, the –OH group signal appears at 3478 cm^{-1}, XG at 3256 cm^{-1}, and in X at 3312 cm^{-1}. As the content of X in the gels increases, the 3256–3478 cm^{-1} ranges of peak detecting the –OH group of stretching vibration, indicating the interaction between XG and PEG molecular chains. The second is featured in the region of 2500–3000 cm^{-1} which is the C–H group stretching vibration. The C–H group signal appears in PEG at 2885 cm^{-1}, XG at 2913 cm^{-1}, and X at 2893 cm^{-1}. The hydrogel signals indicate a higher concentration of XG. A characteristic absorption signal occurs for pure PEG at 537, 862, 1116 and 1476 cm^{-1} for C–O–C, CH$_2$, C–O, and CH$_2$ respectively (Ofokansi *et al* 2016) while for pure XG at 1017, 1394 and 1644 cm^{-1} for COO–, COO– and C$_2$H$_3$O stretching respectively (Faria *et al* 2011, Zhang *et al* 2019). In the case of the bare hydrogel are shown other absorbance peaks at 1110 cm^{-1} (C–O stretching), 1070 cm^{-1} (C–O stretching), and 1608 cm^{-1} (C=C stretching), these signals are indicating its purity (figure 2(b)). The bands corresponding to the doped hydrogel sample are at 1043, 1533, and 3010 cm^{-1} depicting the proper incorporation of the poly-herbal excipients (figure 2(b)). Additionally, in FTIR the 1043 cm^{-1} peak corresponds to the polysaccharide C–O valence vibration (Mak *et al* 2013), and the other two major vibrations at 1533 and 3010 cm^{-1} are due to C–OH and –OH vibrations respectively (Al-Mussawi and Al-Hussani 2019). This –OH vibration possibly comes from the absorbed water of the hydrogel sample. Poly-herbal excipients doped hydrogel shows two extra absorbance bands centered around 1643 and 2130 cm^{-1} depicting the formation of C–OH and C–H bonds respectively (Mak *et al* 2013, Azizi *et al* 2018).

The absorbance of the hydrogel samples was measured after the complete dissolution of the mixture in water. The absorbance spectra were recorded in a UV–Vis spectrophotometer. Figure 2(c) does not show any prominent absorption maximum for the undoped hydrogel sample, whereas, the polyherbal extract doped hydrogel offers a broad absorption maximum centered at around 352 nm, and it corresponds to n–π^* transition of the herbal excipients indicating successful doping. This relates to the proper incorporation of the dopants as seen in XRD and FTIR data.

In FESEM, herbal excipient encapsulated hydrogel showed a more exfoliated structure of the gel
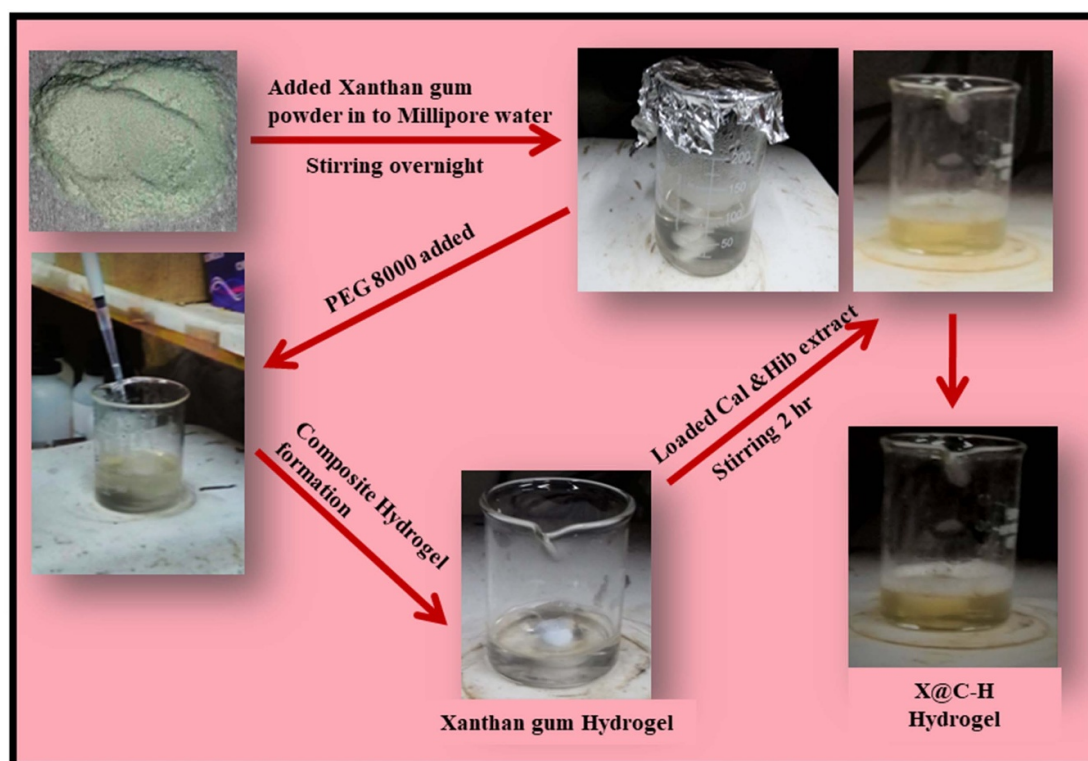
Figure 1. Schematic representation of xanthan gum hydrogel and herbal extract encapsulated hydrogel preparation process.

sample than the bare vehicle (figures 2(d) and (e)). The doped hydrogel also shows a porous structure and less agglomeration. Our synthesized doped sample shows exfoliated microstructure suggesting increased porosity of the sample and reducing the agglomeration and thus providing better attachment probability to the substrate like in contact with a wound. The hydrodynamic diameter of pure hydrogel is 20.144 d.nm as measured by DLS whereas the poly-herbal extract conjugated hydrogel (X@C–H) corresponding value is 1596 d.nm with poly-dispersity index (PDI) 0.64 (figure 2(f)). Additionally, the surface charge of the pure XG hydrogel is 0.136 mv, which is positive and pretty low to be stable enough (supplementary figure S3). Loading of poly-herbal excipient makes this hydrogel negative (−27.7 mV) and is quite stable (supplementary figure S3). It is quite interesting to observe the alteration of microstructure after the doping of poly-herbal excipients into the hydrogel patch. Our synthesized doped sample shows exfoliated microstructure suggesting increased porosity of the sample and reducing the agglomeration and thus providing better attachment probability to the substrate like in contact with a wound. The doped sample depicts an enhanced negative surface charge with a lower PDI (0.64) indicating the extract-encapsulated hydrogel forms a homogenous solution, which is suitable for any biological application. In reality, negative surfaces of the poly-herbal excipient strongly attract the hydrogel towards their surface, which further exfoliates the structure of

the doped hydrogel and opens the clustered surface for better binding with the substrate.

3.4. The absorption capacity of hydrogel patch measured by the swelling study

The drug release capacity of hydrogel was evaluated by its swelling properties. After 24 h it has been found that the weight of bare XG was increased (figure 2(g)) and swollen hydrogel patch maintains its shape better at pH 7.5 than pH 5.4. The high drug loading capacity is due to the large surface area of the hydrogel patch.

3.5. Stability assay of the hydrogel patch samples

The thermal stability has also been measured using the DTA-TGA technique showing the stability of the hydrogel patch up to 200 °C. The thermal stability of the pure hydrogel patch has been tested (figures 2(h) and (i)) to validate their storage and uses. The temperature-dependent mass loss and differential thermograms were analyzed by the DTA-TGA instrument maintaining a heating rate of 10 °C min^{-1} in nitrogen atmosphere (flow rate 50 cc min^{-1}). It is observed that the hydrogel undergoes dehydration at 60 °C–70 °C but no mass loss has been observed in this region. Apart from this, another major thermal transition occurs at 190 °C indicating high stability of the hydrogel sample. In reality, such hydrogel patches have a very fragile structure and need proper ambient conditions to sustain. TGA measurement enables us to find the softening temperature and
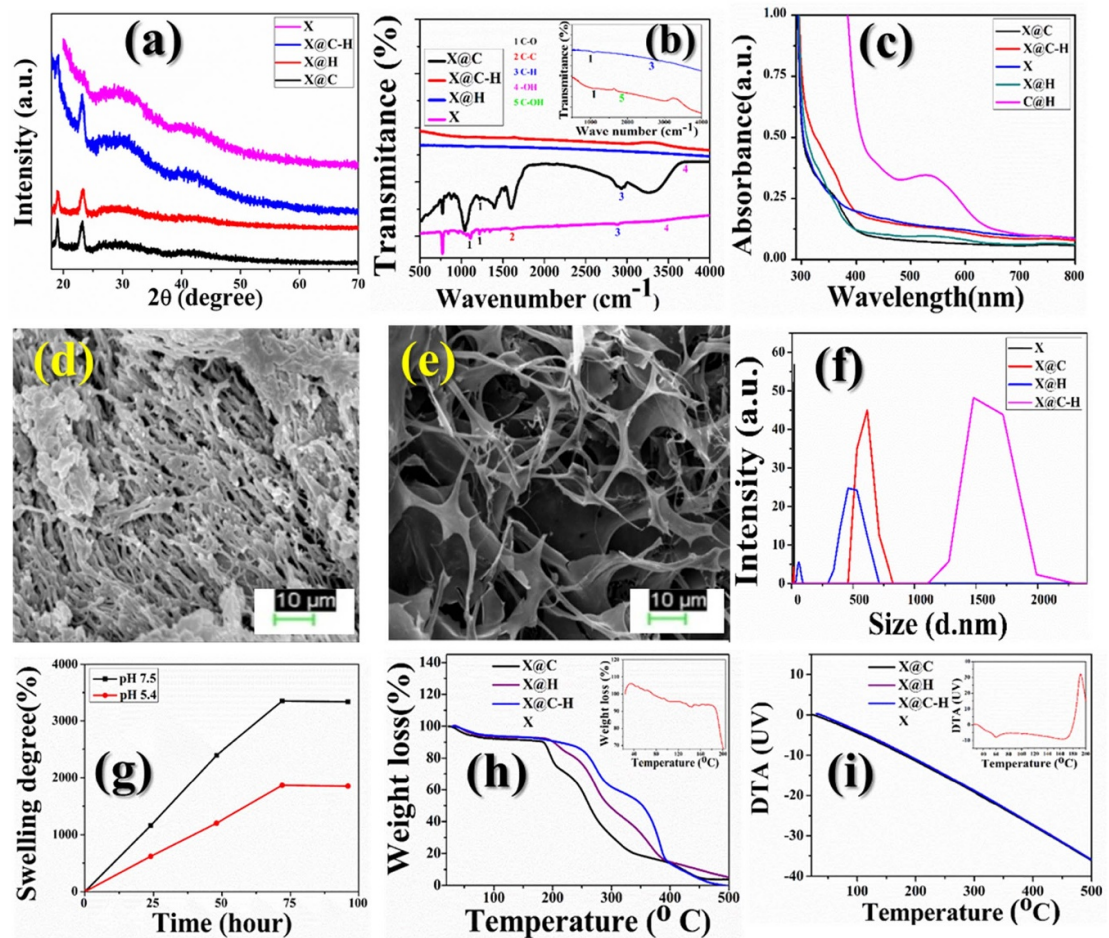
Figure 2. Physical characterization of xanthan gum hydrogel patch, (a) XRD of X, X@C, X@H, and X@C–H; (b) FTIR spectroscopy of X, X@C, and X@H and X@C–H; (c) UV–VIS spectroscopy of X, X@C, X@H, C@H, and X@C–H; (d) and (e) FESEM images of X and X@C–H respectively; (f) DLS of X, X@C, X@H, X@C–H; (g) water absorbance capacity of hydrogel measured by swelling ratio study at variant pH; (h) TGA, and (i) DTA of X, X@C, X@H, X@C–H.

phase formation temperature, which not only signifies its stability but also aids in designing its storage conditions.

The synthesized sample was exposed to various pH ranges (5.3, 7.5, and 9.6) in order to check the structural and chemical stability. It is found that there is no alteration in their absorbance spectra at different pH (supplementary figure S2(b)) and no change in absorbance spectra of the samples with time was observed (supplementary figure S2(a)). Simultaneously dissolving synthesized samples in different buffer solutions (H$_2$O, PBS, and TBS) does not influence their stability (supplementary figure S2(c)). Additionally, pH and time-dependent stabilities of the sample have been found, which reveals the application potential of the hydrogel for biological purposes.

Figure 3. Drug release studies at pH 7, 7.5, 8, and 8.5 of X@C–H hydrogel.

3.6. Herbal excipient encapsulated hydrogel patch showed pH-responsive drug release

The release profile of herbal excipient (drug) encapsulated hydrogel patch at different pH was estimated and shown in figure 3. The DLC and DEE percentages of the XG hydrogel patch were found to be 71% and 85%, respectively. Approximately 55%, 58%, 70%, and 80% of the drug is released from X@C–H hydrogel at pH 7, 7.5, and pH 8, 8.5 (wounded environment) respectively, as shown in figure 3. However, the
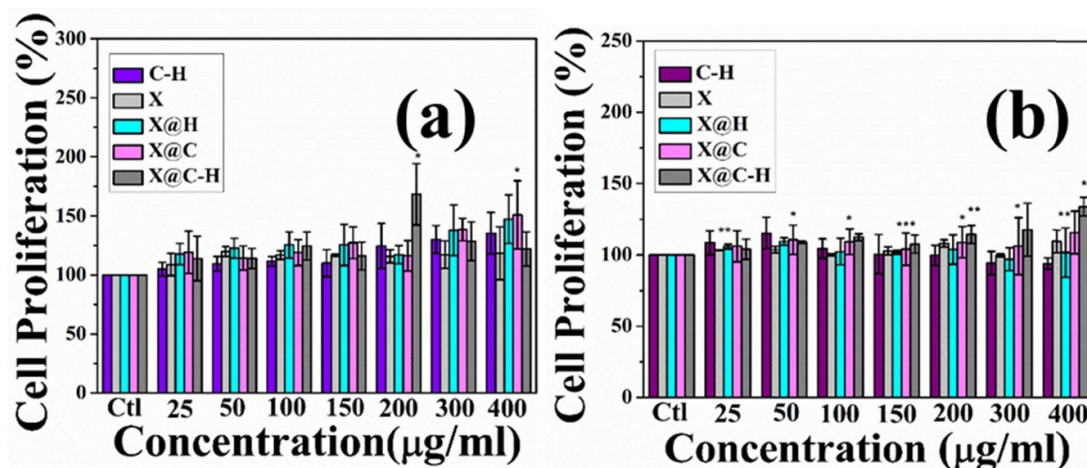
Figure 4. Assessment of cell cytotoxicity and cell proliferation of C@H, X, X@C, X@H on human fibroblast and keratinocyte cell lines (a) WI-38 and (b) HaCaT cells by MTT assays which shows cells number were increasing in a dose-dependent manner. The MTT results were expressed as mean ±SD of three independent experiments and where * ($P < 0.05$), ** ($P < 0.01$), and *** ($P < 0.001$).

present outcomes confirmed that the pH-dependent release is very much more sensitive to in alkaline pH of 8 or 8.5 than the normal pH of 7 or 7.5.

3.7. Synthesized hydrogel promotes cell proliferation

MTT assay was performed to explore the proliferation of WI-38 and HaCaT cell lines. The cells were seeded in 24 well plates and treated with our synthesized C–H, X, X@C, X@H, and X@C–H at different concentrations (0–400 μg ml^{-1}) for 24 h. The maximum proliferation of WI-38 and HaCaT cells at 200 μg ml^{-1} and 400 μg ml^{-1} respectively and are shown in figures 4(a) and (b). We have found bare hydrogel (X) has no cytotoxic effects and X@C–H exhibited significant proliferation in a dose-dependent manner.

3.8. Proliferative effect assessment of the excipient payloaded hydrogel by BrdU assay

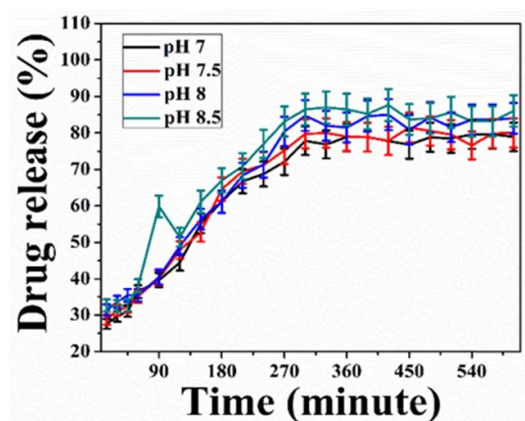We further studied the proliferation effect of polyherbal encapsulated hydrogel patch on WI-38 and HaCaT cells by counting BrdU-positive cells. After labeling with BrdU, cells were observed under a fluorescence microscope and counted for BrdU-positive cells. As shown in figure 5, X@C–H has more BrdU-positive cells (150% of cells are BrdU positive for both the cell lines) compared to X@C and X@H treated cells. Thus, we found more BrdU-positive cells in the fibroblast cell line compared to the keratinocyte cell after the treatment of X@C–H hydrogel. In addition, this polyherbal hydrogel patch significantly promoted the migration of the lung fibroblast cell line.

3.9. Cell migration estimated by scratch assay

To assess the *in vitro* wound healing effect of X, X@C, X@H, and X@C–H hydrogel on WI-38 cell lines, the

migration pattern was observed around the closure of a marked area scratched in confluent monolayer cells. The measure of gap width at the initial time (0 h) and final time (24 h) was calculated and plotted in figures 6(a) and (b). This result suggested an increased migrating ability of fibroblasts in response to the polyherbal extract encapsulated hydrogel patch treatment.

3.10. Expression of the proliferation responsive protein analysis by Western blotting

We next explored the expression of Akt and pAkt protein in X, X@C, X@H and X@C–H treated human lung fibroblast cell line WI-38 and keratinocyte cell line HaCaT. We have observed that, in both the cell lines, expression of pAkt enhanced in the presence of X@C–H than X, X@C or X@H treated cells (figure 7). Here also observed phosphorylation of Akt, when cells were treated with a hydrogel containing herbal excipients, indicating efficient release of excipients.

3.11. *In vivo* study

3.11.1. Excision wound created in male BALB/c mice model and measurement of wound size

We found that X@C–H treated mice also healed within 9 d compared to other treated X, X@C, and X@H mice (figure 8(a)). After 12 d, the wounded area was measured following this process, wound sizes at any given time point after wounding were expressed as a percentage of the initial (day 1) wound area and the rate of wound closure was calculated using ImageJ software (NIH, USA). The rate of wound healing was shown in figure 8(b), on day 12 post-wounding the X@C–H treated groups showed complete wound closure compared to other groups of

Figure 5. Effect of X, X@C, X@H, and X@C–H treated cell proliferation were determined by BrdU staining assay treatment with/without extract in WI-38 and HaCaT cell lines for 24 h and labeled with 10 μM BrdU before immunocytochemical analysis. The representative images of BrdU staining were shown in figures (a) and (b) respectively. The quantitative estimation of BrdU positive WI-38 and HaCaT cells was shown in the respective figures (c) and (d), where * ($P < 0.05$) and ** ($P < 0.01$).

Figure 6. (a) The scratch area was formed in WI-38 monolayer cells and images have taken by a phase contrast microscope ($10\times$) at 0 h and 24 h; (b) X, X@C, X@H, and X@C–H treated cell migration was measured using ImageJ Software and % gap width is calculated with different time point, where * ($P < 0.05$) and *** ($P < 0.001$).

Figure 7. Western blot analysis of Akt (MW 60 kDa) and pAkt (MW 60 kDa) protein in response to X; X@H; X@C and X@C–H. This suggests the upregulation of pAkt protein expression upon delivery of polyherbal excipient encapsulated hydrogel patch in fibroblast and keratinocyte cell lines shown in (a) for WI-38 and (b) for HaCaT; (c) WI-38 and (d) HaCaT represent the band intensity of the proteins and was quantified using ImageJ software.
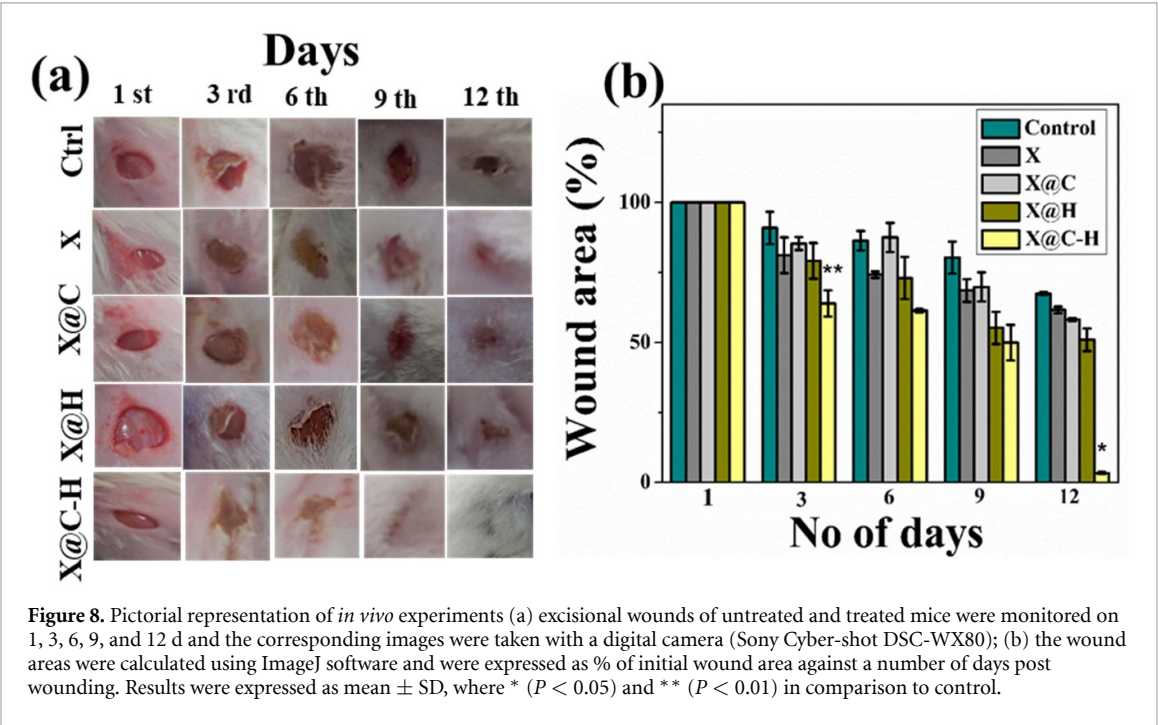
Figure 8. Pictorial representation of *in vivo* experiments (a) excisional wounds of untreated and treated mice were monitored on 1, 3, 6, 9, and 12 d and the corresponding images were taken with a digital camera (Sony Cyber-shot DSC-WX80); (b) the wound areas were calculated using ImageJ software and were expressed as % of initial wound area against a number of days post wounding. Results were expressed as mean $\pm$ SD, where * ($P < 0.05$) and ** ($P < 0.01$) in comparison to control.

mice. The results indicated that the application of bare hydrogel does not induce any toxic effect on the mice neither it promotes the re-epithelialization of the epidermis. However, treatment with X@C–H hydrogel led to extensive re-epithelialization within 9 d and hair follicle appears on dermal sheath cells. Also, there was no sign of scars and hairlessness compared to the others groups.
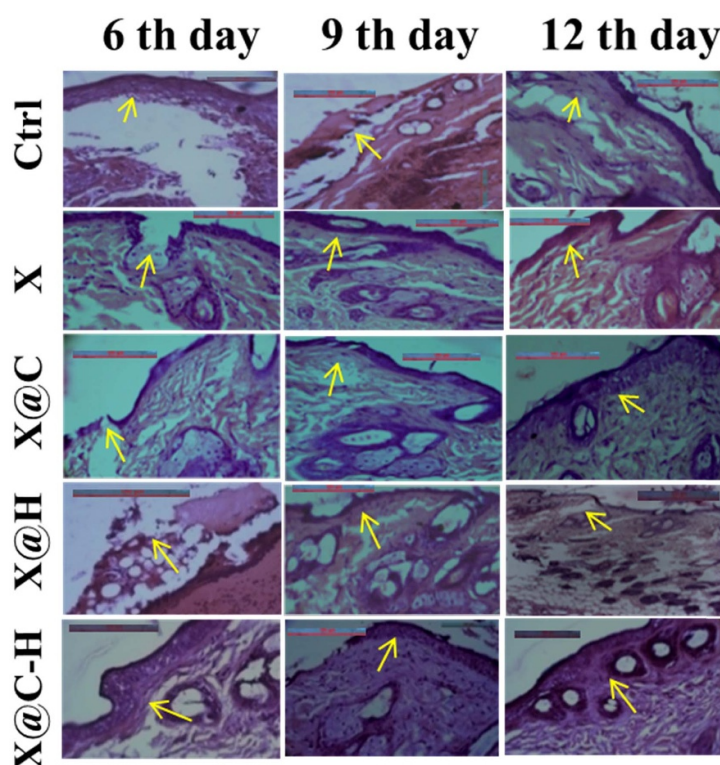
Figure 9. Histological analysis of wounded areas tissue from mice at different post-wounding days (6, 9, and 12) in treated, untreated animals. Original magnification 40X, scale bar-100 μm.

3.11.2. Histological study

A histological study purposes eosin, as well as hematoxylin, was used to envisage the alterations in tissue morphology with the progression of wound healing upon application of various forms of hydrogel like X, X@C, X@H, X@C–H for different time intervals. The slides were observed under a bright-field optical microscope and found the fibroblast numbers are slightly increased in the dermis near a wounded portion with the genesis of new blood vessels (neoangiogenesis). While in control, the wound site was filled with necrotic debris and fibrin. Within 6 d, in the case of X@C–H applied animals, the granulation tissue had developed fully and the regeneration of the epidermis took place. On the other hand, it took 12 d for the formation of granulation tissue after the application of X@C and X@H hydrogels. While in control and bare hydrogel applied animals slowly developed the granulation layer. On day 12, the re-epithelialization of the wounded portion was completed in X@C–H applied animals compared to control, X, X@C, and X@H where re-epithelialization was not completed (figure 9). Hence, we can conclude that the X@C–H hydrogel showed more pronounced wound healing activities.

4. Discussion

Wound healing is a very slow, complex, and overlapping dynamic process that repairs the injured tissue through hemostasis, inflammation, proliferation, and remodeling phases (Amsden 2015, Alibolandi *et al* 2017).

In recent times different types of wound care products have been suggested that are more effective in promoting and regeneration of wounded tissue (Mohsin *et al* 2018). Among them, hydrogels are beneficial for control release of therapeutic agents of different types (Özdemir Dinç and Güner 2017). Here we have synthesized a biocompatible hydrogel patch from the abundantly available XG which acts as a promising vehicle for the delivery of polyherbal excipients using a facile method. For herbal excipients, we have used *C. officinalis* flower which was known to treat burn and ulcer wounds, and *H. rosa-sinensis* flower, known for wound healing and antibacterial property (Talekar *et al* 2017). Our prepared polyherbal ethanolic flower extract showed the presence of phytochemical constituents through the phytochemical screening process. The flavonoids, alkaloids, terpenoids, tannins, saponins, anthraquinones, glycosides, and amino acids are present in the polyherbal extract (supplementary figure S4). The reducing sugar screening result showed yellowish red color, indicating the reducing sugar percentage of the polyherbal extract is low. The result of reducing sugar of polyherbal extract is compared to a known reducing agent like dextrose (supplementary figure S4). This polyherbal extract can be used for wound healing activity because it contains highly therapeutic

and medicinal compounds which play a crucial role against wound infection and promote wound tissue regeneration. This poly-herbal plant extracts along with their encapsulation in a cheap hydrogel and is not reported previously.

The absence of any sharp diffraction line in XRD indicates an amorphous pattern of the pure XG powder (Mohsin *et al* 2018) and PEG 8000 shows two sharp peaks at 19° and 23.33°, it is semi-crystalline type. Therefore, X also carries two diffraction lines at 19° and 23.33° which is similar to PEG 8000 so it is formed a hydrogel. The herbal excipient doped samples X@C, X@H, and X@C–H show diffraction lines at 19.1° and 23.2° revealing the semi-crystalline nature. Additionally, in FTIR the 1043 cm^{-1} peak corresponds to the polysaccharide C–O valence vibration, and the other two major vibrations at 1533 and 3010 cm^{-1} are due to C–OH and –OH vibrations respectively. This –OH vibration possibly comes from the absorbed water of the hydrogel sample. Poly-herbal excipients doped hydrogel shows two extra absorbance bands centered around 1643 and 2130 cm^{-1} depicting the formation of C–OH and C–H bonds respectively. Moreover, the appearance of an absorption band in the UV–Vis spectrum around 352 nm is due to the incorporation of the poly-herbal excipients and it corresponds to n–π^* transition of the herbal excipients indicating successful doping. It is quite interesting to observe the alteration of microstructure after the doping of poly-herbal excipients into the hydrogel patch. The size values of pure hydrogel and doped hydrogel are suitable for hydrogel structure. Zang *et al* synthesized another type of hydrogel by using PVA and XG. Our synthesized doped sample shows exfoliated microstructure suggesting increased porosity of the sample and reducing the agglomeration and thus providing better attachment probability to the substrate like in contact with a wound. The doped sample depicts an enhanced negative surface charge with a lower PDI (0.64) indicating the extract encapsulated hydrogel forms a homogenous solution, which is suitable for any biological application. Additionally, pH and time dependent stabilities of the sample have been found, which reveals the application potential of the hydrogel for biological purposes. The thermal stability has also been measured using the DTA-TGA technique showing the stability of the hydrogel patch up to 190 °C. Such high temperature stability would definitely make this sample usable for biomedical applications.

In reality, negative surfaces of the poly-herbal excipient strongly attract the hydrogel towards their surface, which further exfoliates the structure of the doped hydrogel and opens the clustered surface for better binding with the substrate. The swelling ratio study is the most important property for the

determination of its drug release capacity. The high drug loading capacity is due to the large surface area of the hydrogel patch.

We have found bare hydrogel (X) has no cytotoxic effects and X@C–H exhibited significant proliferation in a dose-dependent manner. The result could be due to the presence of major flavonoid constituents like rutin, quercetin, and gallic acid in Calendula and Hibiscus flower extract (Dinda *et al* 2016, Purushothaman *et al* 2016) which are reported to be significant proliferative activities on fibroblast cells. Thus, we found more BrdU-positive cells in the fibroblast cell line compared to keratinocyte cells after the treatment of X@C–H hydrogel. In addition, this polyherbal hydrogel patch significantly promoted the migration of the lung fibroblast cell line. Phosphorylation of Akt was observed when cells were treated with *C. officinalis* extract in our previous study (Shivananda Nayak *et al* 2007, Dinda *et al* 2016), here also observed phosphorylation of Akt when cells were treated with polyherbal extract encapsulated hydrogel and indicating efficient release of excipients. The *in vivo* results indicated that the application of bare hydrogel does not induce any toxic effect on the mice neither it promotes the re-epithelialization of the epidermis. However, treatment with X@C–H hydrogel led to extensive re-epithelialization within 9 d and hair follicle appears on dermal sheath cells. Also, there was no sign of scars and hairlessness compared to the others groups. It has been reported that ethanol extract from calendula and hibiscus flower attenuates inflammation, enhances fibroblast proliferation, and collagen deposition, and upregulates vascular endothelial growth factor (VEGF) and transforming growth factor (TGF)-β1 expression in excisional wounds (Talekar *et al* 2017). However, we have developed a hydrogel-loaded polyherbal excipient and successfully deliver it to wounds for promoting healing.

5. Conclusion

This study hypothesized that the synthesized cost-effective biocompatible XG hydrogel has the potential to emerge as an ideal carrier for polyherbal excipients for the purpose of different types of wound amelioration in the near future.

Data availability statement

The data cannot be made publicly available upon publication because they are not available in a format that is sufficiently accessible or reusable by other researchers. The data that support the findings of this study are available upon reasonable request from the authors. Data will be available from 27 July 2022.

Acknowledgments

Funding

Ethics declarations

All applicable guidelines for the care and use of animals were followed. The experimental protocols were approved by the Bose Institute, P 1/12, CIT scheme VIIM, Kolkata-700 054, India animal ethics committee.

Conflict of interest

The authors have no conflict of interest to declare.

ORCID iDs

Sukhen Das ⬤ https://orcid.org/0000-0001-8372-3076
Parimal Karmakar ⬤ https://orcid.org/0000-0002-9423-9906

References

Al Masum A, Pal K, Saha I, Ghosh D, Roy S, Chowdhury S G, Islam M M and Karmakar P 2020 Facile synthesis of antibiotic encapsulated biopolymeric okra mucilage nanoparticles: molecular docking, *in vitro* stability and functional evaluation *Adv. Nat. Sci.: Nanosci. Nanotechnol.* **11** 025020

Alibolandi M, Mohammadi M, Taghdisi S M, Abnous K and Ramezani M 2017 Synthesis and preparation of biodegradable hybrid dextran hydrogel incorporated with biodegradable curcumin nanomicelles for full thickness wound healing *Int. J. Pharm.* **532** 466–77

Alle M, Kim T H, Park S H, Lee S H and Kim J C 2020 Doxorubicin-carboxymethyl xanthan gum capped gold nanoparticles: microwave synthesis, characterization, and anti-cancer activity *Carbohydr. Polym.* **229** 115511

Almeida P A D, Nones J, Trentin A G and Nones J 2015 Quercetin and rutin affect the survival and proliferation of human skin-derived multipotent mesenchymal stromal cells *J. Pharm. Pharmacol.* **3** 237–42

Al-Mussawi Z K and Al-Hussani I M 2019 Phytochemical study of Calendula officinalis plant by used Gc-Ms and FTIR techniques *Plant Arch.* **19** 845–51

Amsden B 2015 Novel biodegradable polymers for local growth factor delivery *Eur. J. Pharmacol.* **97** 318–28

Azizi M, Azimzadeh M, Afzali M, Alafzadeh M and Mirhosseini M S H 2018 Characterization and optimization of using Calendula officinalis extract in fabrication of polycaprolactone-gelatin electrospun nanofibers for wound dressing applications *Adv. Mater. Process.* **6** 34–46

Bhaskar A and Nithya V 2012 Evaluation of the wound-healing activity of Hibiscus rosa sinensis L (Malvaceae) in Wistar albino rats *Indian J. Pharmacol.* **44** 694

Choi J, Park Y G, Yun M S and Seol J W 2018 Effect of herbal mixture composed of Alchemilla vulgaris and Mimosa on wound healing process *Biomed. Pharmacother.* **106** 326–32

Das S and Baker A B 2016 Biomaterials and nanotherapeutics for enhancing skin wound healing *Front. Bioeng. Biotechnol.* **4** 82

Dinda M, Dasgupta U, Singh N, Bhattacharyya D and Karmakar P 2015 PI3K-mediated proliferation of fibroblasts by Calendula officinalis tincture: implication in wound healing *Phytother. Res.* **29** 607–16

Dinda M, Mazumdar S, Das S, Ganguly D, Dasgupta U B, Dutta A and Karmakar P 2016 The water fraction of Calendula officinalis hydroethanol extract stimulates *in vitro* and *in vivo* proliferation of dermal fibroblasts in wound healing *Phytother. Res.* **30** 1696–707

Doersch K M and Newell-Rogers M K 2017 The impact of quercetin on wound healing relates to changes in αV and β1 integrin expression *Exp. Biol. Med.* **242** 1424–31

Elegbede R D, Ilomuanya M O, Sowemimo A A, Nneji A, Joubert E, de Beer D, Koekemoer T and van de Venter M V 2020 Effect of fermented and green Aspalathus linearis extract loaded hydrogel on surgical wound healing in Sprague Dawley rats *Wound Med.* **29** 100186

El-Refaie W M, Elnaggar Y S R, El-Massik M A and Abdallah Y O 2015 Novel curcumin-loaded gel-core hyaluosomes with promising burn-wound healing potential: development, *in-vitro* appraisal and *in-vivo* studies *Int. J. Pharm.* **486** 88–98

Faria S, de Oliveira Petkowicz C L, de Morais S A L, Terrones M G H, de Resende M M, de Franca F P and Cardoso V L 2011 Characterization of xanthan gum produced from sugar cane broth *Carbohydr. Polym.* **86** 469–76

Han G and Ceilley R 2017 Chronic wound healing: a review of current management and treatments *Adv. Ther.* **34** 599–610

Hoare T R and Kohane D S 2008 Hydrogels in drug delivery: progress and challenges *Polymer* **49** 1993–2007

Hu X, Wang K, Yu M, He P, Qiao H, Zhang H and Wang Z 2019 Characterization and antioxidant activity of a low-molecular-weight xanthan gum *Biomolecules* **9** 730

Jaiswal L, Shankar S and Rhim J W 2019 Carrageenan-based functional hydrogel film reinforced with sulfur nanoparticles and grapefruit seed extract for wound healing application *Carbohydr. Polym.* **224** 115191

Khairnar M S, Pawar B, Marawar P P and Mani A 2013 Evaluation of Calendula officinalis as an anti-plaque and anti-gingivitis agent *J. Indian Soc. Periodontol.* **17** 741

Khan B A, Khan A, Khan M K and Braga V A 2021 Preparation and properties of high sheared poly (vinyl alcohol)/chitosan blended hydrogels films with Lawsonia inermis extract as wound dressing *J. Drug Deliv. Sci. Technol.* **61** 102227

Lee K, Lee B, Lee M H, Kim B, Chinannai K S, Ham I and Choi H Y 2015 Effect of Ampelopsis Radix on wound healing in scalded rats *BMC Complement Altern. Med.* **15** 1–9

Mak Y W, Chuah L O, Ahmad R and Bhat R 2013 Antioxidant and antibacterial activities of hibiscus (Hibiscus rosa-sinensis L.) and Cassia (Senna bicapsularis L.) flower extracts *J. King Saud Univ. Sci.* **25** 275–82

Mohsin A, Zhang K, Hu J, Tariq M, Zaman W Q, Khan I M, Zhuang Y and Guo M 2018 Optimized biosynthesis of xanthan via effective valorization of orange peels using response surface methodology: a kinetic model approach *Carbohydr. Polym.* **181** 793–800

Murray R Z, West Z E, Cowin A J and Farrugia B L 2019 Development and use of biomaterials as wound healing therapies *Burn. Trauma* **7** 2

Najafpour F, Arabzadeh S, Kalalinia F, Mostajeran N, Laal Mousavi S M, Yazdian-Robati R, Hashemi E and Hashemi M 2022 Evaluation of wound healing effect of Solanum nigrum L. leaf extract-loaded sodium alginate nanoparticles embedded in chitosan hydrogel, *in vivo* study *Nanomed. J.* **9** 34–42

Ofokansi K C, Kenechukwu F C, Ezugwu R O and Attama A A 2016 Improved dissolution and anti-inflammatory activity of ibuprofen-polyethylene glycol 8000 solid dispersion systems *Int. J. Pharm. Investig.* **6** 139

Özdemir Dinç C and Güner A 2017 Solid-state characterization of poly (ethylene glycol) samples prepared by solvent cast technique *Bulg. Chem. Commun.* **49** 15–20

Purushothaman A, Meenatchi P, Saravanan S, Sundaram R and Saravanan N 2016 Quantification of total phenolic content, HPLC analysis of flavonoids and assessment of antioxidant and anti-haemolytic activities of Hibiscus rosa-sinensis L. flowers *in vitro Int. J. Pharm. Sci. Res.* **4** 1342–50

Rathod L, Bhowmick S, Patel P and Sawant K 2022 Calendula flower extract loaded PVA hydrogel sheet for wound management: optimization, characterization and *in-vivo* study *J. Drug Deliv. Sci. Technol.* **68** 103035

Rubio-Elizalde I, Bernáldez-Sarabia J, Moreno-Ulloa A, Vilanova C, Juárez P, Licea-Navarro A and Castro-Ceseña A B 2019 Scaffolds based on alginate-PEG methyl ether methacrylate-Moringa oleifera-Aloe vera for wound healing applications *Carbohydr. Polym.* **206** 455–67

Seeli D S and Prabaharan M 2017 Guar gum oleate-graft-poly (methacrylic acid) hydrogel as a colon-specific controlled drug delivery carrier *Carbohydr. Polym.* **158** 51–57

Sharma R, Kaith B S, Kalia S, Pathania D, Kumar A, Sharma N and Schauer C 2015 Biodegradable and conducting hydrogels based on guar gum polysaccharide for antibacterial and dye removal applications *J. Environ. Manage.* **162** 37–45

Shedoeva A, Leavesley D, Upton Z and Fan C 2019 Wound healing and the use of medicinal plants *Evid.-based Complement. Altern. Med.* **2019** 1–30

Shen H M, Chen C, Jiang J Y, Zheng Y L, Cai W F, Wang B, Lind Z, Tang L, Wang Y H and Shi G G 2017 The N-butyl alcohol extract from Hibiscus rosa-sinensis L. flowers enhances healing potential on rat excisional wounds *J. Ethnopharmacol.* **198** 291–301

Shivananda Nayak B, Sivachandra Raju S, Orette F A and Chalapathi Rao A V 2007 Effects of Hibiscus rosa sinensis L (Malvaceae) on wound healing activity: a preclinical study in a Sprague Dawley rat *Int. J. Low. Extrem. Wounds* **6** 76–81

Sung J H, Hwang R M, Kim J O, Lee H J, Kim J H, Kim Y I and Han S S 2010 Gel characterisation and *in vivo* evaluation of minocycline-loaded wound dressing with enhanced wound healing using polyvinyl alcohol and chitosan *Int. J. Pharm.* **392** 232–40

Talekar Y P, Apte K G, Paygude S V, Tondare P R and Parab P B 2017 Studies on wound healing potential of polyherbal formulation using *in vitro* and *in vivo* assays *J. Ayurveda Integr. Med.* **8** 73–81

Tam J C *et al* 2014 A Chinese 2-herb formula (NF3) promotes hindlimb ischemia-induced neovascularization and wound healing of diabetic rats *J. Diabetes Complicat.* **28** 436–47

Wang T, Liao Q, Wu Y, Wang X, Fu C, Geng F, Qu Y and Zhang J 2020 A composite hydrogel loading natural polysaccharides derived from Periplaneta americana herbal residue for diabetic wound healing *Int. J. Biol. Macromol.* **164** 3846–57

Zhang Q, Hu X M, Wu M Y, Wang M M, Zhao Y Y and Li T T 2019 Synthesis and performance characterization of poly (vinyl alcohol)-xanthan gum composite hydrogel *React. Funct. Polym.* **136** 34–43

Biomedical Materials

PAPER

Facile process of *Hibiscus* mucilage polymer formulation using *Hibiscus rosa-sinensis* leaves to treat second-degree burn and excision wounds

Ishita Saha[1], Sourav Ghosh[2], Shubham Roy[3,4], Tarakdas Basu[2] and Parimal Karmakar[1,*] ⓘ

[1] Department of Life Science and Biotechnology, Jadavpur University, 188, Raja S.C. Mullick Road, Kolkata, 700032 West Bengal, India
[2] Department of Biochemistry and Biophysics, University of Kalyani, Kalyani, 741 235 West Bengal, India
[3] School of Science, Shenzhen Key Laboratory of Flexible Printed Electronics Technology, Harbin Institute of Technology, Shenzhen 518055, People's Republic of China
[4] Department of Physics, Jadavpur University, 188, Raja S.C. Mullick Road, Kolkata, 700032 West Bengal, India
[*] Author to whom any correspondence should be addressed.

E-mail: pkarmakar_28@yahoo.co.in

Abstract

Mucilage is a sticky substance found in various plants and microorganisms and is made up of proteins and polysaccharides. Mucilage from *Hibiscus rosa sinensis* is a complex polysaccharide traditionally used to treat different skin diseases. In our study, we fabricated mucilage polymer from *Hibiscus rosa sinensis* leaves and evaluated its potential application in second-degree burns and excision wounds. The physical properties of Hibiscus mucilage (HM) polymer were demonstrated by using Ultraviolet-visible absorption spectroscopy, x-ray diffraction, Fourier transform infrared spectroscopy, dynamic light scattering, Scanning electron microscopy, Brunauer–Emmett–Tellerand, Swelling ratio. The human cell lines WI-38, and HaCaT have been used for *in-vitro* experiments like MTT, scratch wound, BrdU, ROS scavenging assays, and western blot analysis. The results of the MTT, scratch-wound, and BrdU assay indicated that the HM polymer is nontoxic in nature and also enhances both the properties of cellular migration and proliferation, respectively. On the other hand, the result of the ROS scavenging assay suggested that HM polymer enhances the antioxidant activity of cells while the western blot analysis designated that the HM polymer treatment caused downregulation of the pro-inflammatory cytokine IFN-γ and upregulation of the pAkt (Serine 473) protein, and TGF-β1 signaling pathway. Therefore, all *in-vitro* experimental studies recommended that HM polymer is biocompatible and has antioxidant and anti-inflammatory effects. In the *in vivo* experiment, second-degree burns and excision wounds were created on the dorsal surface of male BALB/c mice. After the sixth day of HM polymer treatment have developed new tissue, hair follicles, blood vessels, α-SMA, and Collagen type-1 fiber on the burn and excision wound area while the 11th day of HM polymer treatment cured the wound area significantly. Therefore, it could be contemplated that HM polymer is a potential agent for treating different wounds in the near future.

1. Introduction

The normal wound healing process is a dynamic and complex phenomenon involving different signaling cascades and immunomodulatory molecules. The healing process is completed in four phases: hemostasis, inflammation, proliferation, and maturation (Eming *et al* 2014). Most of the time, the healing of burn injuries occurs very slowly compared to that of excision wounds because microorganisms grow very fast in the burn-injured portions due to deep cutting (Juncos Bombin *et al* 2020). A burn wound is a type of serious injury that may happen in different ways (thermally, chemically, electrically, or by stitches) and could be life-threatening (Kalantari *et al* 2020). Depending on the diversity and severity, different

wound healing agents have been developed. Among them, hibiscus plant-derived agents are gaining much interest due to their biocompatibility, nontoxicity, and non-allergic nature. Some plant extracts like *Calendula officinalis, Curcuma longa, Annona reticulata, Zanthoxylum bungeanum, Terminalia arjuna*, etc (Shedoeva *et al* 2019) are already proposed to have potential wound healing capability and are expected to translate into wound care management in the near future (Maver *et al* 2018). *Hibiscus rosa sinensis* leaves extract has also been used for antibacterial, anti-allergic, and skin care due to the presence of flavonoids (Gingasu *et al* 2016), alkaloids (Sivaraman and Saju 2021), and triterpenoids (Saponins) (Gupta *et al* 2009), (Patel *et al* 2012), etc. (Nath and Yadav 2015, Mondal *et al* 2016). The flavonoid compounds inhibit nucleic acid and protein synthesis processes of bacteria by altering their membrane permeability (Oliveira *et al* 2016). In contrast, the alkaloids can offer potential benefits in the wound healing process by regulating the inflammation, oxidative stress, angiogenesis, analgesic, collagen synthesis, cell proliferation, and antibacterial effects (Criollo-Mendoza *et al* 2023). Hence, these are very crucial for wound healing. The other phytochemical terpenoids or triterpenoids inhibit the nuclear factor-$\kappa\beta$ (NF-$\kappa\beta$) signaling pathway and reduce scar formation in injured areas (Salminen *et al* 2008).

Currently, some scientists are focused on biopolymeric components because simple extract cannot protect the wound area causing a delay in the healing process. The biopolymers composed of polysaccharides and proteins are being explored for wound dressing/ healing agents that have some potential properties like (1) stimulate the rapid healing process (Singh *et al* 2022), (2) provide a moist environment to the wound site, (3) allow sufficient gas permeability, such as oxygen exchange, (4) have a high fluid absorption capacity to absorb wound exudates, (5) reduce pain and healing time, (6) have exceptional antibacterial activity, (7) have no cytotoxic effects, and (8) accelerate re-epithelialization (Moholkar *et al* 2021). Several types of synthetic (PLGA, PVA, PEG, etc) (Li and Wang 2021) and natural polymers are developed for the protection of the injured area, but synthetic polymers may have some hazardous effects compared to natural polymers (Sinha *et al* 2015, Amini *et al* 2021). Subsequently, several biopolymers like alginate, hyaluronic acid, chitosan, xanthan gum hydrogel, gum acacia hydrogel, etc. have been used for wound management (Juncos Bombin *et al* 2020, Yang *et al* 2021).

Recently, some scientists isolated biopolymeric mucilage by a filtration process from different sources like okra, fenugreek, *Aloe vera, Bryophyllum* sp., *Hibiscus rosa sinensis, Asparagus racemosus, Cassia angustifolia,* etc (Malviya *et al* 2011). It is reported that the hibiscus mucilage can be used to treat a wide range of ointments like skin infections, and skin barrier (Saidin *et al* 2021); a natural remedy for reducing fever, antiinflammation, antioxidant, and antibacterial activity (Vignesh and Nair 2018a); drug delivery system (Dalvadi *et al* 2013); matrix tablet preparation (Kaleemullah *et al* 2017); stabilizing agent for nanoparticle preparation, mucoadhesive nasal gel preparation (Tyagi *et al* 2015), etc (Bahadur *et al* 2018). However, some limited data is available for wound healing or wound care management using *Hibiscus rosa sinensis* mucilage polymer.

This prompted us to fabricate *Hibiscus rosa sinensis* mucilage, where the wound-healing properties of *Hibiscus rosa sinensis* extract and the biopolymeric advantage of *Hibiscus rosa sinensis* can be available simultaneously. Here, we explored the additional properties of HM polymer and applied it to different kinds of wounds [excision and burn wounds (Jahromi *et al* 2018)]. In this study, the HM polymer was featured both chemically and physically, including a demonstration of its amorphous and mesoporous nature; stability, and absorption capacity. The HM polymer treatment caused improved cellular growth and migration, as measured by BrdU and scratch wound assay respectively. Additionally, the ROS scavenging assay and western blot analysis respectively revealed the antioxidant and anti-inflammatory properties of HM polymer. Furthermore, HM treatment for both excision or burn wounds in male BALB/c mice accelerated the re-epithelialization process and the growth of hair follicles within 11 day of treatment protocols. The *in-vitro* and *in-vivo* experimental process is graphically represented in scheme 1. This result suggests that hibiscus mucilage polymer (HM polymer) can be used for different kinds of wound care management.

2. Methods

2.1. Plant material collection
The young and fresh *Hibiscus rosa sinensis* leaves were collected from the Jadavpur University campus, in Kolkata, India. The leaves were then authenticated by the Agri-horticultural Society of India, Kolkata.

2.2. Synthesis of Hibiscus mucilage polymer
The collected *Hibiscus rosa sinensis* leaves were carefully washed with distilled water, and macerated in 500 ml of deionized water, and then allowed to be stirred for 4–5 h. After that, the macerated leaves were boiled for a few minutes. The concentrated hibiscus solution was then filtered through a muslin cloth. The extracted mucilage was purified by acetone and the precipitated mucilage was dried in a hot air oven at 40 °C. The dried sample is known as HM polymer and it is stored for six months at ambient temperature

Scheme 1. The wound healing capacity of HM polymer is depicted through a diagrammatic representation.
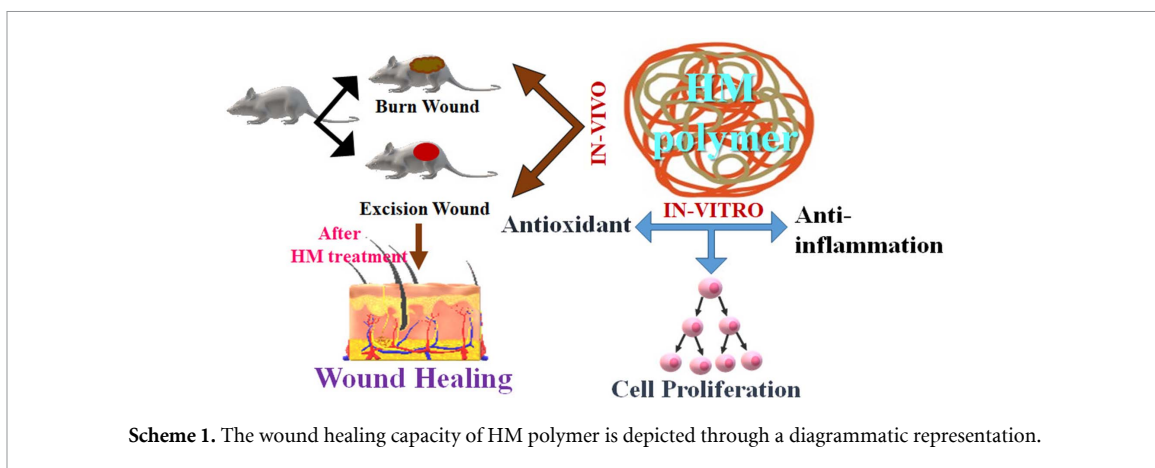
(27 °C–30 °C). The synthesis process is schematically shown in figure S1.

2.3. Physical characterization of HM polymer
The dry HM powder was used in the XRD, FTIR, SEM, and BET studies. The XRD patterns of HM samples were captured using an x-ray diffractometer model D8 from Bruker AXS in Wisconsin, USA. It used a Cu-kα target with a wavelength of 1.5418 A^0 and operated at 35 kV with a scan speed of 1 s/step.

The IR Affinity, Shimadzu was used for the FTIR (Fourier transform infrared spectroscopy) investigation, which covered the 400 cm^{-1}–4000 cm^{-1} wave number range. The samples were made by combining KBr with HM powder and the sample to KBr ratio was 1:50. A hydraulic press mechanism was then used to make the pellets for spectrometry. Additionally, a pure KBr pallet was also constructed for measuring the baseline.

The HM polymer was submerged in distilled water with a concentration of 2 mg ml^{-1} and used for UV–Vis, DLS, and ZETA. UV–Vis (Bio-Tech) absorption spectroscopy was used to measure the absorbance intensity at 250–800 nm wave length. DLS (dynamic light scattering) was used to measure the hydrodynamic size distribution and diameter of particles. The Zetasizer also measured the charges of the samples (NanoZS90, Malvern Instruments Ltd, UK).

For SEM, the dry powder was then cast over carbon grids and coated with gold plasma using a sputtering process. Scanning electron microscopy (Inspect-F50, FEI) was used to analyze the topology of HM.

The pore size of HM polymer and surface area were measured by the most popular technique Gas sorption (both adsorption and desorption) at the clean surface of dry solid powders. BET (Brunauer–Emmett–Teller) specific surface area and pore size distribution of HM polymer were determined by using the Quantachrome Autosorb iQ adsorption instrument. At 77 K and 0–1 bar pressure range, a liquid-nitrogen bath was used to retain the activated samples during an ambient pressure volumetric N$_2$ gas (99.999% purity) adsorption study for HM polymer. Gas or solvent vapour was then allowed to diffuse in the sample tube. The change in gas/vapour pressure in the equilibrium state was used to calculate the quantity of adsorption. The NL-DFT method was used to calculate the pore size distribution from the N$_2$ isotherm at 77 K (Halder *et al* 2021).

2.4. Swelling ratio studies
The water absorbance capacity of HM polymer was measured by swelling studies (Saha *et al* 2023). In the experiment, the dried sample (A$_0$) was accurately weighed, dipped into a petri dish filled with PBS (pH 7.4), and kept the sample for incubation for 24 h at 37 °C. After incubation, the remaining water in the Petri dish was absorbed with tissue paper; the weight of the swelled sample (A$_t$) was measured and the following formula was used to calculate the swelling ratio at time t.

$$\text{Degree of swelling}, \% = \left[(A_t - A_0)/A_0 \right] \times 100.$$

Here A$_t$ and A$_0$ are the weights of the polymer at time t and 0 h respectively.

2.5. Fibroblast cell culture
Human keratinocyte cell line HaCaT (gift from Prof. Runa Sur, Calcutta University, Kolkata, India) and human lung fibroblast cell line WI-38 (NCCS, Pune,) were grown in DMEM (Dulbecco's modified eagle's medium) (Thermo Fisher Scientific (Waltham, MA, USA)) media supplemented with 5% FBS (fetal bovine serum) (Thermo Fisher Scientific (Waltham, MA, USA)), penicillin/streptomycin (100 units/ml) (Thermo Fisher Scientific (Waltham, MA, USA)),

and amphotericin-B (anti-fungal) (Hi-media, India) and the cells were maintained at 37 °C in 5% CO_2 (Heraeus, Thermo Scientific, MA, USA) for all experiments.

2.6. MTT assay

In 24-well plates, human lung fibroblast cell WI-38 and human keratinocyte cell HaCaT were seeded at a density of 2.5×10^4 cells per well. After that, the cells were allowed to be incubated with HM polymer at various concentrations (0, 40, 60, 80, 100, 120, 140, and 160 µg ml^{-1}) for 24 h. Next day of treatment the MTT (3-(4,5-Dimethylthiazol-2-Yl)-2,5-Diphenyltetrazolium Bromide) (SRL, India) dye was added into the cell and incubated for 3 h, at 37 °C. After the completion of the incubation period, the highest cell proliferation concentration of HM polymer was determined by a standard protocol of MTT assay (Saha *et al* 2023). The subsequent cell culture-based experiments were done at the highest proliferation dose of HM for both cell lines separately. The assay was selected as a requirement for additional *in-vitro* and *in-vivo* studies.

2.7. Immuno-cytochemistry and BrdU incorporation assay

BrdU, a thymidine replacement, is used for labeling the DNA of newly proliferating cells. The cell labeling experiment was carried out in accordance with the recommended procedure (Saha *et al* 2023). The experiment is explained here briefly. Firstly, a coverslip was put in a 35 mm culture plate. Then, the WI-38 and HaCaT cells were seeded on the coverslips and treated with HM polymer. After that, 10 µM BrdU (5- bromo $-2'$-deoxyuridine) (Sigma, (St. Louis, MO, USA)) was added to the culture medium, and the cells were allowed to be incubated with the agent for one hour. The coverslips were then taken off from the culture plate, fixed for 30 min with 4% paraformaldehyde, rinsed in PBS, and permeabilized for 10 min with 0.2% Triton X-100 at 4 °C. Following a 30 min exposure to 2 N HCl at room temperature, the cells on the coverslips were blocked with 5% FBS for an hour. A perfect 1:100 dilution of the mouse monoclonal anti-BrdU antibody (BD Biosciences, New Jersey, U.S) was made in wash buffer, and the cells were then treated with the diluted antibody at 4 °C overnight. On the next morning, the coverslips were washed and then incubated with FITC-conjugated goat anti-mouse IgG (Invitrogen, UK) at 1:200 dilutions in wash buffer for 1 h at room temperature under dark conditions. After that, the coverslips were washed and finally attached with slides with the mounting medium containing DAPI (4′6-diamidino-2-phenylindole) (Vector Laboratories, Inc. (CA, USA)). Then cellular images were captured using a fluorescent microscope (Leica, Wetzlar, Germany) with 40 X magnification.

2.8. Scratch-wound-assay

Firstly, the lung fibroblast cell line (WI-38) and the keratinocyte cell line (HaCaT) were seeded separately (3×10^5 cells) in a 35 mm petri plate and incubated for 24 h at 37 °C. A linear wound was created in the monolayer with sterile 200 µl tips. Then the synthesized HM polymer was added into the culture medium at a concentration of 100 µg ml^{-1} for WI-38 and 120 µg ml^{-1} for HaCaT respectively and the cells were incubated for 24 h at 37 °C with 5% CO_2. After 24 h, photographs of the same field of the scratched area were taken to determine the cell migration efficiency under the treatment condition. The performed scratch wound assay was done as per standard methodology (Saha *et al* 2023). This experiment helped with the analysis of the *in-vitro* wound healing study of HM polymer.

2.9. Antioxidant study

The excess production of ROS in injured tissue was neutralized by the antioxidant properties of HM polymer because the maintenance of oxygen-stressed conditions accelerates the process of wound healing (Comino-Sanz *et al* 2021). In this experiment, the cells were seeded firstly on coverslips as per section 2.8, the cells on the coverslips were incubated with 5 mM of N-acetylcysteine (NAC) (Sigma-Aldrich, U.S.) for 3 h, as well as 100 µg ml^{-1} of HM for WI-38 cells and 120 µg ml^{-1} HM for HaCaT cells were treated for 24 h separately. After that, the cells were washed with PBS and subsequently incubated with 100 µM DCF-DA at 37 °C for 30 mins. In this study, DCFH-DA was employed as a probe for ROS. After entering the cells, DCFA-DA is deacetylated into a non-fluorescent compound by the action of cellular esterase. Later, the non-fluorescent compound is oxidized in the presence of ROS and turns into highly fluorescent DCF (2′,7′-dichlorofluorescein). After incubation, the cells were washed in PBS and the cellular images were captured with a fluorescence microscope (Leica, Germany) with 40 X magnification.

2.10. Western blot analysis

The wound healing mediated signaling pathway and protein expressions were analyzed by western blot study. The whole cell lysates of proteins were prepared after HM treatment and then a standard methodology for western blot analysis was followed (Saha *et al* 2023). Here, the primary antibodies Akt (1:1000, rabbit monoclonal, Cell signalling, USA), pAkt (Ser 473) (1:1000, rabbit polyclonal; Cell signalling, USA), TGF-β1 (1:1000, mouse monoclonal, Santacruz biotechnology, USA), IFN-γ (1:1000, mouse monoclonal; Santacruz biotechnology, USA), and GAPDH (1:1000, rabbit monoclonal; Biobharati LifeScience, India) have been used, where GAPDH was used as the loading control. The primary antibody was added membrane and incubated overnight at 4 °C

and the next day the membrane was washed with 1X TBST and added secondary antibody (anti-rabbit or anti-mouse HRP-linked (SRL, India)) and incubated for 1 h at R/T (27 °C–30 °C). The intensity of the membrane was measured with iBRIGHT CL1000 (Invitrogen, U.S.).

2.11. Animal experiments

For these experiments, 25–30 g weight, 6–7 weeks old, male BALB/c mice have been used. The mice were given a limited diet of vitamin-rich pellets and libitum-added water. Animals were monitored and all the experiments were carried out as per guidelines of the committee for purpose of control and supervision of experimental animals (CPCSEA), Government of India, and as approved by the institutional animal ethics committee (IAEC), University of Kalyani.

2.11.1. Experimental design of in-vivo experiments

The mice were divided into six groups each group containing five animals. Three groups were used for excision wounds and another three groups were utilized for burn wounds. For the excision wound model, Group 1: untreated, Group 2: placebo control (silverex Ionic Gel), Group 3: HM polymer treated, and in the case of the burn wound, Group 1: untreated, Group 2: placebo control (silverex Ionic Gel), Group 3: HM polymer treated have been arranged. Mice's dorsal hairs were shaved and washed with 70% ethanol. On the dorsal midline side, one full-thickness excisional wound was made using a 5 mm diameter punch biopsy, and a metal comb was used to create second-degree burns. The mice with excision wounds were monitored on the first, third, sixth, and eleventh days and given treatment on the first, third, and sixth days. In second-degree burn wounds mice were treated on the first, third, sixth, and eighth days and the images were taken on the first, third, sixth, eighth, and eleventh days.

2.11.2. Haematoxylin and eosin staining

The histological study was performed to visualize the changes in injured tissues after the HM treatment. The Haematoxylin staining denoted the nuclear components and eosin signified the cytoplasmic portions along with red blood cells, collagen, muscle fibers, and elastic fibers within the tissue sections (Fischer *et al* 2008). In this experiment, the excised tissue sections were cleaned with PBS, cut into small pieces, and fixed for 24 h in 10% (v/v) neutral buffered formalin (100 ml formalin, 4 g NaH_2PO_4, 6.5 g Na_2HPO_4, and 900 ml H_2O) at room temperature. The procedure for preparing samples for the histological study has been detailed in supplementary section 1. Finally, using a microscope, pictures of tissue sections were taken at 40 X magnification (Leica, Germany).

2.11.3. Immunohistochemistry

The highly effective method, immunohistochemistry (IHC) was used to demonstrate the expression of specific proteins (α-SMA & Collagen type-1) through selective interaction of the antigen-antibody complex formation in tissues. The experiment was carried out using the method described in the Abcam DAB staining protocol, using collagen type 1 (1:50, Santa Cruz Biotechnology, INC, USA) and α-SMA (1:200, Abcam) as primary antibodies and horseradish peroxidase (HRP)-conjugated anti-IgG as the secondary antibody (SRL, India). The detailed procedure has been described in the supplementary section 2. The stained tissue images were captured with a Leica microscope at 40 X magnification. The measurements were undertaken exclusively on the edge of the epidermis. The pixels of positive areas (which correlate with the collagen type 1 and α-SMA activities) and the total areas were analyzed using ImageJ software for each sample in order to obtain an average value together with the corresponding standard deviation value of the microscopic fields. The percentages of stained areas for α-SMA and collagen type 1 protein were to be estimated by ImageJ software.

2.12. Statistical analysis

Every experiment was repeated multiple times and the standard deviation was calculated by all the repeated experiments. The comparisons of the mean of experiments were made by one way ANOVA test (using MS-Excel software) with multiple comparison t–tests, $p < 0.05$ as a limit of significance.

3. Result

3.1. Biophysical properties of Hibiscus mucilage polymer

The XRD pattern of mucilage polymer is shown in figure 1(a). The result indicates that any sharp diffraction maxima are absent in HM polymer therefore, the HM polymer is amorphous in nature.

FTIR analysis was used to evaluate the chemical structure and functional groups of mucilage. The characteristic absorption signal of mucilage polymer was found to be present at 1235.56 cm^{-1}, 2160.71 cm^{-1}, and 2934.44 cm^{-1} for C–O bend (aromatic), C≡C stretch, and C–H stretch respectively (Vignesh and Nair 2018b) moreover, the strong absorption peaks of mucilage polymer at 770.72 cm^{-1}, 1598.36 cm^{-1}, and 1398.82 cm^{-1} were for chloride C–Cl, N–H bending, N=O (Nitro R-NO2) respectively. The C–H stretch at 2934.44 cm^{-1} was also referred to as the presence of the carbohydrates group (Hssaini *et al* 2022). Furthermore, the band at 1737.18 cm^{-1} and its sharp peak denoted the stretching of C=O (aldehyde) for the presence of flavonoids (Oliveira *et al* 2016) and amorphous in nature (Guo *et al* 2010) of polymer accordingly. On the other hand, the strong absorbance peaks at

Figure 1. Physical characterization of hibiscus mucilage polymer (a) the nature of polymer measured with XRD (b) functional groups of polymer evaluated by FTIR spectroscopy (c) absorbance maxima measured by UV–Vis spectroscopy, (d) size measured by DLS, (e) morphology of polymer was measured by SEM and the agglomerate portion of the polymer was mentioned by yellow arrow, (f) absorbance capacity measured by swelling ratio.

1229.24 cm^{-1} for C–O bending, also referred to as alcohol, ether, ester, anhydride, and carboxylic acid. The strong and sharp peaks at 1036.01 cm^{-1} were probably assigned to the C–OH group as well as C–O stretching in the phenol and carbohydrate structure. The absorbance region between 3000–2800 cm^{-1} was most unlikely assigned to C–H, O–H, and NH$_3$ groups, which may be referred to as carbohydrates, carboxylic acids, free amino acids, and phenolic compounds. (Hssaini *et al* 2022). The C–H and O–H stretching between 2900–3380 cm^{-1} absorbance were related to the polysaccharides (Xu *et al* 2012). This result is shown in figure 1(b).

The absorbance of the polymer was measured after the complete dissolution of the mixture in water. UV–Vis spectroscopy was used to determine the absorbance of synthesized components. Our isolated HM polymer formed a broad-spectrum absorbance at 336.14 nm, which is shown in figure 1(c).

The hydrodynamic diameter of the polymer was 1069 d.nm as measured by DLS, and Poly-Dispersity Index (P.D.I) value was 1 (figure 1(d)). Additionally, the surface charge of the pure polymer was −2.68 mV, which was negative and quite stable against coalescence.

The SEM result designated the agglomerate structure of hibiscus mucilage. This agglomerate structure was composed of small particles that are tightly bound together. The agglomerates vary in size and shape depending on the conditions used during

sample preparation (figure 1(e)). The agglomerate structure of HM polymer was marked by a yellow arrow in figure 1(e). After measuring N$_2$ adsorption-desorption experiments, the results of pore sizes and BET surface areas are shown in figure S2. The pore size distribution analysis from N$_2$ sorption data at 77 K and the non-local density function theory (NL-DFT) suggested that the average pore width of HM mucilage polymer was 31.69 Å and the BET surface area was 25.447 m^2 g^{-1}. The HM structure indicated it formed a mesoporous nature that may be ideal for wound management.

The water absorption capacity of HM polymer was evaluated by their swelling properties. After 6 h we observed that the absorbance percentage of HM polymer was 90% which remains the same for up to 24 h (figure 1(f)) moreover swollen polymer maintains its shape with a large surface area at pH 7.5.

3.2. *In vitro* experiment

3.2.1. Demonstration of cell viability, cell proliferation, and cellular migration properties of HM polymer treatment by MTT assay, BrdU assay, and scratch-wound assay, respectively

The cellular metabolic activity and cell viability percentage were measured by the standard MTT assay. The HM treatment, confirms the 100% viability of WI-38 and HaCaT cell lines whereas, 100 μg ml^{-1} and 120 μg ml^{-1} of HM polymer significantly helped to proliferate the cells at about 40% and 50% higher
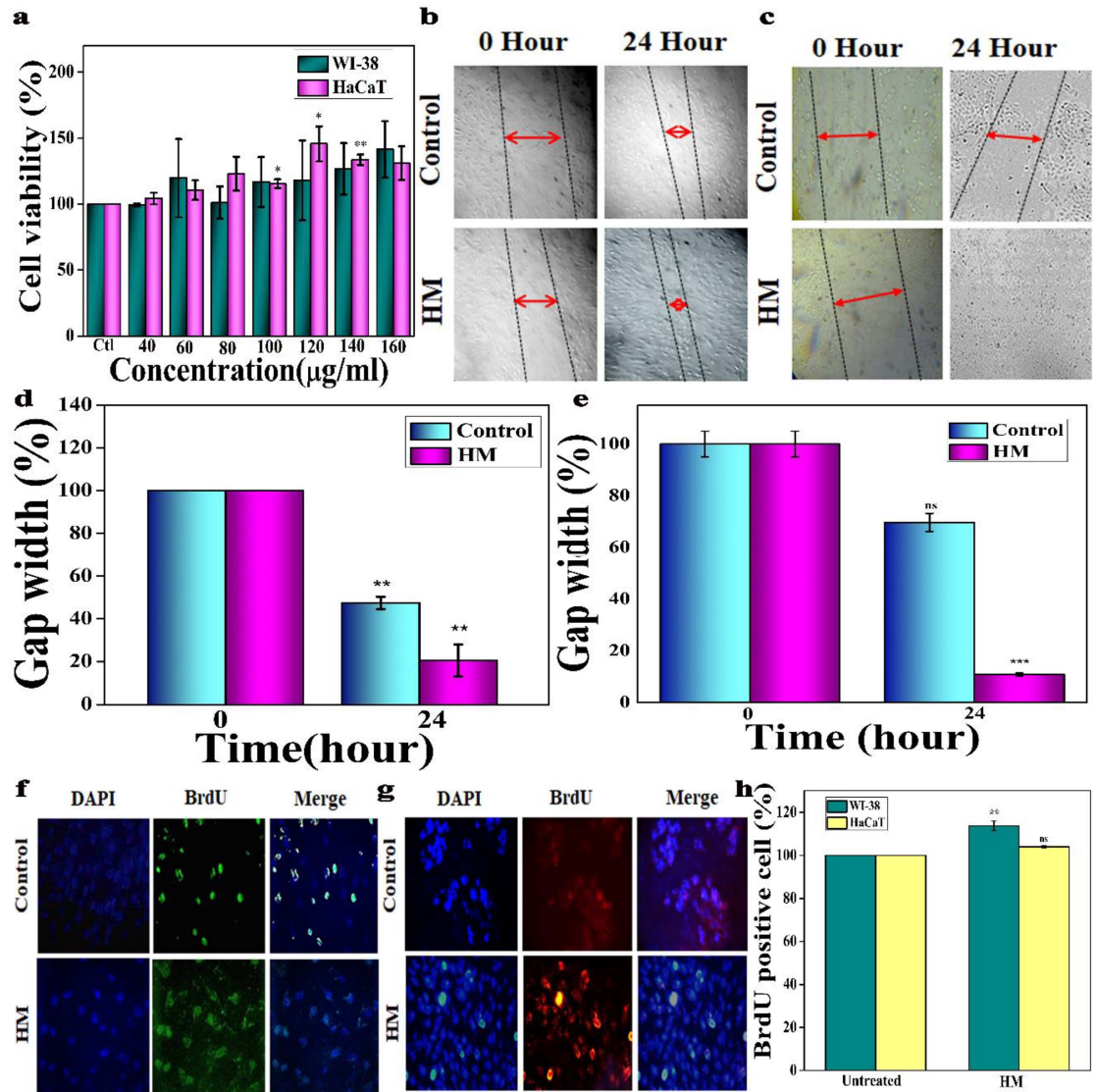
Figure 2. (a) Assessment of cell viability effect of HM polymer by MTT assay; (b), (c) determination of cell migratory efficiency by scratch wound assay; (d), (e) quantitative representation of cell migratory efficiency in terms of 'Gap width'; (b), (d) for WI-38 cell line and (c), (e) for HaCaT cell line; (f), (g) assessment of newly proliferated cells by DNA probing with BrdU staining assay. The representative WI-38 and HaCaT cell images of BrdU staining were shown in figures (f), (g) respectively. The quantitative estimation of BrdU positive WI-38 and HaCaT cells was shown in the respective figure (h). All results were represented as mean $\pm$ SD, * ($P < 0.05$), ** ($P < 0.01$), and *** ($P < 0.001$) in comparison to untreated.

rates, respectively, compared to untreated cells under the same conditions (figure 2(a)). Moreover, our synthesized HM polymer helped with cellular metabolic activity and simultaneously cell proliferation process.

On the other hand, the proliferation efficacy of HM polymer has been confirmed by another experiment, like BrdU assay. A thymidine analog, BrdU was incorporated into the DNA during synthesis of the proliferating cells. Thus BrdU labelling can be considered as direct evidence of proliferating cells. It was found that HM polymer treatment significantly increased the presence of BrdU-positive cells at 10% and 5% in the WI-38 and HaCaT cell lines, respectively, over the untreated cells (figures 2(f)–(h)). This result confirmed the cellular proliferation capability of HM polymer.

Next, the effect of HM polymer treatment on cellular migration, an important property of wound healing, was studied by the scratch-wound assay. Here it has been found that HM-treated WI-38 and HaCaT cells covered the created scratch wound area by 80% and 90% (figures 2(b)–(e)) respectively, compared to mock-treated cells. It is also noted that the HM polymer treatment showed a significantly better effect on the HaCaT cell line compared to the WI-38 cell line in cellular migration. The keratinocyte cell plays a crucial role in tissue migration in the process of wound healing.

3.2.2. Assessment of antioxidant properties (ROS scavenging) of HM polymer by DCF-DA method
The over expressed reactive oxygen species (ROS) in oxidative stressed conditions lead to impaired wound
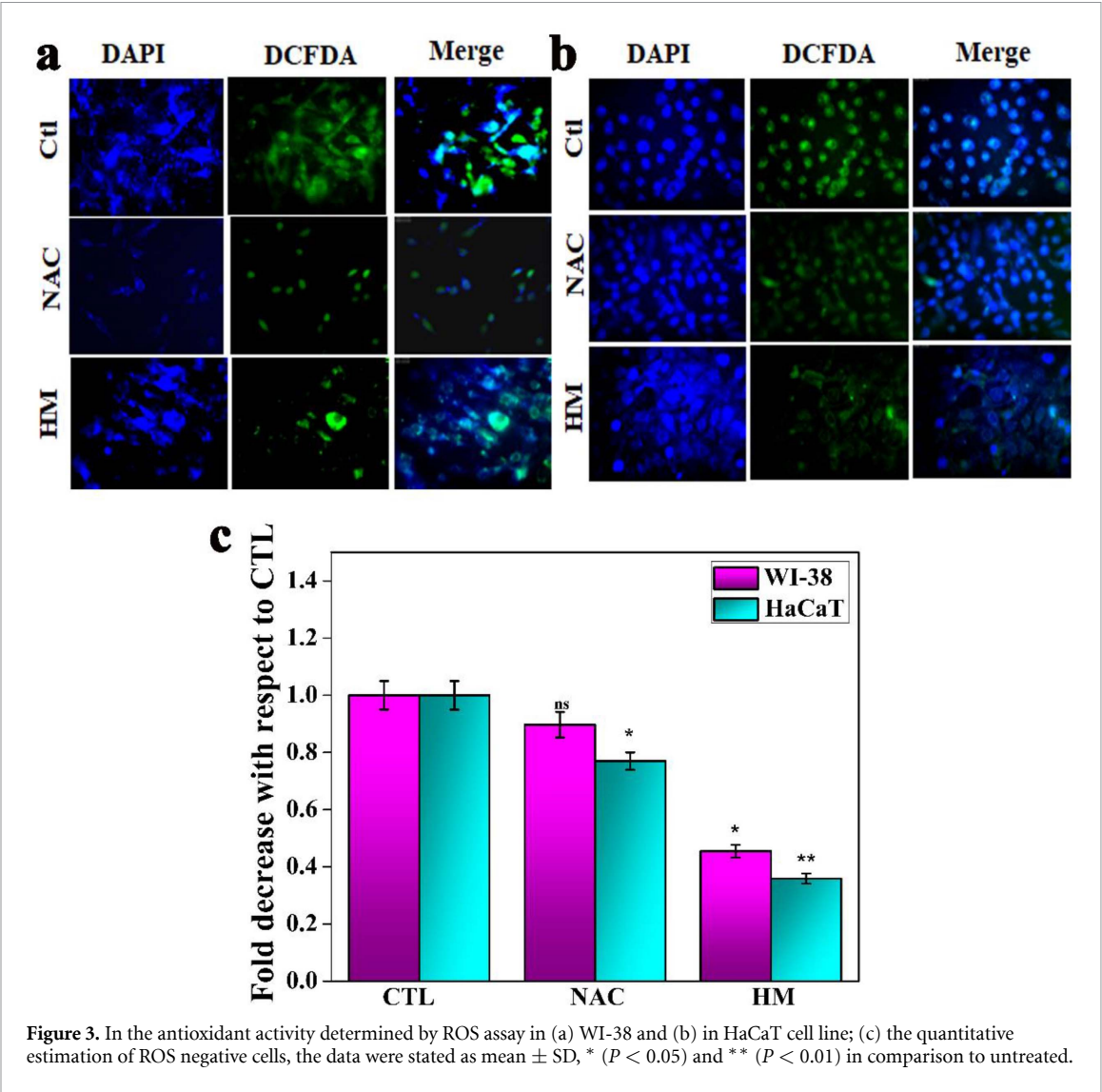
Figure 3. In the antioxidant activity determined by ROS assay in (a) WI-38 and (b) in HaCaT cell line; (c) the quantitative estimation of ROS negative cells, the data were stated as mean $\pm$ SD, * ($P < 0.05$) and ** ($P < 0.01$) in comparison to untreated.

healing. Therefore, antioxidants regulate oxidative stress and thereby accelerate the process of wound healing. The HM-treated WI-38 and HaCaT cell lines were used for the ROS scavenging assay. The ROS production was decreased in NAC-treated cells was 0.1 fold in WI-38 cells and 0.2 fold in HaCaT cell lines compared to untreated cells. On the other hand, the amounts of ROS production in HM-treated WI-38 and HaCaT cell lines were significantly decreased by 0.5 and 0.6 fold, respectively, than that of the untreated cells (figure 3). Thus HM polymer showed better antioxidant properties in comparison to the well-known antioxidant drug NAC.

3.2.3. Assessment of protein and signaling pathway expression of HM polymer treatment through the immunoblot analysis

To provide further evidence for the proliferating potential of HM-treated cells, we determine the pAkt (Ser473), TGF-β1, and IFN-γ protein levels by immunoblot analysis of whole cell extract. The TGF-β1, which is upregulated during granulation tissue formation and IFN-γ play an important role in the inflammation phase of wound healing, it are also assessed by immunoblotting. In this experiment, the various concentrations of cell lysate were selected based on a cell proliferation assay. In figures 4(a) and (c) the relative intensities for the proteins pAkt (Ser 473) were 74%, and 114%; TGF-β1 intensity were 83%, and 106%; and IFN-γ were 128%, and 95% respectively at a concentration of 60 μg ml^{-1}, and 100 μg ml^{-1} of HM treatment compared with untreated WI-38 cells. In the case of the HaCaT cell line, pAkt (Ser 473) intensity were 121%, and 137%; TGFβ1 intensity were101%, and 152%; and IFN-γ intensity were 114%, and 43%, so, in high concentration, respectively at the concentration of 80 μg ml^{-1}, and 120 μg ml^{-1} of HM treatment compared with untreated cells (figures 4(b)–(d)). The HM polymer acts as an anti-inflammatory component, so in high concentration, it decreases the intensity of IFN-γ.
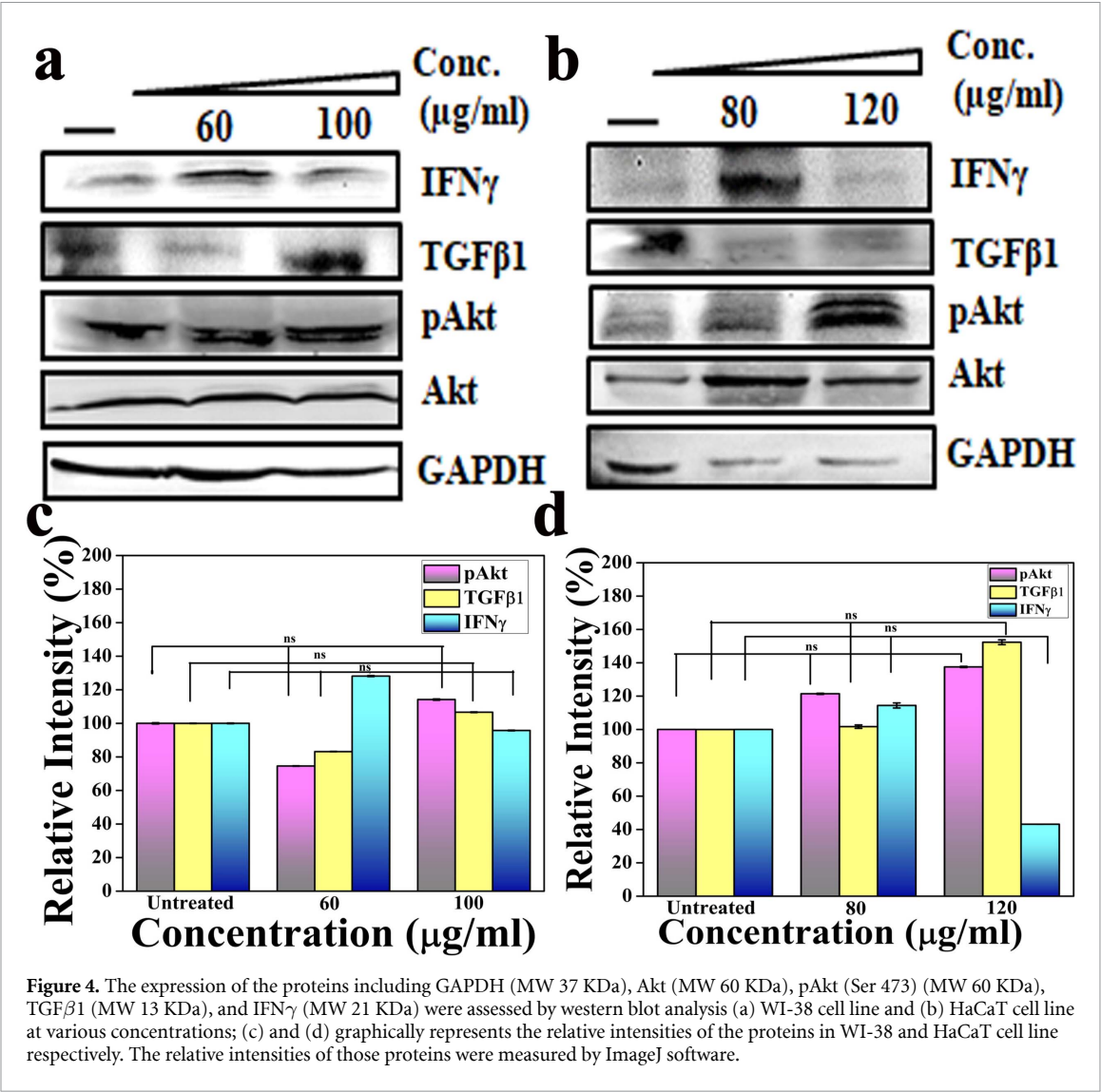
Figure 4. The expression of the proteins including GAPDH (MW 37 KDa), Akt (MW 60 KDa), pAkt (Ser 473) (MW 60 KDa), TGFβ1 (MW 13 KDa), and IFNγ (MW 21 KDa) were assessed by western blot analysis (a) WI-38 cell line and (b) HaCaT cell line at various concentrations; (c) and (d) graphically represents the relative intensities of the proteins in WI-38 and HaCaT cell line respectively. The relative intensities of those proteins were measured by ImageJ software.

3.3. *In vivo* experiment

3.3.1. Measurement of the second-degree burn and excision wound healing area

In BALB/c male mice, the created excision and burn wounds were treated with HM polymer at 8 mg kg^{-1} body weight in both cases. The micrograph images depicted that the HM-treated excision and second-degree burn wound areas were gradually reduced whereas the reduction of wound areas happened abruptly in the silverex ionic gel treated (Placebo control) and the untreated mice (figures 5(a) and (b)). Figures 5(c) and (d) represent the results of a quantitative investigation of the wound healing capacity in HM-treated, placebo control, and untreated murine models. On the 11th day, the HM-treated excision wound area was reduced to 63% while the placebo group recovered the wound area at 50% and the untreated group recovered at 40%, compared to the 1st day of wound creation (figure 5(c)). On the other hand, the 11th day, the HM treatment repaired second-degree burn wounds by 61% than that of untreated group. However, the second-degree burn

wound areas were found to be recovered by 40% in the placebo group and untreated group on the 11th day (figure 5(d)) compared to the 1st day of wound creation. Therefore, this result suggests that the HM polymer has shown better efficacy than the well-known wound healing ointment Silverex ionic gel.

3.3.2. Histological study of excision and second-degree burn wound tissue:

The process of wound healing is coordinated by different types of cells which were detected by histological study. The first phase of wound healing i.e. hemostasis is characterized by a damaged epidermis (Rodrigues *et al* 2019). In the excision wound (figure 6(a)), the epidermis (white arrow) was found to recover on the 6th day of HM and silverex treatment (placebo control) but the epidermis started to recover on the 11th day of untreated. In the case of burn wounds (figure 6(b)), HM treatment promoted the recovery of the damaged epidermis (White arrow) within the 6th day; silverex (Placebo control) and

Figure 5. Measured the wound recovery area after various treatments. (a) excision and (b) second-degree burn woundswere created on the dorsal portion of male BALB/c mice, the quantitative estimation of wound area for (c) excision wound and (d) burn wound, (* is $P < 0.05$,)area was measured by ImageJ software.

Figure 6. Histopathological features of wounded murine tissue (a) excision wounded mice tissue and (b) second-degree burn wounded mice tissue. Where the white arrow is epidermis, the yellow arrow is neutrophil infiltration, the red arrow is blood vessels, the black arrow is granulation tissue, and the sky-blue arrow is hair follicles. Original magnification 40X, scale bar-80 μm.

untreated showed no signs of epidermis recovery after the 11th day.

During the next inflammation stage neutrophils or WBC accumulate to remove necrotic tissue and pathogens by phagocytosis, release of ROS, antimicrobial peptides, and proteolytic enzymes (De De Oliveira *et al* 2016). Inflammatory signs (yellow arrow) were seen to be limited on the third day of HM treatment in both the types of wounds (figures 6(a) and (b)) while in the case of silverex treatment (placebo control) inflammation had been extended to 6th day in burn wound but limited up to 3rd day in case of excision wound. In untreated, neutrophil infiltration has been increased from the 3rd to 6th day of injury for excision wound but in burn wound, inflammation started on the 6th day and it was continued up to the 11th day. The extensive inflammation promotes tissue injury and delays the healing process.

The third phase of healing is a proliferative stage that involves extensive activation of keratinocytes, fibroblasts, macrophages, and endothelial cells to orchestrate wound closure, matrix deposition, and angiogenesis (Tonnesen *et al* 2000). Activation of endothelial cells leads to the process of angiogenesis i.e. development of a new blood vessel (red arrow) on the sixth day for every group of mice but the process of angiogenesis had been continued on 11th days in untreated and placebo groups whereas HM treatment, this process was completed on 6th day in both groups (burn and excision) of mice.

The last phase of wound healing is matrix remodeling which spans the entire injury spectrum of responses, beginning with the initial deposition of a fibrin clot and ending with a mature scar that is rich in collagen type 1. Scar formation was initiated with the development of granulation tissue (black arrow). In the excision wound, granulation tissue started to develop on the 6th day and continued on 11th day of HM treatment but the granulation tissue was not developed in the silverex (placebo control) and untreated conditions, whereas in burn wound, HM treatment and silverex treatment (placebo control) accelerated the process of granulation tissue development within the 3rd day and 6th day respectively and it was continued to the 11th day, but in untreated group the granulation tissue was formed on 11th day.

As healing progresses, collagen type III of granulation tissue is replaced by collagen type I which resurfaces the wound with the development of hair follicles (sky arrow). In the burn and excision wounds, hair follicles started to develop on 3rd day of HM treatment; silverex treated (placebo control) excision and burn wound accelerated the hair follicle formation on the 6th day and 11th day respectively, but in both cases, untreated groups started hair follicle formation on 11th day.

3.3.3. Estimation of α-SMA and type 1 collagen by immunohistochemistry

The formation of neo-connective tissue (activated fibroblast), differentiation of fibroblast into myofibroblast, and new blood vessel formation, etc at the wound site are detected by the expression of α-SMA and collagen type 1 protein in the tissue from the post-wounded area. In excision wounds, the expression of α-SMA (figure 7(a)) increased from 12% to 28% for the untreated group, 12% to15% for the silverex treatment (placebo control), and 48% to 55% for HM treatment from the 6th (sky blue bar) to the 11th (brown bar) day of treatment, whereas the expression of collagen type 1 (figure 7(b)) was 22% to 2%, 2% to 8%, and 32% to 20% in untreated, placebo control and HM-treated tissues respectively within the 6th (sky blue bar) to 11th (brown bar) days of post-wound.

In the case of burn wound (figure 7(c)), the expression level of α-SMA was changed from 18%–68%, 65%–62%, and 70%–35% in untreated, silverex (placebo control), and HM-treated tissues respectively and the percentage of collagen type 1 was changed from 32%–40%, 28%–31% and 48%–25% for untreated, placebo control and HM treated mice respectively (figure 7(d)) within 6th (green) to 11th (purple) days of the treatment regimen.

The result suggested that HM therapy significantly increased the level of collagen type 1 in both types of wounds within the 6th day while HM treatment elevated the expression of α-SMA in excision wounds by the 11th day as well as second-degree burn wounds by the 6th day. As previously reported after the resolution phase of wound healing the number of cells is dramatically decreased by apoptosis of both vascular cells and myofibroblasts (Darby *et al* 2014). On the other hand, this result also significantly suggested that on the 11th day, HM treated second-degree burn, and the excision wound completed its inflammation phase and repaired the injured area.

4. Discussion

In the past, different parts of the *Hibiscus rosa sinensis* plant were used to make traditional medicines (Jadhav *et al* 2009), such as antibacterial, antioxidant, and wound-healing medicines. Most people currently use natural products or biopolymeric materials for health care, such as sodium alginate hydrogel (Bahadoran *et al* 2020), carbopol, hyaluronic acid, chitosan, silk fibroin, xanthan gum, gum acacia, etc. Biopolymer also has certain advantages such as being biocompatible, biodegradable, well available, non-irritant in nature, cost-effective, and lastly, antimicrobial and anti-inflammatory properties making them an ideal component of wound healing (Jani *et al* 2009, Saha *et al* 2023).
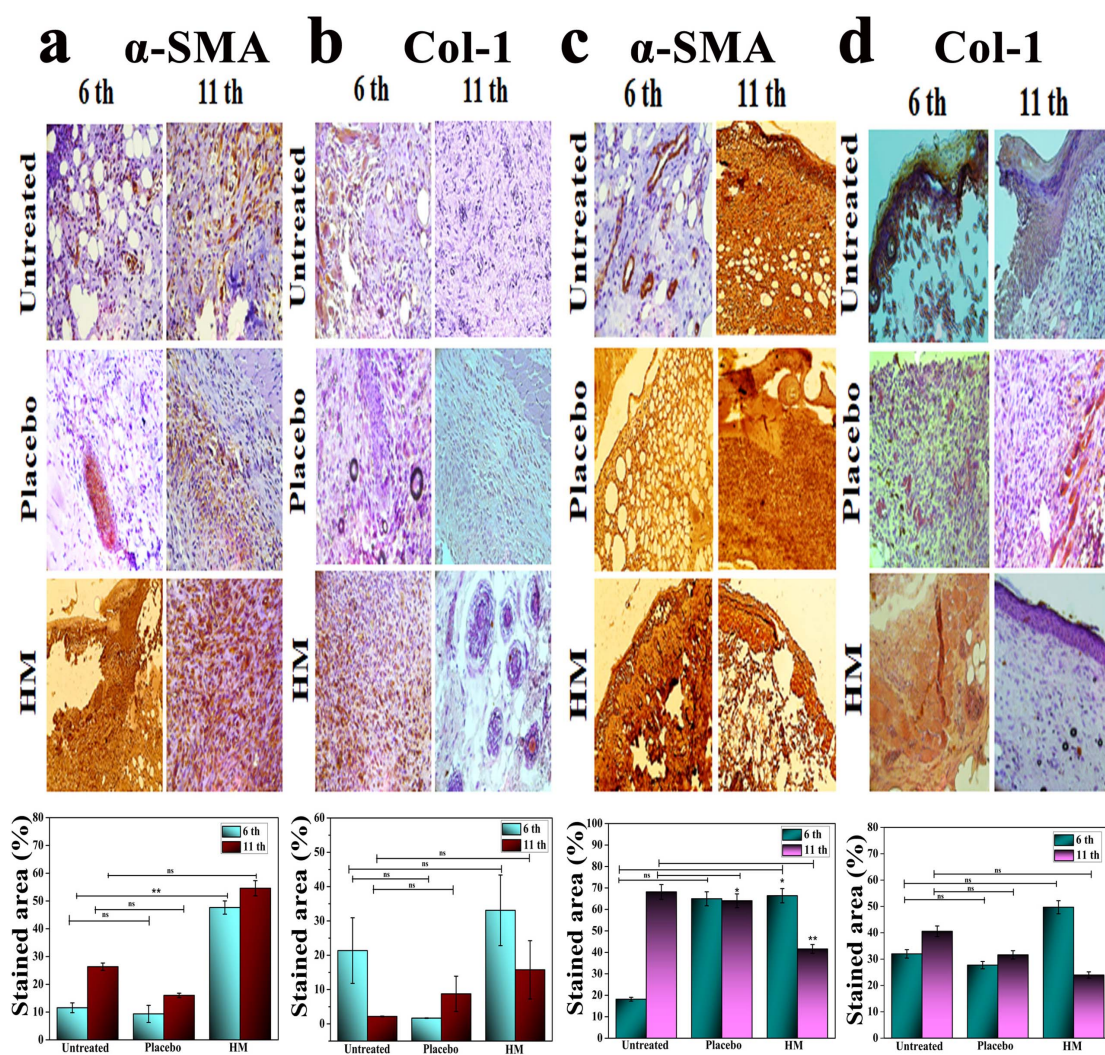
Figure 7. Immunostaining was performed with anti-α-SMA (rabbit, Abcam, 1:200) and anti-type 1 collagen (goat, Santa Cruz Biotechnology, 1:50) as primary antibodies and horseradish peroxidase (HRP)-conjugated anti-IgG as a secondary antibody. The images were taken in 40 X magnification, the scale bar is 80 μm. (a), (b) Immunostaining of excision wound tissue; (c), (d) immunostaining of burn wound tissue; quantitative representation of the stained area in murine tissue in the 6th and 11th days of treatment for α-SMA and collagen type I in excision and burn wounds, respectively. The positively stained areas were calculated using ImageJ software. Results were expressed as mean $\pm$ SD, * ($P < 0.05$) and ** ($P < 0.01$) in comparison to untreated.

Mucilage is a mucoadhesive polymer (Dalvadi *et al* 2013), it is made up of polysaccharides, sugar, uronic acid, and some minerals (Gupta *et al* 2015, Tyagi *et al* 2015, Vignesh and Nair 2018a). Recently, many pharmaceutical industries have focused on plant-derived gum and mucilage polymer as a binder, disintegrant, emollient, emulsifier, gelling agent, etc (Malviya *et al* 2011, Kassakul *et al* 2014, Kaleemullah *et al* 2017). The hibiscus mucilage biopolymer is hydrocolloid, and hydrophilic in nature; carries emulsifier, and gelling properties; and is suitable for topical application on wound healing (Bakr *et al* 2021). In recent times different scientists have used hibiscus mucilage as a drug-loading carrier and applied it to different biological functions like antioxidant, anticonvulsant, hypoglycaemic, antimicrobial activity, etc. (Jani and Shah 2008, Kaleemullah *et al* 2017, Vignesh and Nair 2018a Bakr *et al* 2021, Sen *et al*

2022). Previously reported the *Hibiscus rosa sinensis* mucilage consisted of different types of minerals like Cu (6.42 mg Kg^{-1}), Zn (10.54 mg Kg^{-1}), and Se (0.23 mg Kg^{-1}), which helped for metalloenzymes and antioxidants activity (Bakr *et al* 2021). In this study, Hibiscus mucilage polymer (HM) was developed from *Hibiscus rosa sinensis* fresh leaves. The HM polymer formulation process is facile and less time-consuming. The HM polymer contains different types of wound healing responsive phytochemicals like reducing sugar, flavonoids, and acidic polysaccharides (27% Galactosides, 24% L Rhamnose, 19% D-galacturonic acid, D-galactose, Glucuronic acids etc.) (Jani and Shah 2008, Kassakul *et al* 2014, Vignesh and Nair 2018b, Vignesh and Nair 2018a, Bakr *et al* 2021). The physicochemical properties of HM polymer were characterized by XRD, FTIR, UV–Vis, SEM, DLS, BET, and Swelling ratio. A very low amount of

crystallinity structures is present in hibiscus mucilage extract, as suggested by the existing literature (Ash *et al* 2019, Sen *et al* 2022) while the XRD result indicated HM polymer did not show any crystallinity in structure and it carried only an amorphous pattern. Additionally, FTIR confirms the characteristic vibrational bands and thereby suggesting its purity. The FTIR result also suggested that the polymer is made up of carbohydrates (Zhang *et al* 2023), flavonoids, and phenolic compounds. The flavonoids and phenolic compounds upregulate the cellular expression of antioxidants, anti-inflammation, and proliferation (Oliveira *et al* 2016). Carbohydrate provides energy to the body, they upregulate collagen formation, angiogenesis, inflammatory response, cellular activity, fibroblast formation, cell migration process, leucocyte and neutrophil formation, as well as stimulates various growth factors secretion. (Barchitta *et al* 2019). Castro *et al* stated that carbohydrate, proteins, lipids, and nucleic acids percentages are increased in the body after burn injuries which is associated with the initiation of the hemostasis process along decrease in the metabolic activity and progress of the wound healing process (Vazquez-Zapien *et al* 2023). However, carbohydrates provide support for hemostasis, inflammation, proliferation, and maturation phases of the wound healing process. Therefore, we can conclude that C–H stretches at 2934.44 cm^{-1} for the carbohydrate group, C=O stretching at 1737.18 cm^{-1} for the flavonoid group and C–O stretching at 1036.01 cm^{-1} for the phenolic group are highly responsible functional groups of HM polymer for the second-degree burn and excision wound healing.

The broad spectrum absorbance of HM polymer was observed by UV–Vis spectroscopy. The highest absorption peak of mucilage polymer is at 336.14 nm. The SEM result indicated that the structure of the polymer is agglomerate in nature whereas the BET analysis suggested the mesoporous nature of the polymer. These are quite interesting characteristic features of a polymeric material that can accelerate the process of wound healing.

The swelling ratio study is the most essential property for wound healing agents because exudates absorption from the wounded portion is the most important function for ignition of the process of wound healing (Ruffo *et al* 2022, Lu *et al* 2023).

In vitro studies were conducted for the assessment of wound-healing properties of HM polymer in human lung fibroblast WI-38 and keratinocyte HaCaT cell lines. The actual phenomenon of wound healing i.e. cellular proliferation is promoted under HM treatment. The cell viability, cellular migration, and formation of newly dividing cells were confirmed by MTT assay, scratch wound assay, and BrdU incorporation assays respectively. HM treatment increased cell proliferation by 40% and 50% compared to the untreated condition, and these proliferating cells filled the gap (scratch wound) faster by about 80% and 90% than untreated cells, and increased by 10% and 5% newly dividing cells formation compared to an untreated condition in WI-38 and HaCaT cell lines respectively. The MTT assay suggests that HM polymer is more effective for cell proliferation process because it simultaneously helped for cellular metabolic process. The scratch-wound assay suggests that HM is more effective for migration in keratinocytes than the lung fibroblast cell lines. The keratinocyte cells play an important role in restoring the epidermal fence during the recovery from wound injury (Ter Horst *et al* 2018). The level of reactive oxygen species (ROS) in cells plays a crucial role in cell survivability and wound healing process. Low levels of ROS are beneficial in protecting tissues against infection and by producing cell survival signaling, but when ROS is present in excess, it produces oxidative stress leading to cell damage and an extended pro-inflammatory phase as seen in the case of diabetic wounds (Schieber and Chandel 2014). The synthesized HM was found to decrease the excess level of ROS in cells in a better manner than the well-known antioxidant NAC. Reduction in ROS level may be one of the underlying mechanisms of HM-induced proliferation of fibroblast and keratinocyte cells.

The effectiveness of HM polymer for wound healing was investigated by immunoblot assay. The following proteins: the transforming growth factor-β1 (TGF-β1), pAkt (Ser 473), and IFN-γ play an important role in cellular proliferation and wound healing in the animal body. TGF-β1 plays a dual role in cellular proliferation either stimulatory or inhibitory depending on the cell types. The profibrogenic cytokine TGF-β1 is a powerful activator of connective tissue synthesis and fibroblast proliferation and a critical paracrine signal for the development of pulmonary fibrosis and differentiation into myofibroblasts in the lung (Horng *et al* 2019, Wei *et al* 2019). In the HaCaT cell line, the phosphatidylinositol 3-kinase (PI3K)/protein kinase B (Akt) signaling system controls angiogenesis, metabolism, cell proliferation, differentiation, and migration (Teng *et al* 2021). During wound healing, the wound edge up-regulates p-AKT at serine-473 compared to undamaged skin (Jere *et al* 2019). IFN-γ is a pro-inflammatory cytokine, that is released at the inflammatory phase that at higher doses, degrades the foreign particle, and encourages cellular proliferation, migration, and invasion (Krzyszczyk *et al* 2018) but after a long time effect, it delays the wound healing process and can strongly increase the risk of wound infection (Liu *et al* 2020). Here we have used untreated, 60, and 100 μg ml^{-1} HM-treated WI-38 cell lysate and noticed that 100 μg ml^{-1} is a

suitable treatment concentration for the maximum expression level of TGF-β1 and pAkt (Ser 473) protein and minimum expression level of IFN-γ protein. Similarly, in the HaCaT cell line we used untreated, 80, and 120 µg ml^{-1} HM-treated cell lysate and observed that 120 µg ml^{-1} of HM-treated HaCaT cell lines showed the highest level of TGF-β1 and pAkt (Ser 473) expression and the IFN-γ expression was gradually reduced. Therefore, this result also suggested, that we can use the HM polymer for anti-inflammatory purposes in various wound healing applications.

In the *in-vivo* experiment, the wound healing activity of HM polymer was also investigated in the excision and second-degree burn wounds in male BALB/c mice where HM was found to have better overall action in repairing wound tissue than the commercial drug silverex ionic gel (placebo control). The multi-stage wound healing process is characterized by the involvement of different types of cells like damaged epidermis, neutrophil infiltration, endothelial cells, granulation tissue formation, and hair follicle development. The involvement of different types of cells at a particular phase led to the process of wound closure and scar formation. Scar formation is characterized by the differentiation of fibroblasts into myofibroblasts, whereas the maturity of the myofibroblast is marked by the presence of α-SMA protein. The α-SMA is an important mediator in the contraction and remodeling of the healing scar (Shinde *et al* 2017). The higher level of expression of α-SMA protein on the 6th and 11th days of HM treatment indicates its speedy action on wound closure and on the 11th day the highest expression of α-SMA protein indicates the process of differentiation of myofibroblast is still continuing at the time of excision wound but in case of burn wound, on 11th day of HM treatment the expression of α-SMA was reduced from the expression of α-SMA on 6th day of treatment. The gradual decreasing trend of α-SMA protein designated scar formation, while the maturity of the scar was indicated by the presence of collagen type 1 protein along with the development of hair follicles. The primary constituent of connective tissue, collagen is essential for wound healing because it provides the structural foundation for tissue remodeling, which increases wound strength (Schultz *et al* 2011). The higher expression of collagen type 1 on the 6th and 11th days of HM treatment in both wounds confirmed that HM is more effective as a healing material than silverex Ionic gel (placebo control). In an excision wound, the increasing trend of collagen 1 indicates the maturation process of the scar which means the strength of wound closure is going on, whereas the decreasing level of collagen type 1 in a burn wound indicates the scar maturity has been completed almost. Therefore, the HM is an effective biopolymeric agent for second-degree burn and excision wound healing.

5. Conclusion

To sum up our article, the hibiscus mucilage polymer (HM) is a biocompatible compound and potentially effective in exhibiting antioxidants, anti-inflammation, and cellular proliferation capabilities. Furthermore, HM is found to be a potent excision and second-degree burn wound healing and management material in the murine model. Additionally, the polymer is environment-friendly and has a low manufacturing cost. Thus, it could be used as a desirable substance for potential use in variable biomedical applications or as a drug delivery vehicle.

Data availability statement

The data cannot be made publicly available upon publication because they are not available in a format that is sufficiently accessible or reusable by other researchers. The data that support the findings of this study are available upon reasonable request from the authors.

Ethical statement

All applicable guidelines for the care and use of animals were followed by the Committee for Purpose of Control and Supervision of Experimental Animals (CPCSEA). The experimental protocols were approved by the Institutional Animal Ethics Committee (IAEC), Kalyani University, India (Registration No: 892/GO/Re/S/01/CPCSEA).

Conflict of interest

The authors have no conflict of interest to declare.

ORCID iD

Parimal Karmakar ⓘ https://orcid.org/0000-0002-9423-9906

References

Amini S, Salehi H, Setayeshmehr M and Ghorbani M 2021 Skin barrier modulation by Hibiscus rosa-sinensis L. mucilage for transdermal drug delivery *Polym. Bull.* **79** 1–17

Ash D, Ghosh P, Majee S B and Biswas G R 2019 Hibiscus leaf mucilage as stabiliser for pharmaceutical disperse systems *Int. J. Appl. Pharm.* **11** 6–11

Bahadoran M, Shamloo A and Nokoorani Y D 2020 Development of a polyvinyl alcohol/sodium alginate hydrogel-based scaffold incorporating bFGF-encapsulated microspheres for accelerated wound healing *Sci. Rep.* **10** 1–18

Bahadur S, Roy A, Baghel P, Choudhury A, Saha S and Chanda R 2018 Formulation and evaluation of glipizide tablets utilizing Hibiscus rosasinensis leaves mucilage *Indones. J. Pharm.* **29** 23

Bakr R O, Amer R I, Attia D, Abdelhafez M M, Al-Mokaddem A K, El-Gendy A E N G and Gad S S 2021 In-vivo wound healing activity of a novel composite sponge loaded with mucilage and lipoidal matter of Hibiscus species *Biomed. Pharmacother.* **135** 111225

Barchitta M, Maugeri A, Favara G, Magnano San Lio R, Evola G, Agodi A and Basile G 2019 Nutrition and wound healing: an overview focusing on the beneficial effects of curcumin *Int. J. Mol. Sci.* **20** 1119

Comino-Sanz I M, López-Franco M D, Castro B and Pancorbo-Hidalgo P L 2021 The role of antioxidants on wound healing: a review of the current evidence *J. Clin. Med.* **10** 3558

Criollo-Mendoza M S, Contreras-Angulo L A, Leyva-López N, Gutiérrez-Grijalva E P, Jiménez-Ortega L A and Heredia J B 2023 Wound healing properties of natural products: mechanisms of action *Molecules* **28** 598

Dalvadi H P, Shah D, Saralai M G and Patel J K 2013 Evaluating the mucoadhesive properties of mucilage of hibiscus rosasinensis linn., drug delivery systems *Int J.* **3** 16–21

Darby I A, Laverdet B, Bonté F and Desmoulière A 2014 Fibroblasts and myofibroblasts in wound healing *Clin. Cosmet. Invest. Dermatol.* **7** 301–11

De Oliveira S, Rosowski E E and Huttenlocher A 2016 Neutrophil migration in infection and wound repair: going forward in reverse *Nat. Rev. Immunol.* **16** 378–91

Eming S A, Martin P and Tomic-Canic M 2014 Wound repair and regeneration: mechanisms, signaling, and translation *Sci. Transl. Med.* **6** 265sr6

Fischer A H, Jacobson K A, Rose J and Zeller R 2008 Hematoxylin and eosin staining of tissue and cell sections *Cold Spring Harb. Protocols* **2008** db–prot4986

Gingasu D, Mindru I, Patron L, Calderon-Moreno J M, Mocioiu O C, Preda S and Chifiriuc M C 2016 Green synthesis methods of $CoFe_2O_4$ and $Ag-CoFe_2O_4$ nanoparticles using hibiscus extracts and their antimicrobial potential *J. Nanomater.* **2016** 1–12

Guo L, Sato H, Hashimoto T and Ozaki Y 2010 FTIR study on hydrogen-bonding interactions in biodegradable polymer blends of poly (3-hydroxybutyrate) and poly (4-vinylphenol) *Macromolecules* **43** 3897–902

Gupta S, Parvez N and Sharma P K 2015 Extraction and characterization of Hibiscus rosasinensis mucilage as pharmaceutical adjuvant *World Appl. Sci. J.* **33** 136–41

Gupta V, Bansal P, Garg A and Meena A K 2009 Pharmacopoeial standardization of Hibiscus rosa sinensis Linn *Int. J. Pharm. Clin. Res.* **1** 124–6

Halder A, Maiti A, Dinda S, Bhattacharya B and Ghoshal D 2021 Unraveling the role of structural dynamism in metal organic frameworks (MOF) for excited-state intramolecular proton transfer (ESIPT) driven water sensing *Cryst. Growth Des.* **21** 6110–8

Horng H C, Chang W H, Yeh C C, Huang B S, Chang C P, Chen Y J and Wang P H 2019 Transforming growth factor (TGF)-β1-induced miR-133a inhibits myofibroblast differentiation and pulmonary fibrosis *Cell Death Dis.* **10** 670

Hssaini L, Razouk R and Bouslihim Y 2022 Rapid prediction of fig phenolic acids and flavonoids using mid-infrared spectroscopy combined with partial least square regression *Front. Plant Sci.* **13** 429

Jadhav V M, Thorat R M, Kadam V J and Sathe N S 2009 Traditional medicinal uses of Hibiscus rosa-sinensis *J. Pharm. Res.* **2** 1220–2

Jahromi M A M, Zangabad P S, Basri S M M, Zangabad K S, Ghamarypour A, Aref A R and Hamblin M R 2018 Nanomedicine and advanced technologies for burns: preventing infection and facilitating wound healing *Adv. Drug Deliv. Rev.* **123** 33–64

Jani G K and Shah D P 2008 Evaluation of mucilage of Hibiscus rosasinensis Linn as rate controlling matrix for sustained release of diclofenac *Drug Deliv. Ind. Pharm.* **34** 807–16

Jani G K, Shah D P, Prajapati V D and Jain V C 2009 Gums and mucilages: versatile excipients for pharmaceutical formulations *Asian J. Pharm. Sci.* **4** 309–23

Jere S W, Houreld N N and Abrahamse H 2019 Role of the PI3K/AKT (mTOR and GSK3β) signalling pathway and photobiomodulation in diabetic wound healing *Cytokine Growth Factor Rev.* **50** 52–59

Juncos Bombin A D, Dunne N J and McCarthy H O 2020 Electrospinning of natural polymers for the production of nanofibres for wound healing applications *Mater. Sci. Eng.* C **114** 110994

Kalantari K, Mostafavi E, Saleh B, Soltantabar P and Webster T J 2020 Chitosan/PVA hydrogels incorporated with green synthesized cerium oxide nanoparticles for wound healing applications *Eur. Polym. J.* **134** 109853

Kaleemullah M, Jiyauddin K, Thiban E, Rasha S, Al-Dhalli S, Budiasih S and Eddy Y 2017 Development and evaluation of Ketoprofen sustained release matrix tablet using Hibiscus rosa-sinensis leaves mucilage *Saudi Pharm. J.* **25** 770–9

Kassakul W, Praznik W, Viernstein H, Hongwiset D, Phrutivorapongkul A and Leelapornpisid P 2014 Characterization of the mucilages extracted from hibiscus rosa-sinensislinn and hibiscus mutabilislinn and their skin moisturizing effect *Int. J. Pharm. PharmSci.* **6** 453–7

Krzyszczyk P, Schloss R, Palmer A and Berthiaume F 2018 The role of macrophages in acute and chronic wound healing and interventions to promote pro-wound healing phenotypes *Front. Physiol.* **9** 419

Li H and Wang F 2021 Core-shell chitosan microsphere with antimicrobial and vascularized functions for promoting skin wound healing *Mater. Des.* **204** 109683

Liu W, Yu M, Xie D, Wang L, Ye C, Zhu Q and Yang L 2020 Melatonin-stimulated MSC-derived exosomes improve diabetic wound healing through regulating macrophage M1 and M2 polarization by targeting the PTEN/AKT pathway *Stem Cell Res. Ther.* **11** 1–15

Lu J, Fan X, Hu J, Li J, Rong J, Wang W and Chen Y 2023 Construction and function of robust and moist bilayer chitosan-based hydrogel wound dressing *Mater. Des.* **226** 111604

Malviya R, Srivastava P and Kulkarni G T 2011 Applications of mucilages in drug delivery-a review *Adv. Biol. Res.* **5** 1–7

Maver T, Kurečič M, Smrke D M, Kleinschek K S and Maver U 2018 Plant-derived medicines with potential use in wound treatment *Herbal Med*

Moholkar D N, Sadalage P S, Peixoto D, Paiva-Santos A C and Pawar K D 2021 Recent advances in biopolymer-based formulations for wound healing applications *Eur. Polym. J.* **160** 110784

Mondal S, Ghosh D, Sagar N and Ganapaty S 2016 Evaluation of antioxidant, toxicological and wound healing properties of Hibiscus rosa-sinensis L.(Malvaceae) ethanolic leaves extract on different experimental animal models *Indian J. Pharm. Edu. Res.* **50** 620–37

Nath P and Yadav A K 2015 Acute and sub-acute oral toxicity assessment of the methanolic extract from leaves of Hibiscus rosa-sinensis L. in mice *J. Intercult. Ethnopharmacol.* **4** 70

Oliveira R N, Mancini M C, Oliveira F C S D, Passos T M, Quilty B, Thiré R M D S M and McGuinness G B 2016 FTIR analysis and quantification of phenols and flavonoids of five

commercially available plants extracts used in wound healing *Matéria* **21** 767–79

Patel R, Patel A, Desai S and Nagee A 2012 Study of secondary metabolites and antioxidant properties of leaves, stem, and root among Hibiscus rosa-sinensis cultivars *Asian J. Exp. Biol. Sci.* **3** 719–25

Rodrigues M, Kosaric N, Bonham C A and Gurtner G C 2019 Wound healing: a cellular perspective *Phys. Rev.* **99** 665–706

Ruffo M, Parisi O I, Dattilo M, Patitucci F, Malivindi R, Pezzi V and Puoci F 2022 Synthesis and evaluation of wound healing properties of hydro-diab hydrogel loaded with green-synthetized AGNPS: in vitro and in ex vivo studies *Drug Deliv. Transl. Res.* **12** 1881–94

Saha I, Roy S, Das D, Das S and Karmakar P 2023 Topical effect of polyherbal flowers extract on xanthan gum hydrogel patch-induced wound healing activity in human cell lines and maleBALB/c mice *Biomed. Mater.* **18** 035016

Saidin N M, Anuar N K, Tin Wui W, MeorMohdAffandi M M R and Wan Engah W R 2021 Skin barrier modulation by Hibiscus rosa-sinensis L. mucilage for transdermal drug delivery *Polym. Bull.* **79** 1–17

Salminen A, Lehtonen M, Suuronen T, Kaarniranta K and Huuskonen J 2008 Terpenoids: natural inhibitors of NF-κB signaling with anti-inflammatory and anticancer potential *Cell. Mol. Life Sci.* **65** 2979–99

Schieber M and Chandel N S 2014 ROS function in redox signaling and oxidative stress *Curr. Biol.* **24** R453–62

Schultz G S, Chin G A, Moldawer L and Diegelmann R F 2011 23 principles of wound healing *Mechanisms of Vascular Disease: a Reference Book for Vascular Specialists* p 423

Sen S, Bal T and Rajora A D 2022 Green nanofiber mat from HLM–PVA–Pectin (Hibiscus leaves mucilage–polyvinyl alcohol–pectin) polymeric blend using electrospinning technique as a novel material in wound-healing process *Appl. Nanosci.* **12** 237–50

Shedoeva A, Leavesley D, Upton Z and Fan C 2019 Wound healing and the use of medicinal plants *Evid.-based Complement. Altern.* **2019** 1–30

Shinde A V, Humeres C and Frangogiannis N G 2017 The role of α-smooth muscle actin in fibroblast-mediated matrix contraction and remodeling *Biochim. Biophys. Acta* **1863** 298–309

Singh V, Marimuthu T, Makatini M M and Choonara Y E 2022 Biopolymer-based wound dressings with biochemical cues for cell-instructive wound repair *Polymers* **14** 5371

Sinha P, Ubaidulla U and Nayak A K 2015 Okra (Hibiscus esculentus) gum-alginate blend mucoadhesive beads for controlled glibenclamide release *Int. J. Biol. Macromol.* **72** 1069–75

Sivaraman C M and Saju F 2021 Medicinal value of Hibiscus rosa sinensis: a review *Int. J. Pharmacogn. Chem.* **2** 1–11

Teng Y, Fan Y, Ma J, Lu W, Liu N, Chen Y and Tao X 2021 The PI3K/Akt pathway: emerging roles in skin homeostasis and a group of non-malignant skin disorders *Cells* **10** 1219

Ter Horst B, Chouhan G, Moiemen N S and Grover L M 2018 Advances in keratinocyte delivery in burn wound care *Adv. Drug Deliv. Rev.* **123** 18–32

Tonnesen M G, Feng X and Clark R A 2000 Angiogenesis in wound healing *J. Invest. Dermatol. Symp. Proc.* **5** 40–46

Tyagi S, Sharma N, Gupta S K, Sharma A, Bhatnagar A, Kumar N and Kulkarni G T 2015 Development and gamma scintigraphical clearance study of novel Hibiscus rosasinensis polysaccharide based mucoadhesive nasal gel of rizatriptan benzoate *J. Drug Deliv. Sci. Technol.* **30** 100–6

Vazquez-Zapien G J, Martinez-Cuazitl A, Granados-Jimenez A, Sanchez-Brito M, Guerrero-Ruiz M, Camacho-Ibarra A and Mata-Miranda M M 2023 Skin wound healing improvement in diabetic mice through FTIR microspectroscopy after implanting pluripotent stem cells *APL Bioeng.* **7** 016109

Vignesh R M and Nair B R 2018a A study on the antioxidant and antibacterial potential of the mucilage isolated from Hibiscus rosa-sinensis Linn.(Malvaceae) *J. Pharmacogn. Phytochem.* **7** 1633–7

Vignesh R M and Nair B R 2018b Extraction and Characterisation of mucilage from the leaves of Hibiscus rosa-sinensis Linn.(Malvaceae) *Int. J. Pharm. Sci. Res.* **6** 542–55

Wei P, Xie Y, Abel P W, Huang Y, Ma Q, Li L, and Tu Y 2019 Transforming growth factor (TGF)-β1-induced miR-133a inhibits myofibroblast differentiation and pulmonary fibrosis *Cell Death Dis.* **10** 670

Xu R B, Yang X, Wang J, Zhao H T, Lu W H, Cui J and Hu X L 2012 Chemical composition and antioxidant activities of three polysaccharide fractions from pine cones *Int. J. Mol. Sci.* **13** 14262–77

Yang H, Song L, Sun B, Chu D, Yang L, Li M and Guo J 2021 Modulation of macrophages by a paeoniflorin-loaded hyaluronic acid-based hydrogel promotes diabetic wound healing *Mater. Today Bio* **12** 100139

Zhang Y, Zhu Y, Ma P, Wu H, Xiao D, Zhang Y and Dong A 2023 Functional carbohydrate-based hydrogels for diabetic wound therapy *Carbohydrate Polym.* **312** 120823

Article

Fabrication and Therapeutic Process of a Green Silver-Nanoparticle-Embedded Mucilage Microsphere for Pathogenic-Bacteria-Infected Second-Degree Burn and Excision Wounds

Ishita Saha, Sourav Ghosh, Arunima Mondal, Shubham Roy, Tarakdas Basu, Arunima Sengupta, Deepak Das, and Parimal Karmakar*

Cite This: https://doi.org/10.1021/acsabm.4c00177

Read Online

ACCESS | Metrics & More | Article Recommendations | Supporting Information

ABSTRACT: Multidrug-resistant bacteria are a serious problem in biomedical applications that decrease the wound healing process and increase the mortality rate. Therefore, in this study, we have prepared a green-synthesized silver-nanoparticle-encapsulated mucilage microsphere (HMMS@GSNP) from *Hibiscus rosa sinensis* leaves and applied it to pathogen-infected burn and excision wounds. Biophysical properties like the size, polydispersity index, absorbance capacity, and drug release were measured by different techniques like field-emission scanning electron microscopy, dynamic light scattering, swelling ratio, etc. The strong antibacterial activity of a HMMS@GSNP microsphere was measured by minimum inhibitory concentration assay, minimum bactericidal concentration assay, and agar well diffusion methods. The HMMS@GSNP microsphere enhanced the cell viability, cell proliferation, migration, antioxidant, and antiinflammation activity compared to untreated GSNP and HMMS, as quantified by MTT assay, BrdU assay, scratch wound assay, reactive oxygen species scavenging assay, and Western blot analysis, respectively. In the *in vivo* experiment, we used a methicillin-resistant *Staphylococcus aureus* bacteria-infected, burn-and-excision-wound-created male BALB/c mice model. The HMMS@GSNP-treated burn-and-excision-wound-infected mice showed significant results compared to other groups (untreated, Silverex gel, AgNO$_3$, HMMS, and GSNP), and the mice tissues were utilized for bacteria count, immunoblot analysis, histological studies, and real-time polymerase chain reaction. Thus, the HMM@GSNP microsphere is an excellent therapeutic material that can be used as a topical agent for the management of chronic wound therapy.

KEYWORDS: *antibacterial, antiinflammation, antioxidant, chronic wound healing, microsphere*
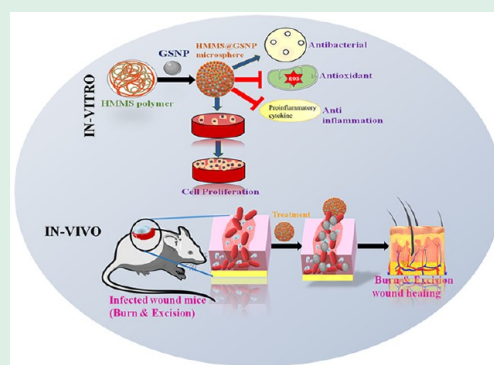
1. INTRODUCTION

Wound healing is a multistep and dynamic process. Acute wounds like burns, cuts, abrasions, surgical wounds, etc., are caused by extrinsic effects, and those wounds are repaired normally by the subsequent phases of wound healing, while chronic wounds like artery or leg ulcers are created by multiple causes.[1] According to the World Health Organization, 50% of patients are infected by antibiotic-resistant bacteria.[2] Usually injured skin is infected by different pathogenic bacteria like *Pseudomonas aeruginosa* (17%), *Staphylococcus aureus* (37%), *Proteus mirabilis* (10%), *Corynebacterium* spp. (5%), *Escherichia coli* (6%), etc., and it migrates into deeper regions of the skin and forms a biofilm on the upper surface of the wounded portion,[3] causing bacteremia or sepsis.[4] Often burn wounds are infected with bacteria and have a lot of exudate. Various types of chemicals, herbal drugs, nanoparticles (like zinc, zinc oxide, silver, titanium dioxide, and zeolite), and antibiotics have been used for the regeneration of injured tissue, but these components may have some hazardous side effects.[5] Additionally, overuse of antibiotics may lead to the development of

resistant bacteria, which ultimately transform into superbugs. Hence, the creation of effective antibacterial drugs has gained more attention for wound healing. Therefore, recently some scientists have focused on natural polymer-coated nanoparticle or biologically synthesized nanoparticle formation to prevent various infections in skin wounds or other organs;[6] for example, Ran et al. fabricated functional DNA nanoflower eye drops for the treatment of MRSA-affected keratitis.[7]

In the past few years, some researchers have used mucilage biopolymers in various forms like microspheres, gel, tablets, etc. Okunlola et al. created a microsphere from the mucilage of okra and employed it as a drug-delivery system.[8] Microspheres are free-flowing, 1−1000-μm-range spherical particles consist-

58 ing of natural or synthetic polymers and efficient for drug
59 loading, controlled release, and targeted delivery processes.[9]

60   The goal of our study is to synthesize a green silver-
61 nanoparticle-encapsulated hibiscus mucilage microsphere
62 (HMMS@GSNP) and apply it to MRSA-infected (methicil-
63 lin-resistant *S. aureus*) burn and excision wounds. Both the
64 green silver nanoparticles (GSNP) and the mucilage polymer
65 (HMMS) are synthesized from *Hibiscus rosa sinensis* leaves.
66 The physical properties of this material were characterized by
67 ultraviolet−visible spectroscopy, X-ray diffraction (XRD),
68 Fourier transform infrared (FTIR), field-emission scanning
69 electron microscopy (FESEM), dynamic light scattering
70 (DLS), ζ potential, thermogravimetric−differential thermal
71 analysis (TGA−DTA), etc. As previously reported, the
72 hibiscus mucilage polymer made up of various types of
73 wound-healing-responsible phytochemicals like galactosides, L-
74 rhamnose, D-galacturonic acid, D-galactose, glucuronic acids,
75 flavonoids, reducing sugar, etc.[10−13] In an *in vitro* experiment,
76 it was applied to human lung fibroblast (WI-38) and
77 keratinocyte (HaCaT) cell lines, and in an *in vivo* experiment,
78 it was applied on a MRSA-infected second-degree-burn-and-
79 excision-wound-developed male BALB/c mice model. The
80 release profile of the HMMS@GSNP microsphere was
81 examined by the incubation process in a phosphate-buffered
82 saline (PBS) medium at pH 7.4, and it was noticed that the
83 HMMS microsphere showed a sustained release profile of
84 GSNP throughout 22 h. At the same time, in the *in vitro*
85 experiment, the HMMS@GSNP microsphere stimulated
86 antibacterial, antiinflammation, cellular proliferation, cellular
87 migration, and antioxidant activity. In the *in vivo* study, we
88 observed that, after 13 days, HMMS@GSNP-treated burn and
89 excision wound groups showed re-epithelization, formation of
90 tissue granulation, development of hair follicles, and decreased
91 scar formation and improved more than 50% bacterial
92 infection compared to untreated and placebo-, $AgNO_3$-,
93 HMMS-, and GSNP-treated groups. Additionally, the
94 HMMS@GSNP microsphere enhanced antiinflammation,
95 antibacterial, and collagen formation activity on MRSA-
96 infected second-degree burn and excision wound mice.

97   Henceforth, our synthesized HMMS@GSNP microsphere
98 was biocompatible and biodegradable and had sustained drug
99 release properties. Additionally, it can promote the healing
100 process in pathogenic bacteria-infected burn and excision
101 wounds.

2. METHODS

102 **2.1. Fabrication Process of GSNP, HMMS, and HMMS@**
103 **GSNP.** The *Hibiscus rosa sinensis* leaves were taken from the Jadavpur
104 University campus in Kolkata, India. The Agri-horticultural Society of
105 India, Kolkata, then validated the leaves.

106 *2.1.1. Synthesis Process of GSNP.* The fresh and young leaves of
107 *Hibiscus rosa sinensis* were collected, washed, and dried at room
108 temperature. The powdered dried leaves were dissolved in distilled
109 water, and after that, the powder aqueous solution was boiled for 5
110 min. The powder solution was filtered by Whatman filter paper 1. A
111 1.7 mM $AgNO_3$ solution was added dropwise to the leaf extract
112 solution in a water bath at a temperature of 90 °C until the prepared
113 GSNP suspension was brown, and it was centrifuged at 9000 rpm for
114 25 min. Last, the pellets were collected, dried at 45−50 °C, and stored
115 at ambient temperature.

116 *2.1.2. Preparation Process of HMMS. Hibiscus rosa sinensis* leaves
117 were carefully cleaned with distilled water, macerated in deionized
118 water, then stirred continuously for 45 min, and boiled for a few
119 minutes. The concentrated hibiscus solution was filtered through a

120 muslin cloth. The isolated mucilage was purified by acetone, and the
121 precipitated mucilage was dried in a hot air oven.

122 *2.1.3. Fabrication Process of HMMS@GSNP.* A total of 5 mg of
123 HMMS polymer was dissolved in 1 mL of water and stirred for 6 h.
124 Then, 2 mg of GSNP was added to the HMMS solution and allowed
125 to stir for 2 h. The mixture was then lyophilized or dried at 45 °C to
126 remove the excess water and stored at room temperature.

127   The preparation process of the HMMS@GSNP microsphere is
128 schematically represented in Figure S1.

129 **2.2. Physical Characterization of Synthesized Components.**
130 The XRD patterns of the HMMS, GSNP, and HMMS@GSNP
131 samples were captured using an X-ray diffractometer model D8 from
132 Bruker AXS, Madison, WI. It used a Cu Kα target with a wavelength
133 of 1.5418 Å and operated at 35 kV with a scan speed of 1 s/step. An
134 IR Affinity (Shimadzu) was used for the FTIR investigation, which
135 covered the 400−4000 cm^{-1} wavenumber range. The samples were
136 made by combining KBr with HMMS, GSNP, and HMMS@GSNP
137 powder, and the sample-to-KBr ratio was 1:50. A hydraulic press
138 mechanism was then used to make the pellets for spectrometry.
139 Additionally, a pure KBr pellet was also constructed for measuring the
140 baseline. The morphologies of HMMS and GSNP were measured by
141 Zeiss EVO 18 Special Edition and FEI Inspect-F50 FESEM
142 microscopes, respectively, and the HMMS@GSNP microsphere
143 morphology was observed by a phase contrast microscope (Leica
144 ICC50 W). The hydrodynamic size and charges of the particle were
145 measured by DLS and a Zetasizer (NanoZS90, Malvern Instruments
146 Ltd., U.K.), respectively. The TGA−DTA study was done using a
147 DTG-60H DTA−TGA instrument.

148 **2.3. Swelling Ratio Study.** We employed a standard method-
149 ology to evaluate the swelling properties of the HMMS polymer and
150 HMMS@GSNP microsphere, as referenced.[14] The HMMS and
151 HMMS@GSNP dry powder samples (S_0) were accurately weighed
152 and immersed in a PBS solution with a pH of 7.5. The samples were
153 placed in a Petri dish, and their weights were observed at 4, 6, 8, and
154 24 h. The weight of the swelled samples, denoted as S_t, was recorded
155 at various time intervals, and afterward, the excess water was wiped
156 with tissue paper. The following formula was used to determine the
157 swelling ratio at time t:

$$\text{degree of swelling (\%)} = [(S_t - S_0)/S_0] \times 100$$

158 where S_t and S_0 represent respectively the weights of the synthesized
159 materials (HMMS and HMMS@GSNP) at time t and 0 h.

160 **2.4. Drug-Release Properties.** The drug release potential of the
161 HMMS@GSNP microsphere was measured by incubation methods at
162 pH 7.5 for 22 h. The percentage of encapsulated GSNP of the
163 HMMS@GSNP microsphere was calculated by absorbance maxima of
164 the silver nanoparticle solution at 450 nm using a spectrophotometer
165 (epoch microplate spectrophotometer, USA). The required amount
166 of HMMS@GSNP microsphere was dispersed in a PBS buffer
167 solution and incubated under continuous mechanical shaking at 37
168 °C. After that 2 h interval, 1 mL of supernatant was taken out to
169 measure the release percentage, and an equal amount of PBS was
170 added to the remaining incubated samples. The drug-loading capacity
171 (DLC) and drug-loading efficiency (DLE) percentages were
172 calculated by the following equations:[15]

$$\text{DLC (\%)} = \{(\text{weight of drug encapsulated in a}$$
$$\text{microsphere/weight of mucilage polymer taken out)}\}$$
$$\times 100$$

$$\text{DLE (\%)} = \{(\text{total amount of drug}$$
$$- \text{free drug in the supernatant})$$
$$/(\text{total amount of drug})\} \times 100$$

173 **2.5. *In Vitro* Experiment.** *2.5.1. Bacteria Culture.* The Gram-
174 negative bacteria *E. coli* DH5α and the Gram-positive bacteria MRSA
175 were maintained in a Luria broth medium obtained from SRL, India.
176 Methicillin antibiotic was added to the *S. aureus* culture, and the

bacterial cultures were incubated at a temperature of 37 °C for an overnight period with continuous mechanical stirring. After 24 h, 200 μL of culture media was extracted from the test tube and placed in a new broth medium. The mixture was then placed under incubation for a duration of 5 h, with continuous mechanical stirring. The newly cultivated bacterial culture was utilized for the intended experimental procedures.

2.5.2. Minimum Inhibitory Concentration (MIC) Assay. The term "MIC" in this study denotes the minimum inhibitory concentration of an antibacterial agent, which is the lowest concentration capable of inhibiting the proliferation of bacteria. Each test tube was filled with a fresh culture medium containing bacteria on the basis of section 2.5.1, and thereafter the bacteria were treated with different doses of GSNP, HMMS, and HMMS@GSNP (0, 5, 10, 20, 40, 50, 60, 80, and 100 μg/mL for *E. coli* and 0, 20, 40, 80, 100, 150, and 200 μg/mL for *S. aureus*). The test tubes were then placed in an incubator at 37 °C and were under constant stirring for a duration of 24 h. The optical density (600 nm) of each test tube was measured after 24 h, and the level of bacterial growth was determined.

2.5.3. Minimum Bactericidal Concentration (MBC) Assay. MBC assay was used to determine the lowest concentration of an antimicrobial agent (such as an antibiotic or disinfectant) required to kill a specific bacterium or microorganism. The HMMS@GSNP-treated bacterial subculture was spread on a sterile agar plate and incubated at 37 °C for 24 h; in that case, the dose was selected on the basis of the MIC value. The MBC value was considered to be the lowest concentration of antimicrobial agent that had not shown any bacterial growth on the agar plates compared to untreated bacteria.

2.5.4. Agar Well Diffusion Method. The zone of inhibition was determined by an agar well diffusion method. The bacteria were cultured in a nutrient broth medium for 24 h at 37 °C. Thereafter, 150 μL of bacteria was spread on the respective antibiotic-treated agar plate and formed a 6-mm-diameter hole in that plate. Then various concentrations of treated samples like GSNP and HMMS@GSNP solution (20,40,50,60,80,100,150, 200, and 300 μg/mL) were added to the well. The Petri dish was incubated at 37 °C overnight. At the end of the period, the inhibitory zone of the Petri dish was examined and measured by *ImageJ* software.

2.5.5. Bacterial SEM. FESEM (INSPECT F-50, FEI) was used for the study of the bacteria cell morphology after treatment of GSNP, HMMS, and HMMS@GSNP. Fresh bacterial cultures were incubated overnight after treatment of GSNP, HMMS, and HMMS@GSNP. The next day the bacteria culture was centrifuged at 8000 rpm, and the bacterial pellet was washed with PBS and fixed with 2% paraformaldehyde. A drop of diluted cell suspension was placed on a coverslip and allowed to vacuum-dry before the SEM study.

2.5.6. Human Fibroblast Cell Culture and Condition. Human lung fibroblast cell line WI-38 was purchased from NCCS Pune, India, and human keratinocyte cell line HaCaT was collected from Prof. Runa Sur's laboratory, Calcutta University, Kolkata, India. These cells were cultured in respective media of Dulbecco's modified Eagle's medium [Thermo Fisher Scientific (Waltham, MA)] with 10% fetal bovine serum [FBS; Thermo Fisher Scientific (Waltham, MA)], penicillin/streptomycin [100 units/mL; Thermo Fisher Scientific (Waltham, MA)], and amphotericin-B (antifungal; Hi-media, India) and incubated at 37 °C and 5% CO_2 [Heraeus, Thermo Scientific (Waltham, MA)].

2.5.7. Cell Viability Study. The WI-38 and HaCaT cell lines were cultured in 48-well plates and subsequently treated with several concentrations of GSNP, HMMS, and HMMS@GSNP. The cells were then incubated at a temperature of 37 °C with a CO_2 content of 5% for a duration of 24 h. After a duration of 3−4 h, the MTT solution should be discarded and subsequently replaced with an extraction buffer, resulting in the formation of a crystal violet color. The absorbance of the resulting formazan crystal color was measured using a spectrophotometer at a wavelength of 570 nm. Finally, the cell viability percent and the proliferation percent were compared with respect to untreated cells.

2.5.8. Scratch Wound Assay. The WI-38 and HaCaT cells were seeded in a 35 mm (3×10^5 cells) plate and created a wounded area with 200 μL tips. The next day the cells were washed with 1× PBS and treated with maximum proliferative concentrations of GSNP (10 μg/mL for WI-38 and 40 μg/mL for HaCaT cell lines), HMMS (80 μg/mL for WI-38 and 60 μg/mL for HaCaT cell lines), and HMMS@GSNP (10 μg/mL for WI-38 and 20 μg/mL for HaCaT cell lines). We took images after 0, 24, and 48 h, and the wounded area was measured by *ImageJ* software.

2.5.9. Immunocytochemistry and Bromodeoxyuridine (BrdU) Incorporation Assay. In this experiment, the *de novo* synthesized DNA was marked with BrdU, which is a thymidine substitute. The standard method was used for cell labeling experiments.[16] The experimental process is briefly described here. WI-38 and HaCaT cells were seeded in coverslips and cultured as per section 2.5.6. The cells were treated with the maximum proliferative concentrations of GSNP (10 μg/mL for WI-38 and 40 μg/mL for HaCaT cell lines), HMMS (80 μg/mL for WI-38 and 60 μg/mL for HaCaT cell lines), and HMMS@GSNP (10 μg/mL for WI-38 and 20 μg/mL for HaCaT cell lines) and incubated at 37 °C for 24 h. The next day 10-μm BrdU was added and incubated for 1 h for immunocytochemical analysis. The coverslips were treated with a 4% paraformaldehyde solution for fixation and afterward permeabilized with a 0.2% Triton X-100 solution for a duration of 15 min. Subsequently, the cells were treated with 2 N hydrochloric acid and incubated for 1 h at ambient temperature. After that, the blocking solution (PBS + 5% FBS) was added to the coverslip and incubated for 1 h at room temperature. During each stage, the coverslips were rinsed with 1× PBS. The cells were treated with a mouse monoclonal anti-BrdU (BD 44) antibody at a dilution of 1:100 in a wash buffer containing 0.5% FBS and 0.05% Tween-20. This incubation was carried out overnight at a temperature of 4 °C. On the second day, following the process of washing, the cells were treated with fluorescein isothiocyanate-conjugated goat anti-mouse IGG (SC-2078) at a dilution of 1:200. This incubation took place at room temperature, in a dark environment, for a duration of 1 h. The slides were prepared by using mounting media that contained 4′,6-diamidino-2-phenylindole and afterward observed using a fluorescence microscope (Leica, Wetzlar, Germany).

2.5.10. Antioxidant Assay. First, cells were seeded on coverslips as per section 2.5.6. Then the cells were treated with 5 mM *N*-acetylcysteine (NAC; Sigma-Aldrich, St. Louis, MO) and incubated for 3 h; on the other hand, cells were treated with the highest proliferative concentrations of the GSNP (10 μg/mL for WI-38 and 40 μg/mL for HaCaT cell lines), HMMS (80 μg/mL for WI-38 and 60 μg/mL for HaCaT cell lines), and HMMS@GSNP (10 μg/mL for WI-38 and 20 μg/mL for HaCaT cell lines) samples. NAC was used as a known antioxidant drug. The next day the cells were washed with 1× PBS, and 100 μm dichlorodihydrofluorescein diacetate was added for 30 min of incubation at 37 °C. Under a fluorescent microscope, the cells were examined, and the number of highly fluorescent cells were counted.

2.5.11. Western Blot Analysis. In an *in vitro* experiment, the cell lysate was prepared from WI-38 and HaCaT cell lines, and it was used for immunoblot analysis. The cells were treated with GSNP (10 μg/mL for WI-38 and 40 μg/mL for HaCaT cell lines), HMMS (80 μg/mL for WI-38 and 60 μg/mL for HaCaT cell lines), and HMMS@GSNP (10 μg/mL for WI-38 and 20 μg/mL for HaCaT cell lines). The standard immunoblot protocol was followed and is described briefly.[17] For Western blot analysis, equal quantities of protein lysates were separated by 8−12% sodium dodecyl sulfate polyacrylamide gel electrophoresis and transferred onto Merck Millipore poly(vinylidene difluoride) membranes at 300 mA for 90 min in a transfer buffer. After transfer, the membrane was blocked with 5% bovine serum albumin (BSA) in 1× 0.1% Tween 20 detergent (TBST) and incubated for 1 h. Subsequently, the membranes were incubated overnight at 4 °C with the required primary antibodies. During each stage, the membranes were rinsed with 1× TBST. The next day the membrane was incubated for 1 h at room temperature with a secondary antibody conjugated to horseradish peroxidase and diluted in 5% BSA. Finally, the membrane was imaged under a Chemi blot machine [Thermo Fisher Scientific (Waltham, MA)]. The intensity of the proteins was measured by *ImageJ* software.

C

2.6. In Vivo Experiment. *2.6.1. Animal Experiment.* In this experiment, we have selected healthy, 20−25 g male BALB/c mice, which were procured from the National Institute of Nutrition (Hyderabad, India). Animal experiments were carried out as per guidelines of the Committee for Purpose of Control and Supervision of Experimental Animals, Government of India, as approved by the Institutional Animal Ethics Committee, Department of Zoology, University of Kalyani. All mice were randomly divided into two main groups, (1) bacteria-infected second-degree burn wound and (2) bacteria-infected excision wound, and each group was divided into six subgroups, with each group containing five mice.

(1) Bacteria-infected second-degree burn wound: group 1, bacteria-injected + burn wound + untreated; group 2, bacteria-injected + burn wound + Silverex ionic gel-treated (placebo); group 3, bacteria-injected + burn wound + AgNO$_3$-treated; group 4, bacteria-injected + burn wound + HMMS-treated; group 5, bacteria-injected + burn wound + GSNP-treated; group 6, bacteria-injected + burn wound + HMMS@GSNP-treated.

(2) Bacteria-infected excision wound: group 1, bacteria-injected + excision wound + untreated; group 2, bacteria-injected + excision wound + Silverex ionic gel-treated (placebo); group 3, bacteria-injected + excision wound + AgNO$_3$-treated; group 4, bacteria-injected + excision wound + HMMS-treated; group 5, bacteria-injected + excision wound + GSNP-treated; group 6, bacteria-injected + excision wound + HMMS@GSNP-treated.

The dorsal hair of mice was shaved with veet cream and cleaned with 70% ethanol. The mice were anesthetized by administration of ketamine (40 mg/kg; Sigma), xylazine (15 mg/kg; Sigma), and tramadol hydrochloride (5 mg/kg; Sigma), and 5-mm-diameter excision wounds were created on the dorsal surface by punch biopsy and second-degree burns were formed on the dorsal surface with the help of a metal comb. The pathogenic bacteria MRSA was applied at a 5×10^8 ratio (cell counts determined by the usual agar plating method) on the upper surface of the burn and excision wound areas. In the burn wound mice, the bacteria were injected on the first and third days, while on the first and sixth days, the bacteria were injected in the excision wound area. The bacterial infection rate was measured by bacterial colony-counting methods. In both cases (postinfected burn and excision wounds), the mice were treated with various dosages, like AgNO$_3$ and GSNP, which were used at 4 mg/kg b.w., as well as HMMS and HMMS@GSNP, which were used at 8 mg/kg b.w. The bacteria-infected burn wound mice were treated on the 6th, 10th, 13th, and 16th days; however, excision wound mice were treated on the 9th, 13th, and 17th days. The wound region was captured by a digital camera and the percentage of wound area was analyzed by *ImageJ* software (NIH, USA). The bacteria-infected burn wound mice were sacrificed on the 6th, 13th, and 20th days, the bacteria-infected excision wound mice were sacrificed on the 9th, 17th, and 20th days, and the tissue samples were used for histological analysis, immunoblot analysis, and real-time polymerase chain reaction (RT-PCR).

2.6.2. Histological Analysis. The postinfected burn and excision wound tissue was sectioned into 4 mm before being paraffinized. The tissue was cleaned three times with xylene and then rehydrated using a graded series of ethanol. Afterward, the slides were stained with hematoxylin and eosin (H&E) stains, followed by dehydration using a graded ethanol series. Afterward, the slides were immersed in xylene and then mounted with a cell mounting medium. The H&E-stained slides were observed under a bright-field optical microscope (Leica DM2500, Germany).

2.6.3. Bacteria Colony-Counting Method. After 48 h of post-infection, the mice tissue was collected from the wounded portion and kept in a sterile 1× PBS buffer for thorough washing. Then the tissue was weighed and homogenized with a tissue homogenizer in a 1× PBS buffer. The homogenate sample was centrifuged at 8000 rpm for 8 min, and the palate portion was mixed with a 1× PBS buffer. Next, the centrifuged tissue was serially diluted in 1× PBS buffer, and 100 μL tissue samples were spread on methicillin-treated agar plates, which were subsequently incubated at 37 °C for 24 h to obtain bacterial colony counts.[18]

2.6.4. Immunoblot Analysis of Mice Tissue. The 6th and 20th days of postinfected burn wound mice tissue was used for immunoblot analysis; similarly, for the excision wound; the 9th and 20th days of mice tissue were used. The tissues from days 6 and 9 in both cases were selected because they represented the pretreatment condition, and day 20 represented the post-treated and recovered condition. The mice tissue was washed with a 1× PBS buffer, and ice-cold RIPA lysis buffer, protease, and phosphatase inhibitor were added. The samples were homogenized by a tissue homogenizer for 5 min in ice conditions, and the homogenized samples were centrifuged at 14000 rpm, 15 min, and 4 °C. The supernatant was collected and stored at −80 °C. The lysate protein was estimated by Bradford methods.[18] Finally, the lysate was used for immunoblot analysis and followed as per section 2.5.11.

2.6.5. RT-PCR Analysis. A RT-PCR technique was used for the quantification of mRNA gene expression. The 6th and 13th day tissues of bacteria-infected burn mice and the 9th and 17th day tissues of bacteria-infected excision wounded mice were used for RT-PCR experiments. The tissue was washed with 1× PBS and isolated using the TRIzol reagent protocol (Invitrogen, cat. no. 15596-026). Then the Qubit 4 machine (Thermo Fisher, Invitrogen, USA) was used for quantification of the RNA concentration; after that, 1 μg of RNA was used for cDNA preparation. Here we have used an iScript cDNA synthesis kit (170889, BIORAD). RT-PCR was performed from the cDNA samples using SsoFast EvaGreen for hypertrophy marker genes α-sma (α-smooth muscle actin) and ctgf (connective tissue growth factor). All primer designs were obtained from IDT, and the primer sequence is mentioned in Table 1. The expression of every gene has been normalized to that of the β-actin gene.

Table 1. Gene Sequence

primer gene	sequence
β-actin (M)	forward 5′-CCTCTATGCCAACACAGTGC-3′
	reverse 5′-CCTGCTTGCTGATCCACATC-3′
ctgf (M)	forward 5′-TCAAGCTGCCTGGGAAATG-3′
	reverse 5′-CAGTTGGCTCGCATCATAGT-3′
α-sma (M)	forward 5′-GTGGCTATTCCTTCGTGACTAC-3′
	reverse 5′-CTGACTCCATCCCAATGAAAGA-3′

2.7. Data Analysis. Every experiment was run more than once, and the standard deviation was calculated by all repeated experiments. Comparisons of the mean of experiments were made by a one-way ANOVA test (using a *MS-Excel* software) with a multiple comparison t-test, with $P < 0.05$ as a limit of significance.

3. RESULT

3.1. Biophysical Properties of Our Synthesized Materials. No diffraction maxima were found in the XRD patterns of HMMS, whereas diffraction maxima were observed at 27.56, 32.06, 38.04, and 46.16° for GSNP. HMMS@GSNP exhibited a small hump at 24.23° and absorbance maxima at 27.86, 32.36, 46.26, 54.88, and 57.33°, respectively. Both characteristic peaks of HMMS and GSNP were detected in HMMS@GSNP. Therefore, based on the XRD pattern, it can be concluded that HMMS has an amorphous nature, GSNP has a crystalline structure, and HMMS@GSNP has a semicrystalline nature (Figure 1a).

In Figure 1b, the GSNP incorporation properties of the HMMS polymer were checked by UV−vis spectroscopy. The undoped HMMS showed broad-spectrum absorbance at 332.35 nm, GSNP showed absorbance maxima at 450 nm, and HMMS@GSNP offers a broad absorption maximum centered at around 441 nm. This result suggested that GSNP doping has been successfully performed on the mucilage polymer matrix.
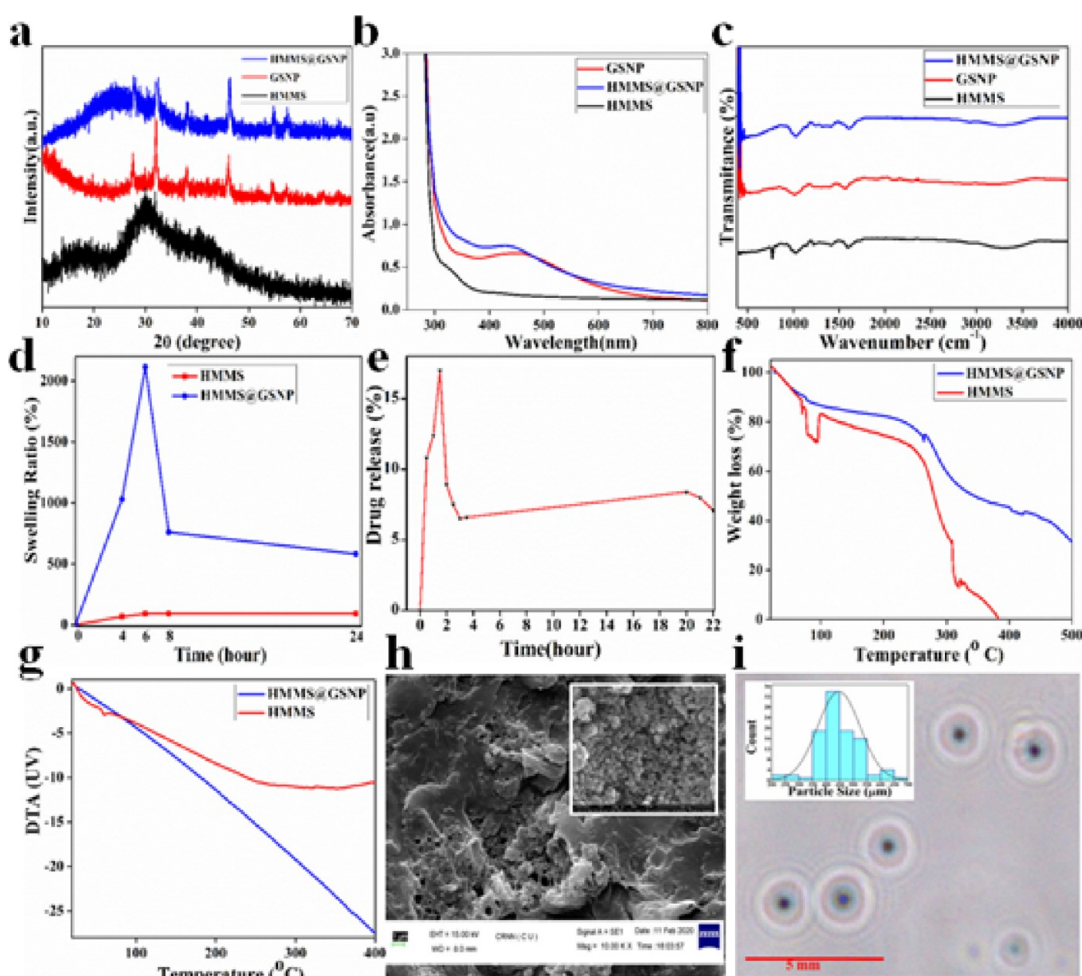
Figure 1. Biophysical properties of synthesized materials: (a) XRD patterns of HMMS, GSNP, and HMMS@GSNP; (b) UV−vis spectroscopy of HMMS, GSNP, and HMMS@GSNP; (C) FTIR spectra of HMMS, GSNP, and HMMS@GSNP; (d) swelling ratios of HMMS and HMMS@ GSNP at pH 7.5; (e) drug-release property of HMMS@GSNP; (f) TGA and (g) DTA of HMMS and HMMS@GSNP; (h) SEM images of HMMS (inset: image of GSNP); (i) phase-contrast microscopic image of HMMS@GSNP (inset: histogram of HMMS@GSNP).

The presence of various functional groups on HMMS, GSNP, and HMMS@GSNP was identified using FTIR. The absorbance peaks for the HMMS polymer were observed at 1022.60, 1417, 1600, and 3302 cm^{-1}, corresponding to the C−H bond (vinyl, monosubstituted alkenes), C−O bond (ethers, aromatic), C≡N bond, and C−H bond (alkyl, methyl), respectively. GSNP exhibited absorbance peaks at 1576 and 1010 cm^{-1} (which are attributed to −CN− stretching of amines)[19] and 1305 cm^{-1} (C−O stretching).[20] In HMMS@ GSNP, the absorbance peaks were observed at 1028, 1600, and 3297 cm^{-1}. An extra absorbance band at 3297 cm^{-1} was observed in the GSNP-doped microsphere, suggesting a possible −OH stretching (Figure 1c). The XRD and FTIR results were indicative of the proper incorporation of dopants in the sample.

The water absorbance capacity of the HMMS@GSNP microsphere was higher than that of the undoped mucilage polymer (HMMS), and it was evaluated by the swelling ratio (Figure 1d). Initially, the HMMS@GSNP microsphere absorbed a large amount of water, rendering the maximum swelling ratio for up to 6 h, and after that, the swelling ratio decreased gradually due to the breakdown of the dry mucilage polymer in the presence of water.

As observed, GSNP was discharged efficiently from the HMMS polymer in a controlled-release fashion. The release profile of GSNP-encapsulated HMMS was measured at pH 7.5 (normal skin pH) at 2 h intervals for 22 h (Figure 1e). The DLC and DLE percentages of the mucilage polymer were found to be 60% and 80%, respectively. The high DLC reveals the extensively large surface area of the HMMS polymer. Approximately 18% drug was released the first 2 h and the rest of the drug was released during the next 20 h.

The thermal stability of HMMS and HMMS@GSNP was measured with the DTA−TGA technique, showing the stability of the polymer up to 500 °C (Figure 1f,g). The temperature-dependent mass loss and differential thermograms were analyzed by the DTA−TGA instrument, maintaining a heating rate of 10 °C/min in a nitrogen atmosphere (flow rate 50 cm^3/min). It was observed that the undoped sample (HMMS) showed a thermal transition at 100 °C. Apart from this, HMMS@GSNP indicated a major thermal transition at 300 °C; therefore, it is highly stable at such a high temperature.

The morphology of the synthesized samples was observed by FESEM and phase-contrast microscopy. The microscopic view of HMMS@GSNP showed a more exfoliated structure of the microsphere than that of the pristine mucilage polymer. While the doped polymer also showed a spherical and porous
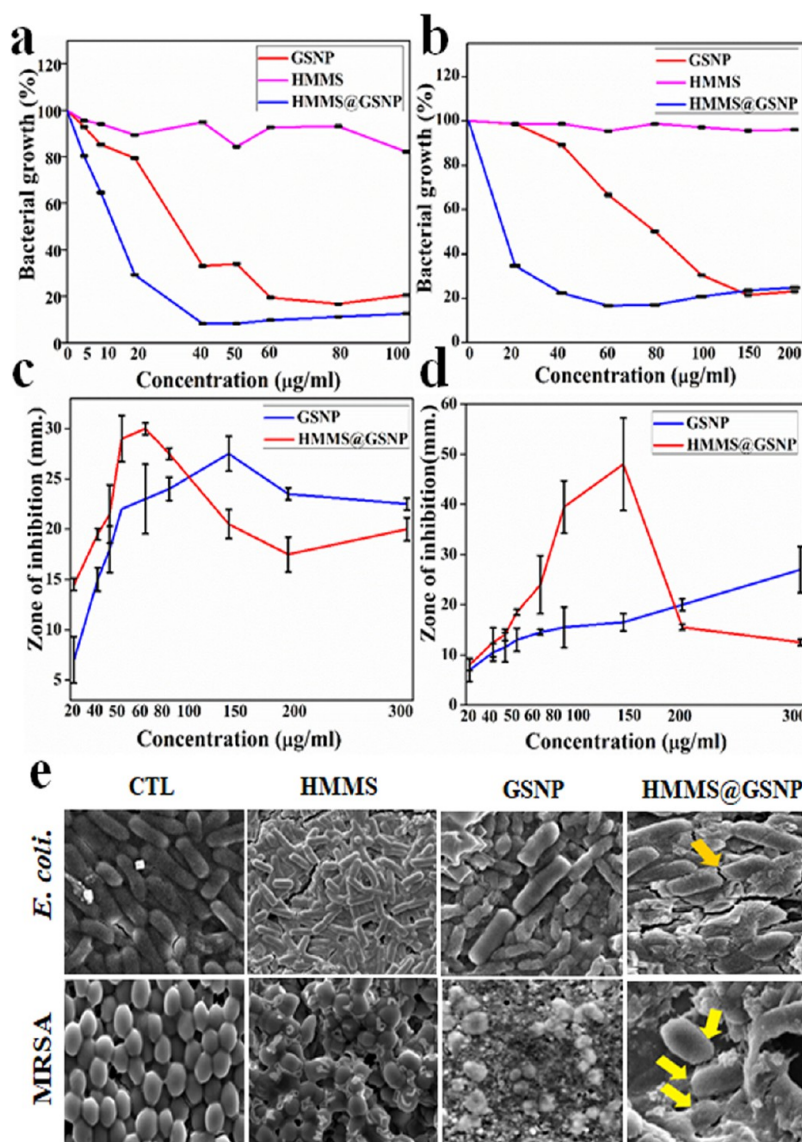
Figure 2. Assessment of the antibacterial activity on *E. coli* and MRSA: (a and b) MIC values of GSNP-, HMMS-, and HMMS@GSNP-treated *E. coli* and MRSA bacteria, respectively. (c and d) Agar well diffusion methods of GSNP- and HMMS@GSNP-treated *E. coli* and MRSA bacteria, respectively. (e) SEM images of GSNP-, HMMS-, and HMMS@GSNP-treated bacteria.

structure (Figure 1i), GSNP showed a spherical structure (Figure 1h, inset), and the undoped polymer was agglomerate in nature (Figure 1h). The incorporation of GSNP into the polymer resulted in increased porosity and reduced agglomeration nature with a microsphere-like structure. All of these properties favored better attachment probability to the substrate-like wound. The size range of the phase-contrast microscopic images of the HMMS@GSNP microsphere was 400−450 μm, and the size distribution of the histogram graph is shown in Figure 1i (inset). The hydrodynamic diameter of pure HMMS was 5545 nm as measured by DLS, whereas the HMMS@GSNP corresponding value was 3200 nm with a polydispersity index (PDI) of 0.381. The hydrodynamic size of GSNP was 191.5 nm, and the PDI value was 0.299. Additionally, the surface charge of pure HMMS was −2.68 mV, and the GSNP surface charge was −38.5 mV. However, doping with HMMS@GSNP resulted in a stable microsphere with a surface charge of 33.1 mV.

3.2. Antibacterial Activity of HMMS, GSNP, and HMMS@GSNP.

The MIC of microorganisms was determined by MIC assay. Here we have used the Gram-negative bacteria *E. coli.* and the Gram-positive bacteria MRSA. The bacteria were treated with HMMS, GSNP, and HMMS@GSNP at different concentrations, and it was observed that HMMS has no effect on the Gram-positive and Gram-negative bacteria. The IC_{50} values of GSNP-treated Gram-negative and Gram-positive bacteria were 30 and 70 μg/mL, respectively, whereas HMMS@GSNP showed IC_{50} values at 12 and 15 μg/mL, respectively. These results are shown in Figure 2a,b.

We also determined the MBC values of GSNP- and HMMS@GSNP-treated *E. coli* DH5α and MRSA bacteria, and the results are shown in Table 2. The bacteriocidal concentrations of GSNP-treated *E. coli* DH5α and MRSA were 40 and 80 μg/mL, respectively, but the HMMS@GSNP-treated bacteriocidal concentrations for *E. coli* and MRSA were 30 and 50 μg/mL, respectively.

Table 2. MIC, MBC, and Their Ratio after HMMS@GSNP Microsphere Treatment against *E. coli* and MRSA

strain	MIC (μg/mL)	MBC (μg/mL)	MBC/MIC
E. coli	12	30	2.5
MRSA	15	50	

The zone of inhibition area was measured by the agar well diffusion method. The maximum inhibitory zone areas against *E. coli* DH5α and MRSA were 27 mm at 150 μg/mL and 25 mm at 300 μg/mL, respectively, when treated with GSNP, whereas upon treatment with HMMS@GSNP, the corresponding zones of inhibition were 30 mm at 60 μg/mL concentration against *E. coli* DH5α and 45 mm at 150 μg/mL concentration against MRSA bacteria (Figure 2c,d).

3.3. Bacterial Morphology Study after GSNP, HMM, and HMM@GSNP Treatment. The bacterial SEM was used to determine the morphological structure of the bacterial sample upon treatment with GSNP, HMM, and HMM@GSNP. We observed that bacterial cell death was induced by cell membrane damage. At the same time, we noticed that HMMS@GSNP had a greater antibacterial effect than GSNP, but HMMS did not show any antibacterial effect (Figure 2e).

3.4. Estimation of the Cell Viability and Migration on HMMS-, GSNP-, and HMMS@GSNP-Treated WI-38 and HaCaT Cell Lines. The cytotoxicity effects of HMMS, GSNP, and HMMS@GSNP were determined by MTT assay. We observed that GSNP-treated WI-38 and HaCaT cell lines showed toxic effects at 40 and 60 μg/mL, respectively. The HMMS polymer had no toxic effect and helped in cell proliferation. The HMMS@GSNP microsphere-treated WI-38 cell proliferated at 10 μg/mL, and the HaCaT cell proliferated at 20 μg/mL. Moreover, the HMMS-polymer-doped GSNP was gradually released into the cell, but free GSNP was directly targeted to the cell; that is why the HMMS polymer doped with GSNP not only reduced the toxic effect of GSNP but also increased cell proliferation. The results are shown in Figure 3a,b.

Scratch wound assay was used for the cell migration study after 24 and 48 h of treatment. Figure S2a shows that, after 24 h, GSNP, HMMS, and the HMMS@GSNP microsphere promoted WI-38 migration, and after 48 h we observed, only the HMMS@GSNP microsphere-treated scratch wound area was completely recovered, while the GSNP- and HMMS-treated wound areas recovered 90% and 80%, respectively, compared to the untreated wound (Figure 3c). Similarly, the HMMS@GSNP-treated HaCaT cell line cured the wound area at 48 h (Figures 3d and S2b). However, for untreated and GSNP and HMMS-treated HaCaT cells, restoration of the wound area was 25%, 60%, and 80%, respectively (Figure 3d).

3.5. Cell Proliferation Ability of Synthesized Materials Measured by BrdU Assay. The proliferation impact of the HMMS@GSNP microsphere on WI-38 and HaCaT cells was further investigated by counting the BrdU-positive cells. Figure 3e reveals that HMMS@GSNP had a higher amount of BrdU-positive cells (172% of cells for WI-38 cell lines and 273% for HaCaT cell lines) than GSNP- and HMMS-treated cells.
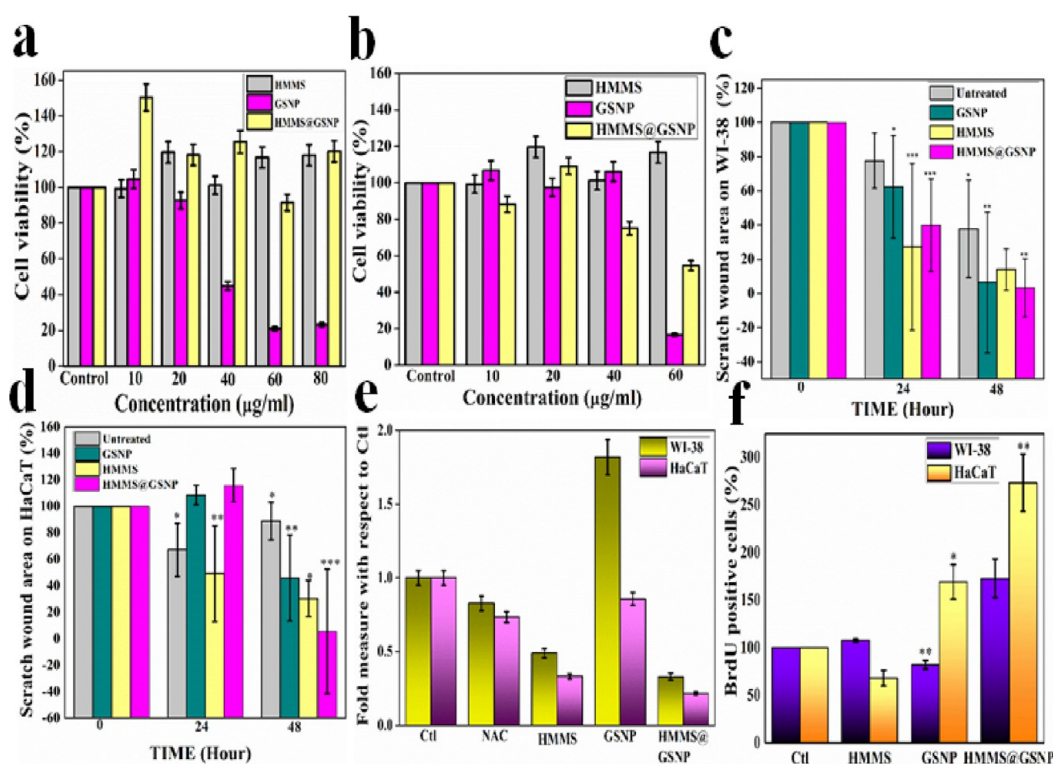

Figure 3. Cell viability, cell proliferation, and migration study of GSNP, HMMS, and HMMS@GSNP treated on human lung fibroblast and keratinocyte cell lines: (a and b) MTT assays on WI-38 and HaCaT cells, respectively; (c and d) scratch wound assay of GSNP-, HMMS-, and HMMS@GSNP-treated human lung fibroblast and keratinocyte cell lines at 0, 24, and 48 h. The effect of HMMS-, GSNP-, and HMMS@GSNP-treated cell proliferation was determined by BrdU staining assay. (e) Quantitative estimation of BrdU-positive WI-38 and HaCaT cells. (f) Antioxidant properties and quantitative analysis of NAC-, GSNP-, HMMS-, HMMS@GSNP-treated WI-38 and HaCaT cell lines. All data were expressed as the mean ± standard deviation and *t*-test values: *, $P < 0.05$; **, $P < 0.01$; ***, $P < 0.001$.
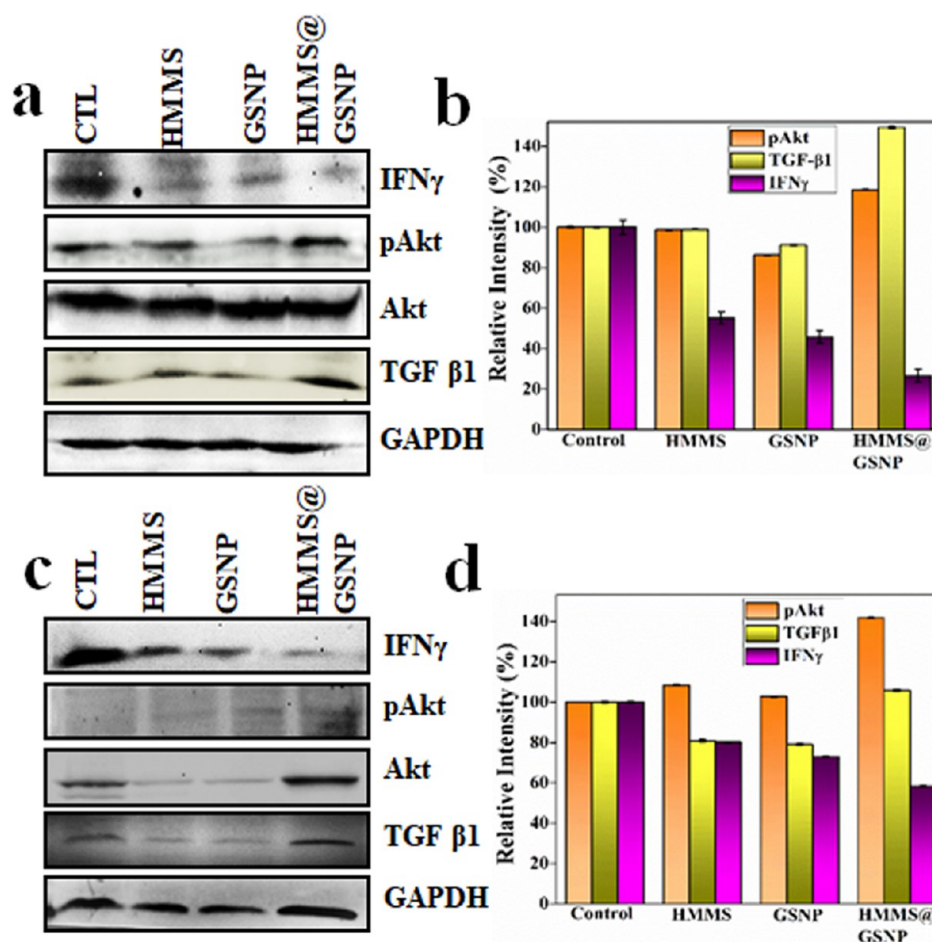
Figure 4. Western blot analysis of Akt (MW 60 kDa), pAkt (MW 60 kDa), IFN-γ (MW 25 kDa), and TGF-β1 (MW 13 kDa) protein in response to HMMS, GSNP, and HMMS@GSNP. This suggests upregulation of pAkt and TGF-β1 protein expression upon delivery of the HMMS@GSNP microsphere in fibroblast and keratinocyte cell lines for (a) WI-38 and (c) HaCaT. (b and d) Band intensities of the WI-38 and HaCat cell lines. The protein intensity was quantified using *ImageJ* software.

3.6. Antioxidant Properties of Synthesized Materials Measured by Reactive Oxygen Species (ROS) Scavenging Assay.

For the ROS scavenging assay, we used NAC-, GSNP-, HMMS-, and HMMS@GSNP-treated human lung fibroblast cell line WI-38 and human keratinocyte cell line HaCaT. Both cell lines were treated with the highest proliferative concentration. We observed that the ROS intensities were decreased by 0.70- and 0.80-fold on HMMS@GSNP-treated WI-38 and HaCaT cells, respectively, whereas the ROS intensities of NAC-, HMMS-, and GSNP-treated cells were 0.82-, 0.49-, and 1.81-fold for the WI-38 cell lines (Figure 3f) and 0.73-, 0.33-, and 0.85-fold for the HaCaT cell lines (Figure 3f). This result suggested that our synthesized HMMS@GSNP microsphere showed a better effect compared to the well-known drug NAC.

3.7. Wound-Healing-Responsive Signaling Pathway Measured by Immunoblot Analysis.

Western blot analysis was used to determine the signaling proteins associated with wound healing after treatment of the cell with either HMMS, GSNP, or HMMS@GSNP. The pAkt (Ser 473) protein was upregulated in both cell lines treated with HMM@GSNP, indicating cellular proliferation. Parts a and b of Figure 4 exhibit quantification of the IFN-γ, pAkt, and TGF-β1 protein expression levels of the HMMS@GSNP-treated WI-38 cell line, and the intensities of these proteins were 26.64%, 118.48%, and 149.29%, respectively, compared to those of the untreated control. In the case of the HMMS@GSNP-treated HaCaT cell line, the IFN-γ, pAkt, and TGF-β1 protein intensities were 58.42%, 141.89%, and 105.85%, respectively, compared to those of the untreated control (Figure 4c,d). We found that HMMS@GSNP downregulated the expression of proinflammatory cytokine IFN-γ and upregulated the expression of pAkt and TGF-β1 for both cell lines compared to GSNP- and HMMS-treated and untreated cells.

3.8. *In Vivo* Experiment. 3.8.1. *Wound Area Measured of Infected Second-Degree Burn and Excision Mice Model.*

In an *in vivo* experiment, we used male BALB/c mice and created a second-degree burn and excision wound on the dorsal surface of the skin. In both cases, the wounded portion of mice was infected by MRSA (treated 5×10^8 ratio) bacteria. We noticed that the second-degree burn wound mice showed inflammation on the 6th day after postinfection, and in excision wound mice, the inflammation started on the 9th day after postinfection. In excision and burn groups of mice, the first treatment was started on the 9th and 6th days, respectively (Figure 5a). In both cases, the mice were treated with Silverex ionic gel (placebo), AgNO$_3$, HMMS, GSNP, and HMMS@GSNP. Silverex ionic gel and AgNO$_3$ are known for wound care ointment and antibacterial drugs, respectively. Parts b and c of Figures 5 represent that HMMS@GSNP-treated second-
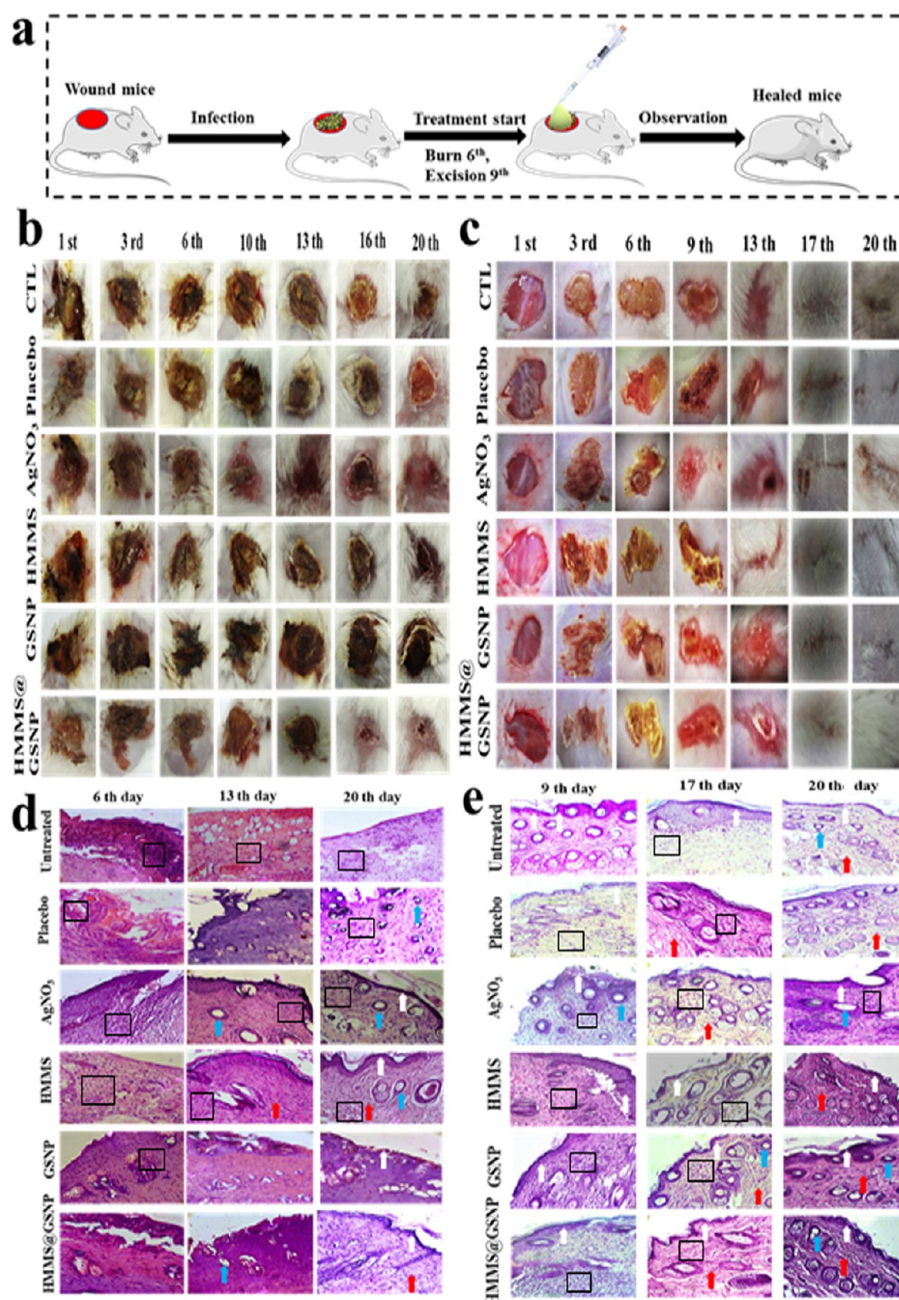
Figure 5. *In vivo* experiment of MRSA-infected burn and excision wound: (a) experimental design of *in vivo* experiment; (b and c) pictorial representation of second-degree burn and excision wounds of untreated and Silverex ionic gel (placebo), AgNO$_3$ (4 mg/kg b.w), GSNP (4 mg/kg b.w), HMMS (8 mg/kg b.w), and HMMS@GSNP (8 mg/kg b.w) treated mice monitored on various days and the corresponding images taken with a digital camera (Sony Cyber-shot DSC-WX80); (d and e) histological images of second-degree burn and excision wounds, respectively. In both cases: white arrow, epidermis; black box, MRSA-infected region; sky-blue arrow, hair follicle; red arrow, blood vessel.

degree burn and excision wound mice have gradually recovered injured areas compared to untreated and placebo-, AgNO$_3$-, HMMS-, and GSNP-treated mice. The HMMS@GSNP-treated postinfected excision wound mice were cured by 66%, the second-degree burn wound area was cured by 83% on the 20th day, and no scar formation was observed. The burn and excision wound recovery result is quantitatively represented in Table 3a,b.

3.8.2. Histological Study of Bacteria-Infected Second-Degree Burn and Excision Wound Tissue. Parts d and e of Figure 5 represent the histological analysis of MRSA-infected second-degree burn and excision wound tissue, respectively.

The morphological changes or progression of the injured portion after treatment of the synthesized component were determined by H&E staining.

The HMMS@GSNP-treated second-degree burn wound mice completely formed the epidermis (white arrow) on the 20th day. Still, the HMMS-, GSNP-, and AgNO$_3$-treated mice started epidermis formation on the 20th day, and the placebo-treated and untreated mice did not form epidermis by the 20th day (Figure 5d). In the cases of excision wounds, the untreated and GSNP- and HMMS-treated mice started epidermis (white arrow) formation on the 17th day, whereas the HMM@

Table 3. Measuring the Wound Area According to the Time after Creation of the Wound[a]

	(a) Second-Degree Burn Wound					
	postinfected second-degree burn wound area (%)					
group	3rd day	6th day	10th day	13th day	16th day	20th day
untreated	115.86 ± 10.60	104.96 ± 12.48	117.05 ± 12.35	118.23 ± 8.65	94.51 ± 11.81	84.67 ± 8.21
Silverex (placebo)	108.37 ± 11.64	114.84 ± 14.30	113.67 ± 17.09	100.96 ± 25.66	105.77 ± 25.21	89.95 ± 17.58
AgNO₃	106.90 ± 7.79	99.886 ± 9.68	91.93 ± 7.03	97.93 ± 7.38	84.85 ± 10.64	99.43 ± 17.13
HMMS	103.47 ± 10.99	76.08 ± 22.62	76.34 ± 15.42	81.57 ± 8.27	71.93 ± 11.32	69.22 ± 11.13
GSNP	95.04 ± 20.79	81.48 ± 21.68	98.63 ± 11.54	106.74 ± 19.17	87.44 ± 21.55	80.56 ± 9.27
HMMS@GSNP	160.96 ± 29.2*	113.60 ± 23*	112 ± 6.81	98.51 ± 12.45	46.87 ± 26.92	34.59 ± 10.48
	(b) Excision Wound					
	postinfected excision wound area (%)					
group	3rd day	6th day	9th day	13th day	17th day	20th day
untreated	70.91 ± 15.78*	103.64 ± 18.57	71.69 ± 19.46	67.12 ± 14.73	59.45 ± 19.22	55.26 ± 15
Silverex (placebo)	86.96 ± 22.48	107.37 ± 23.46	103.39 ± 14.82	80.69 ± 17.66	72.46 ± 25.36	35.98 ± 32.42
AgNO₃	127.49 ± 11.69**	82.55 ± 21.20	64.15 ± 14.21	55.13 ± 9.66	74.41 ± 12.15	84.98 ± 14.07
HMMS	96.36 ± 16.64	79.43 ± 19.07	113.14 ± 21.77	78.20 ± 21.96	56.19 ± 18.45	42.99 ± 15.93
GSNP	100.81 ± 14.41	115.77 ± 15.93	118.27 ± 9.23	82.98 ± 17.08	46.30 ± 20.45	41.64 ± 12.54
HMMS@GSNP	65.12 ± 24.91	85.25 ± 19.27	94.82 ± 10.88	51.33 ± 25.78*	46.45 ± 10.91	17.61 ± 18.78

[a]All data were expressed as the mean ± SD and t-test values: *, $P < 0.05$; **, $P < 0.01$.

GSNP-treated mice started epidermis formation on the 9th day and completely recovered on the 17th day (Figure 5e).

During the inflammation phase, the HMMS@GSNP-treated postinfected burn and excision wound mice removed debris and necrotic tissue from the wound surface, formed blood vessels and a thin layer of epidermis, and decreased the inflammatory portion on the 13th and 17th days, respectively. We also observed that HMMS@GSNP-treated burn wound mice reduced bacterial infection on the 9th day (black box) (Figure 5d) and excision wound mice reduced MRSA infection after the 17th day (black box) (Figure 5e), while untreated and placebo-, AgNO₃-, HMMS-, and GSNP-treated mice reduced infection very slowly compared to the HMMS@GSNP-treated group.

Proliferation is the third phase of wound healing, where keratinocytes, fibroblasts, macrophages, and endothelial cells develop, as well as matrix deposition and angiogenesis start. On the 20th day, the HMMS- and HMMS@GSNP-treated postinfected burn wound mice formed blood vessels (red arrow), but other groups of mice did not develop blood vessels within the 20th day (Figure 5d). In the case of postinfected excision wound mice, they developed blood vessels (red arrows) on the 17th day of HMMS@GSNP-, GSNP-, AgNO₃-, and placebo-treated groups (Figure 5e).

On the 13th and 20th days, HMMS@GSNP-treated postinfected burn and excision wound mice completed the reepithelization process and hair follicles (sky-blue arrow) appeared, respectively, on the wound area, whereas other groups of mice reepithelization processes were not completed. This is a maturation phase of wound healing. The results are shown in Figure 5d,e.

3.8.3. Feature of Bacterial Colonization in the Postinfected Second-Degree Burn and Excision Wound Mice and Subsequent Treatment of the HMMS@GSNP Microsphere. We further evaluated the effect of the HMMS@GSNP microsphere on the bacterial colony count in MRSA-infected second-degree burn and excision wound mice. In the case of second-degree burn wound mice, the treatment started on the 6th day after infection, and similarly, in excision wound mice, the treatment was started on the 9th day. Our result depicted that the number of viable bacteria in HMMS@GSNP-treated second-degree-burn-infected mice was significantly reduced compared to those of other groups. In the second-degree burn wound, after the 20th day, the HMMS@GSNP microsphere reduced bacterial growth by about 40%, yet other groups did not inhibit bacterial growth (Table 4a). Table 4b shows that after the 20th day the HMMS@GSNP-treated MRSA-infected excision wound mice inhibited 75% bacterial growth; on the other hand, the other groups (untreated and treated with placebo, AgNO₃, HMMS, and GSNP) inhibited bacterial growth by less than 30%.

Table 4. Bacterial Colony Count on Postinfected Excision and Second-Degree Burn Wound[a]

(a) Number of Bacterial Colonies on Second-Degree Burn Wound Mice			
	no. of bacterial colonies [log (CFU/mL)]		
group	6th day	13th day	20th day
untreated	15.45 ± 0	15.69 ± 0	15.74 ± 0
Silverex (placebo)	10.52 ± 2.70	11.63 ± 2.22	11.58 ± 2.27
AgNO₃	5.71 ± 5.33	4.93 ± 5.89	4.73 ± 6.02
HMMS	10.76 ± 2.5	10.55 ± 2.82***	15.51 ± 0.13**
GSNP	13.41 ± 1.12***	15.93 ± 0.13**	15.02 ± 0.39***
HMMS@GSNP	16.54 ± 0.61**	13.03 ± 1.53***	10.3 ± 2.98***
(b) Number of Bacterial Colonies on Excision Wound Mice			
	no. of bacterial colonies [log (CFU/mL)]		
group	9th day	17th day	20th day
untreated	17.11 ± 0	16.96 ± 0	15.83 ± 0
Silverex (placebo)	24 ± 4**	24.61 ± 4.5	16.30 ± 0.2
AgNO₃	16.31 ± 0.4***	16.70 ± 0	16.82 ± 0.58
HMMS	15.97 ± 0.65	13.84 ± 2.9	16.52 ± 0.40*
GSNP	16.05 ± 0.6**	16.61 ± 0.04**	16.24 ± 0.26
HMMS@GSNP	23.84 ± 3.88	16.84 ± 0.09	6.01 ± 0.14

[a]All data were expressed as the mean ± standard deviation and t-test values: *, $P < 0.05$; **, $P < 0.01$; ***, $P < 0.001$.
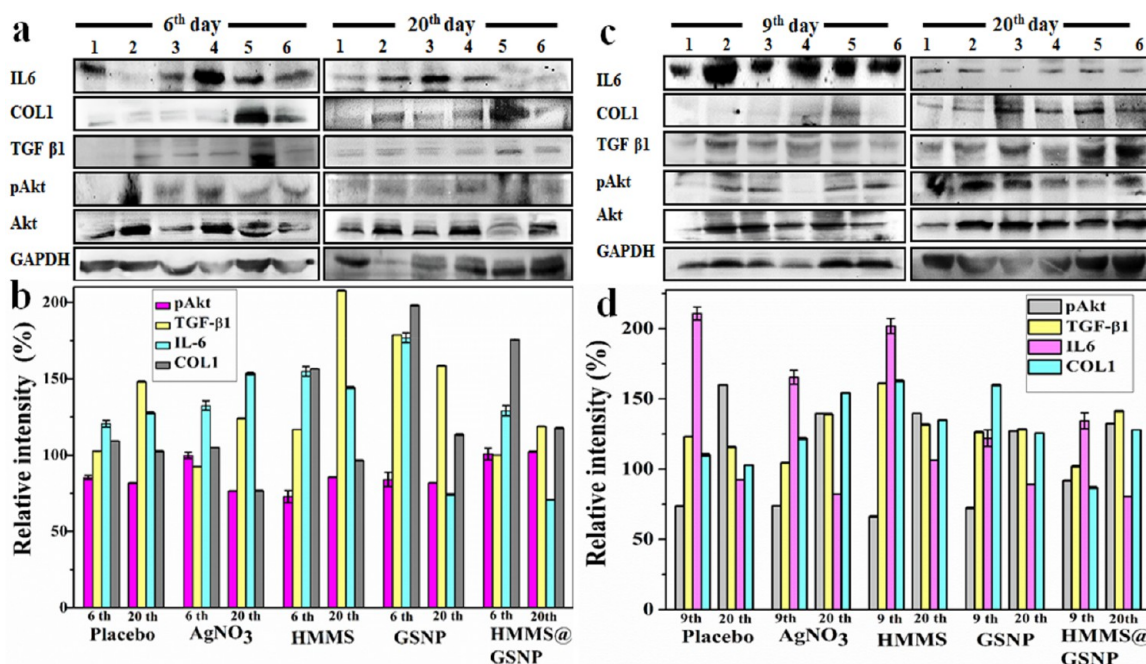
Figure 6. Western blot analysis of postinfected second-degree burn and excision wound mice: (a and b) Akt (MW 60 kDa), pAkt (MW 60 kDa), IL-6 (MW 21 kDa), TGF-β1 (MW 13 kDa), and COL1 (MW 210 kDa) protein expression at the 6th and 20th days of second-degree burn wound-infected mice, respectively; (c and d) Akt (MW 60 kDa), pAkt (MW 60 kDa), IL-6 (MW 21 kDa), TGF-β1 (MW 13 kDa), and COL1 (MW 210 kDa) protein expression at the 9th and 20th days of excision wound-infected mice, respectively. The protein intensity was quantified using *ImageJ* software. In both cases (second-degree burn and excision), untreated was taken as 100%. Lane: 1, untreated; 2, Silverex ionic gel-treated (placebo); 3, AgNO$_3$-treated; 4, HMMS-treated; 5, GSNP-treated; 6, HMMS@GSNP-treated.
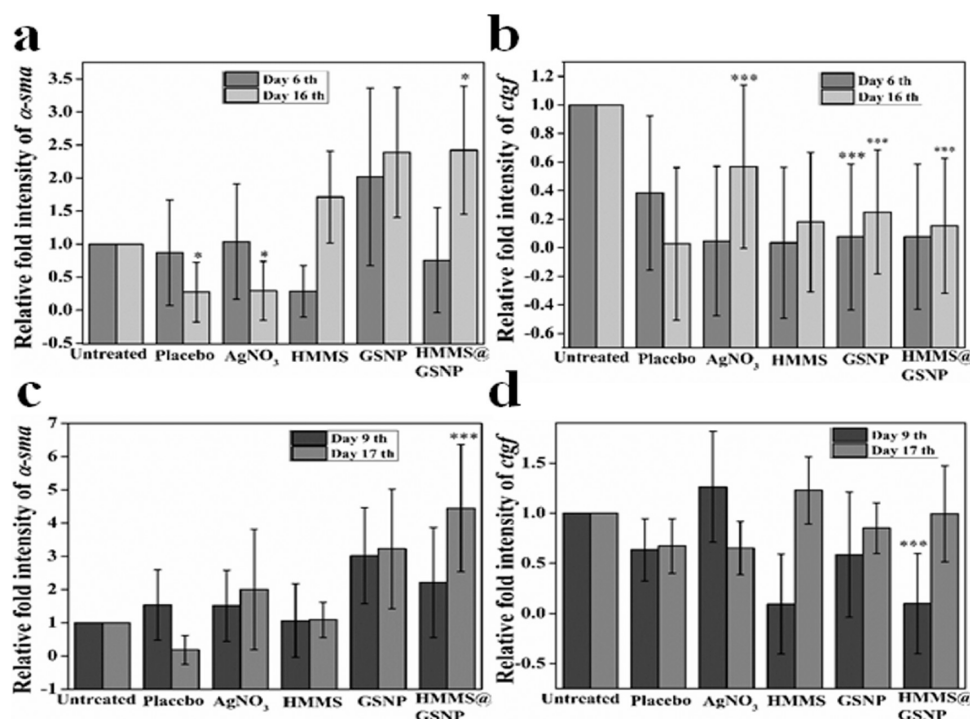

Figure 7. RT-PCR analysis of Silverex (placebo)-, AgNO$_3$-, HMMS-, GSNP-, and HMMS@GSNP-treated postinfected second-degree burn and excision wound mice tissue: (a and b) α-sma and ctgf gene expression of postinfected second-degree burn mice, respectively; (c and d) α-sma and ctgf gene expression of postinfected excision mice, respectively. Here; *, $P < 0.05$; **, $P < 0.01$; ***, $P < 0.001$.

3.8.4. Expression of Proinflammatory Cytokine and Wound-Healing-Responsive Protein Level in Mice after the Bacterial Infection and Subsequent Treatment Was Measured by Western Blot Analysis. After the introduction of MRSA bacteria in the injured area, the expression of proinflammatory cytokines like IL-6, IFN-γ, IL-8, TNF-α, IL-1, etc.,[21] is changed. We examined whether the HMMS@GSNP microsphere could modulate the expression of proinflamma-

tory cytokines and promote wound-healing-responsive proteins of the postinfected burn and excision wound in male BALB/c mice. Here tissues from the 6th and 20th days of second-degree burn wound mice (Figure 6a,b) and 9th and 20th days of excision wound mice were taken for analysis (Figure 6c,d). We observed that the HMMS@GSNP microsphere-treated postinfected burn wound mice resulted in enhanced expression of pAkt (Ser 473) (102%), TGF-β1 (118.86%), and Collagen Type-I (117.74%) and reduced IL-6 expression by 70.8% on the 20th day compared to the untreated control (Figure 6b) as well as on the same day postinfected excision wound mice when treated with the HMM@GSNP microsphere that increased expression of pAkt (Ser 473) (132.39%), TGF-β1 (141.47%), and Collagen Type-I (127.91%) and decreased IL-6 expression (80.41%) compared to the untreated control (Figure 6d). In both cases, the HMMS@GSNP microsphere showed a better antiinflammatory effect and promoted the PI3K pathway, the TGF-β1 pathway, and Collagen Type-I formation compared to the other groups of mice, and the results are depicted in Figure 6.

3.8.5. Molecular Analysis of Postinfected Burn and Excision Wound Mice. Figure 7 exhibits the results of αsma and ctgf gene expression on different days of second-degree burn and excision wound tissue by RT-PCR. Our findings indicated that the α-sma mRNA expression levels were significantly higher in the HMMS@GSNP-treated burn and excision mice compared to the untreated and placebo-, AgNO$_3$-, HMMS-, and GSNP-treated groups (Figure 7a,c). Figure 7b shows that HMMS@GSNP-microsphere-treated second-degree burn wound mice significantly increased ctgf gene expression on the 16th day compared to the pretreated 6th day mice. In the case of the excision wound, the HMMS@ GSNP microsphere promoted the ctgf expression levels (17th day) compared to other groups (Figure 7d).

4. DISCUSSION

Burn and excision wound patients have higher rates of morbidity and mortality due to microbial infections, especially by numerous drug-resistant microorganisms like *S. aureus*, *P. aeruginosa*, *P. mirabilis*, *E. coli*, and *Corynebacterium* spp.[22] Therefore, herbal medicine and synthetic nanoparticles have been practiced for centuries, and even today, natural medicines make up one-third of the top-selling products in the pharmaceutical industry. Recently, green synthesized nanoparticles have become extremely popular compared to chemically synthesized nanoparticles because green synthesized nanoparticles are economical, energy-saving, relatively easier to perform, and environmentally friendly and exhibit low toxicity levels in living cells.[23] Wound dressing and management is the most important factor for the recovery of bacteria-infected wound healing. Nowadays, researchers are using a variety of techniques to prevent bacterial infection, including living probiotic therapy,[24] photodynamic therapy, chemo-dynamic therapy, sonodynamic therapy, nanocomposite therapy, nanoparticle-mediated therapy, etc. Using photo-thermal therapy, Ran et al. created a nanocomposite material to prevent the production of biofilms.[25] Here we report the development process of a plant-derived green silver nano-particle-loaded mucilage microsphere and its therapeutic efficacy against bacteria-infected second-degree burn and excision wound healing. The XRD result of HMMS@GSNP shows some sharp peaks at 27.86, 32.36, 46.26, 54.88, and 57.33°, so it is a semicrystalline type. Our FTIR results also suggested that HMMS@GSNP partly carried both GSNP and HMMS vibrations like 1028 and 1600 cm^{-1}. Therefore, the XRD and FTIR results confirmed that HMMS@GSNP carries some diffraction and vibration lines of GSNP and HMMS, so GSNP is successfully doped in the HMMS polymer. Moreover, the appearance of an absorption band in the UV−vis spectrum around 441 nm is due to the incorporation of GSNP, and it corresponds to the n−π^* transition of GSNP, indicating successful doping. It is quite interesting to observe the alteration of the microstructure after the doping of GSNP into the HMMS polymer.

The morphology of the synthesized HMMS@GSNP was spherical in structure and increased porosity. We also observed that, after GSNP encapsulation, a modified structure of the HMMS polymer and a microsphere-like structure are formed. Thus, the spherical and porous structure provided better attachment probability on the wound surface. The doped sample depicts an enhanced surface charge of the microsphere and forms a homogeneous solution, which is suitable for any biological application. As previously reported, the hydrophilic types of wound dressing materials are suitable for fast wound healing.[26] However, our synthesized HMMS@GSNP micro-sphere is a suitable healing material for infected wounds. The water absorbance capacity of the microsphere is higher than that of the HMMS polymer, and the HMMS@GSNP microsphere participated in sustained drug-release properties, which is the most important characteristic for wound care management as well as drug delivery.

Additionally, the thermal stability has also been measured using the DTA−TGA technique, showing stability of the microsphere up to 300 °C. Such high-temperature stability would definitely make this sample usable for biomedical applications.

In antibacterial experiments, we selected Gram-positive MRSA and Gram-negative *E. coli* bacteria because they commonly occurred in the wound site. As previously reported, silver nanoparticle was used as a broad-spectrum antibacterial agent for many strains[27] but did not protect the wound area from bacterial infection. Advanced wound dressing material should possess antibacterial, antiinflammation, and wound-healing properties. The MIC, MBC, and agar well diffusion results depicted that the HMMS-incorporated GSNP micro-sphere showed a better effect compared to untreated and HMMS- and GSNP-treated bacteria. As previously reported, AgNP inhibited bacterial growth by blocking the respiratory enzyme pathway, destroying cell walls, and cleaving bacterial DNA.[28] Herein, the bacterial SEM images showed that HMMS@GSNP-treated Gram-positive and Gram-negative bacterial growth was inhibited by the bacterial membrane damage process (Figure 2e) perhaps by better deposition of silver ions on the bacterial surface. Similar results were also found in the *in vivo* experiment of the MRSA-infected second-degree burn and excision wound mice model. The mice were treated with MRSA because it is the most widespread pathogenic bacteria for skin and soft tissue infections.[6] The HMMS polymer did not show any significant effect of antibacterial properties compared to the untreated and placebo control samples. GSNP inhibited the bacterial growth and the wounded area recovered very slowly, but HMMS@GSNP inhibited the bacterial growth and simultaneously accelerated the healing process of the second-degree burn and excision wound (Table 4a,b). Our results indicate that the HMMS@

GSNP microsphere may release Ag$^+$ ions from the surface and inhibit microbial growth.

The cytotoxicity of HMMS, GSNP, and HMMS@GSNP was measured by MTT assay, and we used WI-38 (human lung fibroblast) and HaCaT (human keratinocyte) cell lines. In this experiment, we noticed that the HMMS polymer was significantly biocompatible, GSNP showed some toxic effects on both cell lines at a lower concentration than in a previously reported paper,[29,30] while GSNP incorporated in the HMMS polymer reduced the toxic effect and also helped with cell proliferation (Figure 3a,b). In scratch wound assay and BrdU assay, cells were treated with the highest proliferative concentration of our synthesized components, and it was observed that the HMMS@GSNP microsphere stimulated cell migration and proliferation, respectively, compared to other groups. Another important part of wound healing is mediated by oxidative stress, which induces inflammation and inhibits angiogenesis and endothelial function.[31] Previous studies reported that the dysfunction of the endothelial cell was caused by damage to mitochondrial DNA for ROS production through the Sirt3 signaling pathway.[32] The HMMS@GSNP microsphere also stimulated the expression of antioxidant properties in both cell lines, and the results showed that it is more effective in the keratinocyte cell line (Figure 3f). This is perhaps due to the different metabolisms in these two cell lines. Both keratinocytes and fibroblasts play a major role in the proliferation phase like replacement of the damaged ECM and restoration of the tissue structure and function.[33] Several molecular pathways were responsible for cutaneous wound healing like PI3K,[17] Wnt/β-catenin, TGF-β, Notch, Sonic Hedgehog, and ras/MEK/ERK signaling pathway.[34] Some proinflammatory cytokines like IFN-γ, TNF-α, IL-1β, IL-6, and IL-8 significantly increase in response to nuclear factor NF-$\kappa\beta$, which is mostly responsible for the expression of proinflammatory genes.[35] In the early stage of the wound, proinflammatory cytokines protect the wound area from infection, but in the late stage of the wound, proinflammatory cytokines delay the healing process.[36] The GSNP-encapsulated HMMS microsphere induced the expression of PI3K and TGF-β1 in the human cell lines (Figure 4).TGF-β1 plays an important role in the proliferation of fibroblasts, synthesis of ECM components like Collagen Type-I and fibronectin, the transformation of fibroblasts to a myofibroblastic phenotype, and last wound contracture.[34] However, the HMMS@GSNP microsphere promotes the antiinflammatory properties of human cell lines (Figure 4), which is another important part of early wound lesions.

Our *in vivo* result also showed that the topical application of the HMMS@GSNP microsphere stimulates the expression of wound-healing activity in MRSA-infected second-degree burn and excision wound mice. The HMMS@GSNP-treated second-degree burn wound-infected mice started healing on the 16th day, and after the 20th day, it recovered 80% of wounds compared to untreated and placebo-, AgNO$_3$-, HMMS-, and GSNP-treated mice (Table 3a and Figure 5b). Similarly, HMMS@GSNP-treated excision wound-infected mice started healing on the 13th day, and after the 20th day, it recovered 82% of wounds (Table 3b and Figure 5c) and 75% of bacterial infection (Table 4b). Therefore, the outcome of our study also recommended that the treatment dose of the HMMS@GSNP microsphere, at 8 mg/kg b.w. of mice, is suitable for this experiment. The histological result also indicates that the HMMS@GSNP microsphere showed a better effect compared to other treated and untreated groups (Figure 5d,e). The biomaterials in direct contact with biological tissues should have good histocompatibility.[37] During the wound-healing periods, the bacterial infection increases tissue inflammation, delays the healing process, and increases scar formation. Therefore, the immuno cells fight against bacteria, remove cell debris, and secrete different types of proinflammatory cytokines like TNF-α, IL-6, and IL-1β matrix metalloproteinase.[35] Herein, we observed that the HMMS@GSNP microsphere downregulates the expression of IL-6 cytokine protein and upregulates the expression of pAkt (Ser 473) protein, TGF-β1, Collagen Type-1 (Figure 6) protein as well as HMMS@GSNP significantly changes expression of the ctgf and α-sma genes (Figure 7). In the proliferative phase, the collagen acts as a strong angiogenic signal that promotes new blood vessel formation, and it also helps keratinocyte migration.[38] Further, we also observed that the HMM@GNSP microsphere enhances the expression of ctgf and α-sma, which specifically stimulate the granulation tissue formation and accelerate the wound-healing process.

5. CONCLUSION

Therefore, we can conclude that our synthesized HMMS@GSNP microsphere shows antibacterial, antiinflammation, antioxidant, and proliferation activities. The HMMS@GSNP microsphere is biocompatible, biodegradable, and cost-effective, and, additionally, it helps with sustained drug release. As mentioned, this microsphere is a suitable material for chronic wound healing, and it is an ideal candidate for biomedical application.

■ ASSOCIATED CONTENT

ⓢ Supporting Information

The Supporting Information is available free of charge at https://pubs.acs.org/doi/10.1021/acsabm.4c00177.

Additional experimental details including images of the synthesis process (Figure S1) and images of scratch wound assay (Figure S2) (PDF)

■ AUTHOR INFORMATION

Corresponding Author

Parimal Karmakar — *Department of Life Science and Biotechnology, Jadavpur University, Kolkata 700032 West Bengal, India*; Phone: +913324146710; Email: pkarmakar_28@yahoo.co.in

Authors

Ishita Saha — *Department of Life Science and Biotechnology, Jadavpur University, Kolkata 700032 West Bengal, India*; ⓞ orcid.org/0009-0002-7881-4971

Sourav Ghosh — *Department of Biochemistry and Biophysics, University of Kalyani, Kalyani 741235 West Bengal, India*

Arunima Mondal — *Department of Life Science and Biotechnology, Jadavpur University, Kolkata 700032 West Bengal, India*

Shubham Roy — *Shenzhen Key Laboratory of Flexible Printed Electronics Technology, School of Science, Harbin Institute of Technology, Shenzhen 518055, China*; ⓞ orcid.org/0000-0001-5245-3229

Tarakdas Basu — *Department of Biochemistry and Biophysics, University of Kalyani, Kalyani 741235 West Bengal, India*; ⓞ orcid.org/0000-0003-3409-9830

Arunima Sengupta − *Department of Life Science and Biotechnology, Jadavpur University, Kolkata 700032 West Bengal, India*

Deepak Das − *GLA University, Chaumuhan, Mathura 281406 Uttar Pradesh, India*

Complete contact information is available at:
https://pubs.acs.org/10.1021/acsabm.4c00177

Notes

The authors declare no competing financial interest.

■ REFERENCES

(1) Lei, L.; Wang, X.; Zhu, Y.; Su, W.; Lv, Q.; Li, D. Antimicrobial hydrogel microspheres for protein capture and wound healing. *Materials & Design* **2022**, *215*, No. 110478.

(2) *Report signals increasing resistance to antibiotics in bacterial infections in humans and need for better data*; World Health Organization, 2022; https://www.who.int/news/item/09-12-2022-report-signals-increasing-resistance-to-antibiotics-in-bacterial-infections-in-humans-and-need-for-better-data.

(3) Rahmanpour, A.; Farahpour, M. R.; Shapouri, R.; Jafarirad, S.; Rahimi, P. Synthesis and characterization of alumina-based nano-composites of TiO2/Al2O3/Chitosan with antibacterial properties accelarate healing of infected excision wounds. *Colloids Surf., A* **2022**, *644*, No. 128839.

(4) Hirsch, T.; Spielmann, M.; Zuhaili, B.; Koehler, T.; Fossum, M.; Steinau, H. U.; Yao, F.; Steinstraesser, L.; Onderdonk, A. B.; Eriksson, E. Enhanced susceptibility to infections in a diabetic wound healing model. *BMC surgery* **2008**, *8* (1), 1−8.

(5) Wang, L.; Hu, C.; Shao, L. The antimicrobial activity of nanoparticles: present situation and prospects for the future. *Int. J. Nanomedicine* **2017**, *12*, 1227−1249.

(6) Nikpasand, A.; Parvizi, M. R. Evaluation of the effect of titatnium dioxide nanoparticles/gelatin composite on infected skin wound healing; an animal model study. *Bulletin of Emergency & Trauma* **2019**, *7* (4), 366.

(7) Ran, M.; Sun, R.; Yan, J.; Pulliainen, A. T.; Zhang, Y.; Zhang, H. DNA Nanoflower Eye Drops with Antibiotic-Resistant Gene Regulation Ability for MRSA Keratitis Target Treatment. *Small* **2023**, *19* (47), No. 2304194.

(8) Okunlola, A.; Odeniyi, M. A.; Arhewoh, M. I. Microsphere formulations of ambroxol hydrochloride: influence of Okra (Abelmoschus esculentus) mucilage as a sustained release polymer. *Progress in biomaterials* **2020**, *9*, 65−80.

(9) Akin-Ajani, O. D.; Hassan, T. M.; Odeku, O. A. Talinum triangulare (Jacq.) Willd. mucilage and pectin in the formulation of ibuprofen microspheres. *Polymers in Medicine* **2022**, *52* (2), 83−92.

(10) Jani, G. K.; Shah, D. P. Evaluation of mucilage of Hibiscus rosasinensis Linn as rate controlling matrix for sustained release of diclofenac. *Drug development and industrial pharmacy* **2008**, *34* (8), 807−816.

(11) Kassakul, W.; Praznik, W.; Viernstein, H.; Hongwiset, D.; Phrutivorapongkul, A.; Leelapornpisid, P. Characterization of the mucilages extracted from hibiscus rosa-sinensis linn and hibiscus mutabilis linn and their skin moisturizing effect. *Int. J. Pharm. Pharm. Sci.* **2014**, *6* (11), 453−7.

(12) Vignesh, R. M.; Nair, B. R. Extraction and Characterisation of mucilage from the leaves of Hibiscus rosa-sinensis Linn.(Malvaceae). *Int. J. Pharm. Sci. Res.* **2018**, *6* (2), 542−555.

(13) Bakr, R. O.; Amer, R. I.; Attia, D.; Abdelhafez, M. M.; Al-Mokaddem, A. K.; El-Gendy, A. E. N. G.; El-Fishawy, A. M.; Fayed, M. A.; Gad, S. S. In-vivo wound healing activity of a novel composite sponge loaded with mucilage and lipoidal matter of Hibiscus species. *Biomedicine & Pharmacotherapy* **2021**, *135*, No. 111225.

(14) Johnson, A.; Kong, F.; Miao, S.; Lin, H. T. V.; Thomas, S.; Huang, Y. C.; Kong, Z. L. Therapeutic effects of antibiotics loaded cellulose nanofiber and κ-carrageenan oligosaccharide composite hydrogels for periodontitis treatment. *Sci. Rep.* **2020**, *10* (1), No. 18037.

(15) Wu, J.; Zhang, Z.; Gu, J.; Zhou, W.; Liang, X.; Zhou, G.; Han, C. C.; Xu, S.; Liu, Y. Mechanism of a long-term controlled drug release system based on simple blended electrospun fibers. *J. Controlled Release* **2020**, *320*, 337−346.

(16) Zhang, D.; Ouyang, Q.; Hu, Z.; Lu, S.; Quan, W.; Li, P.; Chen, Y.; Li, S. Catechol functionalized chitosan/active peptide microsphere hydrogel for skin wound healing. *Int. J. Biol. Macromol.* **2021**, *173*, 591−606.

(17) Saha, I.; Roy, S.; Das, D.; Das, S.; Karmakar, P. Topical effect of polyherbal flowers extract on xanthan gum hydrogel patch—induced wound healing activity in human cell lines and male BALB/c mice. *Biomedical Materials* **2023**, *18* (3), No. 035016.

(18) Mukherjee, R.; Dutta, D.; Patra, M.; Chatterjee, B.; Basu, T. Nanonized tetracycline cures deadly diarrheal disease 'shigellosis' in mice, caused by multidrug-resistant Shigella flexneri 2a bacterial infection. *Nanomedicine: Nanotechnology, Biology and Medicine* **2019**, *18*, 402−413.

(19) Valli, J. S.; Vaseeharan, B. Biosynthesis of silver nanoparticles by Cissus quadrangularis extracts. *Mater. Lett.* **2012**, *82*, 171−173.

(20) Philip, D. Green synthesis of gold and silver nanoparticles using Hibiscus rosa sinensis. *Physica E: Low-Dimensional Systems and Nanostructures* **2010**, *42* (5), 1417−1424.

(21) Zgheib, C.; Xu, J.; Liechty, K. W. Targeting inflammatory cytokines and extracellular matrix composition to promote wound regeneration. *Advances in wound care* **2014**, *3* (4), 344−355.

(22) Sharma, B. R.; Harish, D.; Singh, V. P.; Bangar, S. Septicemia as a cause of death in burns: an autopsy study. *Burns* **2006**, *32* (5), 545−549.

(23) Elkordy, A. A.; Haj-Ahmad, R. R.; Awaad, A. S.; Zaki, R. M. An overview on natural product drug formulations from conventional medicines to nanomedicines: Past, present and future. *Journal of Drug Delivery Science and Technology* **2021**, *63*, No. 102459.

(24) Chen, Z.; Cai, Z.; Zhuang, P.; Li, F.; Cui, W.; Li, Z. Living probiotic biomaterials for osteoporosis therapy. *Biomedical Technology* **2023**, *1*, 52−64.

(25) Ran, M.; Gounani, Z.; Yan, J.; Rosenholm, J. M.; Zhang, H. Ca2+ enhanced photosensitizer/DNase I nanocomposite mediated bacterial eradication through biofilm disruption and photothermal therapy. *Nano Select* **2022**, *3* (7), 1201−1211.

(26) Qian, S.; Zhao, B.; Mao, J.; Liu, Z.; Zhao, Q.; Lu, B.; Mao, X.; Zhang, L.; Cheng, L.; Zhang, Y.; Cui, W.; Sun, X. Biomedical applications of Janus membrane. *Biomed. Technol.* **2023**, *2*, 58−69.

(27) Bruna, T.; Maldonado-Bravo, F.; Jara, P.; Caro, N. Silver nanoparticles and their antibacterial applications. *International Journal of Molecular Sciences* **2021**, *22* (13), 7202.

(28) Shaikh, S.; Nazam, N.; Rizvi, S. M. D.; Ahmad, K.; Baig, M. H.; Lee, E. J.; Choi, I. Mechanistic insights into the antimicrobial actions of metallic nanoparticles and their implications for multidrug

resistance. *International journal of molecular sciences* **2019**, *20* (10), 2468.

(29) El-Naggar, N. E. A.; Hussein, M. H.; El-Sawah, A. A. Bio-fabrication of silver nanoparticles by phycocyanin, characterization, in vitro anticancer activity against breast cancer cell line and in vivo cytotxicity. *Sci. Rep.* **2017**, *7* (1), 10844.

(30) Potara, M.; Bawaskar, M.; Simon, T.; Gaikwad, S.; Licarete, E.; Ingle, A.; Banciu, M.; Vulpoi, A.; Astilean, S.; Rai, M. Biosynthesized silver nanoparticles performing as biogenic SERS-nanotags for investigation of C26 colon carcinoma cells. *Colloids Surf., B* **2015**, *133*, 296−303.

(31) Ding, Q.; Sun, T.; Su, W.; Jing, X.; Ye, B.; Su, Y.; Zeng, L.; Qu, Y.; Yang, X.; Wu, Y.; Luo, Z.; Guo, X. Bioinspired multifunctional black phosphorus hydrogel with antibacterial and antioxidant properties: a stepwise countermeasure for diabetic skin wound healing. *Adv. Healthcare Mater.* **2022**, *11* (12), No. 2102791.

(32) Zhou, X.; Chen, M.; Zeng, X.; Yang, J.; Deng, H.; Yi, L.; Mi, M. T. Resveratrol regulates mitochondrial reactive oxygen species homeostasis through Sirt3 signaling pathway in human vascular endothelial cells. *Cell death & disease* **2014**, *5* (12), e1576−e1576.

(33) Ter Horst, B.; Chouhan, G.; Moiemen, N. S.; Grover, L. M. Advances in keratinocyte delivery in burn wound care. *Advanced drug delivery reviews* **2018**, *123*, 18−32.

(34) Amini-Nik, S.; Yousuf, Y.; Jeschke, M. G. Scar management in burn injuries using drug delivery and molecular signaling: current treatments and future directions. *Advanced drug delivery reviews* **2018**, *123*, 135−154.

(35) Pourkarim, R.; Farahpour, M. R.; Rezaei, S. A. Comparison effects of platelet-rich plasma on healing of infected and non-infected excision wounds by the modulation of the expression of inflammatory mediators: experimental research. *European Journal of Trauma and Emergency Surgery* **2022**, *48* (4), 3339−3347.

(36) Huang, Y.; Bai, L.; Yang, Y.; Yin, Z.; Guo, B. Biodegradable gelatin/silver nanoparticle composite cryogel with excellent anti-bacterial and antibiofilm activity and hemostasis for Pseudomonas aeruginosa-infected burn wound healing. *J. Colloid Interface Sci.* **2022**, *608*, 2278−2289.

(37) Huang, Y.; Mu, L.; Zhao, X.; Han, Y.; Guo, B. Bacterial growth-induced tobramycin smart release self-healing hydrogel for Pseudomonas aeruginosa-infected burn wound healing. *ACS Nano* **2022**, *16* (8), 13022−13036.

(38) Mathew-Steiner, S. S.; Roy, S.; Sen, C. K. Collagen in wound healing. *Bioengineering* **2021**, *8* (5), 63.

(12) PATENT APPLICATION PUBLICATION

(21) Application No.202331006688 A

(19) INDIA

(22) Date of filing of Application :02/02/2023

(43) Publication Date : 10/02/2023

(54) Title of the invention : FABRICATION OF GREEN SILVER NANOPARTICLE-EMBEDDED MICROSPHERE AND THERAPEUTIC ACTIVITY AGAINST BACTERIA INFECTED BURN AND EXCISION WOUND

(51) International classification : A61P0017020000, A61K0033380000, A61L0026000000, A61K0009160000, A61L0015420000	**(71)Name of Applicant :** **1)Jadavpur University** Address of Applicant :188, Raja Subodh Chandra Mallick Rd, Jadavpur, Kolkata, West Bengal 700032 Kolkata ----------- ---------- **Name of Applicant : NA** **Address of Applicant : NA** (72)**Name of Inventor :** **1)Ishita Saha** Address of Applicant :Department of Life Science and Biotechnology, Jadavpur University, 188, Raja Subodh Chandra Mallick Rd, Jadavpur, Kolkata, West Bengal 700032 Kolkata ------------ -----------
(86) International Application No :PCT// Filing Date :01/01/1900	
(87) International Publication No : NA	**2)Prof. Parimal Karmakar** Address of Applicant :Department of Life Science and Biotechnology, Jadavpur University, 188, Raja Subodh Chandra Mallick Rd, Jadavpur, Kolkata, West Bengal 700032 Kolkata ------------ -----------
(61) Patent of Addition to Application Number :NA Filing Date :NA	
(62) Divisional to Application Number :NA Filing Date :NA	**3)Sourav Ghosh** Address of Applicant :Department of Biochemistry & Biophysics, University of Kalyani, Kalyani, West Bengal, India, 741235 Kalyani ----------- ----------- **4)Prof. Tarakdas Basu** Address of Applicant :Department of Biochemistry & Biophysics, University of Kalyani, Kalyani, West Bengal, India, 741235 Kalyani ----------- -----------

(57) Abstract :

A process of fabrication of green silver nanoparticle-embedded mucilage microsphere is disclosed, wherein the process comprises of green synthesis of a silver nanoparticle, synthesis of mucilage microsphere and the process of encapsulation of silver nanoparticle in mucilage microsphere. Particularly, the process of encapsulation of silver nanoparticle in mucilage microsphere comprises of dissolving about 5 mg of the mucilage in 1mL of water using a magnetic stirrer for 6 hrs, adding about 2 mg of the silver nanoparticle into the mucilage and stirred for about 2 hrs and lyophilizing the silver nanoparticle-mucilage mixture to remove the excess water and stored at room temperature. The synthesized microspheres can be used in wound dressing material due to its high-water absorption capacity and it also acts as a proliferating agent for increasing pathogenic bacteria infected burn and excision wound healing activity. This microsphere is applied topically on the upper surface of skin injuries.

No. of Pages : 25 No. of Claims : 10

Contents lists available at ScienceDirect

Spectrochimica Acta Part A: Molecular and Biomolecular Spectroscopy

journal homepage: www.elsevier.com/locate/saa

Real-time sensitive detection of Cr (VI) in industrial wastewater and living cells using carbon dot decorated natural kyanite nanoparticles

Souravi Bardhan [a], Shubham Roy [a], Sanghita Das [a], Ishita Saha [b], Dhananjoy Mondal [a], Jhilik Roy [a], Dipak Kr. Chanda [c], Solanky Das [d], Parimal Karmakar [b], Sukhen Das [a,*]

[a] Department of Physics, Jadavpur University, Kolkata 700032, India
[b] Department of Life Science and Biotechnology, Jadavpur University, Kolkata 700032, India
[c] School of Materials Science and Nano-Technology, Jadavpur University, Kolkata 700032, India
[d] Department of Geology, Jadavpur University, Kolkata 700032, India

HIGHLIGHTS

- Synthesis of carbon dot doped natural kyanite nanostructure has been reported.
- Selective detection of Cr (VI) in industrial wastewater and live cells is found.
- Limit of detection is found to be $\sim 0.11\ \mu M$ against hexavalent chromium.
- Theoretical and experimental validation of the detection mechanism is reported.

GRAPHICAL ABSTRACT

Cost-effective and time-efficient synthesis of natural mineral (kyanite) based biocompatible, fluorometric sensor for highly selective and sensitive detection of Cr (VI) in aqueous media, industrial wastewater and living cells.
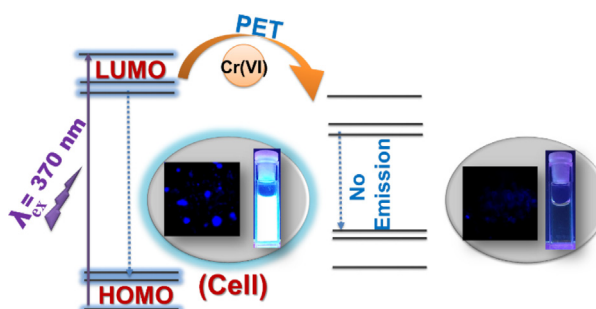
ARTICLE INFO

ABSTRACT

This article reports a facile strategy to detect hexavalent chromium (Cr (VI)) using a naturally formed mineral (kyanite) based fluorometric sensor. Nitrogenous carbon dots have been incorporated into natural kyanite (KYCD) nanoparticles causing a stable bright blue fluorescence compared to its pristine counterpart. This sensing probe structurally stabilizes and resists the agglomeration of carbon dots, thus retaining fluorescence quality for a longer period. The promising bright blue fluorescence has been utilized further to detect Cr (VI) in wastewater and living cells. Ease of synthesis, low cost, and stability of the system offers the benefit for large-scale production, which is convenient for industrial production the sensing probe. The sensor shows high selectivity and sensitivity (LOD and LOQ of 0.11 μM and 0.36 μM respectively in case of linear fitting, whereas 0.26 μM and 0.88 μM respectively for full range plot) towards hexavalent chromium in presence of other interfering elements. A detailed study of photoinduced electron transfer (PET) mediated rapid 'turn off' sensing mechanism was carried out using Time-Dependent Density functional (TDDFT) calculations. The sensing efficacy of the probe remains unaltered under a wide range of pH and can be effective in various water types. Onsite sampling and probing of Cr (VI) in tannery wastewater has been performed to validate its real-life efficiency that yields excellent results. The sensor can effectively detect chromium at a cellular level (HeLa cells) in a similar way as the bright blue fluorescence diminishes in presence of the quenching ion. Experimental in vitro studies along with theoretical docking analysis has been conducted to substantiate such issues and a higher

---

* Corresponding authors.
  E-mail address: sdasphysics@gmail.com (S. Das).

Facile synthesis of antibiotic encapsulated biopolymeric okra mucilage nanoparticles: molecular docking, *in vitro* stability and functional evaluation

Abdulla Al Masum[1,5], Kunal Pal[2,5], Ishita Saha[2], Deblina Ghosh[2], Shubham Roy[3], Sougata Ghosh Chowdhury[2], Md Maidul Islam[4,6] and Parimal Karmakar[2,6]

[1] Department of Life Sciences, Presidency University, Kolkata-700073, India
[2] Department of Life Science and Biotechnology, Jadavpur University, Kolkata-700032, India
[3] Department of Physics, Jadavpur University, Kolkata-700032, India
[4] Aliah University, ll-A/27, Action Area II, Newtown, Kolkata-700156, India

E-mail: maidulaliah@gmail.com and pkarmakar_28@yahoo.co.in

CrossMark

Abstract

The biocompatible, biodegradable okra mucilage nanoparticles (MNPs) were synthesised by a facile synthesis process and characterised by employing XRD, FTIR and FESEM studies. These were then encapsulated with the antibiotics (streptomycin, ampicillin and kanamycin) which are widely used in several pathogenic conditions. These antibiotics are susceptible to functional degradation upon exposure to adverse conditions like high temperature, UV, etc. The encapsulation of antibiotics within the mucilage matrix was testified with the aid of x-ray diffraction (XRD), FTIR, UV-vis, dynamic light scattering (DLS) as well as molecular docking estimations. These mucilage nanoparticles were then encapsulated with antibiotics when applied against bacterial strains like *Escherichia coli DH5α* and *Staphylococcus aureus.* The results demonstrated augmented bactericidal activity in comparison to the bare form of antibiotics. Our results further depict that the encapsulation of these antibiotics within the mucilage nanoparticles enhances their functionalities and also stabilises these antibiotics in conditions like elevated temperature, UV exposure and prolonged storage. Additionally, Rhodamine-B a fluorescent dye was encapsulated within the okra mucilage nanoparticles and is readily internalised by the human lung fibroblast cells, WI-38. Thus, our findings implicate that these synthesised MNPs are truly multi and can emerge as a promising therapeutic intervention in the coming years.

Keywords: okra mucilage, nanoparticles, antibiotics, stability, biological activity
Classification numbers: 2.04, 2.05, 5.08

1. Introduction

Nanotechnology involves the synthesis and application of matters in the nanoregime [1–3]. It encompasses the fields like development of potential drug delivery agents [4, 5], biosensors [6, 7] and advancements in disease diagnosis. The natural polymers are usually biogenic in origin. Generally natural polymers comprise of several monosaccharides that are interlinked by glycoside bonds and they also have high molecular weights [8]. There has been an upsurge in the use of natural polymers for the numerous pharmaceutical formulations [9, 10]. Biogenic polymers are used in several pharmaceutical fields in various forms such as microspheres, nanomatrix, liquid formulations as wells as transdermal or buccal films [11, 12].

---

[5] These authors contributed equally to this work.
[6] Authors to whom any correspondence should be addressed.

Taylor & Francis
Taylor & Francis Group

Check for updates

A comparison on the biochemical activities of Fluorescein disodium, Rose Bengal and Rhodamine 101 in the light of DNA binding, antimicrobial and cytotoxic study

Mukti Mohammad[a], Ishita Saha[b], Kunal Pal[b], Parimal Karmakar[b], Prateek Pandya[c], Harun Al Rasid Gazi[a] and Md. Maidul Islam[a]

[a]Department of Chemistry, Aliah University, Kolkata, India; [b]Department of Life Science and Biotechnology, Jadavpur University, Kolkata, West Bengal, India; [c]Amity Institute of Forensic Sciences, Amity University, Noida, India

Communicated by Ramaswamy H. Sarma

ABSTRACT

Biochemical activities of Fluorescein, Rose Bengal and Rhodamine 101 were studied by DNA binding, antibacterial and cytotoxic studies. DNA binding studies were done using spectroscopic, thermodynamic and molecular modeling techniques. Antibacterial activities were investigated against a gram-negative bacteria *Escherichia coli* and a gram-positive bacteria *Staphylococcus aureus*. Cytotoxic activities were studied against Wi-38 cell line. We observed these dyes bound to minor groove of DNA and structural diversity of dyes affect the phenomenon. No significant antibacterial and cytotoxic activities of these dyes were found in our observations.

$$\Delta G = \Delta G_{con} + \Delta G_{t+r} + \Delta G_{hyd} + \Delta G_{pe} + \Delta G_{mol}$$
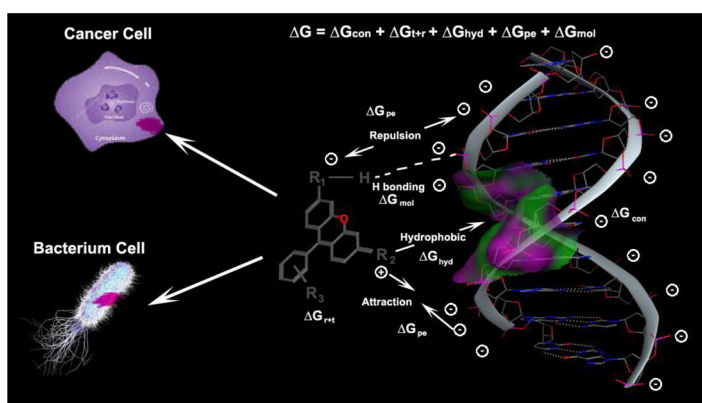
Introduction

Now a day, study on the biochemical activities of dyes is an interesting area of research. From the recent studies, it was proved that malachite green is highly toxic due to its mutagenic effect (Culp & Beland, 1996; Srivastava et al., 2004). Tartrazine and carmoisine two organic azo dyes can adversely affect the function of vital organs like liver, kidney even at very low dose (Amin et al., 2010).

One of the important biochemical activities of dyes are their affinity towards DNA. Several fluorescent dyes are used for specification, staining and photosensitization of DNA molecule (Afzal et al., 2016; Maurye et al., 2017; Zarrintaj et al., 2018). DNA replication may be inhibited due the binding of dyes, which in turns lead these dyes to act as antimicrobial

(El-Ghamry et al., 2018; Venugopal et al., 2020)and cytotoxic agents against carcinoma cells (Cheng et al., 2019; Shi et al., 2016).

Our previous study showed that three xanthene group of dyes Rhodamine B (Islam et al., 2013), Rhodamine 123 (Masum et al., 2014) and Rhodamine 6 G (Al Masum et al., 2016) are good DNA binder molecules, which motivated us to continue the study with other derivatives of these group of dyes such as Fluorescein (FS), Rose Bengal (RB) and Rhodamine 101 (R101; Figure 1).

Fluorescein (uranine), a xanthene group of dye is used frequently in ophthalmology and optometry field as diagnostic dye (Stein, 1957). Walthall and Stark showed that fluorescein has an acute toxicity against *Daphnia pulex* (Walthall & Stark,
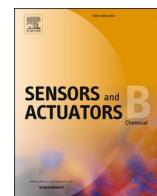
Contents lists available at ScienceDirect

Sensors and Actuators: B. Chemical

Polymeric carbon dot/boehmite nanocomposite made portable sensing device (Kavach) for non-invasive and selective detection of Cr(VI) in wastewater and living cells

Shubham Roy [a,1], Souravi Bardhan [a,2], Dhananjoy Mondal [a], Ishita Saha [b], Jhilik Roy [a], Solanky Das [c], Dipak Kr. Chanda [d,3], Parimal Karmakar [b], Sukhen Das [a,*,4]

[a] *Department of Physics, Jadavpur University, Raja S.C. Mullick Road, Kolkata 700032, India*
[b] *Department of Life Science and Biotechnology, Jadavpur University, Kolkata 700032, India*
[c] *Department of Geological Sciences, Jadavpur University, Kolkata 700032, India*
[d] *School of Materials Science and Nano Technology, Jadavpur University, Kolkata 700032, India*

ARTICLE INFO

ABSTRACT

This work reports a handheld fluorometric probe, namely 'Kavach' for monitoring hexavalent chromium in industrial wastewater and living systems. Kavach is capable to detect chromium contamination in a rapid and facile way. The device is made of a thin layer (~1 mm) of carbon dot decorated boehmite nanostructure (BH@CD) incorporated in a layer of poly vinylidene fluoride-co-hexafluoropropylene (PVDF-HFP) membrane. The doped membrane has an excellent blue fluorescence upon UV excitation (355 nm) and alters its fluorescence level when exposed to Cr(VI). In reality, tiny carbon dots leach out from the nano-matrices to produce secondary contamination. Incorporation of the BH@CD into the polymeric matrix of PVDF-HFP significantly reduces such contamination and makes this material a potential sensing probe. This photoinduced electron transfer (PET) based sensor is tremendously selective and sensitive (LOD ~66 nM) towards aqueous chromium. The performance of the probe remains unaltered in different pH and water qualities. Additionally, this material can sense chromium in living cells, which has been validated theoretically using molecular docking and observed experimentally using fluorescence microscopy. Kavach is truly a handheld, reusable and non-invasive sensing probe against Cr(VI), which can be employed for on-site low-cost detection.

1. Introduction

The toxic industrial effluents are enormously causing harm to the water bodies. These effluents, such as Cr(VI), Fe(III), Pb(II), *etc.* are mostly carcinogenic and mutagenic in nature [1a]. Such toxins are not only polluting water and water bodies but also cause severe harm to the environment and thus need proper detection and removal. Traditionally, various detection techniques, like inductively coupled plasma mass spectroscopy (ICP-MS), atomic absorption (AAS) are well adopted in detecting such heavy metals in water [1a]. But, recently fluorometric sensors have gained enormous interest due to their tremendous

sensitivity and rapid detection of various ions, molecules and biological elements [1b]. Biocompatible fluorescent materials have been used widely for fabricating such excellent sensing materials, but a well-devised handheld sensor is yet to be achieved. Mostly, fabrication of a fluorescent sensor device is difficult due to the limited availability of free-standing, flexible and reusable sensing materials, when it comes to heavy metal detection in aqueous media [2]. Several heavy metal sensors have been developed recently, among them carbon dot and its derivatives are showing great potential in this field [3–5].

Carbon dot (c-dot) is a nanostructure made of sp²- hybridized carbon atoms known for excellent fluorescence properties [6a]. The

---

ORIGINAL ARTICLE

Biocompatible Carbon Dot Decorated α-FeOOH Nanohybrid for an Effective Fluorometric Sensing of Cr (VI) in Wastewater and Living Cells

Bidisha Ghosh[1] · Shubham Roy[1] · Souravi Bardhan[1] · Dhananjoy Mondal[1] · Ishita Saha[2] · Saheli Ghosh[1] · Ruma Basu[3] · Parimal Karmakar[2] · Kaustuv Das[1] · Sukhen Das[1]

Abstract

This article reports the fluorometric detection of toxic hexavalent chromium Cr (VI)) in wastewater and Cr (VI) contaminated living cells using *in-situ* grown carbon quantum dots into the goethite (α-FeOOH) nano-matrix. The synthesized nano-hybrid shows enormous potential in determining the chromium contamination levels in various types of water samples. This selective fluorometric probe is enormously sensitive (LOD 81 nM) toward hexavalent chromium, which makes it a dedicated chromium sensor. Moreover, the sensing mechanism has been assessed using Stern–Volmer's equation and fluorescence lifetime experiments showing the simultaneous occurrence of photoinduced electron transfer and the inner filter effect. This chromium sensor has also been employed to assess the contamination level in real-life industrial wastewater. The performance of this probe in a real-life wastewater sample is quite commendable. Further, this biocompatible fluorometric probe has been used to demonstrate the in-vitro sensing of Cr (VI) in HeLa cells. The rapid detection mechanism of hexavalent chromium in living cells has been validated using theoretical docking simulations. Henceforth, this fluorometric sensor material could open new avenues not only in wastewater monitoring but also in biomedical applications.

Introduction

Natural sources like weathering of rocks, volcanic eruptions, and mining are counted to be potential sources of heavy metal contamination [1]. Heavy metals are those that have a specific density of 5gm/cm^3 and have the ability to affect the environment and living organisms [2].

Bidisha Ghosh and Shubham Roy are authors contributed equally in this work.

✉ Kaustuv Das
kaustuv12@gmail.com

✉ Sukhen Das
sdasphysics@gmail.com

[1] Department of Physics, Jadavpur University, Kolkata-700032, India

[2] Department of Life Science and Biotechnology, Jadavpur University, Kolkata-700032, India

[3] Department of Physics, Jogamaya Devi College, Kolkata- 700026, India

Of all the heavy metals known chromium is one of the most toxic heavy metals, commonly prevalent in nature as trivalent chromium Cr (III) and hexavalent Cr (VI) [3]. Cr (VI) has been regarded as 100-fold toxic and mutagenic than its lower oxidative counterpart Cr (III) [4]. As an effluent, it is often improperly discharged mainly into waterbodies from printing, electroplating, and tanning industries and thereby promoting biomagnification, scale rot, and osmoregulatory dysfunction of fish [5]. Cast iron pipes and ductile iron pipes are mostly lined with cement mortar that contains a considerable amount of chromium and thus chromium leaches out from the cement mortar lining into the drinking water [6]. It has been seen that Cr (VI) exposure to Swiss mice causes a sharp decrease in leucocyte and erythrocytes with an additional deforming of echinocyte formation from erythrocytes [7]. Cr (VI) has been recognized as a group-1 carcinogen by World Health Organization (WHO) as it can disrupt DNA via reactive oxygen species (ROS) generation, a maximum limit of 50 μgL^{-1} has been set by WHO [8, 9].

Considering the toxicity of the numerous organic and inorganic fluorophores and chromophores there is a need

Thesis
By: Ishita Saha

As of: Apr 1, 2024 3:33:53 PM
21,450 words - 265 matches - 164 sources

Similarity Index

13%

Mode: Similarity Report ▾

Thesis

ORIGINALITY REPORT

13%

SIMILARITY INDEX

MATCH ALL SOURCES (ONLY SELECTED SOURCE PRINTED)

★www.mdpi.com   3%
Internet

| EXCLUDE QUOTES | ON | EXCLUDE SOURCES | OFF |
| EXCLUDE BIBLIOGRAPHY | ON | EXCLUDE MATCHES | OFF |